TRANSACTIONS ON ENGINEERING SCIENCE AND TECHNOLOGY

Edited by :

Dr. Sandip Chanda, Dr. Rajesh Dey, Mr. Avijit Karmakar, Mr. Partha Sarathi Bhattacharya,
Mr. Snehashis Das, Mr. Braja Gopal Dey, Mr. Sohan Goswami

TECHNIQUE POLYTECHNIC INSTITUTE

PANCHROKHI, SUGANDHYA, HOOGHLY, 712102

| March 4th - 5th, 2022
| Hooghly ,West Bengal, INDIA

EDITION : I

ISBN : 978-93-92818-00-4

www.tpiconference.in
tpiconfa@gmail.com

Transactions on Engineering Science and Technology

A Periodic Proceedings Book of
TECHNIQUE POLYTECHNIC INSTITUTE
Approved by AICTE and Affiliated to WBSCTVES&D

1st Edition: March, 2022

Sandip Chanda, Rajesh Dey, Avijit Karmakar, Partha Sarathi Bhattacharya, Snehashis Das, Braja Gopal Dey, Sohan Goswami - Editors

Transactions on Engineering Science and Technology Edition: 1

Selected contributed articles/papers of the National Conference on "Emerging Trends in Engineering Science & Technology (NCETET-2022)" organized by Technique Polytechnic Institute March 4th - 5th, 2022.

Technique Polytechnic Institute
Village - Panchrokhi, Post - Sugandhya
District - Hooghly, State - West Bengal
Pin - 712102
Email - techniqueedu@gmail.com

Institute Website: **www.** techniqueedu.com

First Published in **March, 2022**
Printed in India

A catalogue record is available at **Technique Polytechnic Institute Library**

ISBN: 978-93-92818-00-4

TECHNIQUE POLYTECHNIC INSTITUTE

(A three years Diploma Engineering Institute)
APPROVED BY AICTE & AFFILIATED TO WBSCTVESD
Campus : Panchrokhi, P.O.-Sugandhya (Near Hooghly Rly. Station), Hooghly, W.B., Pin : 712 102
Ph : 033 2686 3682, 9830482096, 9674982097
e-mail : techniqueedu@gmail.com, tnp.tpi@gmail.com, **Website** : www.techniqueedu.com

Sri Tapas Kumar Saha
Chairman, Governing Body
Technique Polytechnic Institute

Date: 4th March, 2022

Message

On behalf of the Governing Body it's my proud privilege & honour to welcome you all to the National Conference on "Emerging Trends in Engineering Science & Technology" conducted by the Technique Polytechnic Institute, Hooghly, to be held on 4th. & 5th. March, 2022.

This is a great opportunity to gather with many researchers and to be a part of the discussions and presentations by leading experts in India about the new advances and innovations in the field of Engineering Science & Technology.

I wish to thank in advance the conference committee for extending their valuable time in organizing the programme and all the participants, reviewers, and other contributors for their collaborative efforts.

I wish the conference a grand success.

TECHNIQUE POLYTECHNIC INSTITUTE

(A three years Diploma Engineering Institute)
APPROVED BY AICTE & AFFILIATED TO WBSCTVESD
Campus : Panchrokhi, P.O.-Sugandhya (Near Hooghly Rly. Station), Hooghly, W.B., Pin : 712 102
Ph : 033 2686 3682, 9830482096, 9674982097
e-mail : techniqueedu@gmail.com, tnp.tpi@gmail.com, **Website :** www.techniqueedu.com

Sri. Soumendranath Basu
Advisor, Academic and Administration,
Technique Polytechnic Institute
& Former Additional Director,
DTET, Govt. of West Bengal

Date: 4th March, 2022

Message

As the Advisor, Academic and Administration, Technique Polytechnic Institute, Hooghly, It is my privilege and honour to welcome you all to the National Conference on "Emerging Trends in Engineering Science & Technology" which is going to be held on 4th & 5th March, 2022.

The conference aims to bridge the researchers working in academia through presentations and keynote addresses by eminent personalities in current technological trends in Engineering Science & Technology.

I congratulate the team of organizers and management of Technique Polytechnic Institute, Hooghly, for organising National Conference on such an important topic.

I wish the organizers as well as the dignitaries and the participants to make this conference a grand success.

I wish all of you success, health, happiness and prosperity!

TECHNIQUE POLYTECHNIC INSTITUTE

(A three years Diploma Engineering Institute)
APPROVED BY AICTE & AFFILIATED TO WBSCTVESD
Campus : Panchrokhi, P.O.-Sugandhya (Near Hooghly Rly. Station), Hooghly, W.B., Pin : 712 102
Ph : 033 2686 3682, 9830482096, 9674982097
e-mail : techniqueedu@gmail.com, tnp.tpi@gmail.com, **Website :** www.techniqueedu.com

Dr N R Banerjea
Former Vice Chancellor
Bengal Engineering and Science University
Shibpur
& Member of IQAC
Technique Polytechnic Institute

Date: 4th March, 2022

Message

I am pleased to offer my felicitations and best wishes to the Principal, faculty members, supporting staff, students for very successfully organising the National Conference on Emerging Trends in Engineering Science and Technology under the aegis of Technique Polytechnic Institute, Sugandhya, Hooghly, on March 4-5, 2022, with the able guidance of the Governing Body of the Institute and inspiring association of academics and practising engineers, researchers from India and abroad.

The papers presented were of high standards and invigorating for the participants and delegates. These are being published in the form of a compendium which would be worth preserving for reference.

I expect the technical education leadership of the Country and the State will not hesitate to shower their blessings on this rural Polytechnic in all their similar endeavours.

Content

Remedial methods for Geomechanical threats associated to River Hydraulics: Selected Case Studies in India

Ghritartha Goswami
Department of Civil Engineering
North Eastern Regional Institute of Science and Technology
Nirjuli, Arunachal Pradesh, India
er.ghritartha@gmail.com

Joydeep Dutta
Silchar Water Resources Circle
Govt. of Assam
Silchar, Assam, India
duta_iit@yahoo.co.in

Sudip Basack
Elitte College of Engineering, Affiliation
MAKA University of Technology
Kolkata India
basackdrs@hotmail.com

Bini Kiron
Department of Civil Engineering
North Eastern Regional Institute of Science and Technology
Nirjuli, Arunachal Pradesh, India
itachikiron@gmail.com

Habung Bida
Department of Civil Engineering
North Eastern Regional Institute of Science and Technology
Nirjuli, Arunachal Pradesh, India
habungbida1@gmail.com

***Abstract*—For each and every geologist, engineers, and hydrologist the study of river science and engineering has been and would be, one of the important study areas to be reckon with. The open channel flow such as river and associated hydraulics often initiate several geomechanical hazards including silting, scouring, meandering, migration, and floods. Such sort of hazard may lead to disastrous consequences if adequate remedial measures are not undertaken. In this paper the selected case study has been chosen for the northern and north-eastern parts of the India where such sort of phenomena has been witnessed such as Kosi and the Brahmaputra River. The relevant conclusions have been drawn in this paper. In this paper, two above selected cases in India have been described. Here are the important observations which are made have been briefly summarized: the first study is the alluvial basin of the Kosi river, with a maximum peak migration rate of 2.5744 km/year. Such migration could produce significant erosion and siltation, introducing severe civil and environmental hazards. By constructing appropriate barrage and associated hydraulic structures can reduced such risks. For the second case i.e., Dibrugarh town the foremost hazard observed was frequent flood which was associated with immense land erosion and migration of river channel. By the construction of spurs and the associated hydraulic structures, the solution has been demonstrated effectively. The research work is in progress and interesting results are presented in the full-length paper**

Keywords— Flood, Marginal embankment, River hydraulics, River migration, spur

I. INTRODUCTION

From ancient civilization to the modern today, river played a key role in changing the livelihood of the human-being as well as changing the land pattern of the Earth. A river is a stream of water that typically originates from the mountains, glaciers, springs and thereafter flows through the plain and finally destines them to the sea. Initially it passes through the rocky terrain of high altitudes with very high flow velocity and then gradually meanders towards the plain area where silting and scouring of the flow channel occurs. The flow velocity gradually decreases as it reaches the mouth of the sea. This final portion of the sea is called tidal river where river is affected by the tidal fluctuations of the sea [1]. Silting of the river is caused mainly due to the low velocity of the flowing water. When the bed slope of the river is below its critical value, the velocity of the river goes below the threshold value thus beginning the silting process. It occurs in aggrading river whereas the scouring takes place in degrading river. When the bed slope of the river is in its critical value, the river attains a stable condition with neither silting nor scouring situation. On reaching the mouth of the sea, the river divides itself into several branches forming deltas [2].

The meandering of the river is the deviation of its flow path from its axial direction. The river bends successively to form reverse curvature. Aggrading river carries significantly high number of silts resulting in siltation. Due to silting, the channel area of the river decreases and hence the flow velocity increases. This increased velocity of the river scours the opposite bank of the river thus introducing bends of reverse curvature and meandering takes place [3]. This process is the root cause of the geomechanical hazards of the river. Here is the need for remedial measures arise to prevent the unpredictable events which may arise due to river erosion. Flood flows with high velocity results in deep scouring which undermines the bank of the river. Spurs and groynes constructed at right angle to the embankment are used for protection of river erosion [4].

II. STUDY AREA

This paper focuses on the hydrological and geomechanical hazards of the river Kosi in Bihar and river Brahmaputra in Assam, as shown in Fig.1. It also briefs the remedial measures taken in both the rivers over the past few decades. In both the study areas, the nature of the geomechanical hazards of river mitigation was found to be similar as well as the remedial measures taken were in multi-level and multi-phases.

The river Kosi originating from Sun Kosi near Triveni in Nepal is a trans-boundary river flowing through Tibet, Nepal, and India. It is also called ‘Saptakoshi’, the Seven Rivers. It stretches for a length of 42 Km in Nepal, crossing across the mountainous terrains and then enters India at Bhimnagar, Bihar. It then flows for a length of 260 Km until it reaches the river Ganga near Kursela. The accumulation of sediments in the Kosi River is one of the world’s largest alluvial fans. It has a lateral shifting of over 120 Km and surrounded by ridges heavily attributed with silt charge especially during monsoon season [5].

The Brahmaputra River originating from the Kailash Manasarover flows through Tibet as the Yarlung Tsangpo River and enters India through the Upper Siang District of Arunachal Pradesh. It covers the North-Eastern parts of

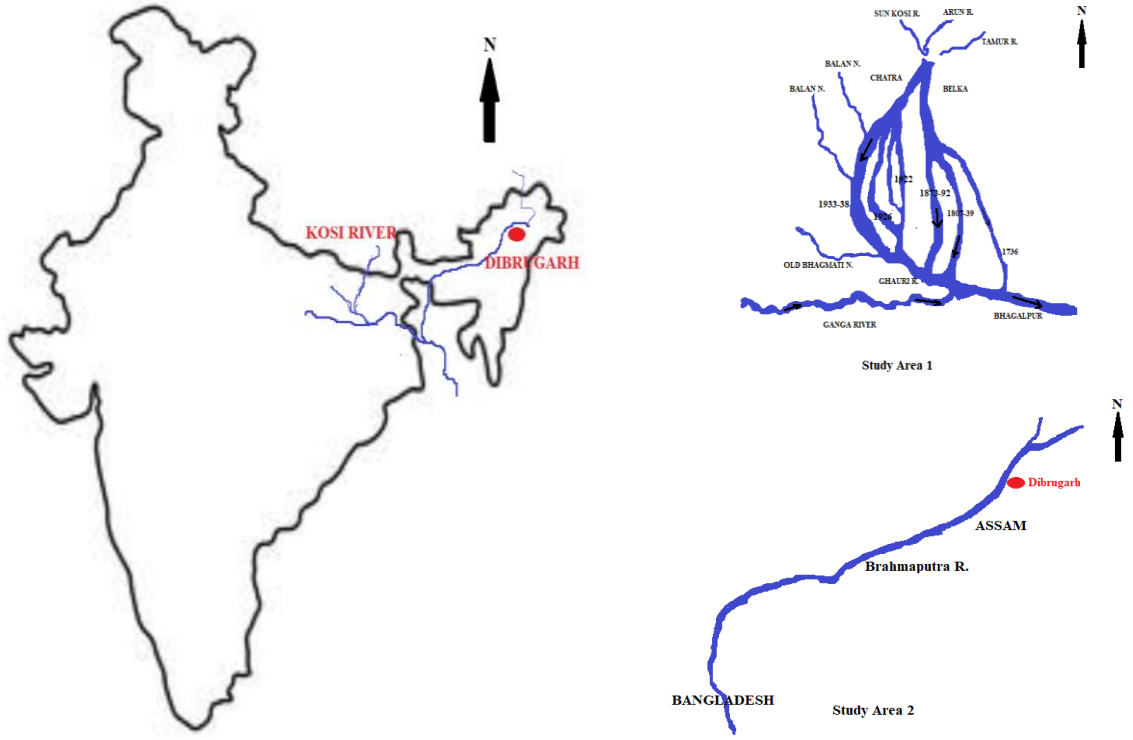

Fig 1. Case Study Areas

India and extends up to Bangladesh. In India, it is bounded by the Great Himalayan range on the North, the Patkai and Naga hills on the East and the Khasi hills on the south. It flows westward in India and joins the Padma River in Bangladesh. It is considered as one of the largest rivers of the world. It is ranked fifth all around the world in terms of average annual discharge, annual sediment load, and catchment area and for its length. Also, the river has highest specific yield in the world with 0.22 cumec/km^2 [6].

III. Case Study: 1

A. Kosi River

The state of Bihar in India is surrounded by Nepal in the north, while the states of Jharkhand, West Bengal and Utter Pradesh in the south, east and west, respectively. Bihar is a flood prone state with nearly 50% annual loss due to flood. Every year, the river Kosi in Bihar with their number of tributaries, initiate flood devastation in the monsoon period by inundation and erosion. The recurring annual disaster of the state of Bihar in India is particularly associated with flood of the Kosi River in the northern part. On account of the resulting huge damages and suffering of the people, the river is named as the 'river of sorrow', like the yellow river of China.

B. Hydrological and Geomechanical Hazards

Bihar is a flood prone state. The river Kosi, with its numerous tributaries causes recurring floods especially in the monsoon season as a result of inundation and erosion. This recurring flood causes huge damages to the structures and loss to human lives. Therefore, the river is also called as 'The River of Sorrow'. During the last 150 years, it has been observed that the river has been migrated 110 Km westward. Due to this migration, siltation took place in an area of about 13,000 Km2 in India and 1000 Km2 in Nepal. In the upstream of Chhatri, a very steep gradient of 1V:5H were likely found to be refilled during dry seasons. Borehole data taken from the study area near Belka hill region with borehole sample 2650 mm indicated 900 mm medium sand layer, 125 mm coarse sand and boulders, 150 mm of medium sand and 1475 mm of gravels and boulders in sequence. It gives a clear indication that as the river enters plain terrain, the coarser materials accumulate first and then the smaller ones [7]. It was found that the average flood gradient of 8.73 x 10-4 downstream of the barrage constructed at 42 Km reach from Chhatri to Bhimnagar was gradually flattened to 0.61 x 10-4 at about 130 Km downstream. The average migration rate of the river observed is shown in Table 1 and Fig 2.

TABLE I. Average rate of migration of Kosi River

Year	Period of movement (years)	Approximate distance migrated (km)	Rate (km/year)	Total westward migration (km)
1736-1770	34	10.7803	0.3171	10.7803
1770-1823	53	9.3322	0.1761	20.1125
1823-1856	33	6.1142	0.1853	26.2267
1856-1883	27	12.872	0.4767	39.0987
1883-1907	24	18.5035	0.7710	57.6022
1907-1922	15	10.9412	0.7294	68.5434
1922-1933	11	28.962	2.6329	97.5054
1933-1950	17	17.699	1.0411	115.1744

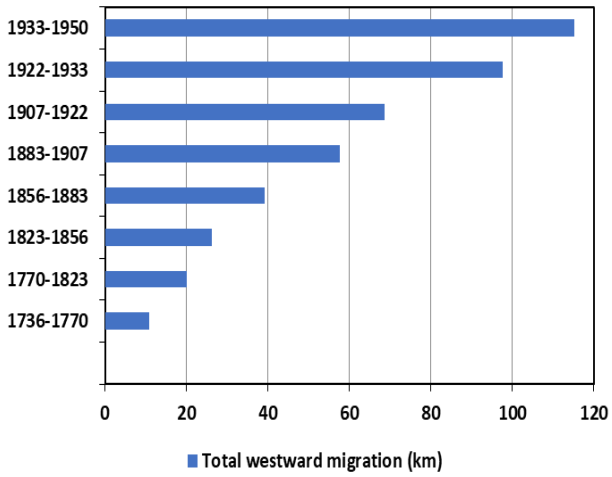

Fig 2. Year-wise westward migration

The existing transverse slope in the terrain of the study area might be the possible reason of the westward migration. Also, the direction of the open channel flow occurring at the right angles to the contour increased the tendency to scour and erosion, which in turn aided the expansion of the channel and river migration. Similar observations are also found in the case of erosion gullies, which also cross the contours at right angles [8]. Excessive sediment load (about 0.43 million ton/year/km2) during flood is another reason for river migration which may also attribute to large variation in stream variation, slope, and geological young rock formation [9].

C. *Remedial measures*

To overcome the geomechanical hazards, extensive construction of marginal embankments was taken up from the year 1955 onwards. On the eastern side of the river, an embankment of 101 Km was built downstream of Bhimnagar and 118 Km on the western side. The spacing between the eastern and the western embankments varied from 5 to 8 Km. Afflux bunds were constructed on both the sides of the barrage having 40 Km length on the east and 14 Km on the west [10]. Also, a sluice-type barrage of about 2 Km length and 54.25 meter width was constructed. It was provided with multiple gates and facilities for pedestrian and vehicular passage. As observed, a sluice-type barrage is an effective river training work [11]. Spurs were also provided on both the upstream and downstream of the barrage. This construction of embankment effectively reduced the flood occurrence as it shifted the main current from western bank to the eastern bank.

Before the construction of the barrage, up to a reach of 102 Km downstream of Chhatri, the river was found to be degrading followed by aggrading. After the construction of the barrage, up to a reach of 42 Km was found to be aggrading. From the barrage, up to 16 Km, the river was found degrading and further downstream up to 100 Km was found to be aggrading [12], as shown in Fig 3. The estimated annual sediment load of 95 Mm3 was reduced to about 15.6 Mm3. However, measurements after banking indicated an average deposit rate of 84 Mm3/year [13].

Other remedial measures were also undertaken and improvised. Study of the past river discharge and water level data were done to investigate the overbank spilling due to rise in the flood level. Study was also done to control the erosion of the riverbank to mitigate the risk involved. According to the National Commission of Agriculture (1976), the change in cropping pattern would reduce the damage from flooding. The population of the area were provided awareness about the limitations of flood protection and given proper guidance to be followed during emergency to protect their life. Also, adequate public services were provided to the people affected by flood and erosion by providing shelters and livelihoods.

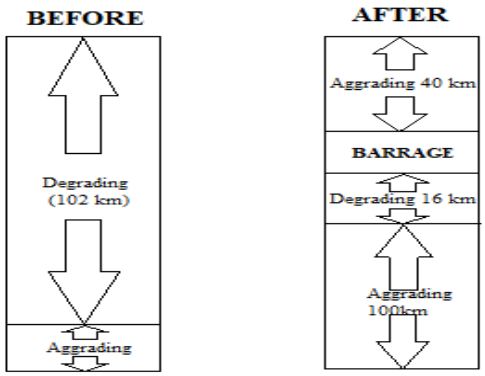

Fig 3. Sediment load comparison of river Kosi near Chatra

IV. Case Study: 2

A. *Dibrugarh Town*

Dibrugarh is a town in the state of Assam of Northeastern region of India. It is located near the basin of river Brahmaputra. The river Brahmaputra originates from the glaciers of Manasarover Lake, Kailash Ranges in Tibet. From its origin to the outfall in the Bay of Bengal, it stretches over a total length of 2,880 Km. The river enters India through the Yang-Yap pass in the state of Arunachal Pradesh. The river flows with the name Siang in Arunachal Pradesh and then enters Assam with other two tributaries namely Dibang and Lohit. From this confluence point, the river is called as Brahmaputra. The river passes through major cities and town like Dibrugarh, Jorhat, Tezpur, Guwahati, Dhubri, etc., and finally enters Bangladesh, covering a stretch of 720 Km of alluvial plains. While travelling through Bangladesh, it swings at nearly right angle towards south and merges with river Jamuna. The united river Jamuna (Ganga) and Padma (Brahmaputra) merges together to form river Meghna, which finally falls in the Bay of Bengal [14].

B. *Hydrological Hazards*

The total catchment area of Brahmaputra in India is approximately 240,000 Km2 with average monsoon discharge of about 40 x 103 m3/s. The river shifted its course over the period due to this high discharge and sediment load. The river, before reaching India follows a very steep gradient and drops to 4.8 Km in the stretch of 2000 Km. The average gradient of the river has been reduced from 2.4 x 10-3 in Arunachal Pradesh to 0.1 x 10-3 in the valleys of Assam.

This sudden change in the gradient leads the river to be braided [15].

Earlier Dibrugarh town was located on the bank of river Dibru. The river Brahmaputra and Dibru were few kilometers away from each other, but due to scouring of river Brahmaputra towards the southern bank, paved the way for river Dibru to merge with Brahmaputra. Dibrugarh, which is located on the bank of river Brahmaputra, is under highly erosion prone zone. The earthquake of 1930 in Assam is one of the main reasons for the creation of this erosion prone zone. It has caused several landslides especially on the southern bank of Dibrugarh town. At the same time, the flow of river was attacking the riverbank at 60˚, resulting in excessive erosion of the bank. The river migration rate was observed to be 1.32 km2/year. These hydro-geological hazards caused significant damage to the buildings, civil infrastructure, open lands and tea gardens of the Dibrugarh town [6, 14, 15].

C. Remedial Measures

The Government of Assam together with Government of India undertook several remedial measures to mitigate such hazards. In 1953, Government constructed a stone revetment of about 460 meters length on the worst affected bank of river Brahmaputra, which was washed away by the 1954 flood, due to high erosion. Therefore, the Government entrusted the Central Water Commission and the Central Water and Power Research Station to investigate and study the affected area and come up with a better proposed designs for protection work [16]. Thereafter in 1954, 5 stone spurs with slope 1V:1.4H to 1V:1.5H was constructed. The length of the 4 spurs were 61 meter each and one spur with 122 meter length. Timber pile spurs were also constructed normal to the bank. Initially each of the timber pile spur were 61m long, which was later shortened to 30m-45m, and six numbers of timber pile spur were added. Also, brush wood protections of the banks were provided between the spurs.

Few minor construction works were executed during the year 1955-1961. Additional stone spurs of 42.7 m length were constructed on the upstream of first stone spur and 610 m length on the downstream of the fifth stone spur for the purpose of flow diversion. To further protect the town from flooding, a 10 Km long earthen dyke was also constructed. Butt heads at pile spurs were provided along with additional double rows of T shaped piles. The protection works of 1963-1964 consisted of two phases. In the first phase, two semi-permeable spurs each 45.8 m long and 6 permeable spurs were constructed. Along with, additional revetments of length 55 m and 36.6 m were provided on the upstream and downstream respectively. After the first phase construction, heavy erosion took place. Therefore, in the second phase, additional 1 semi-permeable and 7 permeable timber spurs were constructed along with 1 subsidiary dyke on the downstream. The secondary work of 1965-1966 included few more impermeable spurs of 15 m length each. Boulder aprons were provided, and revetments were constructed between the spurs to strengthen the pile spurs.

The major protection works of 1967-79 consisted of five phases. The reason for this major protection work was the hydro-geological hazard of 1967-1969, where a vast area including Mathola tea garden was eroded by river Brahmaputra. The first phase was undertaken in 1970, where 3 timber spurs and 29 stone spurs were constructed at the critically affected riverbank. The second phase of 1973 included construction of three bank heads, under the recommendation of the Government, to control the erosion of the riverbank. The erosion continued, therefore in the third phase (1975), 8 permeable spurs with stone apron were constructed to strengthen the river bends. However, the flood of 1977 eroded about 300 m deep chunks of bed area resulting severe damage to this structure. As the post-flood protective measures, the fourth phase (1977-1978) was undertaken. Ten timber dampeners with boulder apron were constructed. These structures were also damaged in the next flood. After further Government recommendation, the fifth phase (1978-1979) was undertaken. A land spur was constructed having length of 299 m with 3.5 m apron width and 1.5 m apron thickness. It was also provided with crest level of 1.5 m above high flood level and side slope of 1 vertical to 5 horizontals. This land spur is still the key structure in guarding the river from erosion and flood control under the entire Dibrugarh Town Protection Work.

V. Critical Analysis

The geomechanical and hydro-geological hazards in the above two case studies have been observed to be varying though in both the cases river migration takes place accompanied with scouring and erosion. Therefore, the remedial measures undertaken were also different. In the case of Kosi River, the hydraulic structures constructed were firm and stable, whereas in case of the Dibrugarh town, the hydraulic structures were unstable. Hence, it is analyzed that the protection of river and flood control measures are necessarily site specific, and they vary from place to place.

VI. Conclusion

Geomechanical and hydro-geological hazards can lead to serious disaster if proper mitigation measures are not embraced. In the first case study, the alluvial river basin of Kosi River was observed to be migrating westward. The peak migration rate was found to be as high as 25,744 Km/year. The migration of river caused several recurring floods, which lead to scouring in the monsoon season and siltation during the dry season. The construction of the barrage across the river was found quite effective in controlling flood and erosion of riverbanks in the downstream. The annual sediment loss was also reduced after the construction of the barrage. Thus, construction of appropriate barrage helped in mitigating the risks of geomechanical and hydro-geological hazards in the Kosi River.

In the second case study, the geomechanical and hydro-geological hazards of the Brahmaputra River in the Dibrugarh town of Assam was considered. The frequent flood accompanied with erosion of the riverbed and riverbank was found to be the most concerned hazard. It also led to the migration of the river channel. The remedial measures undertaken included construction of spurs, dykes, head butts, boulder apron and Bankhead's. The hydraulic structures were found to be unstable due to rigorous flooding each year, until the construction of the land spur in1979. After 25 years of trial-and-error construction of hydraulic structures, land spur was found to be most effective, standing firm and stable.

From the above two case studies, it can be concluded that the hazards from the river hydraulics and the required river protection works are necessarily site specific. The scope for future study in the selected sites is wide open in the field of hydrology, geology, flood control measures, river training works, erosion and many more. The study would benefit immensely to both the researchers and practicing engineers.

ACKNOWLEDGMENT

The authors thankfully acknowledge research data collected from various departments of Government of India and Assam, for this study. Assistances were also received from late Prof. Bharat Singh, former Vice Chancellor, University of Roorkee, India.

REFERENCES

[1] Grant, G. E., O'Connor, J. E. and Wolman, M. G., A river runs through it: conceptual models in fluvial geomorphology, Treatise on Geomorphology, vol. 9, pp. 6-21, 2013.

[2] Julien, P. Y., River Mechanics, Cambridge University Press, 2nd Edition, 2018.

[3] Yang, C. T., On river meanders, Journal of Hydrology, vol.13, pp. 231-253, 1971.

[4] Herb Wiebe (2006). River Flooding and Erosion in Northeast India. Technical Report, Northwest Hydraulics Consultants, Alberta, Canada.

[5] Chakraborty, T., Kar, R., Ghosh, P., Basu, S., Kosi megafan: historical records, geomorphology and the recent avulsion of the Kosi River, Quaternary International, vol. 227, no. 2, pp. 143–160, 2010.

[6] Shrivastava, R.J. and Heinen, J.T., Migration and home gardens in the Brahmaputra valley, Assam, India". Journal of Ecological Anthropology, vol. 9, pp. 20–34, 2005.

[7] Chakraborty, T., Kar, R., Ghosh, P. and Basu, S., Kosi megafan: Historical records, geomorphology and the recent avulsion of the Kosi River, Quaternary International, vol. 227, no. 2, pp. 143-160.

[8] Armani, A., Principles of River Hydraulics, Springer link, 1999.

[9] Sinha, R., Gupta, A., Mishra, K., Tripathi, S., Nepal, S., Wahid, S. M. and Swarnkara, S., Basin-scale hydrology and sediment dynamics of the Kosi river in the Himalayan foreland, Journal of Hydrology, vol. 570, pp. 156-166.

[10] Devkota, L., Giri, S., Crosato, A. and Baral, B. R., Impact of the Koshi barrage and embankments on river morphology and dynamics, Proceedings, 7th International Conference on Water Resources and Renewable Energy Development in Asia, Danang, Vietnam, 2013.

[11] Basack, S., Goswami, G., Deka, P., Borah, P. P. and Mastorakis, N., Analysis and control of flow parameters through sluice gate in dam, International Journal of Mechanics, vol. 14, pp. 22-27, 2020, DOI: 10.46300/9104.2020.14.3

[12] Uttarakhand River Rejuvenation Committee, Action Plan for Rejuvenation of River Kosi, District. US Nagar, Uttarakhand, Priority IV, 2019.

[13] Gole, C.V. and Chitale, S.V., Inland delta building activity of Kosi river, Journal of the Hydraulics Division, Proceedings of the American Society of Civil Engineers, vol. 92, no. HY2, pp 111–126, 1966. https://doi.org/10.1061/JYCEAJ.0001406

[14] Gilfelloni, G. B., Sarma, J. N. and Gohain, K., Channel and bed morphology of a part of the Brahmaputra river in Assam, Journal of Geological Society of India, vol. 62, pp. 227-235, 2003.

[15] Roy, N. and Pandey, W. B., Socio-economic appraisal of flood hazard among the riparian communities: case study of Brahmaputra valley in Assam; India, Proceedings, 19th EGU General Assembly, Vienna, Austria, 2017, p.17653.

[16] Brahmaputra Board, Annual Report 2018-2019, Basistha, Guwahati, p. 148, 2019.

[17] Samantaray, S. and Sahoo, A., Estimation of flood frequency using statistical method: Mahanadi river basin, India, H2Open Journal, vol. 3, issue 1, pp. 189-207, 2020.

[18] K. G. Renard, G. R. Foster, D. K. Weesies, and D. C. Yoder, Predicting Soil Loss by Water: A Guide to Conservation Planning with the Revised Soil Loss Equation (RSULE), no. 2, U.S. Department of Agriculture, Washington DC, USA, 1997.

[19] Di, L., Zhou, J., Chen, L., Huang, K., Wang, Q. and Zha, G., Flood risk analysis based on a stochastic differential equation method, Journal of Flood Risk Management, vol. 12, Suppl. 1, pp. 1-10.

[20] Flood Management Organization, Handbook for Flood Protection, Anti Erosion & River Training Works, Central Water Commission, Government of India, 2012.

[21] Basack, S., Goswami, G. and Nimbalkar, S., Analytical and numerical solutions to selected research problems in geomechanics and geohydraulics, WSEAS Transactions on Applied and Theoretical Mechanics, vol. 16, pp. 222-231, 2021, http://dx.doi.org/10.37394/232011.2021.16.25

THE EFFECT OF COARSE AGGREGATE SIZES ON THEIR PHYSICAL PROPERTIES

LaldintluangaH
ORCID: 0000-0002-6180-9757
laldin99@gmail.com

Rebecca Ramhmachhuani
Department of Civil Engineering
Mizoram University
Aizawl, India

***Abstract*— Rock aggregates are the most fundamental material of highways, railroads, and other construction activities. Rocks from two different quarries were evaluated to determine the impact of aggregate size on the performance of materials. This study is to find out the effect of size on physical parameters of aggregate used in flexible and rigid pavement. In order to determine the effect of aggregate size on their physical properties, different sieve sizes were selected. The sizes are divided into four categories according to IS sieve standards: R1 (20 mm-16 mm), R2 (16 mm-12.5 mm), R3 (12.5 mm-10 mm), and R4 (10 mm-4.75 mm) for aggregate impact value, aggregate crushing value, water absorption, and specific gravity. It is observed that the larger size of aggregate has given better results in their physical parameters.**

Keywords*— *Particle size, materials strength, properties of rock, flexible pavement

I. INTRODUCTION

Aggregate on road construction was hugely important as it affects the overall performance based on the aggregate strength, durability, and resistance to sustained load after construction. The aggregate used in this study is river stones obtained from Niawhtlang and crushed aggregates (crushed stone) obtained from Hlimen quarry. Aggregate characteristics such as particle size, shape, and texture influence hot mix asphalt pavement performance and serviceability. Low resistance to deformation will ensue if the aggregate structure is weak, while too excellent stability in the aggregate structure may result in brittleness and low resistance to impact. In uniformly graded aggregates, particles are uniformly decreasing size, coarse to fine to dust. Such aggregate structures have a fairly uniform stress distribution. This type of grading is particularly important in utilising smooth, round aggregates such as alluvial sand and gravel. Careful grading control can yield high stability from aggregates possessing little strength [1].

The important fundamentals to consider in selecting aggregate size and gradation are that a large quantity of the maximum size aggregate within the size limits should be used for non-skid pavement. A uniformly graded aggregate is suggested for workability and freedom from segregation [2]. Permeability is a matter of pore size rather than void volume. Workability is most affected by the quantity and grading of coarse aggregate. Particle alignment tends to increase with the increasing size of aggregate particles [3]. As the nominal maximum size of the aggregate is increased, the amount of water needed for the same workability is reduced. Therefore, strength is greater at the same cementitious material content because the w/c is lower. But in the high-strength range, over 40 MPa, higher compressive strengths are usually obtained at a given w/c with a smaller nominal maximum-size aggregate. Similarly, higher flexural strength is obtained at a given w/cm with a smaller nominal maximum size aggregate [4]. Aggregates with good physical and mechanical properties can substantially improve the engineering properties of asphalt mixtures [5,6]. High density and good crush resistance can prevent aggregates from breaking under repeated vehicle loads and improve the fatigue resistance of asphalt pavements [7, 8, 9]. Aggregates with low water absorption can improve the low-temperature performance of mixtures [10, 11,12].

II. OBJECTIVES AND SCOPES

In this study, the effect of aggregate size on rock's physical properties is examined, along with the possibility of using a larger stone in flexible pavements. Mizoram terrain is, according to the Geological Survey of India, an immature topography, and the physiographic expression consists of several almost north–south longitudinal valleys containing series of small and flat hummocks, mostly anticlinal, parallel to sub-parallel hill ranges and narrow adjoining synclinal valleys with series of topographic highs. The general geology of western Mizoram consists of repetitive

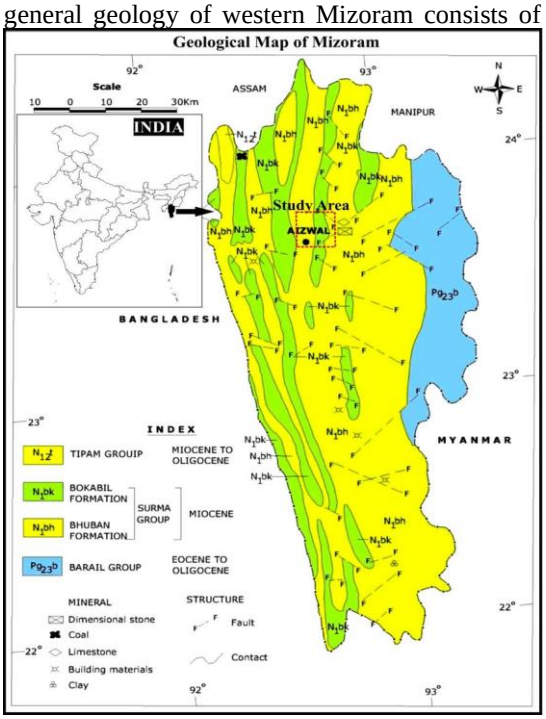

Figure 1. Geological Map of Mizoram

succession of Neogene sedimentary rocks of the Surma Group and Tipam Formation such as sandstone, siltstone, mudstone and rare pockets of shell limestone. The eastern

part is the Barail Group [13]. As stipulated by IRC 37-2018 and MORT&H, the performance of rock size gradation used in the construction of flexible pavements is not satisfactory in terms of durability, mainly when applied to sedimentary rock that has a high absorption value. In Mizoram, most rocks cannot withstand repeated wheel loads in the presence of moisture during the long monsoon rainy season. Hydro-geological factors have also contributed to the longevity of the asphalt pavement. As a result of this study, there will be scope for using the coarse aggregate of larger size, especially on the friable and quickly disintegrated rock under weathering action. In relation to the same volume of rock, larger aggregate has better load resistance and lower water absorption.

III. MATERIALS AND METHODOLOGY

A. Material

Coarse aggregate is used for base and sub-base courses for flexible and rigid pavements. The aggregates which pass through 75 mm IS sieve and retained on 4.75 mm IS sieve is known as coarse aggregates. Aggregates influence to a great extent the load transfer capability of pavements. They are tested for strength, toughness, hardness, and water absorption. The aggregate size includes maximum size, size range, and gradation. Materials selections for the study are from two different quarries.

B. Methods

Two different coarse aggregates were selected and divided into four ranges of sizes. Each range of coarse aggregate were tested using physical and mechanical properties tests such as aggregate impact value, aggregate crushing value, water absorption and specific gravity test. The gradation ranges from A to G is adopted for classification of aggregate size in the Abrasion test. To determine the physical properties of rock, tests are performed to determine the performance of coarse aggregate in constructing flexible pavement under various loads, including impact, abrasion, and water absorption. The aggregate (rock) sizes are divided into the normally adopted size of four ranges of aggregate size as per IS sieve standards: R1 (20 mm-16 mm), R2 (16 mm-12.5 mm), R3 (12.5 mm-10 mm), and R4 (10 mm-4.75 mm) for aggregate impact value, aggregate crushing value, water absorption, and specific gravity. The size-dependent performance of rock with regard to physical properties is the main focus of the study.

IV. RESULTS AND DISCUSSIONS

Rock types within Mizoram area are mostly consist of sedimentary rocks. The two quarries are selected for these studies are from Hlimen and Niawhtlang quarry rock.

A. Effect of Aggregate Size in Aggregate Impact Value (AIV)

AIV is the test that measures toughness. As shown in Figures 2 and 3, larger sizes of aggregates have given better impact values. It means that a larger size of aggregate has a higher resistance to withstand more impact load compared to a smaller size of aggregate.

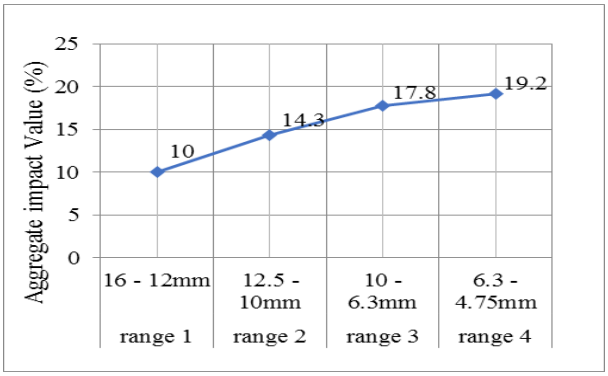

Fig.2:Aggregate Impact Value (Niawhtlang Quarry) with different size of rock

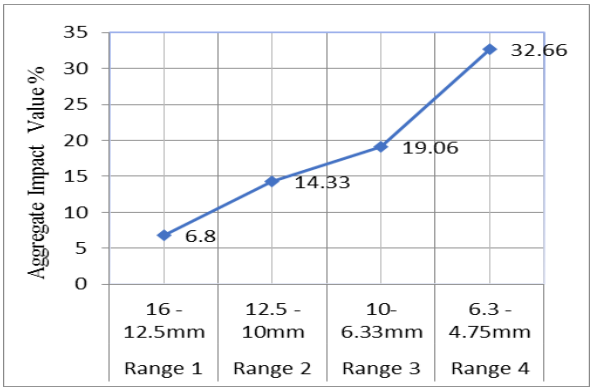

Fig.3: Aggregate Impact Value (Hlimen Quarry) with different size of rock

B. Effect of Aggregate Size in Water Absorption Value:

Water absorption values (WAV) measures the ratio between dry weight aggregate and saturated surface dry weight of aggregate to dry weight of aggregate. Larger sizes of aggregates have given lower absorption values compared to smaller sizes as shown in Figures 4 and 5. This may be due to the depth of water penetration remaining the same regardless of the size at a specific period of time. The quantity of water absorbed by large or smaller a size of aggregates remains the same.

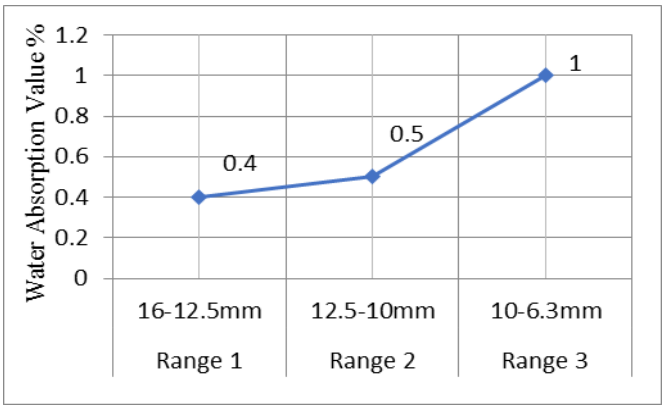

Figure.4 Water Absorption Value (Niawhtlang quarry) with different size of rock

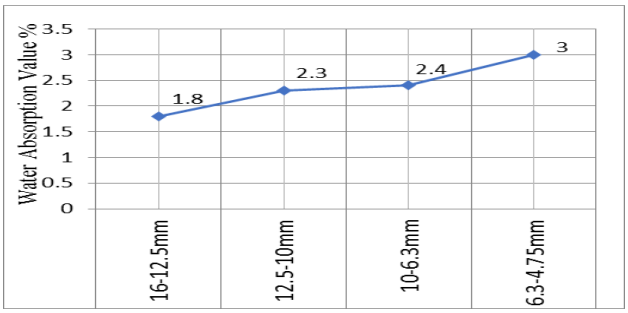

Figure.5 Water Absorption Value (Hlimen quarry) with different size of rock

C. Effect of Aggregate Size on Specific Gravity Test:

The specific gravity of rock measures the density of rock with respect to the density of the equal volume of water. The specific gravity values with respect to a particle size of aggregate do not change much as shown in Table.1. The size of the aggregate does not affect much as the density of aggregate remains the same for a particular rock.

TABLE .1 SPECIFIC GRAVITY VALUES FOR DIFFERENT SIZE OF AGGREGATE

Niawhtlang quarry rock		**Specific gravity value**
Sieve size	12.5-10mm	2.5
	16- 12.5mm	2.51
Hlimen quarry rock		**Specific gravity value**
Sieve size	16-12.5mm	2.5
	12.5-10mm	2.52
	10-6.3mm	2.54
	6.3-4.75mm	2.6

D. Effect of Aggregate Size on Los Angeles Abrasion Value (LAAV)

The percentage wear of the sample aggregates due to rubbing with steel balls and the falling impact of balls are determined as a percentage in the observation value. LAAV test involves two kinds of action i.e impact (pounding force) and abrasion (frictional force). In flexible pavement, these two action forces reflect the actual conditions of the site. It has been observed that gradations with a higher sieve size (coarser aggregates) have a lower level of abrasion, as shown in figure 6. The time required to wear away a larger size of the rock is more compared to the time required to disintegrate the smaller size of aggregate. LAAV test involves the combination of different gradation sizes of aggregate as shown in table 2. At a larger particle size, the desired value of abrasion is obtained, and the desired result is found in ascending order by aggregate size, i.e. D<C<B<A<G<F<E, grade E has the largest aggregate size, while grade D is the smallest. As the particle size increases, the abrasion value decreases. Los Angeles abrasion test has different gradation which is adopted to conduct the study. The Abrasion Value test was not performed on Niawhtlang quarry rock.

TABLE.2 GRADATION OF AGGREGATES FOR LAAV

Sieve Size		**Weight in gm of test sample for grade**						
Passing (mm)	**Retained (mm)**	**A**	**B**	**C**	**D**	**E**	**F**	**G**
80	63					2500		
63	50					2500		
50	40					5000	5000	
40	25	1250					5000	5000
25	20	1250						5000
20	12.5	1250	2500					
12.5	10	1250	2500					
10	6.3			2500				
6.3	4.75			2500				
4.75	2.36				5000			

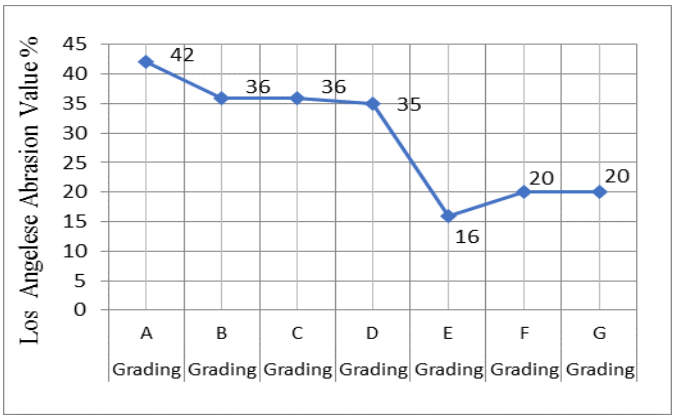

Figure.6 LAAV (Hlimen quarry) with different gradation of rock

E. Effect of Aggregate Size on Aggregate Crushing Value

Aggregate Crushing Value is used to measure the crushing strength of aggregate. As the size of aggregate gets larger, the crushing value decreases. The larger size has the ability to resist more loads (traffic load) due to individual thickness of aggregate that imparts more strength as shown in figure:7. Hlimen quarry rock sample is used here to fine the effect of particle size on crushing value.

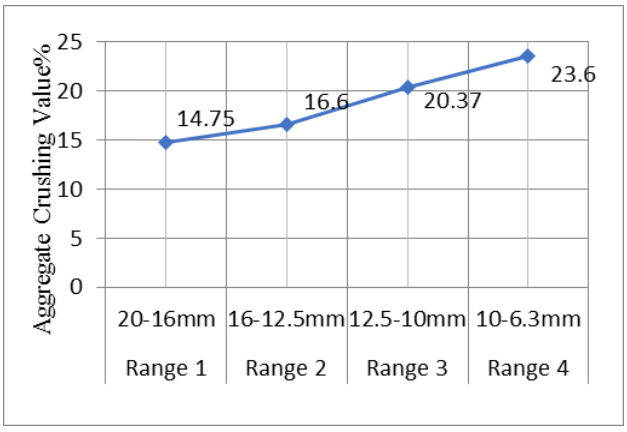

Figure.7: Aggregate Crushing Value with different size of Hlimen rock

V. Conclusion

The size of the aggregate plays a significant role in its permeability and strength. In high moisture content in the pavement structure, weak aggregate cannot withstand repeated traffic loads. This study will pave the way for introducing a larger size aggregate or boulder in the base layer of the pavement to counter the problem of early disintegration of rock in the presence of moisture under load. In areas where the rainfall intensity exceeds 2m/year with a high water absorption value of the rock, it is required to have good subsurface drainage and high loading capacity. Based on the resilient data obtained from the investigation, the following conclusions can be drawn:

The nature of the rocks, being sedimentary and having high water absorption of Hlimen rock, has shown a lower value of physical properties of rock under the application of load compared to Niawhtlang rock. The larger size of aggregate has been found to have higher toughness (impact), strength (crushing) and abrasion resistance than the smaller size of aggregate. Larger sizes of aggregates have given lower absorption values as the depth of water penetration remained the same regardless of the size and weight of aggregate.

References

[1] J. R Benson,"The Grading of Aggregates for Bituminous Construction". ASTM Symposium on Mineral Aggregates, 1948, pp. 117-133.

[2] N. W. McLeod, "Review of Design of Subgrades and of Base Courses and Selectionof Aggregates". Proc. Nat. Bituminous Conf., 1937, pp. 75-80.

[3] T. E Stanton Jr, F. N Hveem,"Role of the Laboratory in Preliminary Investigation and Control of Materials for Low Cost Bituminous Pavements". HRB Proc., Vol. 14, Part II, 1935, pp. 14-54.

[4] S.O Beam, Ajamu, J.A. Ige ,"Effect of Coarse Aggregate Size on the Compressive Strength and the Flexural Strength of Concrete". Ajamu Int. Journal of Engineering Research and Applications ISSN: 2248-9622, Vol. 5, Issue 1(Part 4), January 2015, pp.67-75.

[5] Liu, Y. J., and M. Tia. 2012. "Creep property of concretes with different types of coarse aggregates." Appl. Mech. Mater. 174: 308–313.

[6] Walubita, L. F., and A. E. Martin. 2010. "Characterizing the relaxation modulus properties of HMA mixes based on the uniaxial strain-controlled testing." Road Mater. Pavement Des. 11 (3): 529–557.

[7] Cai, X., K. H. Wu, W. K. Huang, and C. Wan. 2018. "Study on the correlation between aggregate skeleton characteristics and rutting performance of asphalt mixture." Constr. Build. Mater.179 (Aug): 294–301.

[8] Xu, M., Z. C. Li, and J. Chen. 2014. "The effect of aggregate property on shear performance of asphalt mixture." [In Chinese.]J. ShandongJiaotong Univ. 22 (3): 62–65.

[9] Haddock, J. E., and B. D. Prowell. 2001. Determination of aggregate specific gravity and its effect on HMA mixture performance. STP 1412.West Conshohocken, PA: ASTM.

[10] Faheem, A. F., H. Wen, L. Stephenson, and H. Bahia. 2008. "Effect of mineral filler on damage resistance characteristics of asphalt binders (with discussion)." J. Assoc. Asphalt Paving Technol. 77: 885.

[11] Gong, X., P. Romero, and Z. Dong. 2017. "Investigation on the low temperature property of asphalt fine aggregate matrix and asphalt mixture including the environmental factors." Constr. Build. Mater.156 (Dec): 56–62.

[12] Airey, G. D., A. C. Collop, S. E. Zoorob, and R. C. Elliott. 2008. "The influence of aggregate, filler and bitumen on asphalt mixture moisture damage." Constr. Build. Mater.22 (9): 2015–2024.

[13] Geology and mineral resources of Manipur, Mizoram, Nagaland and Tripura (Report). Miscellaneous publication No. 30 Part IV. Vol. 1 (Part-2). Geological Survey of India, Government of India. 2011.

Analysis of High Impedance Fault in IEEE 9 bus system by Signal Processing Tools using MATLAB/Simulink Model

Sudipta Das
Student, Dept. of Electrical Engineering,
Narula Institute of Technology,
Agarpara,WB
Kolkata, India
sudipta19x@gmail.com

Pratyusha Biswas Deb
Assistance Professor, Dept. of Electrical Engineering
Narula Institute of Technology,
Agarpara,WB
Kolkata, India
pratyushabiswas85@gmail.com

***Abstract*— In this paper, a signal processing technique is used for detecting HIF with saving the time with correct value. High Impedance Faults (HIFs) is a common disturbance problem in the power transmission and distribution line today. HIF cannot be detected specifically by the electrical protection systems due to its low faults current and due to its high impedance nature. HIFs are not identified by protection system easily as this type of fault has currents with values close to those in the steady-state condition in transmission and distribution system. Asymmetry, nonlinearity, and randomness in nature are also additional features of HIFs, due to the presence of electrical arcs in HIF. Fire hazards and electrical shocks are the main concern regarding HIFs. Also, today harmonic rich content of distribution grids plays a significant role in increasing confusion for protection devices. Therefore, the improvement of effective fault identification techniques, substantially for HIFs is very essential which will help to neat and clean transmission and distribution operation of electrical power. So, our paper aims to propose a methodology capable of identifying HIFs. We use Fourier Transform (FT) method. It is one of the mathematical techniques use in power system fault analysis. It is employed in this work as a fundamental mathematical derivation to obtain its discrete and fast equivalent algorithm that are used in this research. The HIF current has low and high-frequency components in its spectrum, which can be extracted from the signals using frequency domain techniques, as the FT. Therefore, the application of FT with a Fast Fourier Transform (FFT) algorithms usually used in digital relay protection algorithms, as they present a fast response. Also, these transforms can be combined with machine learning techniques for a developed system. So, FFT is an important and best technique for HIF detection. So, to maintain the safe and stable operation of power grid and power system measuring units (PMU), high-precision harmonic component detection is very necessary. Fast Fourier Transform (FFT) is the most commonly used method for harmonic analysis and HIF detection. Furthermore, when we apply this FFT technique then it gives the correct result for pre-fault and at fault condition with saving the time.**

Keywords— High Impedance Fault - HIF, Fourier Transform - FT, Fast Fourier Analysis -FFT, Power System Measuring Units - PMU, MATLAB/Simulink

I. INTRODUCTION

A 3-phase AC power system operating under normal condition has a standard magnitude of both current and voltage which is equally distributed across each phase. But when a fault occurs on the system, then fault cause heavy current called short circuit current to flow in system, unbalanced voltage and reduce the effective impedance of the system which may destroy or damage the protective equipment connected in the system. The High Impedance Fault (HIF) current random behavior and its low magnitude cause difficulties for a reliable detection by traditional protection methods. Therefore, the hazards for grid devices, people's safety, associated with HIFs, motivate a better, suitable detection techniques. Short-circuit currents are harmful for two reasons-the first is that even a short-time flow of heavy current will overheat the equipment, the second is that the flow of short-circuit currents through the current carrying parts produces forces of electrodynamic interaction which may destroy or damage the equipment. This is why all the elements of any electrical installation are designed and selected for a thermal and a dynamic stability sufficient to withstand the largest possible flow of short circuit current that may occur in the given installation.

The severest conditions in service are those of the switching devices during a short circuit. These devices are circuit breakers and the fuses, whose function is to interrupt the fault current within a short period or time (0.05 -0.3 second) and thereby switch out the faulty section. Due to harmonics power system equipment like relay, circuit breaker and others are working with malfunction so, they don't work properly so fault current detection and over voltage detection are get failed and a fault occurs in the total system. So, short circuit current analysis and harmonics analysis with quick function is most important task for the protection function. If the fault current analysis is done quick then protective equipment can do their operation within the time.

Therefore, HIF occurrence is a major challenge for distribution networks. Also, the electric arc leads to distinctive features on the fault current waveform as well as a peculiar frequency spectrum. Consequently, several types of research stimulate the use of harmonic content to detect HIF faults. Thus, this paper presents a study of a variant of the FT, called Fast Fourier Transform (FFT)."

In this paper, Short circuit current analysis and harmonics analysis is done with the Fast Fourier transform (FFT). So, the fault current FFT analysis is done for protection operation of total electrical system within the time for completing the fault clearing operation within the 'critical fault clearing time' to maintain the steady state stability

II. SYSTEM MODELLING

This section presents the methodology proposed in this paper concerning implementing an electrical system, the HIFs, and other events related to electrical transmission and distribution systems, which are required to prove the method's

robustness. Therefore, the simulations were carried out according to the following subsections.

A. *HIF*

High Impedance Faults (HIFs) on distribution feeders are defined as abnormal electrical conditions that cannot be detected and cleared by conventional protection schemes, due to their low fault current. Faults resulting from neighbouring objects making prolonged contact with the energised line can endanger human life, potentially causing severe electrical burns, electrocution or fires. Additionally, the arcing associated with HIF may also lead to serious damage to the power system. HIF occur when the energized overhead distribution feeder conductors have undesired physical contact with a quasi-insulating object nearby, such as asphalt road, gravel or tree limbs. The current from this type of fault may be not large enough to be detected by conventional protection devices. Therefore, the downed energised conductor may become a potential hazard to public safety. Furthermore, arcing is often associated with these faults.

HIF typically caused by: broken conductor in touch with ground and other surfaces but still connected to source, Intermitted contact with tree limbs or other objects, contaminated or falling equipment etc.

B. *Test System*

All developed and developing countries depend upon electrical energy for industrial, commercial, agricultural, domestic and social purposes. Therefore, the basic infrastructure, that is, generating stations and transmission and distribution lines have become a crucial part of modern socio-industrial landscape. So, we choose IEEE-9 BUS System for standard calculation and simulation here. where 3 generators are connected with 3 Transformer, then power is transmitted over transmission line and it distributed in 3 load buses and 1 bus specified as swing bus. It is a specially designed grid system which has 9 buses arranged in a specific pattern in accordance to IEEE norms. Simulation will be applied on this test system.

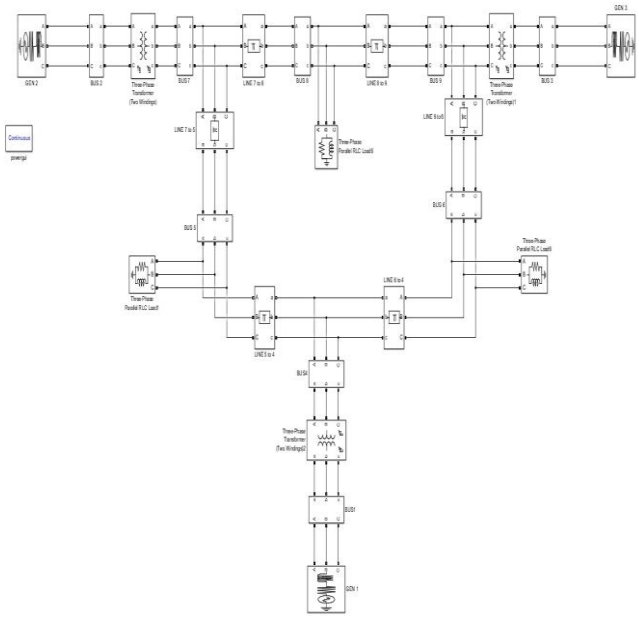

Fig 1: IEEE 9-Bus standard system

C. *Simulation Software*

MATLAB is a programming and numeric computing platform software used to analyze data, develop algorithms, and create models and design systems and simulation.

In this paper, we use MATLAB 2014a software for create the total 9-Bus system Simulink model and total experiments has done.

III. PROPOSED METHODOLOGY

The proposed HIF detection method in this study aims to identify HIF by monitoring the phase current, using only the substation as an observable point. By the analysis of the phase current spectrograms and the state of the art.

In the case of HIF detection, the signal processing technique is popular and this give most correct result.

A. *Fourier Transform*

Frequency domain techniques can be used for obtaining the signals harmonic content. Since the FT can extract information about the magnitudes of the various signal frequencies and because it is widely used in the protection systems of Electric Power Systems (EPS), it is used in the methodology proposed by this work.

For defining the Fourier transform of an integrable function

$$\hat{f}(\xi) = \int_{-\infty}^{\infty} f(x)\, e^{-2\pi i x \xi}\, dx, \quad \forall\, \xi \in \mathbb{R}. \tag{1}$$

The Fourier transform is denoted here by adding a circumflex to the symbol of the function. When the independent variable x represents time, the transform variable ξ represents the frequency.

Under suitable conditions f is determined by $\hat{f}$ via the inverse transform:

$$f(x) = \int_{-\infty}^{\infty} \hat{f}(\xi)\, e^{2\pi i x \xi}\, d\xi, \quad \forall\, x \in \mathbb{R}. \tag{2}$$

That is known as the Fourier inversion theorem.

In order to observe certain signal frequencies, the size, and consequently the number of samples in each window, can be changed, thus modifying the frequency resolution Δf of the signal with a sampling frequency fs and N is number of samples.

$$\Delta f = \frac{fs}{N} \tag{3}$$

Inter-harmonics are commonly found in HIF current waveforms, because they are associated with the random length variation of the electric arc during fault situations. In this condition, the larger the amplitude of the variation, the larger the number of inter-harmonic frequencies.

There are some processes of FT:

Continuous Fourier Transform (CFT), Discrete Fourier transform (DFT), Discrete Time Fourier Transform (DTFT), Fast Fourier transforms (FFT), Short Time Fourier transform (STFT).

B. *Discrete Fourier Transform*

In mathematics, the discrete Fourier transform (DFT) converts a finite sequence of equally-spaced samples of a function into a same-length sequence of equally-spaced samples of the discrete-time Fourier transform (DTFT), which is a complex-valued function of frequency. The interval at which the DTFT is sampled is the reciprocal of the duration of the input sequence. An inverse DFT is a Fourier series, using the DTFT samples as coefficients of complex sinusoids at the corresponding DTFT frequencies.

The discrete Fourier transform transforms a sequence of *N* complex numbers

$$\{\mathbf{x_n}\} := x_0, x_1, \ldots, x_{N-1} \quad (4)$$

into another sequence of complex numbers, $\{\mathbf{X_k}\} := X_0, X_1, \ldots, X_{N-1},$ which is defined by

$$X_k = \sum_{n=0}^{N-1} x_n \cdot e^{-\frac{i2\pi}{N} kn} = \sum_{n=0}^{N-1} x_n \cdot \left[\cos\left(\frac{2\pi}{N} kn\right) - i \cdot \sin\left(\frac{2\pi}{N} kn\right)\right], \quad (4)$$

where the last expression follows from the first one by Euler's formula. The transform is sometimes denoted by the symbol *F*, as in $\mathcal{F}(\mathbf{x})$ or $\mathbf{X} = \mathcal{F}\{\mathbf{x}\}$ or $\mathcal{F}\mathbf{x}$.

The discrete Fourier transform is an invertible

The inverse transform is given by:

$$x_n = \frac{1}{N} \sum_{k=0}^{N-1} X_k \cdot e^{i \frac{2\pi}{N} kn} \quad . \quad (5)$$

The DFT has seen wide usage across a large number of fields. All applications of the DFT depend crucially on the availability of a fast algorithm to compute discrete Fourier transforms and their inverses, a fast Fourier transform (FFT).

C. *Fast Fourier Transform*

A fast Fourier transform (FFT) is an algorithm that computes the discrete Fourier transform (DFT) of a sequence, or its inverse (IDFT). Fourier analysis converts a signal from its original domain (often time or space) to a representation in the frequency domain and vice versa. The DFT is obtained by decomposing a sequence of values into components of different frequencies. An FFT rapidly computes such transformations by factorizing the DFT matrix into a product of sparse (mostly zero) factors. As a result, it manages to reduce the complexity of computing the DFT from $O(N^2)$, which arises if one simply applies the definition of DFT, to $O(N\log N)$, where N is the data size and N=2 here. The difference in speed can be enormous, especially for long data sets where N may be in the thousands or millions. In the presence of round-off error, many FFT algorithms are much more accurate than evaluating the DFT definition directly or indirectly. Because $\lim_{N\to\infty} \frac{\log_2 N}{N} = 0$ it is a typical fast algorithm. Fast algorithms of this type of recursive halving are very typical in scientific computing. So, FFT is faster than DFT.

Applying DFT using a FFT algorithm reduces the time complexity required in practical applications. Thus, this work uses the FFT calculation in specific signal windows, making it possible to obtain values in the magnitude of all frequencies during the entire fault time. Therefore, the way the FFT is calculated for a discrete signal.

IV. SOLUTION METHOD

Total work is done with the following stage by stage:

- First, IEEE 9-BUS standard system is created with MATLAB Simulink model with standard value and run it in steady state performance using MATLAB 2014a software.
- Stage 2, In the system HIF is created at some location and done the simulation.
- Stage 3, after simulation we collected all date of faults.
- Stage 4, at last with creating the faults the FFT analysis is applied and all data are collected.

V. RESULT AND SOLUTION

Transmission line protection is an important issue in power system because 85-87% of power system faults are occurring in transmission line. This dissertation work gives technique to classify the different faults on transmission line for quick and reliable operation of protection schemes.

Transmission line faults are of mainly five types: L-G, L-L, L-L-G, L-L-L and L-L-L-G. But the effect of L-L-L and L-L-L-G faults is same. So, here we are considering only L-L-L fault. In all four different faults are classified after faulty condition is detected in the system..order to detect the existence of HIFs, we propose to use FFT. The traditional approach uses FFT to detect HIF current of the event in a large size frame. By doing this, one could miss the existence of the HIF in the transient state where the duration of occurrence is very short.

All the fault cases are discussed in the results initially all the types of faults are made near bus 2 and bus 7. The cases of faults made at a distance of 25km is considered for the result analysis. Here , take the values andd graphs of FFT for every type of HIF. By the result, It is observed that the how faults are detected very quickly with applying the FFT signal processing technique .

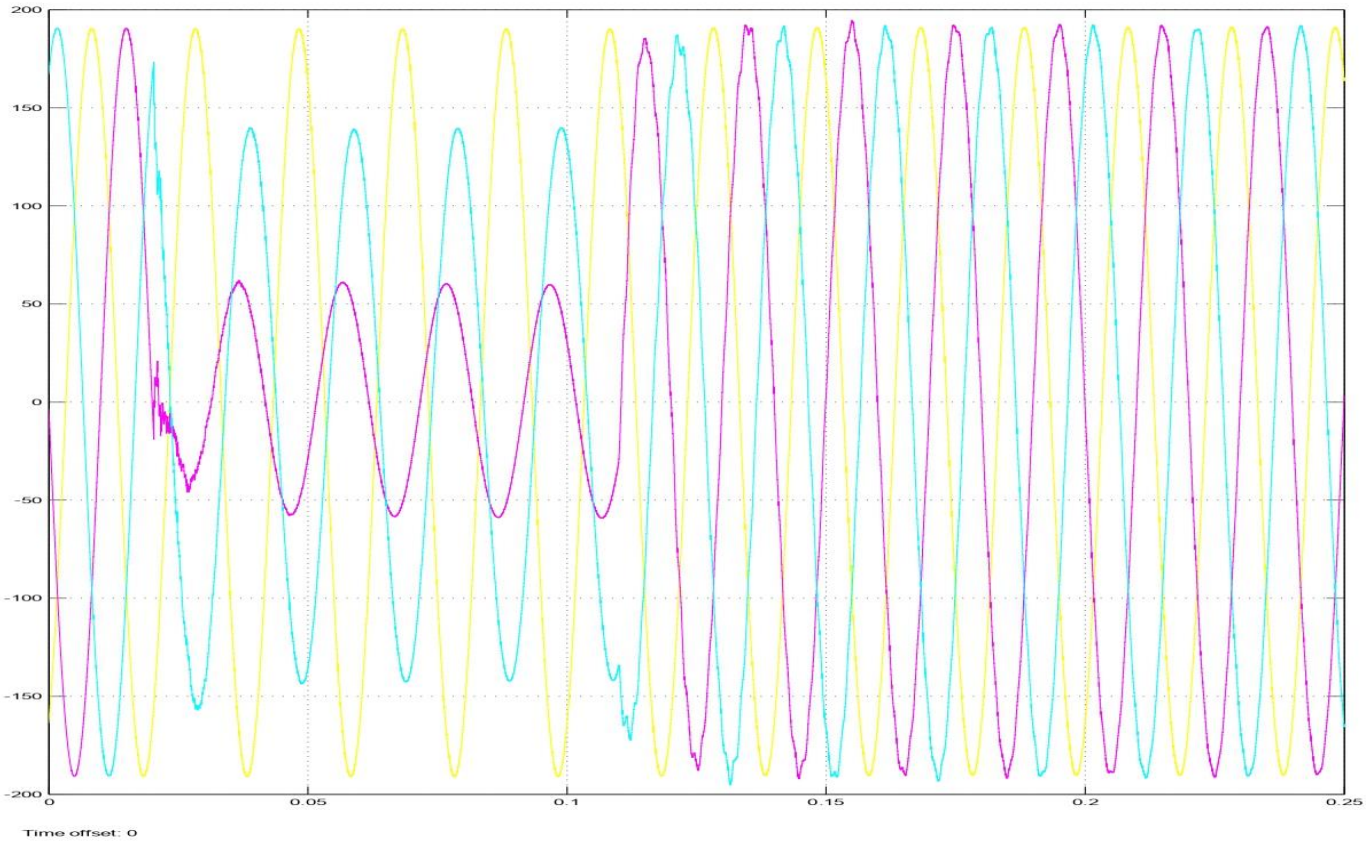

Fig 2: Fault current of 3 phase for line-to-line fault

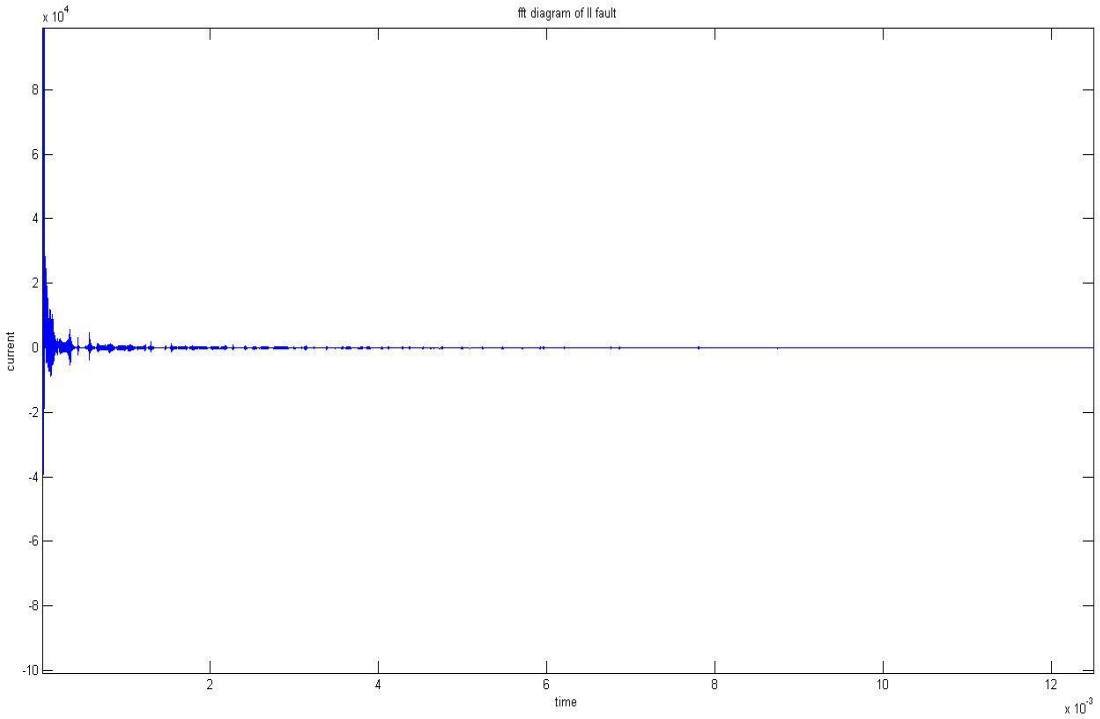

Fig 3: Line to line fault current FFT analysis

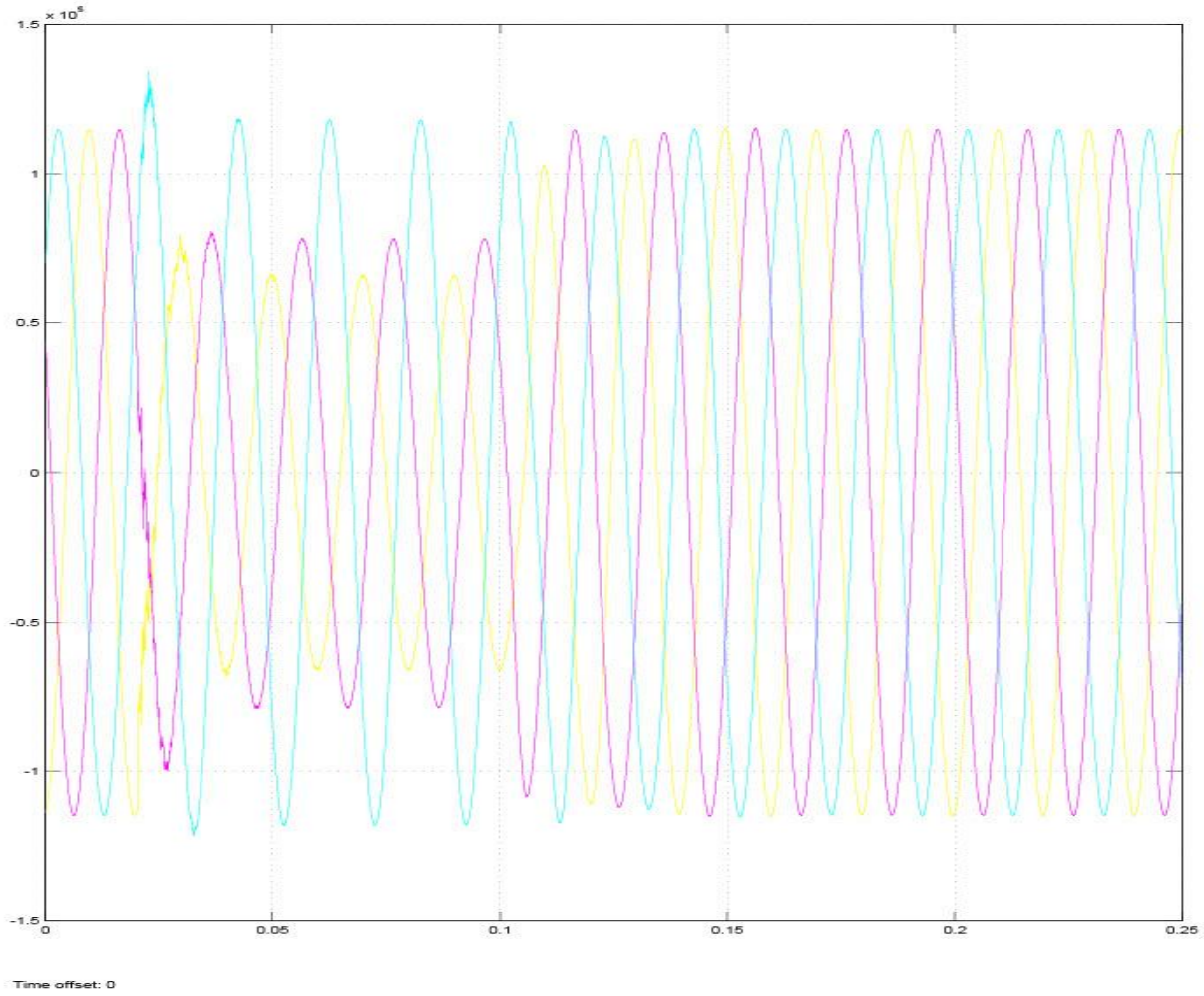

Fig 4: Fault current of 3 phase for line to line to ground fault

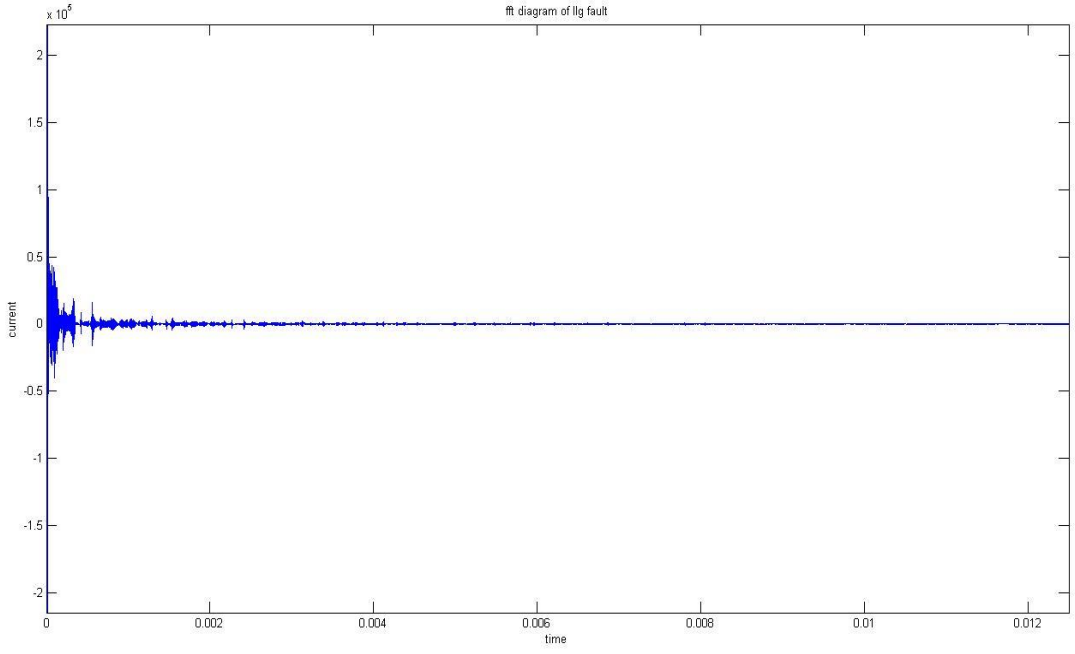

Fig 5: Line to line to ground fault current FFT analysis

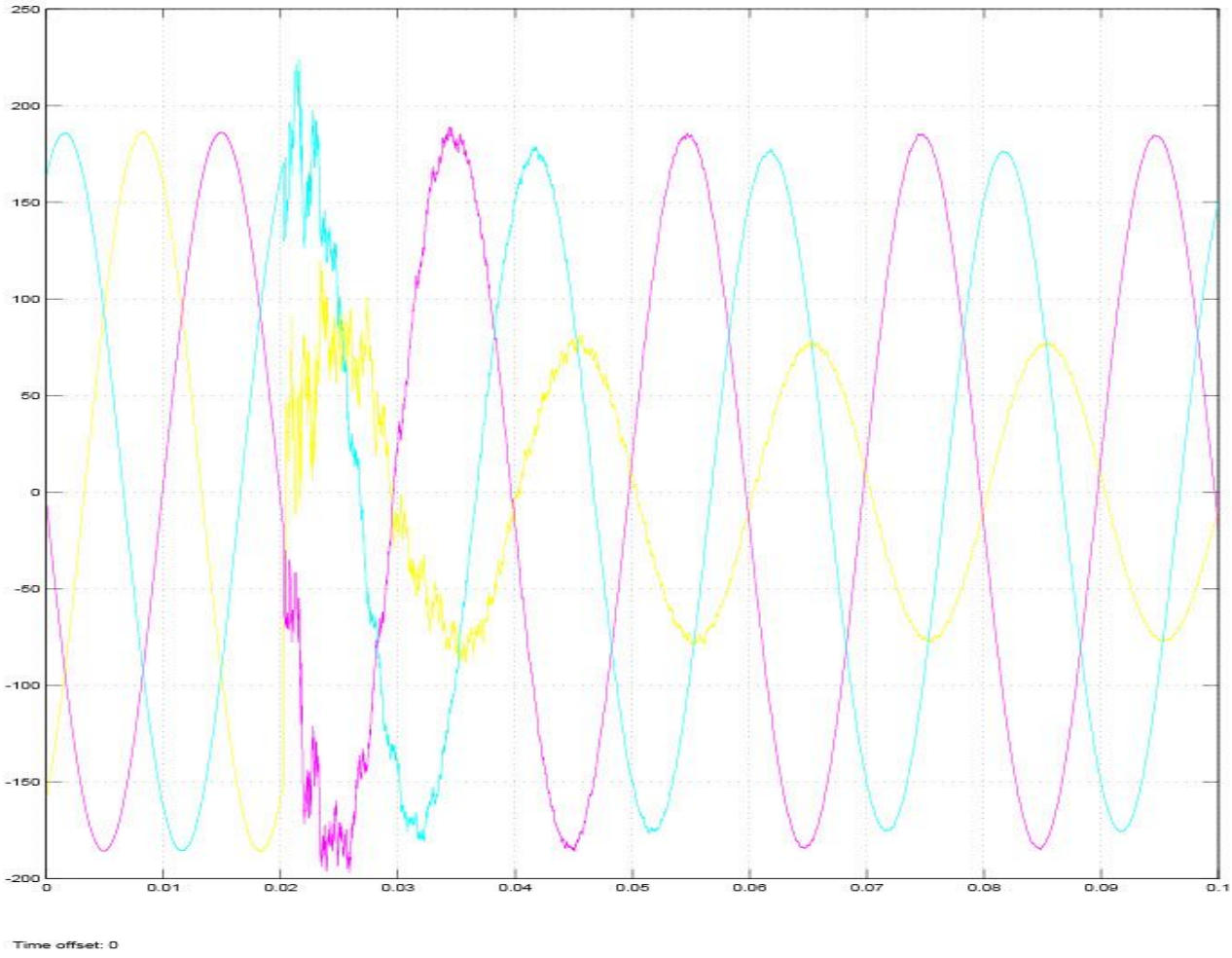

Fig 6: Fault current of 3 phase for line to ground fault

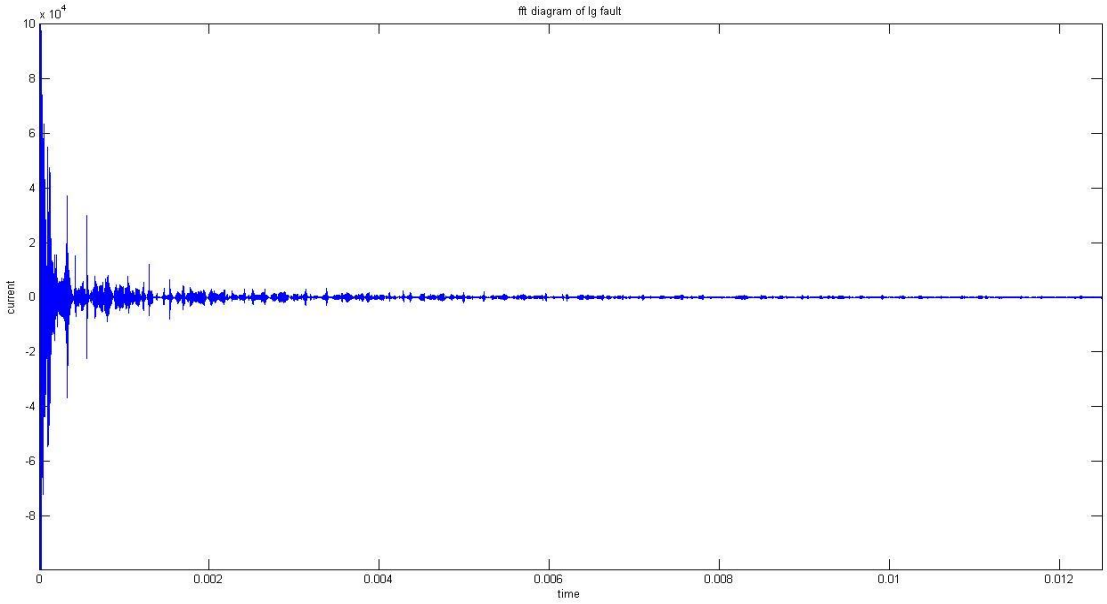

Fig 7: Line to ground fault current FFT analysis

It is observed that during the HIF, the value of current decrease from the nominal value, as shown in the diagram. When the Fault is removed, the system attends its normal value. Whereas the for the voltages, at the time of occurrence of the fault, there is large surges at that instant while the nature of the waveform is retained.

It is showed that if a HIF fault is happened then normal fault graph value is how much lower and fault detection time is delayed. But when FFT is applied then it is showed that how the time is saved and voltage and current magnitude is increased for detect the fault.

If a HIF detection method has only one sensor at the substation, it would be necessary to use the low-frequency content, which can be done either by harmonics or inter-harmonics. On the other hand, if the sensor is nearby the HIF location, it would be possible to use the current higher frequencies energy amplitude and variation for HIF detection.

VI. CONCLUSION

The behaviour of HIF faults is quite diverse, and there is general agreement that no single technique is capable of securely identifying all HIF fault scenarios. However, a large percentage of HIF faults can be detected; utilities which presently do not employ any form of HIF detection will significantly benefit from rolling out available technologies. Furthermore, the main advantages of this proposition are its high rates of identification, when inserting the HIF in buses far from the measurement spot, the wide range of non-HIF events that were tested to confirm the method selectivity, as well as its simplicity. For future studies, the method can be applied in other test systems with topology variations.

As it can be seen, no report of false detection has been witnessed during the abovementioned cases. The low current in three-phase and single-phase conditions has also no influence on the proposed method accuracy. It should Low currents have shown to reduce the distinct difference among the second and third order harmonic, since magnitude of current will not vary significantly before and considered and no misbehaviours in HIF detection were found. However, by implementing the sum of even harmonics, this problem has been averted.

Finally, based on the result of the simulation, the HIF is detected with high accuracy the saving the time by using FFT.

In future, the protection system provided for the system should have fast response. According to this analysis, fast fault clearing and load shedding methodologies can be adopted for system stability and for detection of fault location.

For future studies, the method can be applied in other test systems with topology variations like intelligence Artificial Neural Network (ANN).

REFERENCES

[1]. “Analysis of High Impedance Faults Current Using Fourier, Wavelet and Stockwell Transforms” Gabriela N. Lopes, Universidade de São Paulo, Luiz H. P. C. Trondoli, José Carlos M. Vieira; 2021-02-14.

[2] Jonas Villela de Souza, Gabriela Nunes Lopes, José Carlos Melo Vieira and Eduardo N. Asada “High Impedance Fault Detection in Distribution Systems: An Approach Based on Fourier Transform and Artificial Neural Networks” 5thWorkshop on Communication Networks and Power Systems (WCNPS 2020).

[3] Torres-Garcia, V.; Guillen, D.; Overs, J.; Escalante- Ramirez, B.Rodríguez-Rodríguez, J.R. “Modelling of high impedance faults in distribution systems and validation based on multiresolution techniques” Compute. Electr. Eng. 2020, 83, 106576. [CrossRef]

[4] “Modified FFT based high impedance fault detection technique considering distribution non-linear loads: Simulation and experimental data analysis”. Adel Soheili, Javed Sadeh, Reza Bakhsi. Elec. Power and Energy Systems:2017.

[5] Érica Mangueira Lima, Caio Marco dos Santos Junqueira, Núbia Silva Dantas Brito, Benemar Alencar de Souza, Rodrigo de Almeida Coelho, Hugo Gayoso Meira Suassuna de Medeiros. (2018) “High impedance fault detection method based on the short-time Fourier transform”. ISSN 1751-8687.

[6] Power System Fault Analysis Using Signal Processing Technique Vaibhav S.Yendole, Prof. Kiran A.Dongare ; Vol. 6, Issue 8, August 2018 , IJIREEICE.

[7] Theron, J.C.J.; Pal, A.; Varghese, A. “Tutorial on high impedance fault detection” In Proceedings of the 2018 71st Annual Conference for Protective Relay Engineers (CPRE), College Station, TX, USA, 26–29 March 2018

[8] “Simulation Models for Different Power System Faults”-Manish Srivastava, Sunil Kumar Goyal, Amit Saraswat, G.Gangil. IEEE-ICADEE 2020.

[9] Brito, N.S.D., de Souza, B.A., dos Santos, W.C., et al.: ‘Analysis of the influence of the window used in the short-time Fourier transform for high impedance fault detection’. 2016

[10] Carvalho, D., Macedo, J.R., Resende, J.W., Castro, F.C., and Bissochi, C.A. (2015). “Proposition of an interharmonic based methodology for high-impedance fault detection in distribution systems”. IET Generation, Transmission & Distribution, 9(16), 2593–2601.

The statistical analysis of Groundwater at Durgapur using GIS

Chhanda Mondal Roy
Assistant Professor, Department of
Civil Engineering, HOD
(Dr.B.C.Roy Polytechnic)
Dr. B.C.Roy college group of Institute
Research scholar of NIT Durgapur
Durgapur West Bengal, India
mondalchhanda@gmail.com/
chhanda.mondal@bcrec.ac.in/

***Abstract*— Groundwater is the most suitable source of our drinking water. Contamination of such water sources is a big problem that creates a health hazard. The groundwater quality has been studied at the different points located in the Durgapur Sub-Divisional area. The water sample's physical and chemical parameters were evaluated during all seasons. The parameters like alkalinity, total dissolved solids, hardness, colour, turbidity, pH, dissolved oxygen were tested in the laboratory. To assess the quality of groundwater, each parameter has been compared with the standard desirable limit of that parameter in drinking water as prescribed by IS 10500-2012 and a comparison of different parameters. Statistical analysis has been performed and a correlation coefficient matrix has been evaluated.**

Keywords*— Groundwater, pH, turbidity, DO, TDS, hardness, correlation coefficient, and statistical analysis.

I. INTRODUCTION

In the world, water is the universal solvent. Water is an important resource for humans existing in our world. In our day-to-day life water is an essential thing. Below the land surface everywhere groundwater is available. 0.6% of groundwater in the world is suitable for drinking [1]. Groundwater is less polluted than compared to surface water but now-a-days due to increasing civilization enhanced population, urbanization, and industrialization groundwater is getting polluted. It is contaminated directly by the mixing of disposal of hazardous wastewater and industrial effluents to the groundwater [1].

The objective of the study is to assess the quality of groundwater of the industrial area of Durgapur locality for using drinking. Physico-chemical parameters of groundwater have been determined and statistical analysis has been performed. The correlation coefficient matrix of different water parameters has been determined. The Geological Information System (Arc GIS 10.8) is also used for mapping and selecting the position for collecting groundwater [5].

II. STUDY AREA

A. *Location of sampling point*

Durgapur is one of the important industrial areas, its geographical area is 154 km^2 and its latitude is 23^{o}55' N and 87^{o}32'E. Our study area is Durgapur industrial zone. Yearly rainfall is 1391ml. There are four groundwater collecting points in our project. That points are Bhiringi, City Centre, Rajbandh, and C Zone (shown in Fig. 1). Four water samples were collected from every sampling point and the total collected samples were eighteen. The study area is located between 23^{0}47' N to 23^{0}56'N latitudes and 87^{0}276' E -87^{0}293'E [4].

B. *Geology*

Durgapur area is situated on the bank of the river basin. It enters the alluvial plain of Bengal and the topography is an undulating character. It is just beyond the coal-bearing area of Raniganj. Its laterite decomposition consists of composing rock of quartz grain and sandy gravel beds. These are true conglomerates and laterite gravel [2].

C. *Climate condition and Rainfall and Temperature*

The summer season is hot and dry and the rainy season is hot and cloudy here. The temperature of the Durgapur region typically varies from 53^{o}F 1938.55 mm (annual value to 99^{o}F but rarely below 48^{o}F and above 107^{o}F.[3] The maximum amount of rainfall) and lowest rainfall are 1119mm [10]

D. *Table 1. Location of sampling point*

Sample No.	Location of sampling point		
	Place	***Latitude***	***Longitude***
S1.	Bhiringi	23^{o}5569'N	87^{o}2768'E
S2.	City centre	23^{o}5391'N	87^{o}3647'E
S3.	Rajbandh	23^{o}4768'N	87^{o}3935'E
S4.	C- Zone	23^{o}5542'N	87^{o}3163'E

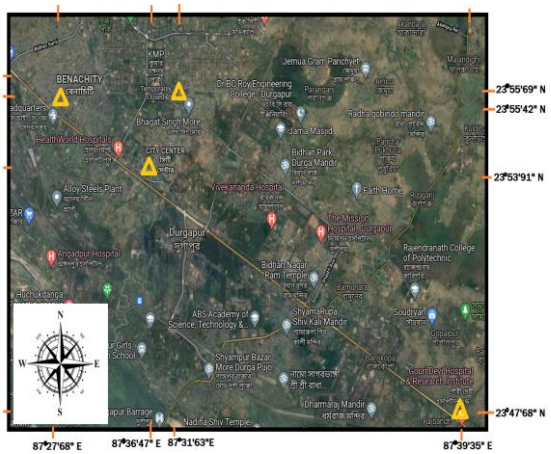

Fig.1: Groundwater collecting point of Durgapur zone

III. Material and Method

Water samples were collected at four different points (already mentioned) and at every point, four samples were collected. Water samples were collected in cleaned polythene bottles. The collected water was kept in the sterilized bottle separately. The following parameters like pH, total hardness, turbidity, color, DO, BOD, and COD. Were tested in our laboratory (shown in Fig. 2) by following standard methods (shown in Table 2).

TABLE 2. List of Parameters and Methods of Determination

Sl. No.	Method	
	Parameters	***Method of determination***
1.	PH	pH meter
2.	Total hardness (mg/l)	EDTA method
3.	Turbidity	Nephelometric turbidity meter
4.	DO	DO meter
5.	BOD	BOD incubator
6.	COD	COD incubator with the spectrophotometer

Fig. 2: Photos of a few laboratory tests.

IV. Results and Discussion

After testing, the above-mentioned physio-chemical parameters of collected water, the mean value, and standard deviation were calculated and shown in Table 4. From Table 4, it is observed that the pH value of groundwater is mostly alkaline and its range is 7.0 - 8.4. According to IS 10500-2012, the permissible limit of pH value is 6.5 to 8.5. It is seen that from table 3 the pH of all samples are within the permissible limit.

Turbidity value range is 0.5 -1 mg/l. Where the Desirable limit according to the Indian Standard for Turbidity of groundwater is 1 NTU and the Permissible limit according to the World Health Organization for Turbidity of groundwater is 5 NTU, so all belong in the desirable limit [7].

TDS is one of the important parameters of groundwater. From Table 3 it is observed TDS range is 430 to 520 mg/l. So high-level concentration is 520 which is above the desirable limit. but it is below the permissible limit. According to WHO, it's the permissible limit and desirable limits are 1500 mg/l and 500 mg/l respectively. Durgapur zone underground soil texture is rocky type, so different types of minerals are deposited in water [8].

The hardness of the water in the groundwater range is 240 to 340 mg/ l. It depends on bivalent cations like Ca^{++} and $Mg^{++,}$ etc. In the groundwater different minerals are available also. Where the desirable limit and permissible limit according to the Indian Standard for the hardness of groundwater are 300mg/l and 600mg/l respectively.

Iron: Iron in water occurs in soil rocks and minerals. In the ground, different aquifers contact with solid minerals as a result water is mixed with minerals. The iron concentration level range is 0 to 50.0 mg/l. According to WHO 's recommendation, it is below 0.3 mg/l. It is observed from Table 3, the iron level is 0.063 – 0.182 mg/l. So, it is within the permissible limit [4].

A. Correlation Analysis

The correlation analysis was found using all variables. Correlation analysis shows linear relationships among the variables. A high correlation point represents a strong relationship between the two variables, and a low correlation represents weakly related variables. It gives some idea to the increasing and decreasing tendency of the Physico-Chemical parameter and its relation.

B. Correlation between variables

The correlation coefficients are represented in Table 5. It represents 49 correlation coefficients. From Table 5 it is observed that turbidity with other parameters (like TDS, DO, Alkalinity, Hardness, and Iron) are positive correlation that means these parameters increase then turbidity also increases. The correlation coefficient among TDS and alkalinity is the maximum negative value. TDS and alkalinity have a strong negative correlation.

FIG 3: PICTURES OF THE SOURCES OF COLLECTED WATER

TABLE 3: COLLECTED SAMPLE DADA

Parameters	COLLECTED SAMPLE				
	Unit	**S1**	**S2**	**S3**	**S4**
pH	---	7.62, 7.91, 7.64, 7.89,	8.4, 8.3, 8.3, 8.2,	7.60, 7.62, 7.64, 7.42,	7.96, 7.92, 7.86, 8.12,
Turbidity	NTU	0.60, 0.61, 0.72, 0.75,	0.90, 0.85, 0.81, 0.90.	0.82, 0.80, 0.83, 0.81,	0.90, 0.82, 0.85, 0.90,
Total Dissolved Solids	mg/l	517.5, 509.5, 490.3, 510.2,	475.16, 463.17, 456.60, 458.60	485, 492, 501, 488	453.07, 443.01, 460.50, 452.01
Dissolved Oxygen (DO)	mg/l	5.16, 5.51, 5.65, 5.51	6.86, 6.10, 6.28, 6.30	5.65, 5.71, 5.45, 5.85,	5.64, 5.71, 5.91, 5.44

Parameters	COLLECTED SAMPLE				
	Unit	S1	S2	S3	S4
Alkalinity	mg/l	190, 180, 192, 196	180, 193, 196, 184	198, 190, 192, 212	280, 285, 275, 272
Hardness	mg/l	340, 320, 326, 322	260, 263, 265, 258	321, 312, 310, 321	274, 271, 276, 272
Iron	mg/l	0.063, 0.060, 0.079, 0.076	0.182, 0.180, 0.184, 0.100	0.072, 0.082, 0.085, 0.085	0.091, 0.086, 0.081, 0.088

TABLE 4. BASIC STATISTICS OF GROUNDWATER

Parameters	Statistics				
	Unit	*Min*	*Max*	*Mean*	*Standard Deviation*
pH	---	7.62	8.4	7.91	0.3267
Turbidity	NTU	0.5	1	0.75	0.2061
Total Dissolved Solids	mg/l	437.3	517.5	473.26	30.82
Dissolved Oxygen(DO)	mg/l	5.16	6.86	5.795	0.6258
Alkalinity	mg/l	180	300	237.5	53.0919
Hardness	mg/l	340	240	280	37.4165
Iron	mg/l	0.0630	0.182	0.10025	0.0479

TABLE 5. CORRELATION MATRIX

parameter	Correlation Matrix						
	pH	*Turbidity*	*TDS*	*DO*	*Alkalinity*	*TH*	*Iron*
pH	1						
Turbidity	0.093	1					
TDS	-0.236	0.118	1				
DO	0.231	0.771	0.01	1			
Alkalinity	-0.365	0.020	-0.916	-0.404	1		
TH	-0.013	0.129	0.814	-0.505	-0.585	1	
Iron	0.369	0.886	0.146	0.989	-0.702	-0.051	1

V. CONCLUSION

The statistical analysis of collected sample data of groundwater has been performed in this study. The samples of groundwater have been collected from the area of the Durgapur Sub-Division. The different parameters of the groundwater sample are within the permissible limit as per the World Health Organization. Finally, a correlation coefficient matrix is provided based on the test results for future reference.

ACKNOWLEDGMENT

I would like to thank Dr. B.C.Roy College Institute group to offer lab facilities for the research works.

REFERENCES

[1] M Jamuna "Statistical Analysis of groundwater Quality Parameters in Erode District, Taminadu, India" ISSN 2277-3878, Volume -7, Nov 2018

[2] Dr. Jayashri Roy "the geological characteristics of the western part of bardhaman district". e ISSN 2348 –1269, Volume – 6.

[3] Mohit Raja; Chirag Kumar; Rohan Jayesh; Kamalika Tiwari; Chhanda Mondal Roy "Instrumental Analysis of Groundwater and Water Quality Index in Fuljhore, Durgapur using GIS" IEEE *Xplore*: 18 June 2020. DOI: 10.1109/NCETSTEA48365.2020.9119932

[4] D. Hossain1, M. S. Islam1, N. Sultana2 and T. R.Tusher1 Assessment of Iron Contamination in Groundwater at Tangail Municipality, Bangladesh ISSN 1999-7361

[4] Ajithkumar, T.T., Thangaradjou, T. and Kannan, L. 2006. Physicochemical and biological properties of the Muthupettai mangrove in Tamil Nadu. J. Mar. Biol. Ass. India, 48: 131-138. 1."Assessment of Water Quality Index of Damodar river near coal city Dhanbad" Md. Asif Ekbal and Ashutosh Ramteke. Energy Research and Environmental Management. ISBN 978-81-930585.

[5] "Water Quality Index of Groundwater in Haridwar District", Uttarakhand, India Gopal Krishan, Surjeet Singh, R.P. Singh, and N.C. Ghosh National Institute of Hydrology, Roorkee, Uttarakhand January 2016.

[6] 3. "Heavy metal contamination of groundwater in Guwahati city," Assam, India manoshi lahkar1, k.g. Bhattacharyya, International Research Journal of Engineering and Technology (IRJET) e-ISSN: 2395-0056.

[7] 3. A review study on "Quality Assessment of groundwater resource in Centre India region" Arun Verma1, Prof R. K. Bhatia, Prof Atul Sharma.

[8] 4. Ali 1, New generation -adsorbents for water treatment chem. Rev 112(2012),5073-5091.

[9] 5. Debalina Kar, Arnab Banerjee, Debnath PalitAssessment of Water Quality of Some Selected Sites of Durgapur Industrial Belt, West Bengal, India through Distribution and Abundance of Larval Chironomidae in Relation with Physicochemical Characteristics of Water January 2011.

[10] 'Six Years Major Historical Urban Floods in West Bengal State in India: Comparative Analysis Using Neuro-Genetic Model ' Nihar R. Samal1, 2,, Pankaj K. Roy3, Mrinmoy Majumadar3, S. Bhattacharya2, Malabika Biswasroy3 Science and Education Publishing, *American Journal of Water Resources*, 2014 2 (2), pp 41-53. DOI: 10.12691/ajwr-2-2-3

Affordable Cold Storage for Preservation of Tomatoes before exporting to the Market

Uttam Das
Post Graduate Scholar
Department of Mechanical Engineering
Jalpaiguri Government Engineering College
Jalpaiguri, India
uttamcobpoly@rediffmail.com

Asim Mahapatra
Assistant Professor
Department of Mechanical Engineering
Jalpaiguri Government Engineering College
Jalpaiguri, India
a.mahapatra2000@gmail.com

***Abstract*— A refrigerated storehouse is the most effective system of conserving vegetable quality like tomatoes, but its high cost deters relinquishment by the planter, smallholder directors, and entrepreneurs. Several low-cost cooling styles have been developed, but they cannot maintain the recommended deep freeze- storehouse temperature. Numerous types of fruit and vegetables taste best when they're gathered completely ripe and also consumed or reused. Leafy vegetables and sauces also don't keep long after crop. With fruit and vegetables from the home garden, speedy consumption and further processing are no problem, but consumers also want a certain shelf life in addition to good quality and full aroma for bought products. This poses a challenge to farmers for fruit and vegetable like tomatoes because the metabolism of the products continues indeed after the crop when gathered in the optimal condition, the quality of the gathered material decreases continuously – it loses taste and constituents and changes its appearance and thickness until it's at some point is no longer comestible. Tomatoes are perishable fruit that makes them deteriorate fleetly during the post-harvest chain. Thus, it is required to give an affordable refrigeration storehouse system to enhance the quality and shelf life of the tomato for rural as well as unborn use. In the following companion, the reader will learn how solar cold storehouses may be used for the preservation of tomatoes and will be affordable to growers and smallholders, producers as well as entrepreneurs.**

Keywords*— *Tomatoes, cold storage, and solar power

I. INTRODUCTION

Tomato is considered one of the most important vegetable crops worldwide for fresh request and reused products due to its health and profitable significance. West Bengal has secured the first rank in vegetable products and tomato is one of the most consumed vegetables in the study area. [1]. It has been reported that tomato fruit has a considerable value of the most important antioxidants similar to the lycopene, carotenoids, vitamin C, and minerals, which can play a vital part in suppressing the development of some mortal conditions including prostate, colon, and bone cancers [2]. Also, consumption of about 100 g of tomato can supply the mortal body with 40% of the recommended diurnal lozenge of vitamin C which can enhance the vulnerable system, lower blood pressure and cholesterol [3]. Likewise, tomatoes are classified as climactic fruit and deteriorate fleetly after crop due to soft textures and their vulnerability to microbial infection. Tomatoes are gathered at colorful maturity stages, including green mature, swell, turning, light red, and full red. The most favored stages for consumers are the light and full red stages, which decay extensively after crop. Fruit and vegetable quality is substantially affected by postharvest conditions similar to transportation and storehouse conditions [4]. Post-harvest losses of fruits and vegetables are estimated to be between 30 and 40%, contributing towards a significant portion of a total loss due to lack of storage facilities and poor infrastructure. Several methods are available for the preservation of food, the most common being preservation through heat exclusion [5]. A reduction in energy consumption and the utilization of sustainable and renewable energy technologies are essential to meet the increasing demand for cooling, using environmentally friendly methods [6]. Thus, it is required to give an affordable refrigeration storehouse system to enhance the quality and shelf life of the tomato for unborn use maintain postharvest quality and protract the shelf life of tomatoes. Solar cold storehouse may be used for the preservation of tomatoes and it'll be affordable to growers because of its availability and low costing concerning others.

Fig 1. Wastage of tomatoes due to lack of affordable cold storage

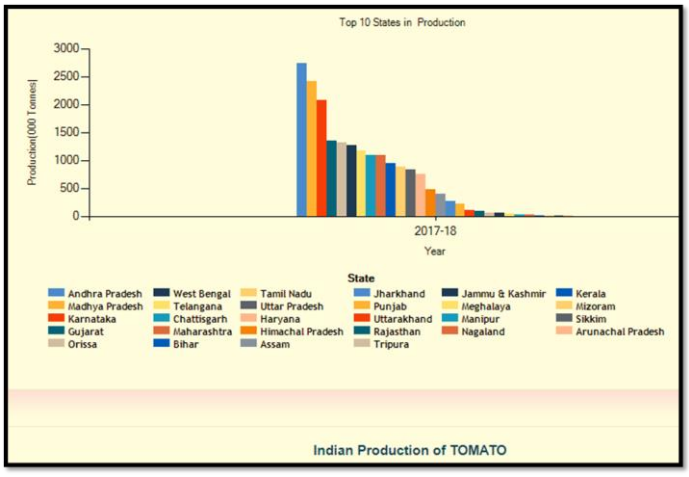

Fig. 2 [7]

II. AREA AND PRODUCTION OF TOMATO FOR MAJOR PRODUCING DISTRICTS IN WEST BENGAL.

		A: Area in '000 Ha P: Production in '000 MT			
States	***District***	***2015-16***		***2016-17***	
		Area	***Production***	***Area***	***Production***
West Bengal	COOCH BEHAR	3.31	148.75	3.32	153.24
	24 PARAGANAS NORTH	4.18	134.53	4.19	135.95
	NADIA	4.80	109.14	4.82	115.84
	MURSHIDABAD	4.87	101.56	4.88	101.89
	ALIPURDUAR	3.39	100.52	3.40	100.75
	24 PARAGANAS SOUTH	4.94	92.19	4.95	93.25
	PURULIA	5.54	80.50	5.55	80.70
	MEDINIPUR WEST	4.21	70.66	4.21	71.56
	PURBA BARDHAMAN	2.97	50.50	2.98	62.45

Horticultural Statistics at a Glance 2018

Production of tomatoes in the District. Cooch Behar

From the above statistics, it can be observed that the state of West Bengal is in 6th position in India in the production of tomatoes and the district Coochbehar is in the 1st position in West Bengal in the production of tomatoes. But due to the lack of post-harvesting management, the farmers are reluctant to produce tomatoes in large quantities. So proper post-harvesting technic like refrigerated cold storage within the budget will motivate them for mass production of tomatoes.

III. Principles of Refrigeration

Refrigeration is the process of removing heat from an area or a substance and usually is done by an artificial means of lowering the temperature. A cold storage house system like any other refrigerating system of the same magnitude employs the vapour absorption refrigeration system. This Vapour Absorption Refrigeration System is the modification of the vapour compression refrigeration systems. However, unlike vapour compression refrigeration systems, the input to absorption systems is in the form of heat. Hence these systems are also called heat-activated or thermal energy-driven systems. Since conventional absorption systems use liquids for the absorption of the refrigerant system, these are also sometimes called wet absorption systems. Parallel to vapour compression refrigeration systems, vapour absorption refrigeration systems have also been commercialized and are widely used in various refrigeration and air conditioning applications. Since these systems run on low-grade thermal energy, they are preferred when low-grade energy such as waste heat or solar energy is available. Since traditional absorption systems generally use naturally accepted refrigerants such as water or ammonia they are environment friendly.

Solar Refrigeration:

A refrigerator that runs on electricity supplied by Solar Energy is known as solar refrigeration.

Solar-powered refrigerators may be most generally used in the coming generation.

Need for solar refrigeration:

- Need refrigeration in areas not connected to a power grid
- Need to minimize environmental impact and energy cost
- Estimate eventuality of solar energy to meet these requirements
- Estimate effectiveness of three types of solar refrigeration

Types of solar refrigeration:

- Photovoltaic Operated Refrigeration Cycle
- Solar Mechanical Refrigeration
- Absorption Refrigeration

Photovoltaic Operated Refrigeration Cycle:

Vapor compression cycle system with a power input from Photovoltaic cells.

DC electric power output system from PV runs the compressor of a conventional cycle

Considerations:

Should match voltage imposed on PV array to the motor characteristics and power requirements of the refrigeration cycle

Forgiven operating conditions (solar radiation and module temperature), single voltage provides maximum power output.

Must find compressor motor nearly matched to the electric characteristics of the PV module.[8]

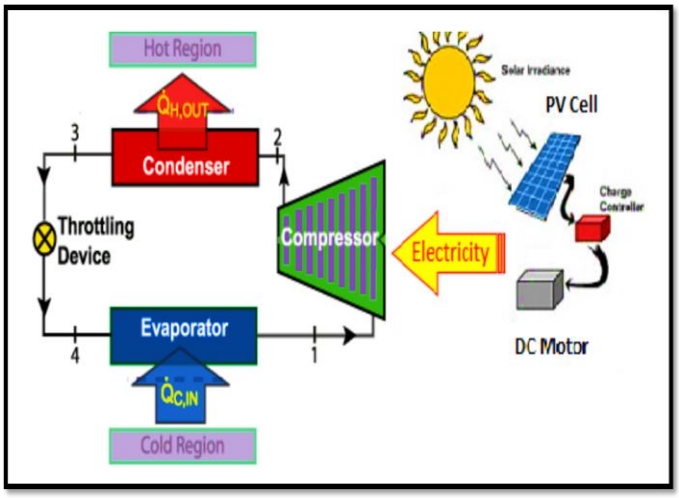

FIG. 3 PHOTOVOLTAIC OPERATED REFRIGERATION CYCLE [9]

Solar Mechanical Refrigeration:

Vapor compression cycle with a power input from solar Rankine cycle.

Considerations:

Efficiency optimization based on delivery temperature

The efficiency of the Rankine cycle increases with increased heat exchanger temperature.

The efficiency of solar collectors decreases with an increase in temperature.

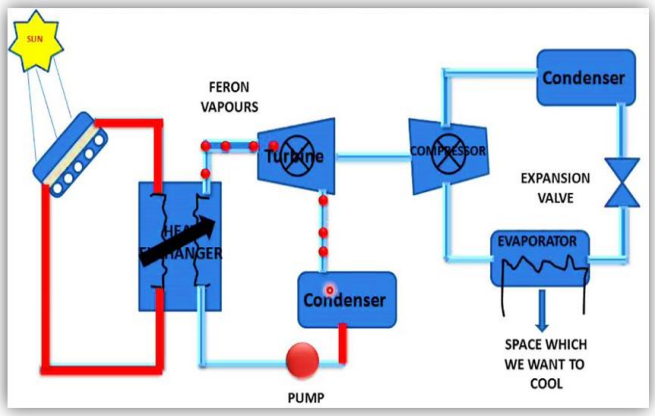

Fig. 4 Solar Mechanical Refrigeration

Absorption Refrigeration:

- Condenser, throttle, evaporator function the same way
- Replaces compressor with "thermal compression system".
- Ammonia is working fluid
- Insignificant mechanical power input (pump instead of compressor).
- Absorption into a water solution allows it to be pumped.
- Desorbed in generator (rectifier required to separate water).
- Heat into the generator provided by solar collectors
- The pressurization is completed by dissolving the refrigerant in the absorbent, in the absorber section.
- Subsequently, the solution is pumped to high pressure with an ordinary liquid pump.
- In this way, the refrigerant vapour is compressed without the need for large amounts of mechanical energy that the vapor-compression air conditioning systems demand.

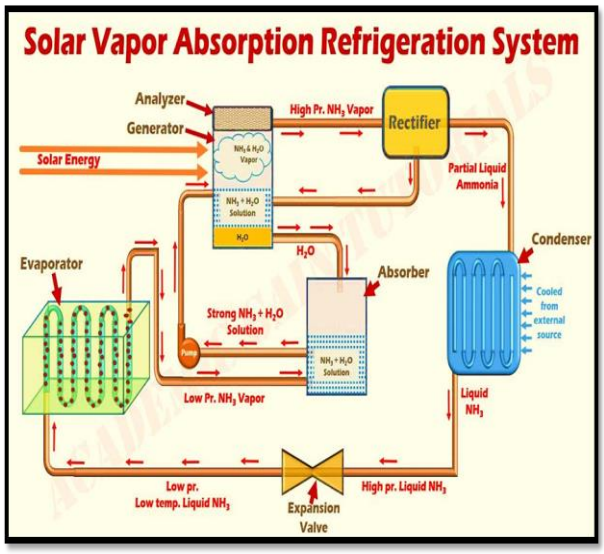

Fig. 5 Processes of vapour absorption refrigeration system

Fig. 6 Mini Cold storage with Solar Panel

IV. Storage Conditions and Ecology:

How active the metabolism of fruit and vegetables is indeed after the crop can be seen from the growing of half-green tomatoes. For growing tomatoes, the storehouse temperature is 4.5 °C to 7 °C, relative moisture 85% to 90%, and cold storehouse life needed about 1 to1.5 weeks. For mature (green) tomatoes, storehouse temperature is needed about12.5°C to15.5°C, relative moisture 90%, and storehouse life 3 to 4 weeks.

The design of Cold Storage largely depends on

• Product to be stored

• Temperature and moisture conditions to be maintained

• Volume of the product

• Period of Storage

Heat load calculations

Cold storage capacity for 1000 kg (1 ton) tomatoes requires a storage volume of approximately 120 ft^3 because nearly 50-60 % of the total volume is utilized for storage purposes. For this purpose one storage of size, 6ft x 5ft x 4ft (120 ft^3) is considered. If the height of the cold storage is 4ft then the base of the cold storage will be 6ft x5ft.

Transmission load

- The dimensions of the cold store may be 6ft long, 5ft wide, and 4ft high.
- Consider the ambient air is 30°c at 50% RH, The internal air is 5°C at 90% RH
- The walls, roof, and floor are all insulated with 0.26ft polyurethane with a U value of 0.028W/ft^2. °C

To calculate the transmission load following formula will be used

$$Q = UA(\frac{To - Ti}{24x1000})$$

-Q= kWh/day heat load

- U = U value of insulation (value is known) (W/ft^2. °C)
- A = surface area of walls roof and floor (ft^2)
- Ti = The air temperature inside the room in (°C)
- To = The ambient external air temperature in (°C)

To calculate “Area” is fairly easy, it is just the size of each internal wall, so drop the numbers in to find the area of each wall, roof, and floor.

Side 1 = 6ft x 4ft = 24ft^2
Side 2 = 6ft x 4ft= 24ft^2
Side 3 = 5ft x 4ft = 20ft^2
Side 4 = 5ft x 4ft = 20ft^2
Roof = 5ft x 6ft = 30ft^2
Floor = 5ft x 6ft = 30ft^2

Then it can run these numbers in the formula to calculate the floor separately to the walls and roof as the temperature difference is different under the floor so the heat transfer will therefore be different.

Walls and roof

$$Q = UA(\frac{To - Ti}{24x1000})$$

$$Q = 0.028x118(\frac{30 - 5}{24x1000})$$

$$Q = 2(\text{approx.})\ \text{kWh/day}$$

[118ft² = 24ft² + 24ft² + 20ft² + 20ft² + 30ft²]

Floor

$$Q = UA(\frac{To - Ti}{24x1000})$$

$$Q = 0.028X30(\frac{10-5}{24x1000})$$

$$Q = 0.1\ kWh/day$$

If the bottom isn't isolated then it is needed to use a different formula grounded on empirical data.

Total daily transmission heat gains = 2kWh/day + 0.1kWh/day = 2.1kWh/day

if the cold room is in the direct sun then it is needed to regard for the sun's energy also.

Product load – Product exchange

Next, it should be calculated the cooling load from the product exchange that being the heat brought into the cold room from new products which are at an advanced temperature.

For this example here will be storing tomatoes, so it can look up the specific heat capacity of the tomatoes but do remember if it is required for freezing products then the products will have a different specific heat when cooling, freezing, and subcooling so it'll be needed to account and calculate this separately, but in this example, here it is just cooling.

There is 1000kg of new tomatoes arriving each day at a temperature of 25°C and a specific heat capacity of 3.60kJ/kg.°C

The following formula can be used

$$Q = mX\mathbf{Cp}(\frac{Ti - Tsh}{3600})$$

- Q = kWh/day
- CP = Specific Heat Capacity of tomatoes (kJ/kg.°C)
- m = the mass of new tomatoes each day in (kg)
- Ti = the initial entering temperature of the products in(°C)
- Tsh = the temperature within the storehouse in(°C)

Calculation

$$Q = mX\mathbf{Cp}(\frac{Ti - Tsh}{3600})$$

$$Q = 1000X3.60(\frac{25-5}{3600})$$

$$Q = 20\ kWh/day$$

Product load – Product respiration

Next, to calculate the product respiration, this is the heat generated by living products similar to fruit and vegetables. These will induce heat as they're still alive, that's why it is required to cool them to decelerate down their deterioration and save them for longer.

For this illustration, here it is taken as 1.91 kJ/ kg per day as an average but this rate changes over time and with temperature. In this illustration, here are using rules of thumb value just to simplify the computation since this cooling load isn't considered critical. If it were to calculate for a critical load they should use lesser perfection. In this illustration, the store maintains a hold of1000 kg of tomatoes

To calculate this the formula is -

$$Q = (\frac{mX\mathbf{resp}}{3600})$$

- Q = kWh/day
- m = mass of tomatoes in storage (kg)
- resp = the respiration heat of the tomatoes (1.91kJ/kg)

$$Q = (\frac{1000X1.91}{3600})$$

Q = 0.52kWh/day

For the product section, it'll sum together the product exchange of 20 kWh/day and respiration load of 0.52kWh/day to get a total product load of 20.52 kWh/day.

Total cooling load

To calculate the total cooling load here all the values calculated

Transmission load: 2.1kWh/day
Product load: 20.52 kWh/day

Total = 22.62 kWh/day

Safety Factor

Safety factors should also apply to the computation to regard crimes and variations from design. It's typical to add 10 to 30 percent onto the computation to cover this, in this case, it is considered as 20 percent for illustration so well just multiply the cooling load by a safety factor of 1.2 to give a total cooling load of 27.1 kWh/ day.

Refrigeration cooling capacity sizing

The last thing that should be demanded to do is calculate the refrigeration capacity to handle this burden, a common approach is to a normal of the total day-to-day cooling burden by the run time of the refrigeration unit. For this, it's projected that the unit to run about 14 hours per day which is fairly typical for this size and type of store. So the total cooling burden of 27.1 kWh per day, divided by 14 hours means the refrigeration unit conditions to have a capacity of about 2kW to sufficiently meet this cooling load. [10]

V. Price of 2kW Solar System

Below is the ultimate 2021 price list Inclusive of all Levies of 2kw on-grid, solar system.

2kW On Grid Solar System

The On-grid solar system works with the grid and net-metering is applicable on the 2kw solar system. 2kW solar system is the most extensively chosen solar system installed each over India.

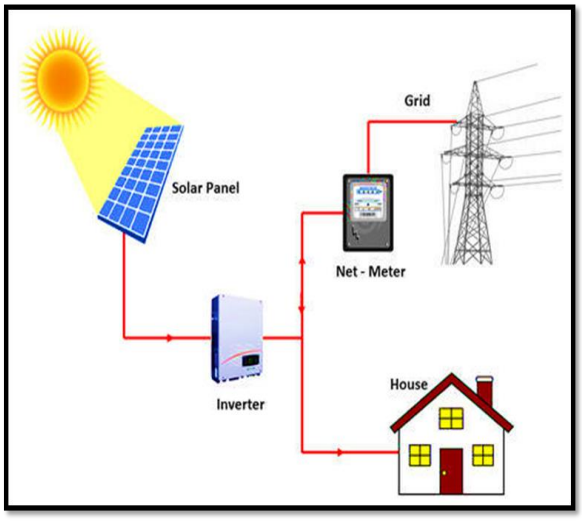

Fig. 7 Grid cum Solar System

Technical Information:	
Particulars	***Description***
Solar system capacity	2kW
Solar panel Quantity	6 No.s
Solar Inverter	2kW – On grid inverter
Accessories	Fasteners, Cable Tie, Crimping Tool, Earthing Kit, Lighting Arrestor
System warranty	**25 years**
MC4 connector	2 Pair
DC wire	30 meters
AC wire	20 meters
Space Required	Approx. 200 sqft
Average generation	8 units per day
Total cost	1,02,872

[11]

Advantages of 2kW On-Grid Solar System

• Costs less compared to other types of the solar system

• Save electricity bills up to 100 percent

• Eligible for over to 70% of government subventions on solar

• Exploit 100 percent solar power produced by 2kW solar panels

• Export the excess solar power to the electricity grid

• No limitation of loads, run all connected load with grid sharing

. • Life 25-30 times [12]

What Solar Panels Do at Night?

At present time, as the solar panels can produce power during the day, the question also develops“ how will solar panels supply power overnight when there's no sunlight?” The primary results may help to resolve that problem. Solar- plus- storehouse technology allows solar panel systems to store excess electricity to the battery or supply to the grid and consumed overnight when solar panel product is dormant, either connected to the electric grid sever or a battery. Thanks to grid connections and solar energy storehouses, solar panels are a sustainable round-the-timepiece energy result. It will also solve the problem of battery demand for storehouses. Near future, if Silicon can be replaced with the material whose band-gap is equal to energy provided by moonlight then solar panels or say, Lunar Panel can be used at night for electricity generation.

VI. CONCLUSION:

A good deal of experience is required to make a perfect calculation of a cold store's refrigeration requirement and this should therefore only be done by a qualified and experienced person. The above calculation is not complete but it will serve two purposes. It allows the reader to make a similar type of calculation for the storage capacity and thereby obtain an approximate refrigeration requirement. It moreover helps the reader to appreciate the number of factors that have to be taken into account for calculating the heat load and also gives some idea of relative importance design procedure used can be applied to scale up the capacity. This paper assists the economic analysis for manufacturing solar absorption refrigeration for mini cold storage like tomatoes, fruits, and vegetables.

REFERENCES

[1] Abdelgawad, K.F.; El-Mogy, M.M.; Mohamed, M.I.A.; Garchery, C.; Stevens, R.G. Increasing Ascorbic Acid Content and Salinity Tolerance of Cherry Tomato Plants by Suppressed Expression of the Ascorbate Oxidase Gene. Agronomy 2019, 9, 51.

[2] Tsaniklidis, G.; Charova, S.N.; Fanourakis, D.; Tsafouros, A.; Nikoloudakis, N.; Goumenaki, E.; Tsantili, E.; Roussos, P.A.; Spiliopoulos, I.K.; Paschalidis, K.A.; et al. The role of temperature in mediating postharvest polyamine homeostasis in tomato fruit. Postharvest Biol. Technol. 2021, 179, 111586

[3]. Zeng, C.; Tan, P.; Liu, Z. Effect of exogenous ARA treatment for improving postharvest quality in cherry tomato (Solanum lycopersicum L.) fruits. Sci. Hortic.2020, 261, 108959. [CrossRef]

[4]. Al-Dairi, M.; Pathare, P.B.; Al-Yahyai, R. Effect of Postharvest Transport and Storage on Color and Firmness Quality of Tomato. Horticulturae 2021, 7, 163. [CrossRef]

[5] Alghool, D.M.; Elmekkawy, T.Y.; Haouari, M.; Elomri, A. Optimization of design and operation of solar assisted district cooling systems. Energy Convers. Manag. 2020, 6, 100028.

[6] Chidambaram, L.A.; Ramana, A.S.; Kamaraj, G.; Velraj, R. Review of solar cooling methods and thermal storage options. Renew. Sustain. Energy

[7]www.academia.edu/39849565/Solarrefrigeration_140708074548_phpapp01_converted.

[8]agriexchange.apeda.gov.in/India%20Production/India_Productions.aspx?cat=Vegetables&hscode=1088.

[9] Alazazmeh AJ, Mokheimer EM (2015) Review of Solar Cooling

[10]https://theengineeringmindset.com/cooling-load-calculation-cold-room/

[11] https://www.upsinverter.com/utl/2kw-solar-system

[12]https://www.omsolar.in/3kw-solar-system-price-features-and-advantages/.

_____

How Electronic Energy Levels Get Modified in Potentially Bound Forms (Atoms, Molecules, Crystals)

Subhajit Samaddar
Dept. of Physics
RKMRC (Narendrapur)
Kolkata, India
ssamaddar1988@gmail.com

Debiprasad Jana
Dept. of Physics
RKMRC (Narendrapur)
Kolkata, India
djana.physcis@gmail.com

Malay Purkait
Dept. of Physics
RKMRC (Narendrapur)
Kolkata, India
mpurkait_2007@rediffmail.com

***Abstract*—Electron in free state is not at all similar to that in bound system. A bound system is nothing but a system with modified potentials. The nature of potential effects on the solution of Schrodinger's equation. Hence the distribution of energy levels is modified along with. A free electron movement gives rise to continuous spectra but this is not the case always. In case of atoms the nature of barrier potential changes as one increases number of electrons from one (Hydrogen atom), two (Helium atom), three, four (Alkali atoms) and so on. In case of molecules the overlap of atomic orbitals and their symmetry have substantial effects on the energy spectra. Lastly, whenever one deals with lattice in case of crystalline structure the periodicity as well as defects in some of the concerns influence the energy spectra. Whenever the average potential due to core ions and neighbouring electrons are replaced by the periodic potentials which are quite obvious in case of crystalline structure, an array of allowed and forbidden bands of energy are availed. The allowed bands consist of series of sharp energy levels the numbers and spacing of which again are functions of nature of the potential energy barrier.**

Keywords—quasi-free electron, binding energy, energy levels, energy bands, energy spectra)

I. INTRODUCTION

Free electron motion is an abstract idealization in the real field. In the classical domain one speaks of a continuum. There is no story of discretization. The dispersion relation is continuous in form. Even if in case of quantal treatment where there is no potential barrier one finds Schrodinger's equation resembling with simple harmonic type. So, the solution is obvious to be of sinusoidal form or linear combination of such forms. The value of wave-vector varies continuously from 0 to ∞. Thus, the dispersion relation takes the form- $E=\frac{\hbar^2 k^2}{2m_e}$ [$\hbar$-Plank's constant, k-Wave-vector, m_e- Mass of electron]. Whenever a potential well or potential barrier is envisaged which has finite length. So, boundness of potential causes discretization of energy. The aforementioned equation turns into $E=\frac{n^2\pi^2\hbar^2}{2m_e L^2}$ on application of the proper boundary conditions [n=1,2,3,….∞ (Principal quantum number, m_e - mass of electron, L- leghth of well/barrier]. So, energy is an explicit function of n and L. the functional dependence shows that although having occurrence of discrete character the bound state-levels do not maintain uniform distance from each other. As the quantum number n increases, the energy levels get more and more separated. In case of hydrogen and Alkali atoms the same energy equation acquires the form $E\sim\frac{1}{n^2}$ and $E\sim\frac{1}{(n-\mu)^2}$ respectively, where μ is quantum defect [1]. In these bound states the energy levels get closer with increase of principal quantum number resulting in a nearly continuum at higher frequency. This is quite obviously obtained through "Bohr's Correspondence Principal" [2] which is eminently known as a merger between classical and quantal theory. Again, if one looks at simple harmonic potential i.e. $V=\frac{1}{2}sx^2$ the energy levels are found to be equidistant. In case of vibronic diatonic molecule along its axis the same spectra is observed but in real life some sorts of anharmonicity happens to exist which refrains the energy levels from being equidistant. The levels get closer and closer as vibrational quantum number increases. The emission and absorption lines merge to a continuum finally. It is conclusive that whenever the lines are equidistant the bonding remains stronger than when anharmonicity appears to make the levels closer. Now, let's turn at rotational molecules. For low to moderate energies, the energy levels are determined by mere kinetic energy which falls in the category of rigid rotor [3] but above a certain energy this model fails. Then the centrifugal distortion potential enters along with the mere kinetic energy. This results in shift of the lines toward lower frequency with increase in rotational quantum number in power of three [4]. So, the emission and absorption lines are also no more equidistant. They come closer with increase of rotational number. i.e. the bond weakens and the levels are less stable for molecules to sustain.

The solid-state structure is most complicated. It is classified into two sections- one is amorphous and the other is crystalline. We will confine ourselves to crystal which consists of three salient properties running holding their hands together. They are- lattice, basis and periodicity [5]. Basis compromises with atoms, molecules, ions. Different types of potentials, usually combination of short range and long-range parts [6] actually remains effective among the bases pairwise. The lattice structure happens to be in equilibrium state for some distance among the atoms pairwise. The distribution of electron clouds obviously has an effect over formation of sustainable bonds along with ion cores. The lattice constants and parameters determine the dimension of potential well and barrier as mentioned earlier. Those are generally of atomic dimensions. The difference lies in the nature of potential. For constancy of barrier potential, the simple harmonic solution is obtained in case of E>V [E-Total energy of electron, V- Height of Barrier]. The barrier potential is most likely to be of periodic nature for the lattice property. The difference here occurs in the nature of wavefunction and energy-wave-vector relationship. The dispersion relation is not only discontinuous but also complicated. This property is quite pronounced at the edge of the material. It may be understood that as a fact that

sharing of outer shell electrons among the ion cores splits the original energy level into several levels which gives rise to band structure. More detailing gives that a band structure rather than distinct sharp edges relying on the potential as evident from "Bloch's theorem" and "Kronig Penny model" [7]. In case of periodic potential several bands of energies are found along with band gap. So, all the domain are not accessible for the electrons. The orders of magnitude of band gap are decider of whether a material will be metal or insulator or semiconductor.

II.THEORY

This section will be divided into three separate subsections. The first one will be dedicated to atoms, second one will be dedicated to molecules and the third one will be dedicated to lattice.

A. Atomic Binding

First of all the atomic spectra of Hydrogen atom is considered. Out of Bohr's theory of quantization of angular momentum one finds radius of Bohr's orbit to be $r_n = n^2 a_0$ [n-Principal quantum no., a_0- Bohr's radius]. Putting it into energy equation one obtains energy of electron in the n-th orbit to be $E_n = -\frac{13.6}{n^2}$ electron-volt. According to this semiclassical theory all the energy levels with different azimuthal numbers (l) have same energy. This concept had existed until the appearance of "Vector Atomic Model" [8]. In the year of 1925 G.E. Uhlenbeck and S.A. Goudsmit introduced the quantal concept spin. The circular motion of the electron causes orbital angular momentum. This angular momentum interacts with spin angular momentum which gives rise to L-S. coupling. This very perturbation removes l-degeneracy. The modified energy acquires the form-

$$\Delta E = [\, j(j+1)-l(l+1)-s(s+1)\,] \qquad (1)$$

l- angular momentum quantum number

s- spin angular quantum number

j= l+s- total angular quantum number

s=1/2 holds for electron. That's why there is a doubling of each of the spectral lines which is said to be fine structure.

The next simplest structure is di-electronic Helium atom. It is tackled with three different ways.

The first one is independent electron model. Here, The total Hamiltonian discards the static correlation [9] term pertaining to the interaction between the electrons. It follows the total energy is the sum of two semiclassical terms as in Hydrogen atom which reads as-

$$E_n = -\frac{Z^2}{2}\left(\frac{1}{n_1^2}+\frac{1}{n_2^2}\right) \qquad (2)$$

Z - Atomic number

n_i(i=1,2,…..) - Principal quantum numbers

The ground state energy is found to be -108.8 electron-volt. It is very much less relative to the experimentally found value (-79 electron-volt).

The second one is to include the correlation term $\frac{1}{r_{12}}$ in the Hamiltonian [$\overrightarrow{r_{12}} = |\overrightarrow{r_1} - \overrightarrow{r_2}|$]. r_1 and r_2 are the positions of the electrons relative to the nucleus. While put in the energy shift formulation of the 1st-order perturbation one gets the energy value to be $\frac{5}{8}$ Z. The calculational procedure follows as [10]. The result is improved, still there is excess in value as compared to the experiment.

Third approach considers of screening effect. It is thought that the charge of the nucleus is screened to each due to occurrence of the other electron in the Helium atom. The nuclear charge Z is replaced with Z_{eff}= Z-S where, S is the screening parameter. The first order calculation gives the energy shift to be-

$$\Delta E = -2\, Z_{eff}\,(\, Z - Z_{eff}\,) \qquad (3)$$

Combining with above two formalisms one obtains the total energy to be-

$$E = -Z_{eff}^2 + \frac{5}{8} Z - 2\, Z_{eff}\,(\, Z - Z_{eff}\,) \qquad (4)$$

The application of Ritz variational principle [11] the value of Z_{eff} is found to be Z-$\frac{5}{16}$. So, the value of screening parameter S will be $\frac{5}{16}$. The corrected value of energy of ground state Helium has been found to be $\approx$ -74.8 electron-volt which is much more conforming with the experimentally obtained value -79 electron-volt.

As electron is a fermion, it has to obey Pauli's exclusion principle. Electron is a spin-$\frac{1}{2}$ particle. It is identified by two different co-ordinates; one is position and the other is spin. In case of Helium atom two electrons do exist. They may align parallelly to produce total spin S=1 or antiparallelly to produce total spin S=0.The former is called Ortho-Helium and the latter is called Para-Helium. In case of Ortho-Helium, less amount of repulsion occurs. So, the energy of this state is lower relative to Para-Helium. The energy levels in Para and Ortho states are not similar. In Ortho state the energy levels start from 2s rather than 1s. The inter-state distances are different for the two sets.

Now, it's time to enter more into many electron atoms. Here also the same two factors i.e. inter-electronic correlation and screening effect are challenges. Due to occurrence of the screening parameter the simple Coulombic potential is modified as-

$$V(r_i) = -\sum_{i=1}^{N} \frac{Z - S(r_i)}{r_i} \qquad (5)$$

Where, Z-Nuclear Charge, r_i-Distance of the i-th electron from the nucleus, $S(r_i)$- Screening experienced by the i-th electron of the atom. So, the screening parameter is no more a constant as Helium. It is function of distance from the nucleus. This non-Coulombic but symmetric potential removes l-degeneracy. If one discards the correlation term along with a contribution from the non-Coulombic symmetric term (residual Coulomb Hamiltonian) the

Schrodinger's equation in satisfied. In the eigenvalue equation the energy is function of both n and l. In actual sense, correlation term is an electrostatic term. Consideration of relativistic correction [12] introduces a term-

$$\sum_i \frac{1}{2m_e{}^2c^2}\,\frac{1}{r_i}\frac{dV(r_i)}{dr_i}(\vec{L}.\vec{S}) \qquad (6)$$

This is called LS-coupling term which is of paramount importance in case of many-electron target. In case of lighter atoms the electrostatic repulsion is not too strong to break L-S coupling. But, in case of heavier atoms the pairwise electrostatic repulsion is strong enough to break L-S coupling. So, jj-coupling is important here. It can be also inferred that in case of lighter atom the L-S term acts as perturbation whereas in case of heavier atoms the residual Coulomb Hamiltonian acts as perturbation (fine-structure consideration) [13].

The discussion remains incomplete without inclusion of Alkali spectra. These metals are highly metallic in character. Elementary knowledge says that outside the complete core, here lies only one unpaired electron. So, the core contributes as optically inactive $^1S_0$ structure and the unpaired electron is mostly responsible for the corresponding spectral structure. The core electrons here do have a screening effect for which the outermost electron cannot see the entire nuclear charge. Again this is responsible for removal of l-degeneracy which was absent for Hydrogen atom. This very comparison is given due to the fact that both the Hydrogen atom and Alkali atoms have one active electron. The energy already has been given previously where quantum defect is an implication of screening.

B. Molecular Binding

The discussion will be limited to simple molecules only. What we understand as molecule is an amalgamation of at least two nuclei and distribution of electron cloud over them. The type of bonding and overlap act as decider of energy in this regard. The simplest molecular structure is H_2^+. It is a homonuclear molecular ion. Bohr-Oppenheimer Approximation [14] assumes the motion of electron is much faster than the motion of nucleus. Hence, the nucleus may be assumed to be at rest. This approximation is basic in all sorts of molecular energy spectra. A simple harmonic motion model is supposed to be in between two heavy nuclei and a molecule is in stable condition due to stable equilibrium there in. A small displacement from the equilibrium r_0 position causes a restoring force F= -K (r-r_0). Out of the Heisenberg's uncertainty principal $\Delta p\Delta x \approx \hbar$, from the dimension of molecule one may have an idea of energy of electron inside. Doing a bit of simple algebra electronic energy is found to be 10^3 times greater than that of vibrational energy and 10^6 times greater than that of rotational energy [15]. In case of homonuclear molecule the external energy cannot change the rotational state of molecule due to not having permanent dipole moment. The external energy also cannot trigger the vibrational energy also due to same reason. It is easier to disturb electrons in the molecule. The change of distribution is associated to change of dipole moment and so one can have rotation al and vibrational energy band structure along with.

Another two very important factors are bonding and antibonding. Molecular orbital is just a wavefunction to find electron in a molecule i.e. concept of molecularized electron [16] comes into play. This is a probabilistic interpretation. So, the individual electronic entity is lost. In case of bonding orbital the electron clouds of two protons of a di-atomic molecule are accumulated between them.so, the overlap is pronounced. On the other hand, in case of antibonding orbital the there occurs a depletion of electrons between the protons resulting in reduction of overlapping. So, the bonding orbital is of larger strength of bond and stabler than that of antibonding [17,18]. Another important parameter is the bond order [18] which determines the strength of bond.

The simplest representation of molecular orbital is Linear Combination of Atomic Orbitals [19,20] which is given as-

$$\varphi = C_1\psi_1 \pm C_2\psi_2 \pm \ldots\ldots \pm C_N\psi_N$$
$$= \sum_{i=1}^{N} C_i\psi_i \qquad (7)$$

Where, the (+) and (-) signs imply bonding and antibonding respectively. Here, the ψ_i's represent component atomic orbitals with similar symmetry.

Another important and the most worth mentioning theory is Hartree-Fock Self Consistent Field (HF-SCF) theory. This theory in indispensable to understand many body physics. In case of molecule one has five type of energy terms-electronic kinetic energy, ionic kinetic energy, inter-ionic interaction, ion-electron interaction and inter-electronic correlation. As per Born-Oppenheimer Approximation one neglects kinetic energy of ions. The electrostatic interaction among bare ions (pairwise) are kept apart from calculation. The prime aim is to solve again the electronic Schrodinger's equation. The electronic correlation term acts perturbation. The introduction of the Fock function is for the sake of minimization of the total energy [21]. Nevertheless of having the electronic interaction term the solution of the equation is approximated to be expressed as product of single electronic wave funtions. But in case of electron (fermion) there is an association of spin co-ordinates along with spatial co-ordinates. The product form-

$$\varphi_i = \prod_i \psi_i(r_i) \qquad (8)$$

is called Hartree's product. The one overlook the General Hartree-Fock or Z- averaged Perturbation Theory [22] the wavefunction $\psi_i(r_i)$ is expressed as product of spatial and spin co-ordinates [21]. But, there is a problem of antisymmetrization which is resolved by Slater's determinant. The occurrence of Permutation operator

appears as solution. The sequential as well as recurring combination of sum (subtraction) of products help minimize the inconsistency. Actually, H-F solution endorses to make possible the complex asymmetric part in form of eigenvalue equation with the alliance of Roothan equation. The overlap integral is annulled by the transformation of basis to orthogonal one. The description is given in [21]. The Hartree-Fock Roothan equation reads as [19.]-

$$\sum_s C_{si}\hat{F}\,\chi_s = \varepsilon_i \sum_s C_{si}\,\chi_s \qquad (9)$$

where, $\hat{F}$ is Hartree-Fock operator such that-

$$\hat{F} = \hat{H}^{core}(1) + \sum_{j=1}^{n/2}[2\hat{J}_j(1) - \hat{K}_j(1)] \quad (10)$$

The first term denotes unperturbed part, J denotes Coulomb integral and K denotes exchange integral. ε_i is binding energy of electron obtained by diagonalizing the Slater's determinant.

C. Crystalline Binding

In case of free/quasi-free electrons [23] there remains continuous states of accessibility. But, the scenario changes in case of complex type potentials. For the sake of simplicity we will concentrate on periodic type potentials, consisting of an array of potential wells and barriers.

In the forthcoming discussion we will concentrate on Bloch Theorem and Kronig-Penney model. These two theorems are intertwined with each others and the common ground lies in the periodicity of potential in the solid-state crystalline structure. Bloch's theorem expresses the solution of Schrodinger's equation to be expressed as-

$$\psi(r) = e^{\pm ikr}\,\mu_k(r) \qquad 11.(A)$$

subject to $\mu_k(\vec{r} + \vec{a}) = \mu_k(\vec{r})$ 11.(B)

The Schrodinger's equation is a second order differential equation. It comprises of two independent solutions- f(r) and g(r). From the periodicity of potential there will be also two more solutions - f(r+a) and g (r+a) but from the rule of mathematics they must depend on f(r) and g(r). what happens as a consequence is that the ratio of $\psi(r + a)$ and ψ(r) is a constant say (δ). Here, the summary will only be retained without mentioning the entire calculation [24,25]. The invariance of the Wronkskian [26] allows the parameter δ to be expressed in form of a simple quadratic equation. Application of Sridharacharya's rule, one finds two types of determinants; one producing real root and the other producing imaginary root. Both are correct mathematically. But, the real root obstacles physical acceptance because of the pre-assumed finite nature of physically acceptable wavefunction in quantum mechanics. This does disallow the energy values to be accessible everywhere as was in classical mechanics and the quantal picture so far. There are forbidden regions also. Nowfrom, two modifications of paradigm with take place- firstly, the existence of allowed energy bands will be separated by forbidden bands and the frequency will no more remain proportional with wave number [27].

Now, array of consecutive wells and barriers will be taken in account. Here the periodicity will be (a+b) [a for well and b for barrier]. Actually well stands for distance between two mobile ions and the barriers occur at the position of ions. Obviously the energy of electron is greater than the uniform potential V_0 . Two schrodinger's equations are found. Imposing Bloch theorem with periodicity (a+b) and the conditions for continuity of logarithmic differential gives four linear equations with four unknown parameters. For the non-zero solution to exist the determinants whose elements are the coefficients of four unknowns to be zero, which gives [28]-

$$P\frac{\sin\alpha a}{\alpha a} + \cos\alpha a = \cos ka \qquad 12.(A)$$

where,

$$P = \frac{mV_0 ba}{\hbar^2} \qquad 12.(B)$$

(m is electron's mass and $\hbar$ is reduced Plank's constant, k is the associated wave vector, α is supposed to be measure of electronic energy). P is a measure of how strongly the electron is bound to the respective potential well. The right hand part of the equation 12.(A) is a cosine function. This confines the left hand portion between -1 and +1 which is again a restriction or constraint whatever one may say on the energy i.e. the E-k curve should not be continuous. An alternation of allowed and forbidden energy bands are formed. In case of infinitely strong bond ($P \to \infty$) the energy bands are squeezed into lines separated by gaps i.e. line spectrum is formed. On the other hand in case of infinitely weak bond ($P \to 0$) energy band is restored. In the intermediate zone one finds band width to be decreasing with strengthening of the bond.

It is already discussed that the E-K diagram is discontinuous in nature. So, Brillouin zones [29] are formed. Let's concentrate on the first Brillouin zone [30]. Combining simple electrodynamic equation with the quantum with simple quantal formalism a wonderful expression of mass is obtained which is reduced mass. This reduced mass is actually the indicator of how much bound is the electron in the crystalline structure. It is denoted as-

$$m^* = \frac{\hbar^2}{\frac{d^2E}{dk^2}} \qquad (13)$$

The binding energy of the electron in the lattice is best understood by the factor-

$$f_k = \frac{m}{m^*} \qquad 14.(A)$$

$$= \frac{m}{\hbar^2}\frac{d^2E}{dk^2} \qquad 14.(B)$$

This denotes that upto the point of inflection of E-K curve i.e. upto highest level one happens to obtain free electron. These free electrons are the only elements which take essential as well as sufficient part in electrical conduction process. So, it is quite evident that the extent to which the allowed energy bands in a solid remains filled up is the determinant of how good or poor conductor the material is [31,32]. In case of filled or nearly filled allowed energy

bands one obtains less effectively free electrons, hence the material is insulating in nature. Whereas, the materials in which energy bands are almost empty the number of effectively free electrons are much probable resulting it to be metallic in character. In the intermediate range one obtains semiconductor. In the standard notation the above definitions are defined as absolute zero temperature.

III. Conclusion

In the entire article two types of character of electron; bound and unbound are discussed. In atomic and molecular level the binding energy opens the door for research toward ionization, capture, excitation [33-38]. In the solid state the different acoustic, electrical, thermal and optical properties may be studied. Immense scopes of research are there involving various type of potentials in this regard.

ACKNOWLEDGEMENT

Thanks to Dr. Malay Purkait for resource and Mr. Debiprasad Jana for Technical Assistance. I am indebted to RKMRC (Narendrapur) Physics lab for the inspiration.

REFERENCES

[1] Physics of Atoms and Molecules; Bransden B.H. Joachain C.J.; Longman Computational & Technical Co-published with John Wiley & Sons.Inc…. (New Work) (1983) pp (360)

[2] Quantum Physics; 3rd Edition; Gasiorowicz S. John Wiley & Sons (Asia) (2005) pp (20)

[3] Fundamentals of Molecular Spectroscopy; Fourth Edition; Banwell C.N. McCASH E.M. McGraw-Hill International (UK) Limited (1994) pp (33-37)

[4] Fundamentals of Molecular Spectroscopy; Fourth Edition; Banwell C.N. McCASH E.M. McGraw-Hill International (UK) Limited (1994) pp (33-37)

[5] Solid State Physics; Dekker A.J: Macmillan India Limited, First Published in United Kingdom (1958) pp (1-4)

[6] Solid State Physics; Puri R.K. Babbar V.K. S.Chand & Company Ltd. (I.S.O. 9001: 2000 Company) pp (76-78)

[7] Solid State Physics; Puri R.K. Babbar V.K. S.Chand & Company Ltd. (I.S.O. 9001: 2000 Company) pp (177-185)

[8] Concepts of Atomic Physics; Kuila S.P. (New Central Book Agency (P) Ltd (London) (2018) pp (356)

[9] Samanta R. Purkait M. Mandal C.R. (2011) Phys. Rev. A 83 032706

[10] Quantum Physics; 3rd Edition; Gasiorowicz S. John Wiley & Sons (Asia) (2005) pp (218-220)

[11] Quantum Physics; 3rd Edition; Gasiorowicz S. John Wiley & Sons (Asia) (2005) pp (224-226)

[12] Quantum Physics; 3rd Edition; Gasiorowicz S. John Wiley & Sons (Asia) (2005) pp (188-191)

[13] Concepts of Atomic Physics; Kuila S.P. (New Central Book Agency (P) Ltd (London) (2018) pp (404-407)

[14] Fundamentals of Molecular Spectroscopy; Fourth Edition; Banwell C.N. McCASH E.M. McGraw-Hill International (UK) Limited (1994) pp (162-163)

[15] Fundamentals of Molecular Spectroscopy; Fourth Edition; Banwell C.N. McCASH E.M. McGraw-Hill International (UK) Limited (1994) pp (163)

[16] Kraft G. Kramer M. (1993) Adv. Radiat. Biol. 17 1-51

[17] What is the difference between bonding and antibonding orbitals?; https://byjus.com

[18] Bond order and lengths- Chemistry Libre Texts; https://chem.libretexts.com

[19] Quantum Chemistry; Levin I.A. Pearson (2008): Sixth Edition pp (487)

[20] Pople J.A. Santry D.P. Segal G.A. (1965) J. Chem. Phys. 43 10 S 129-135

[21] An Introduction to Hartree-Fock Molecular Orbital Theory; Sherril C.D.: School of Chemistry and Biochemistry; Georgia Institute of Technology: June (2000)

[22] Steven E. Wheeler et. al. (2008) J. Chem. Phys. 128 074107

[23] Solid State Physics; Puri R.K. Babbar V.K. S.Chand & Company Ltd. (I.S.O. 9001: 2000 Company) pp (175)

[24] Solid State Physics; Puri R.K. Babbar V.K. S.Chand & Company Ltd. (I.S.O. 9001: 2000 Company) pp (177-179)

[25] Solid State Physics; Dekker A.J: Macmillan India Limited, First Published in United Kingdom (1958) pp (240-242)

[26] Wronskian- Wikipedia; https://en.m.wikipedia.org

[27] Solid State Physics; Dekker A.J: Macmillan India Limited, First Published in United Kingdom (1958) pp (239)

[28] Solid State Physics; Puri R.K. Babbar V.K. S.Chand & Company Ltd. (I.S.O. 9001: 2000 Company) pp (183)

[29] Brillouin Zone- Wikipedia https://en.m.wikipedia.org

[30] Solid State Physics; Puri R.K. Babbar V.K. S.Chand & Company Ltd. (I.S.O. 9001: 2000 Company) pp (190)

[31] Solid State Physics; Puri R.K. Babbar V.K. S.Chand & Company Ltd. (I.S.O. 9001: 2000 Company) pp (191-193)

[32] Solid State Physics; Dekker A.J: Macmillan India Limited, First Published in United Kingdom (1958) pp (251-252)

[33] Samaddar S. Halder S. Mondal A. Mandal C.R. Purkait M. Das T.K. J. Phys. B: (2017) At. Mol. Opt. Phys. 50 065202

[34] Samaddar S. Purkait K. Halder S. Mondal A. Mandal C.R. Purkait M. (2019) 13 413-426

[35] Samaddar S. Jana D. Purkait K. Purkait M. (2020) J. Phys. B: At. Mol. Opt. Phys. 53 245202

[36] Halder S. Mondal A. Samaddar S. Mandal C.R. Purkait M. (2017) Phys. Rev. A 96 032717

[37] Mondal A. Halder S. Mukherjee S.C. Mandal C.R. Purkait M. (2017) Phys. Rev. A 96 032710

[38] Jana D. Purkait K. Samaddar S. Haque A. Purkait M. (2022) Applied Radiation and Isotopes 182 110100

Dark Matter, A Newtonian Approach

Anirban Naskar
Electrical Engineering
Narula Institute Of Technology
Kolkata, India
iamaninaskar2001@gmail.com

***Abstract*—In this paper I have tried to present a case for dark matter using a Newtonian approach. I have also tried to present the evidence for the same.**

In the first three sections of the paper, I have established a relationship between gravitation and velocity using Newton's laws and then showed how the rotation velocities of the galaxies in the Coma cluster do not follow the predicted values of the velocities and finally how inclusion of extra mass can explain the apparent disagreement of the observed phenomenon with the predicted values.

In the next two sections I have tried to provide some evidence for the presence of dark matter in our universe.

Keywords—Dark matter, Universe, Gravitational lensing, Spacetime

I. Introduction

Our entire universe isn't what we see it to be or think it to be. Everything we see in the universe is made up of known visible matter but still, that only accounts for only about 4.6% of the total matter energy density of the universe. Then one question arises in our mind? Where's the rest of it? recent studies have found that our universe is only 4.6% visible matter or normal matter as We know it, about 24% of the entire universe is dark matter and the remaining 71.4% consists of dark energy.

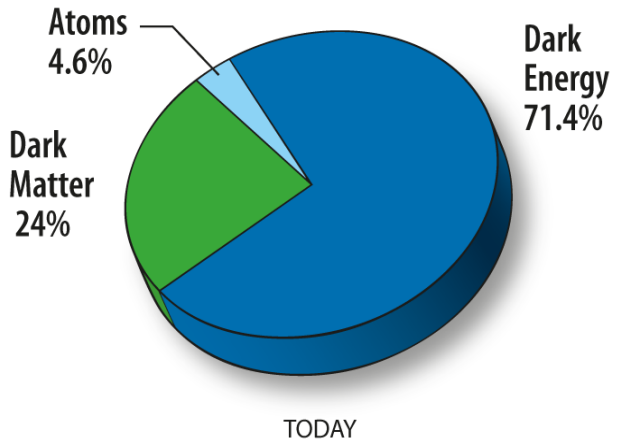

Dark matter was discovered by Dr. Fritz Zwicky in the year 1933 while he was observing the Coma cluster of galaxies. Dr. Zwicky was analyzing the relative velocities of the galaxies under the influence of gravity of the system. Before we go to the topic of how he managed to do that let us first take a look at some basic principles of gravity to better understand Zwicky's results and how did he arrive at his conclusion. It is important to note that, although here I'm using a Newtonian approach to explain dark matter (a relatively simpler approach), Dr. Zwicky used something called the "virial theorem" that gives a general equation for the average kinetic energy of particles bounded by potential forces.

II. Gravitation and Velocity

According to Newton's universal law of gravitation.

$$F = \frac{GMm}{R^2} \quad \ldots\ldots\ldots\ldots (1)$$

We know in stable orbit conditions;

$$F = \frac{mv^2}{R} \quad \ldots\ldots\ldots\ldots\ldots (2)$$

Where ***F*** is the force of gravity, ***M*** is the center of mass of the gravitationally bounded system, ***m*** is the mass of the individual body under consideration of which the orbital velocity ***v*** due to gravity is being measured.

Equating equations 1 and 2 we get,

$$\frac{mv^2}{R} = \frac{GMm}{R^2}$$

So, we get,

$$v = \sqrt{\frac{GM}{R}} \quad \ldots\ldots\ldots\ldots\ldots\ldots (3)$$

As we can see velocity due to gravity is a function of distance from the gravitational center of mass. Equation (3) tells us that if there is a gravitationally bounded system where a body with mass ***m*** orbits around the center of mass of the system with mass ***M***, then the orbital velocities of the body is a function of distance from the center mass of the system denoted by ***R***. Now according to equation (3),

$$v = \sqrt{\frac{GM}{R}}$$

but as we can see both ***G*** and ***M*** are constants in the system, we can write the equation as follows,

$$v = \frac{K}{\sqrt{R}}$$

or we can say that,

$$v \propto \frac{1}{\sqrt{R}}$$

from the above expression we can say that as we move farther away from the gravitational center of mass, we

would see the orbital velocities of the bodies in the system decreasing in accordance with the above relation. Given below is a classic example of the above derived result. It shows how the orbital velocities of planets decrease as we move farther away from the gravitational center of mass of the solar system, in other words, The Sun.

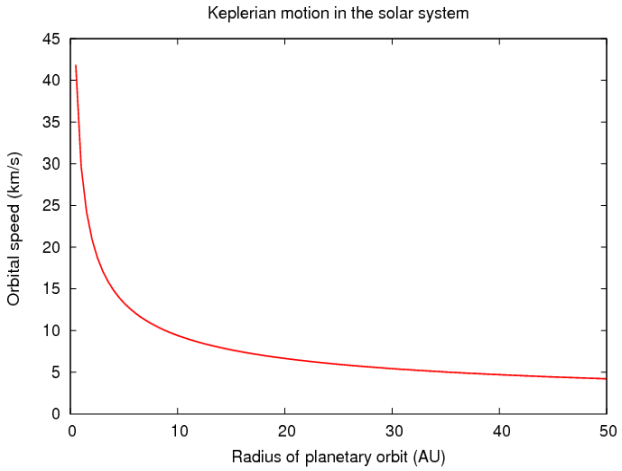

Precisely this is what Dr. Zwicky intended to find. Imagine a galaxy, in it there are trillions of stars orbiting around its galactic center. Now we can assume that as we move farther and farther away from the galactic center the orbital velocities of the stars will gradually decrease. So, what did Dr. Zwicky find?

III. Dr. Zwicky's Results and How It Leads to Dark Matter

Dr. Zwicky used virial theorem to predict the orbital velocities of galaxies of the Coma cluster around the common center of mass of the system. We can do the same thing by the Newtonian approach. We can take the help of the expression for the orbital velocities of gravitationally bounded objects derived in the earlier section of this paper and predict the velocity distribution of the stars in those galaxies with respect to their distance from their respective galactic centers. Then we can plot the predicted results on a graph and intend it to match with the results obtained from the observations made. Did Dr. Zwick's observations match the predictions that he made or the predictions that we made with our Newtonian approach? The answer is no! The analysis of the observed data showed that the velocities of the stars orbiting at the outer edge of the galaxies were roughly equal in magnitude with the orbital velocities of the stars orbiting near the galactic center. Dr. Zwicky's observed results were way off from his predicted plot. These results force us to ask the question, "is there something wrong with Newtonian physics? Or is there a deeper reality hidden behind it waiting to be discovered?" There is a little chance that the former is right because Newtonian mechanics lays the groundwork for the entire classical physics and it is among one of the most successful ways to explain the universe in the macroscopic scales. We have that confidence on Newtonian mechanics that it cannot be wrong. This leaves room for the later statement to be true in some sense, so we can insist on the later statement, there must be some deeper mystery hidden inside waiting to be discovered.

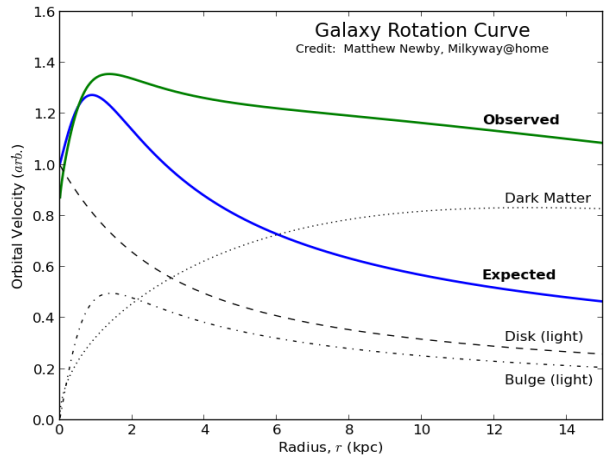

Rotation Curve of the Galaxy

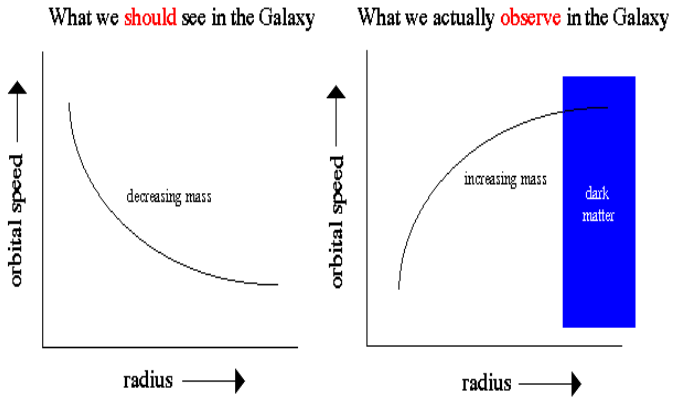

So why were the stars having velocities they shouldn't have? To answer this, we need to go back to equation (3). Imagine a star orbiting the galactic center at a distance ***R,*** so it should have a velocity equal to,

$$v = \sqrt{\frac{GM}{R}}$$

but instead, we find it to have a velocity

$u > v$.

But we know ***G*** cannot change, since it is the universal gravitational constant and we know that the star is at a distance ***R***, so the only parameter that needs to change here in order to account for the extra velocity is ***M***, in other words the galactic system must have some hidden extra mass that is responsible for the extra orbital velocities of the stars. And since the effect is spread throughout the galaxy, the extra mass must be distributed roughly uniformly throughout the entire galaxy. So how much extra mass is present in the galaxy apart from the visible matter or known form of matter?

Let the extra mass of the galaxy due to the mysterious form of matter be ***m***, so according to the expression of velocity we derived earlier,

$$u = \sqrt{\frac{G(M+m)}{R}} \quad ; \ldots\ldots. (4)$$

$$u^2 = \frac{G(M+m)}{R} \quad ;$$

$$u^2 = \frac{GM}{R} + \frac{Gm}{R} \quad ;$$

$$u^2 = v^2 + \frac{Gm}{R} \quad ; \text{[from equation (3)]}$$

$$u^2 - v^2 = \frac{Gm}{R} \quad ;$$

$$m = \frac{R\,(u^2 - v^2)}{G} \quad \ldots\ldots\ldots\ldots\ldots(5)$$

The result obtained above is a very crucial one, it tells us how much of extra unknown form of matter must be present in the galaxies in order for the stars to have the extra orbital velocities around the galactic centers. And as we can see that ***G*** is very small and *R* usually is large, so the value of ***m*** must be significantly large. Dr. Zwicky called this significantly large extra unknown mass, "The Dark Matter". This extra mass does not come from the ordinary matter as we know it, rather it comes from a totally unknown form of matter which we don't know much about. It is important to note that the word "Dark" in the name doesn't have anything to do with color, it represents our ignorance, that how little we know about this form of matter.

IV. Other Evidences for Dark Matter

We don't know what dark matter is or where does it come form, but one thing we certainly know is that it's out there, its present in the interstellar space it's present in the intergalactic space, basically dark matter is present everywhere. So, what are the evidences?

A. Gravitational Lensing:

According to general theory of relativity matter and energy can bend the fabric of spacetime, more massive the body or the matter energy density more it bends the fabric of spacetime. Since everything in this universe is confined within the fabric of spacetime they are bound to follow the curvature wherever it leads and this eventually gives rise to a force called gravity. So, if we ask," what causes gravity?'' Einstein would answer in this fashion, "matter tells spacetime to bend and curve and spacetime tells matter to follow the curvature''. One interesting consequence of this result is that light is also made up of particles called photons, and since photons are particles, they are bound to follow the curvature of spacetime. In other words, gravity will force light to bend around massive objects, the same light ray that prefers to travel in a straight line otherwise. Now we know how convex lenses work and how it magnifies an image. Light rays while passing through a lens bends due to the difference in refractive index and that eventually creates the effect of magnification. Similarly light rays while passing from near a massive object ends up bending in a similar way creating a lensing effect. And this is called gravitational lensing.

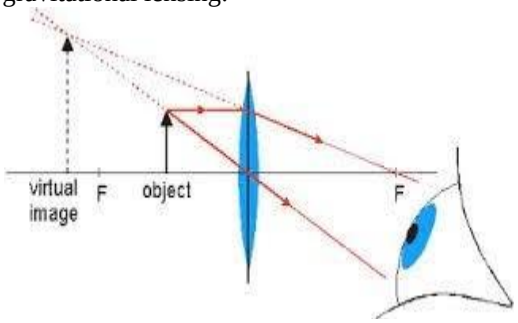

How convex lenses work to produce a magnified virtual image

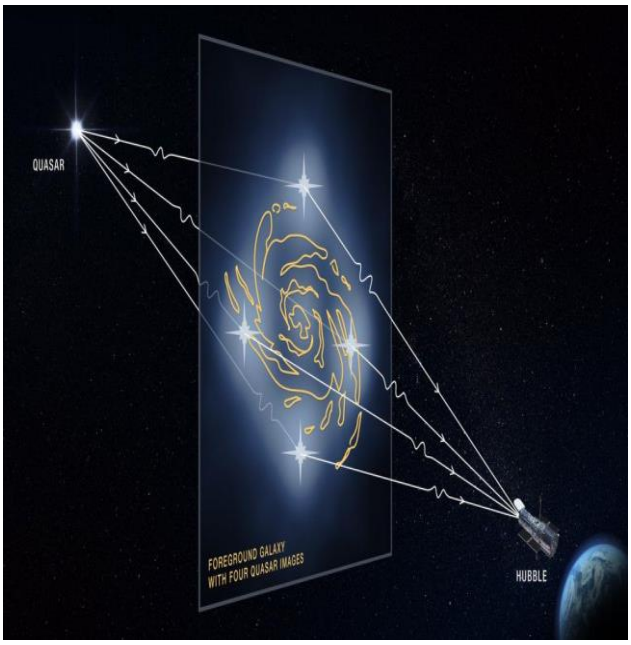

How gravitational lensing works to produce a magnified virtual image of the distance quasar

What does this have to do anything with dark matter? Well just as general theory of relativity leads us to gravitational lensing it also tells us by how much amount a light ray should bend around an object of given mass. So, by observing the light coming from a distant galaxy we can calculate its mass and then we can apply the mathematics of general relativity to calculate by how much the light coming from the background galaxies should bend around the galaxy under observation. But when we make an observation of the light coming from the background galaxies, we find that the degree of lensing is higher than expected and the mass of the foreground galaxy is not enough to account for the extra lensing. Which quite inevitably leads us to the conclusion that there is some extra

unknown form of matter present in the galaxy the nature of which is still unknown to us which is responsible for the extra lensing.

B. Geometry of the universe:

what do we mean when we say geometry of the universe? Imagine the fabric of spacetime as a giant curtain. As we know from the results of general relativity that matter bends spacetime, so if the universe has too much matter in it the space shall bend too much until it closes in on itself. Just like the giant curtain, if you put some weight on it will bend inward, if you keep on adding more and more weight eventually the curtain will get so much bent that it's two opposite ends will come together and form a closed structure this is called positive curvature. But if there is too less matter present in the universe the expansion of the universe will cause the fabric of the universe to bend in the opposite direction which will never really close but will go on bending forever, imagine the curtain being stretched from all sides and you don't add enough weight to keep it bending inward, this is called negative curvature which will cause the universe to have a horse saddle like structure. What if there is just enough matter that makes the fabric of spacetime bend inward counteracting the tendency of the fabric to bend outward due to cosmic expansion? In other wards if there's just enough matter present it can stop the universe from bending in either way and can result in a flat universe. Now this is not something our mind can grasp. How can three-dimensional space be flat or bend in a certain way? But we are just three-dimensional beings stuck with our three-dimensional imaginations. Imagine you were a two dimensional being living in a piece of paper. Only spatial dimensions you are aware of are back and forth and left and right. You would have no idea about a third dimensions top and bottom and most certainly you would not have a shred of imagination of how the paper can be bent in certain ways, for example like a bow.

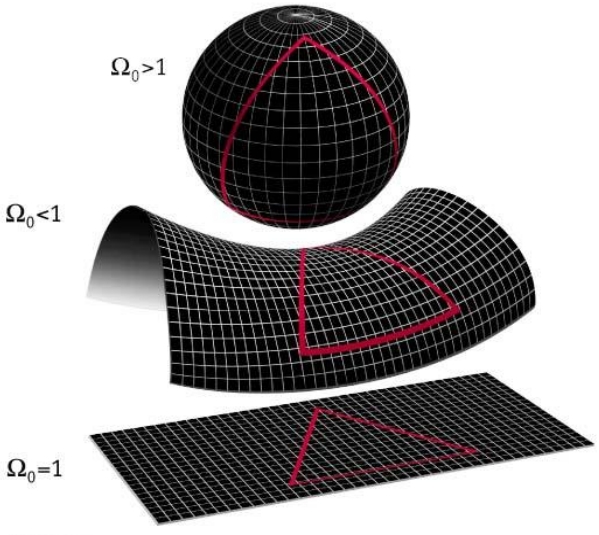

Three possible geometries of our universe

Now the question arises, which kind of universe do we live in? The analysis of the data obtained from the Cosmic Microwave Background Radiation (CMBR) shows us that we live in a flat universe. That is in our universe there is just enough matter to make it flat. But there's a problem with this picture, when we set out to find how much matter is present in the universe, we find that the total amount of known matter that accounts for all the stars planets and galaxies in the universe only represents 5% of the total matter required to make the universe flat, how can this be possible? We know that the universe is flat but still the other 95% of matter in the universe is missing. Discovery of dark matter turned up to be a major clue to solve that problem and a missing piece of this great puzzle.

If dark matter wasn't there, gases could never have collapsed to form galaxies and galactic clusters. Dark matter provided that foundation for our universe to exist the way it exists today.

V. PROPERTIES *OF DARK MATTER*

We still don't have a clear understanding of what dark matter is or where does it come from, but still, we can make educated guesses about some properties that dark matter must have or else the universe wouldn't look the way it is now. Some of these properties are,

- It is nothing like the matter as we know it.
- It does not interact with light or else we would have detected it by now.
- It does not interact with ordinary matter in any known way other than gravity.
- It bends the fabric of spacetime around its vicinity just like any matter with mass would do according to the laws of general relativity, as a result it shows gravitational effects.
- It does not clump together.

But as of now still the concept of dark matter remains a mystery to us till date. Huge efforts are being made to detect dark matter in our solar system, but till now all such attempts have been proved to be fruitless. All we can say is our solar system doesn't have enough dark matter to show significant gravitational anomaly or the effects of dark matter is only evident in large scale structures like galaxies and galaxy clusters. We simply don't know enough about dark matter to setup and design experiments to detect it yet. But we certainly know enough to tell that it is out there. The very goal of science is to chart unknown territories of knowledge, we might not know enough for now but who knows when someone new will come up with a new breakthrough and turn our scientific understanding upside down all over again.

ACKNOWLEDGMENT

I would like to thank the Indian Space Society because I got the inspiration to write this paper after attending their conference. I would also like to thank my friend Ms. Shrestha Dey for encouraging me to write this paper and finally I would like to thank my teacher Dr. Pratyusha Biswas Deb for encouraging and providing me the necessary guidance for the publication of this paper.

REFERENCES

[1] Dr. Lawrence M Krauss, "A Universe From Nothing, why there is something rather than nothing", Simon & Schuster 2012, pp. 25,31,34-35,40-41,72,87

[2] Dr. Stephen W Hawking, “A Brief History Of Time”, A Bantam Book : 9780553175219, pp. 152-157

[3] Dr. Stephen W Hawking, “The Theory of Everything, the origin and fate of the universe lecture series”, Jaico Books,Special anneversary edition, pp. 19,36

[4] Dr, Brian Greene, “ The Hidden Reality”, Penguine Books, pp. 24-25

[5] https://www.nature.com/articles/d41586-019-02603-

[6] Lawrence M. Krauss, “A Universe from Nothing”, Radcliffe Institute lecture https://youtu.be/vwzbU0bGOdc

A REVIEW ON SMART HOME TECHNOLOGIES

Anjana Sengupta
Electrical Engineering Department,
Technique Polytechnic Institute,
Hooghly, India
anju.aeccrj@gmail.com

Kaustav Mallick
Electrical Engineering Department
Technique Polytechnic Institute,
Hooghly, India
kaustavmallick91@gmail.com

Saikat Ray
Electrical Engineering Department
Technique Polytechnic Institute,
Hooghly, India
saikatray1999@gmail.com

***Abstract*— In the near future Smart homes will be the benchmark of next level comfortable homes. IOTs like node MCU, GSM module, Arduino has been pushing smart technologies to new limits in last few years. Smart homes will be important not only on comfort perspective but also for effective and efficient use of electrical energy thereby resulting in reduction of our daily energy consumption and minimising wastage. This paper highlights the fundamental concept of smart homes and some important smart home technologies that can be implemented. The paper as well includes challenges of smart home.**

Keywords— Arduino, sensors, Smart home, home automation, smart irrigation system.

I. INTRODUCTION

The concept of smart home and buildings is being treated as one of the most popular emerging ideas in present world scenario. Smart building is a type of building with reasonable investment, efficient energy management, and comfortable and convenient environment, designed by considering the optimized relationship among structure, system, service, and management. It is the outcome of the application of information technology and control technology into traditional buildings as well as ample internet availability. With vast expansion of digital technology and internet facilities, implementation of different ideas related to smart home has become much more feasible than before. With increase in demand of residential complexes and consequently reduction in natural resources designing energy efficient buildings is the demand of the hour. These systems involved in smart homes can be safer, more convenient, energy saving as well as time saving gifting us intelligent home life. User-cantered intelligent design promotes the sustainable development of smart buildings. It gives the user, the ability to control any electronic device without even reaching out for a remote controlling unit.

The network is required for communication of the automation to the controlling device. It can be both wired and wireless. The controlling devices are used for managing the system, IOT or internet of things is an upcoming technology that allows us to control hardware devices through the Internet.

II. BACKGROUND OF SMART BUILDINGS

The 80s' observed shift towards intelligent buildings which perfectly also matched up with the worldwide property boom towards the end of the '80s. There was also a requirement for these new buildings to be as efficient as possible, and therefore the concept of "intelligent buildings" could fill this void. The advancements in technology and different environmental factors directed to the conception of automated building systems which formed the fundamental concept of "intelligent buildings", a term first coined in 1981 by the United Technology Building Systems (UTBS) Corporation, United States. Initially, intelligent buildings used single and multi-function electronic systems to centrally control certain physical factors like heating, ventilation, and air conditioning systems thereby improving building efficiency and minimizing energy consumption via the integration of information technology. In 1991, with the easy availability of internet to the public changed so many aspects of lives of people, including their way of working in professional fields, mode of communication, and interaction with technology. Buildings began to change as well. Offices were encouraged to a more open-plan environment to encourage people to be more collaborative. This resulted in need of buildings to be as energy-efficient as possible. With the introduction of the internet which became much more widely available, these intelligent buildings were developed to be "Smart Buildings" in the 2000s. People are much more conscious of the changing environment and want to reduce our

effect on it. A major percentage of the common people is but unaware of ways by which we can contribute to the sustainable development.

III. IMPORTANCE OF SMART HOME IN MODERN TECHNICAL SCENARIO:

- *To saving unnecessary energy consumption: -*

The smart home technology industry mainly focuses on reducing unnecessary use of electrical energy. However, it does not implies that smart home technologies will reduce home energy use overall.

- *Wireless control of home appliances (Switch and Voice mode): -*

Development of application would include features of switch and/or voice modes to control the applications which will significantly reduce human efforts. In this time where we are avoiding contacts to avoid spread of identified and unidentified viruses, having voice mode control is a blessing.

- *Monitoring status of appliances: -*

It gives the option of being aware of the energy consumption or the mode of operation. Being able to view the status of home appliances on the application, helps to have a better Home Automation System.

- *Extensible platform for future enhancement: -*

With a strong existing possibility of adding and integrating more features and appliances to the system, the designed systems will be highly extensible in nature.

- *User friendly:-*

The systems are extremely easy to use once designed. The applications are mostly through mobile applications. The increased smart phone literacy makes the application of the technology user friendly.

IV. SMART HOME TECHNOLOGIES

The wireless communication system mostly used nowadays are microwaves, infrared (IR), radio frequency (RF), Wi-Fi, Bluetooth, and so on. Furthermore some of smart home network standard can work using both wired systems and wireless systems.

Some of the technologies which can be easily applied in residential buildings are:

- *Smart water level indicator with automatic water pump controlling system:*

In accordance with the recent scenario, there is huge amount of water wastage from residential areas, industrial and commercial areas which may lead to its scarcity in near future. Some areas are already facing scarcity.

Nowadays everybody has overhead tank at their homes. Objective of this system is to indicate water level and control the water pump to avoid overflow of water. The idea can be adopted and is used to determine and control the level of water in overhead tanks and prevent wastage. The most popular way to implement this idea is by using Arduino microcontroller; codes were written in order for it to perform as water level controller.

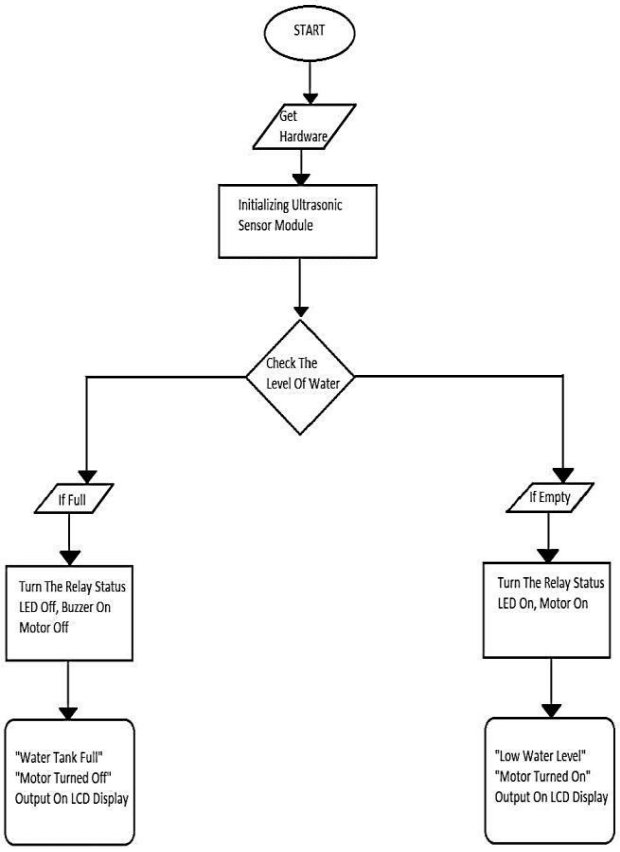

Fig. 1. Program Flow Chart

This smart system involves Ultrasonic sensor module which sends the sound waves in the water tank and detects reflection of sound waves that is ECHO. In order to do that we need to trigger the ultrasonic sensor module to transmit signal by using Arduino and then wait to receive ECHO.

Arduino calculates the time between triggered and received ECHO.

Distance= (travel time/2) * speed of sound

Where speed of sound = 340 metres per second. By using these methods, we get distance from sensor to water surface. After that to calculate water level we need to calculate the total length of water tank. As soon as length of water tank is known then we can calculate the water level by subtraction resulting distance coming from ultrasonic from total length of tank. And we will get the water level distance which can be easily calculated as the percent of water, and can be displayed on LCD.

The advantage of this system over existing conventional ways is that no one will be required to pay attention as to when the tank is filled and tank is overflowing. The system will therefore save a human resource and also the water resource.

- *Solar powered smart irrigation system:*

This concept is often implemented in gardens also as in green buildings and may also be controlled remotely.

This system can easily be developed using Arduino UNO powered by solar array. The system reads the moisture content from the sensor and switches on the motor when the moisture is below the set limit. When the moisture level rises above the point, the system switches off the led indicator. The status of the tank motor and therefore the moisture level are going to be displayed on a 16×2 LCD display. Monitoring of the moisture content of the soil is going to be done by employing a soil moisture sensor. The water level of the tank is monitored by employing a float switch which automatically switches off the motor when the reservoir is filled. The relay module controls the switching On or Off of the pump.

The advantage of this system over existing conventional method is that the reservoir will get automatically filled up as and when required. The soil will also have required moisture level. It will therefore help in avoiding under watering as well as overwatering of soil. Human resource and resource of water will again be saved.

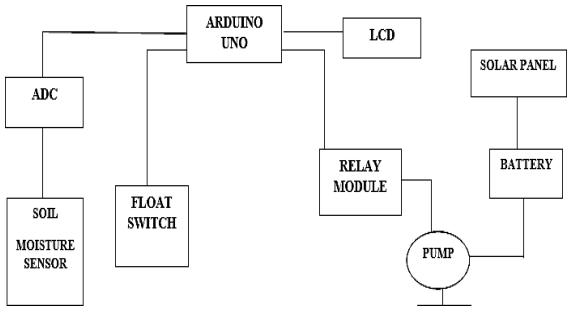

Fig. 2. Block diagram for Solar powered smart irrigation system

- *Smart home automation system:*

The home automation systems are used for controlling the indoor & outdoor lights, heat, ventilation, air conditioning in the house, to lock or open the doors & gates,

to control electrical & electronic appliances and so on using various control systems with appropriate sensors.

Home automation is a combination of hardware, communication medium, and electronic interfaces that work to integrate everyday devices with one another via the Internet. Each device has sensors and is connected through Wi-Fi to manage them from our Smartphone or tablet whether we're at home, or from any remote location having internet facilities. Sensors can monitor deviations in physical conditions of the environment. Home automation systems can then adjust those settings (and more) to our preferences. This is the expansion and advancement of wired automation which uses wireless technologies like IR, Zigbee, Wi-fi, GSM etc. Also, Node MCU with the Relay board is one of the most common hardware that can be used for providing the controlling of home equipment via smart phone.

The system involves the control of Node MCU's GPIO from a webpage on any device connected on the same network as the board. The status of the GPIO's controls the coil of the relays and causes the relay to alternate between normally open (NO) and normally close (NC) condition depending on the state of the GPIO, thus effectively turning the connected appliance "ON" or "OFF".

The advantage of this system over the existing conventional methods is that the system will help old aged, specially-abled people to operate the equipment from their mobile phone. The application can be used without the same switch being touched by multiple persons.

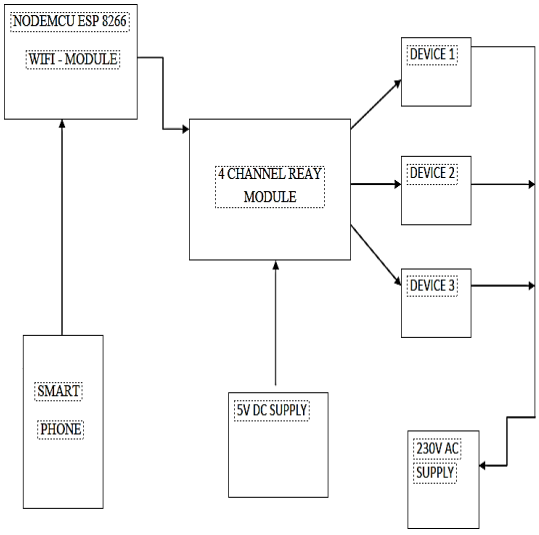

Fig. 3. Block diagram for Smart home automation system

The system will therefore be a low cost, reliable and scalable home automation system that can be operated by remotely switching ON or OFF any household appliance. The system would use a microcontroller and the result would be very user friendly. It may use short messaging system, voice call or a tap on app to switch stages. It may include an electronic smart metering system too. This system can be operated even if away from home. The smart metering system will keep the consumer aware of the energy consumption. The consumer may then plan and reduce energy usage.

- *Smart fire and smoke protection system:*

This system finds its application widely in kitchen for safety purpose. System will detect fire hazards and toxic gases within a limited range. This system will alert anyone near to this incident by putting on the buzzer. This automatic protection system will automatically spread water. This system can be designed using Arduino, temperature sensors. If any gas leakage occurs then it will detect the gas with the help of MQ2 sensor. It will alert anyone near to the incident by using buzzer. Even if fire hazard occurs, it will detect it quickly and the alarming system will work again. This automatic protection system will automatically spread water if any kind of fire hazard occurs.

The system is cost effective and easily applicable to homes. It will reduce accidents due to gas leakage.

- *Smart light intensity controlling system:*

This concept finds a huge scope in lighting system of staircase, lawns, or outdoor lighting areas of the homes. This idea emphasizes automatic turning on or turning off lights that is decided by the intensity of natural light. It also ensures the efficient control of intensity of light in presence of object. If there is movement of object in a particular zone, the movement will result in glowing of the lights with maximum intensity otherwise light intensity will be reduced as a result of which power is saved to some extent. By using this system lot of energy can be saved. Whenever there is sufficient sunlight in surroundings, LDR behaves like high Resistance while in darkness this LDR behaves as low resistance Path and allows the flows of electricity, this LDR's operates with the help of IR sensors, these sensors are activated under low illumination conditions and these are controlled by an microcontroller. When any object comes in the range of IR sensors, as IR LED emits the radiations and reflected back to IR photodiode by the object. Hence, object is detected. The switching of the LEDs is operated through coding applied in Arduino using Arduino Software.

The system helps avoiding unnecessary staircase lights being kept ON even when no one is there.

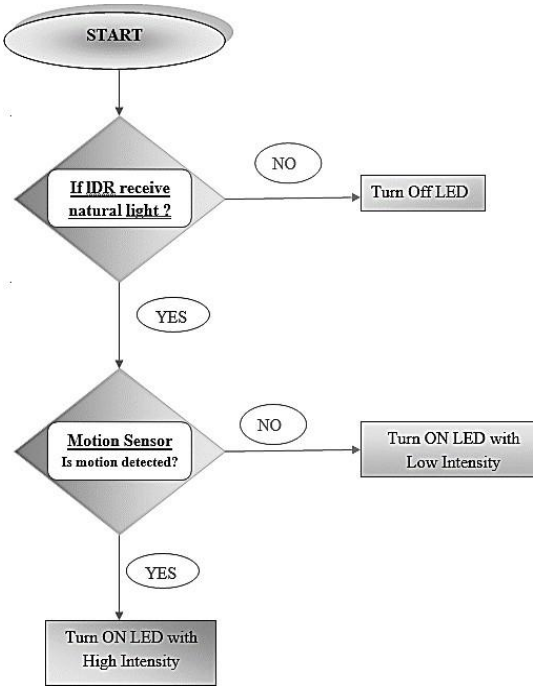

Fig. 4. Block diagram for Smart light intensity controlling system

V. SMART HOME CHALLENGES:

The main challenge of smart home is that all the appliances involve smart technology which may be very costly. During the consistent operation of various integrated devices, there may be delay or interruption with any new devices. Bandwidth consumption is another challenge for IoT connectivity. Managing bandwidth in home network also become challenging with the increasing number of personal and household devices. In a connected IoT network of devices, reliability of bidirectional signalling plays a pivotal role in for collecting and routing data between devices and in this case IoT data streams plays the role. All the devices in the smart home network may communicate to a server to collect data, or the server responds the devices effectively.

VI. FUTURE SCOPE:

The introduction of these technologies will bring a boom in the job generation for engineering graduates in both manufacturing and repairing and maintenance. The smart technologies will also awaken common people about the advantages of engineering.

The technologies may then be applied for small scale industries and also large-scale industries.

VII. CONCLUSION

New revolutions in communication systems and AI, has provided residential houses to reach new dimension of quality of life and security as well as reduction in energy wastage. Smart homes obviously have the ability to make life easier and more convenient. Smart home technology promises tremendous benefits for an elderly person living alone as they can easily fulfil their need via minimum physical effort. This paper based on the meaning of smart resident buildings and summarily description of few main points concerning smart home. these documents could provide a good basis of further research, design and eventual implementation.

REFERENCES

[1] Iot And Its Connectivity Challenges in Smart Home S. Pradeep1, T. Kousalya2, K. M. Aarsha Suresh3, Jebin Edwin4, International Research Journal of Engineering and Technology (IRJET)

[2] Smart buildings features and key performance indicators Joud Al Dakheel 2020: etal.:review,https://doi.org/10.1016/j.scs.2020.1023 28

[3] Drushti Desai1, Hardik Upadhyay, Security and Privacy Consideration for Internet of Things in Smart Home Environments, International Journal of Engineering Research and Development, 10(11), (2014), pp. 73-83.

[4] Moataz Soliman, Tobi Abiodun, Tarek Hamouda, Jiehan Zhou, and Chung-Horng Lung, “Smart Home: Integrating Internet of Things with Web Services and Cloud Computing”, IEEE International Conference on Cloud Computing Technology and Science, 2013, pp. 317-320

[5] M. Al-Qutayri, H. Barada, S. Al-Mehairi, and J. Nuaimi, “A Framework for an End-to-End Secure Wireless Smart Home System”, IEEE International Systems Conference Montreal, Canada, April 7-10, 2008Y. Yorozu, M. Hirano, K. Oka, and Y. Tagawa, “Electron spectroscopy studies on magneto-optical media and plastic substrate interface,” IEEE Transl. J. Magn. Japan, vol. 2, pp. 740–741, August 1987 [Digests 9th Annual Conf. Magnetics Japan, p. 301, 1982].

[6] M. Young, The Technical Writer’s Handbook. Mill Valley, CA: University Science, 1989.

AN OVERVIEW ON COGENERATION SYSTEM

Sayak Pal
Lecturer
Electrical Engineering Department
Technique Polytechnic Institute,
Hooghly, India
sayakpal30@gmail.com

Shamik Chattaraj
Lecturer
Electrical Engineering Department
Technique Polytechnic Institute,
Hooghly, India
chattaraj.shamik@gmail.com

Snehashis Das
Lecturer
Electrical Engineering Department
Technique Polytechnic Institute,
Hooghly, India
snnehashis@gmail.com

Tamal Hazra
Student
Electrical Engineering Department
Technique Polytechnic Institute,
Hooghly, India
tamalhazra02@gmail.com

***Abstract*— The contribution of cogeneration plants to a reduction in primary energy consumption will be important not only in lowering emissions to the atmosphere but also in cutting production costs by increasing the overall efficiency of fuel conversion to the electricity and heat used by process industries. Some basic factors of cogeneration, tri-generation & multi generation system have been discussed in this paper. Relation between cogeneration and gas turbine has been shown here. This paper shows basic details of cogeneration and some of its applications.**

Keywords*— *Cogeneration, Efficiency, Tri-generation

I. INTRODUCTION

Fossil fuel crisis is a very much talkative topic in now days. Fossil fuel is the main source of energy throughout the world. Due to its depleting layer, maximum countries in the world are searching for new resources of energy. Renewable energy is one of the results of that search. But concept of cogeneration can also be helpful to mitigate the energy crisis. But cogeneration is not new concept. It came to Europe in the last segment of 1880s and in the USA early 1900s. During this time maximum industries produced their own electrical energy from coal fired power plants. Many of these industrial plants used the exhaust steam for its industrial process purposes. But due to some unavoidable circumstances, the cogeneration concept came to halt. In early 1970s when the fuel cost started to uprising and uncertainty of fuel supply, again triggered the cogeneration [1]. It was in particular for bigger industries where different types of large quantities steams were needed. In very recent small cogeneration systems have introduced to make inroads in the food, pharmacy, light manufacturing industries etc.

II. COGENERATION

It is the combination of two energy sources from a primary energy source. The primary energy sources typically mechanical energy and thermal energy. Mechanical energy can be used in generator for production of electrical energy or to drive various types of motors, fans, and pumps etc. which are

used in various industrial activities. Thermal energy has application in production of steam, hot water, hot air for cooled water etc. Cogeneration is also known as combined heat and power (CHP) [1]. Cogeneration has various applications in different sectors of economic activities. The system efficiency some time reaches to 85% which can be shown by given figure.

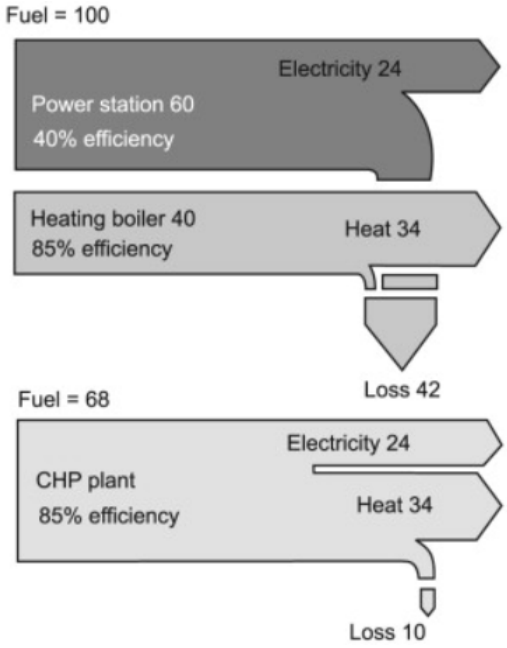

Fig. 1. Advantage of cogeneration

From the above figure, it is considered that power station will need 24 units of electrical energy and boiler needs 34 units of heat energy and also consider total fuel is 100 units. The input fuel (separately) to power plant is 60 and in boiler are 40 respectively. It is because for plant and boiler the efficiencies are 60% and 85% respectively. Fuel loss is 100-(24+34)=42. It is totally uneconomical system. But if cogeneration (CHP) considers, with 85% efficiency, only 68 fuel units are required and loss only 10 units of fuel. So in cogeneration total system efficiency is highly improved, less amount of fuel is needed and loss decreases considerably. Cogeneration also reduces emission of greenhouse gases. Production of electrical energy on site remove utility burden on the network and transmission losses.

III. MAIN COMPONENTS OF COGENERATION

There are mainly four main components present in a cogeneration facility. They are as follows (a) prime mover or turbine (b) a turbo alternator (c) A heat recovery boiler is installed to generate steam from energy contained in the exhaust gas of the turbine. Energy extraction can be

maximized by set up a standard economizer at the output side coif the heat recovery boiler & (d) control system.

IV. MAIN COMPONENTS OF COGENERATION

Technology	Fuel	Typical Size (MWe)	Electrical Efficiency	Heat to power ratio (HTPR)	Overall Efficiency
Spark ignitionn reciprocating engine	Natural gas / bio gas / diesel	0.0 0.3 to 6	25% to 43%	1:1 to 3:1	70% to 92%
Compression ignition reciprocating engine	Natural gas / bio gas / diesel / heavy fuel oil	0.2 to 20	35% to 45%	0.5:1 to 3:1	65% to 90%
Combied cycle turbine	Natural gas / bio gas / diesel / heavy fuel oil	3 to 300	35% to 55%	1.1:1 to 3:1	73% to 90%
Open cycle turbine	Natural gas / bio gas / diesel	0.2 5 to 50	25% to 42%	1.5:1 to 5:1	65% to 87%
Back pressure Steam turbine	None	0.5 to 500	7% to 20%	3:1 to 10:1	Maxi mum 80%
Extraction steam turbine	None	1 to 100	10% to 20%	3:1 to 8:1	Maxi mum 80%

V. FACTORS FOR SELECTION OF COGENERATION SYSTEM

The following factors can be considered in regarding cogeneration selection.

- Normal and terminal load (maximum or minimum) demand and steam load demand on the plant.
- Importance of electrical load or steam load.
- Load variation or fluctuation with respect to time.
- Types of fuel available for the process (Natural gas/bio gas/diesel/heavy fuel oil).
- Life span of various systems in the plant and maintenance cost.
- Local environmental conditions: space available, soil conditions, raw water availability, infrastructure etc.
- Project cost and long term benefits.
- Total project completion time.

VI. TRI-GENERATION & MULTI- GENERATION

Tri-generation is the combination of cooling, heating and power. It is the simultaneous process of electrical power production, heating and cooling from a single energy sources. The single energy source may be a fossil fuel or renewable energy source. One common tri-generation system is to use high temperature heat to drive steam turbine after that low temperature heat is used to produce cooling. The main difference of cogeneration and tri-generation is that in later part both heating and cooling are produced simultaneously. In tri- generation a cooling absorption system is used for providing cooling from thermal energy. To improve the overall efficiency the existing tri- generation system can be converted into multi- generation system. Output will be more than three products from single energy resources. In multi- generation system part of the electricity or cooling or heating is often utilized to produce an extra product viz. hydrogen or dry cleaning purpose etc. multi-generation increases system efficiency which reduces the energy losses. It indicates reducing of fuel usage as well as less amount of CO_2 emission. Ultimately multi-generation helps to minimize the global warming effect by this process. Below figure shows how system efficiency increases from single output to multi output.

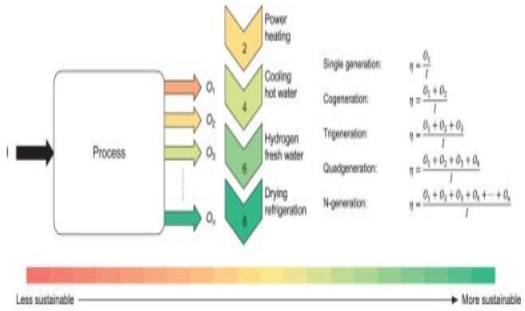

Fig. 2. Multi-generation energy efficiencies as the number of output increases [3]

VII. COGENERATION & GAS TURBINE:

Process plants are often used cogeneration because they want better return on investment (ROI)[4] on the process than utility. In this case cogeneration is more useful than two separate two sources of energy i.e. electrical and thermal. In process control plants both the energies are required. The following calculations are important to understand the whole methodology.

Consider, E=electric energy generated, ΔH=heat energy from process steam, Q=heat added to the plant from fuel.

Now cogeneration efficiency, ηco= (E+ΔH)/Q.

For separate electricity and steam generation, the heat added the unit of total energy is ((e/ηe)+(1-e)/ ηh), where e= electric fraction of total energy output=(E/E+ΔH), ηe=electric efficiency, ηh= heat efficiency. The combined efficiency for separate generation is ηc=1/((e/ηe)+(1-e)/ ηh). In most of the cases, ηco > ηc , which gives better ROI.

VIII. APPLICATION OF COGENERATION

Cogeneration is utilized in following process control industries such as petrochemicals, Fertilizers, Sugar, textiles, paper, food & dairy, hotel.

REFERENCES

[1] Alipour, Manijeh, Behnam Mohammadi-Ivatloo, and Kazem Zare. 2014. “Stochastic RiskConstrained Short-Term Scheduling of Industrial Cogeneration Systems in the Presence of Demand Response Programs.” Applied Energy 136 (December): 393– 404.

[2] doi:10.1016/j.apenergy.2014.09.039.

[3] Brown, Tom, David Schlachtberger, Alexander Kies, and Martin Greiner. 2016. “Sector Coupling in a Highly Renewable European Energy System.” In 15th Wind Integration Workshop. Vienna.

[4] https://www.sciencedirect.com/science/article/pii/B9780124172036000053

[5] https://www.sciencedirect.com/science/article/pii/B9780750679695500089

[6] European Commission. 2016. “An EU Strategy on Heating and Cooling. COM(2016) 51 Final.” doi:10.1017/CBO9781107415324.004. European

[7] Union. 2012. “Directive 2012/27/EU of the European Parliament and of the Council of 25 October 2012 on Energy Efficiency.”

[8] Grohnheit, Poul Erik. 1993. “Modelling CHP within a National Power System.” Energy Policy 21 (4): 418–29. doi:10.1016/0301-4215(93)90282- K.

[9] Haghrah, A., M. Nazari-Heris, and B. Mohammadi-ivatloo. 2016. “Solving Combined Heat and Power Economic Dispatch Problem Using Real Coded Genetic Algorithm with Improved Mühlenbein Mutation.” Applied Thermal Engineering 99 (April): 465–

[10] 75.doi:10.1016/j.applthermaleng.2015.12.136.

[11] International Energy Agency. 2014. “Linking Heat and Electricity Systems.” Paris.

[12] International Renewable Energy Agency. 2016. The Power To Change : Solar and Wind Cost Reduction Potential To 2025.

[13] Lowe, Robert. 2011. “Combined Heat and Power Considered as a Virtual Steam Cycle Heat Pump.” Energy Policy 39 (9). Elsevier: 5528–34. doi:10.1016/j.enpol.2011.05.007. in a Highly Renewable European Energy System.” In 15th Wind Integration Workshop. Vienna.

[14] https://www.sciencedirect.com/science/article/pii/B9780124172036000053

[15] https://www.sciencedirect.com/science/article/pii/B9780750679695500089

[16] European Commission. 2016. “An EU Strategy on Heating and Cooling. COM(2016) 51 Final.” doi:10.1017/CBO9781107415324.004. European

[17] Union. 2012. “Directive 2012/27/EU of the European Parliament and of the Council of 25 October 2012 on Energy Efficiency.”

[18] Grohnheit, Poul Erik. 1993. “Modelling CHP within a National Power System.” Energy Policy 21 (4): 418–29. doi: 10.1016/0301-4215(93)90282- K.

[19] Haghrah, A., M. Nazari-Heris, and B. Mohammadi-ivatloo. 2016. “Solving Combined Heat and Power Economic Dispatch Problem Using Real Coded Genetic Algorithm with Improved Mühlenbein Mutation.” Applied Thermal Engineering 99 (April): 465–75.doi:10.1016/j.applthermaleng.2015.12.136.

[20] International Energy Agency. 2014. “Linking Heat and Electricity Systems.” Paris.

[21] International Renewable Energy Agency. 2016. The Power To Change : Solar and Wind Cost Reduction Potential To 2025.

[22] Lowe, Robert. 2011. “Combined Heat and Power Considered as a Virtual Steam Cycle Heat Pump.” Energy Policy 39 (9). Elsevier: 5528–34. doi:10.1016/j.enpol.2011.05.007.

CFD assessment of MHD induced half sinusoidal bottom heated thermo-gravitational convective transport of hybrid nanofluid in porous cavity

Alankrita Chattopadhyay
Department of Mechanical Engineering,
Medinipur Sadar Govt Polytechnic,
Paschim Medinipur 721102, India
Email: alankritachatterjee8637@gmail.com

Joydeep De
Department of Mechanical Engineering,
Medinipur Sadar Govt Polytechnic,
Paschim Medinipur 721102, India
Email: joy.bibhu@gmail.com

Barun B. De
Department of Mechanical Engineering,
Medinipur Sadar Govt Polytechnic,
Paschim Medinipur 721102, India
Email: barunde123@gmail.com

Shovan Dogra
Department of Mathematics,
Medinipur Sadar Govt Polytechnic,
Paschim Medinipur 721102, India
Email: shovansd39@gmail.com

Sobhan Pandit
Department of Mechanical Engineering,
Medinipur Sadar Govt Polytechnic,
Paschim Medinipur 721102, India
Email: sobhanpandit100@gmail.com

Milan K Mondal*
Department of Mechanical Engineering,
Medinipur Sadar Govt Polytechnic,
Paschim Medinipur 721102, India
Email: milanmondal@gmail.com

***Abstract* - A narrative loom in possessions of externally induced thermomagnetic field, nonuniform heating profile frequency, amplitude on fluid flow and heat transport of Cu-Al2O3 blended nanoparticles mixed with water called hybrid nanofluid within porous cavity is lucidly investigated in the present work. The problem geometry is half sinusoidal heated profile at bottommost wall anchored in a range of frequencies (f), amplitude (I) and cooled at the side walls. Fluids enter through two ports of bottom section of side walls and going out mid-center port of top wall. Finite Volume Method (FVM) is adopted for sprouting lab based numerical simulation and same is implemented for solution of governing complex equations. The exploration is conceded underneath the result of an option of important parameters as Re, Ri, Ha, Da, ε, ϕ. Heat lines, streamlines, Isotherms contours and linked heat transport rate of these parametric induced cases are examined scrupulously. This is examined that the energy transmit rate is augmented at elevated Re, Ri, Da and ϕ with the rising frequency whereas Ha values reduce average Nusselt values.**

Keywords: *— Non-uniform heating; half sinusoidal frequency; hybrid nanofluid; magnetohydrodynamic (MHD); Heat lines.*

I. INTRODUCTION

Over the decade, 'Nano' a small word with immense potentiality has been promptly devious itself into the world's realization. Nano science has stimulated from humankind of future to civilization of present. Technology adopted Nano material has been battering its existence reflect on industry, and numerous applications are already standardized. Erstwhile nanomaterials acquire unique, useful chemical, physical, and mechanical property; they might be utilized for an extensive assortment of applications be fond of next-gen computer technology, aeronautical mechanism, spaceship applications, and several others. Ultimately growth of nano technology products is owing to next industrial insurgency. Accepting major challenges in potential engineering apparatus and devices in recent times, this study explores the fundamental physics of mixed convection heat transport beneath external induced MHD field throughout a intricate porous configuration in a half sinusoidal heated enclosed area. The varied applications of allied issues replicated for example electronic device, heat exchangers, solar thermal appliance, and food processing engineering, MEMs and large numbers of others. Consequently, thermal supervision in convection contained by flow diminishing porous media and field of MHD amid heated source to cold sink has been a important topic of apprehension [1–3]. This sort of effect with heater and cooler base added intricate magneto-thermos-flow concern with additional multi-physical status. In this point of view, benefit of heating non-uniformly in porous enclosure is stated by Biswas et al. [4]. Afterward, Manna et al. [5] investigated that sinusoidal heating be able to an effectual way for enhancing heat transport rate in a thermos-flow system. Further comprehensive assessments on thermos-convective study with hybrid nanofluid or nanofluid are convincingly reported in references. [3, 5–7]. Bouncy-dominated convective flow in porous cavity containing special fluid adopting varying boundary provisions are highlighted by Ramakrishna et al. [7]. In the recent investigation, useful characteristic of Cu-Al_2O_3 blended pure water hybrid nanofluid non-uniform heating consequence under the control of heating with sinusoidal profile has been exhaustively scrutinized by Mondal et al. [14] and Tayebi and Chamkha [8].

Through this massive collection of accessible literatures, this is apprehended that half sinusoidal non-uniform

heating relevance is applicable in a diversity of thermos-fluid structure for investigating heat transport added to suitable control to this system [9, 10]. Accordingly, intend of this examination is to learn magneto-thermo mixed convection with Cu-Al_2O_3-water packed porous enclosure with bottom wall heated half sinusoidally revealed in Fig. 1. Heating contour is employed at wall of enclosed space adopting nondimensional parameter as "amplitude (*A*)". Fluids enter through two ports of bottom section of side walls and going out mid-center port of top wall. The hot fluid is liberating heat throughout cold side walls along with fluid flown in cavity. Consequently, the present study is formulated and inspired by need to analyze thermos-flow and transport process of a half sinusoidal bottom heated area beneath a range of significant parameters like Reynolds, Hartmann, Darcy number and Cu-Al_2O_3 blended hybrid nano scale particles concentrations in water. The outcomes are presented by contour maps of streamlines, isotherms, heatlines and Nusselt average. Heatlines is the visualization tools to demonstrate the heat flux flow process from heat source to sink. In present work, the incorporation of flow in and out along with supplementary multi-physical events is a new role in this research area.

II. PHYSICAL DOMAIN AND FORMULATION

A schematic diagram of the problem geometry including the boundary settings is described in Fig. 1. The computational domain is two-dimensional (in *x*-*y* plane) square enclosure with length *L* and height *H* (*L* = *H*) composed of superposed hybrid nanofluid-porous substance. The enclosure is heated half sinusoidally (temperature T_h) at bottom wall is permitted to exchange heat with side walls (temperature T_c, such that $T_h > T_c$). Top wall are thermally insulated. Two bottom portions (of w_i = 0.1*L*) of both side walls are opened through which hybrid nanofluid, Cu−Al_2O_3-water enter and mid portion (of w_o = 0.2*L*) top wall is opened by which hot fluid going out. Enclosure is also composed of, saturated porous substances. External generated a uniform magnetic field of strength *B* may be induced (horizontally from left side wall) over entire length of enclosure.

The governing hyperbolic nonlinear equations are obtained for a 2-D flow of continuity, X and Y-momentum and energy which are non-dimensional with length scale by *L*, velocity scale by V_w, also temperature and pressure expressed by $\theta = (T - T_c)/(T_h - T_c)$ $P = (p - p_a)/\rho V_w^2$ respectively. Consequential dimensionless equations are

$$\frac{\partial U}{\partial X} + \frac{\partial V}{\partial Y} = 0 \tag{1}$$

$$\frac{1}{\varepsilon^2}\left(U\frac{\partial U}{\partial X} + V\frac{\partial U}{\partial Y}\right) = -\frac{\rho_f}{\rho}\frac{\partial P}{\partial X} + \frac{\nu}{\nu_f}\frac{1}{\varepsilon \mathrm{Re}}\left(\frac{\partial^2 U}{\partial X^2} + \frac{\partial^2 U}{\partial Y^2}\right) - \left(\frac{\nu}{\nu_f}\frac{1}{\mathrm{Da}\,\mathrm{Re}} + \frac{F_c\sqrt{U^2+V^2}}{\sqrt{\mathrm{Da}}\,\varepsilon^{3/2}}\right)U \tag{2}$$

$$\frac{1}{\varepsilon^2}\left(U\frac{\partial V}{\partial X} + V\frac{\partial V}{\partial Y}\right) = -\frac{\rho_f}{\rho}\frac{\partial P}{\partial Y} + \frac{\nu}{\nu_f}\frac{1}{\varepsilon \mathrm{Re}}\left(\frac{\partial^2 V}{\partial X^2} + \frac{\partial^2 V}{\partial Y^2}\right) - \left(\frac{\nu}{\nu_f}\frac{1}{\mathrm{Da}\,\mathrm{Re}} + \frac{F_c\sqrt{U^2+V^2}}{\sqrt{\mathrm{Da}}\,\varepsilon^{3/2}}\right)V + \frac{\rho_f}{\rho}\frac{\sigma}{\sigma_f}\frac{\mathrm{Ha}^2}{\mathrm{Re}}V + \frac{(\rho\beta)}{\rho\beta_f}\mathrm{Ri}\,\theta \tag{3}$$

$$\left(U\frac{\partial \theta}{\partial X} + V\frac{\partial \theta}{\partial Y}\right) = \frac{\alpha}{\alpha_f}\frac{1}{\mathrm{Re}\,\mathrm{Pr}}\left(\frac{\partial^2 \theta}{\partial X^2} + \frac{\partial^2 \theta}{\partial Y^2}\right) \tag{4}$$

where,

$$\mathrm{Re} = \frac{V_w H}{\nu_f};\ \mathrm{Pr} = \frac{\nu_f}{\alpha_f};\ \mathrm{Da} = \frac{K}{H^2};\ F_c = \frac{1.75}{\sqrt{150}};\quad \mathrm{Ha} = B_o H\sqrt{\sigma_f/\mu_f};\ \mathrm{Ri} = \frac{\mathrm{Gr}}{\mathrm{Re}^2};\ \mathrm{Gr} = \frac{g\beta_f (T_h - T_c)H^3}{\nu_f^2}; \tag{5}$$

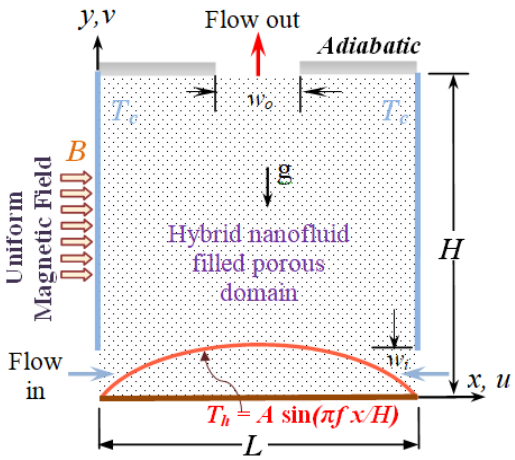

(a) Problem geometry and boundary

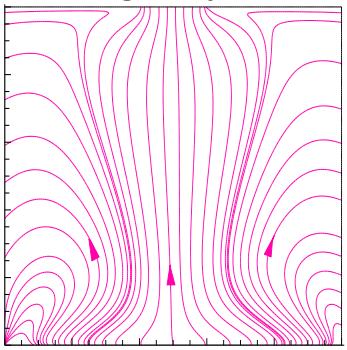

(b) Heatlines

Fig. 1. Schematic problem geometry of (a) physical domain (b) heat flow visualization.

In equations (1) – (4), non-dimension parameters are assigned by Reynolds number Re, Richardson number Ri, Grash of number Gr, Prandtl number Pr (= 5.83, constant), Darcy number Da, For chheimer coefficient F_c, and Hartmann number Ha. Also non-dimensional velocity components are *U* in *X* and *V* in *Y* coordinates and *g* is acceleration due to gravity. Likewise, subscript '*f*' and 's' are employed to specify the thermos-physical properties for host fluid and solid nano scale particles respectively. The symbol 'ϕ' is used to symbolize the blend of hybrid-nanoparticles volumetric fraction. Effectual properties of hybrid nanofluid could be defined as

Mass density:

$$\rho = (1-\phi)\rho_f + \phi_{Al_2O_3}\,\rho_{Al_2O_3} + \phi_{Cu}\,\rho_{Cu} \tag{6}$$

sp. heat capacity:

$$(\rho c_p) = (1-\phi)(\rho c_p)_f + \phi_{Al_2O_3}(\rho c_p)_{Al_2O_3} + \phi_{Cu}(\rho c_p)_{Cu} \quad (7)$$

Thermal expansion:

$$(\rho\beta) = (1-\phi)(\rho\beta)_f + \phi_{Al_2O_3}(\rho\beta)_{Al_2O_3} + \phi_{Cu}(\rho\beta)_{Cu} \quad (8)$$

Thermal conductivity:

$$k = k_f\left[\frac{(k_s+2k_f)-2\phi(k_f-k_s)}{(k_s+2k_f)+\phi(k_f-k_s)}\right] \quad (9a)$$

$$\phi k_s = \phi_{Cu}k_{Cu} + \phi_{Al_2O_3}k_{Al_2O_3} \quad (9b)$$

Electrical conductivity:

$$\sigma = \sigma_f\left[1+\frac{3(\sigma_s/\sigma_f-1)\phi}{(\sigma_s/\sigma_f+2)-(\sigma_s/\sigma_f-1)\phi}\right] \quad (10a)$$

$$\phi\sigma_s = \phi_{Cu}\sigma_{Cu} + \phi_{Al_2O_3}\sigma_{Al_2O_3} \quad (10b)$$

Thermal diffusivity:

$$\alpha = \frac{k}{(\rho c_p)} \quad (11)$$

Viscosity:

$$\mu = \frac{\mu_f}{(1-\phi)^{2.5}} \quad (12)$$

The imposed boundary conditions for the current numerical simulation are as follows:

$U = V = \partial\theta/\partial Y = 0$ - top adiabatic wall

$U = V = 0,\ \theta = 0$ - left and right-side walls,

$\theta = A\sin(\pi f\ x/\mathrm{L})$, $V = U = 0$ for heated bottom wall

Flow in, $U = \pm 1$ (in either side), and flow out, $V = 1$

The average distribution of heat transport uniqueness over the active walls of the enclosure are calculated by the average Nusselt number (Nu) as formulated by

$$\mathrm{Nu} = \frac{k}{k_f}\int_0^1 \left(-\frac{\partial\theta}{\partial Y}\Big|_{X=0}\right) dX \quad (13)$$

Localized contour fluid-flow patterns within computational domain envisaged employing streamlines, which is considered from determined velocity fields by producing stream function ψ and is articulated as

$$-\frac{\partial\psi}{\partial X} = V \text{ and } \frac{\partial\psi}{\partial Y} = U \quad (14)$$

Additionally, transportations of heat flow are foreseen by by means of heat lines contour. The perception of heat lines is used here to signify the pathway of heat flux flow. The heat lines are principally produced from energy equilibrium in steady-state state and it is determined from heat function (Π), which may be formulated as

$$-\frac{\partial\Pi}{\partial X} = V\theta - \frac{\partial\theta}{\partial Y} \text{ and } \frac{\partial\Pi}{\partial Y} = U\theta - \frac{\partial\theta}{\partial X} \quad (15)$$

III. NUMERICAL METHODOLOGY

The governing equations (1) – (4) in conjunction with suitable boundaries identify a set of nonlinear, non-dimensional coupled differential equations are solved in succession by means of indigenous CFD program implementing FVM approach. The set of equations are initially converted into algebraic forms, which are being iteratively solved through TDMA solver and ADI sweep using SIMPLE algorithm. Non-uniform staggered grid (160×160) distributions are used for the discretization. Converging solutions are acquired throughout the iteration procedure, in anticipation of normalized maximum values of residuals and continuity mass defect go with less than 10^{-8} and 10^{-10}, respectively.

IV. RESULTS AND DISCUSSION

In current investigation, effect of half sinusoidal heating of bottom most walls with varying frequency on heat transfer and both way flow of blended hybrid nanofluid inside porous cavity under MHD effect is investigated in mixed convection. Consequences of varied related parameters are analyzed broadly for a choice of parametric variation as: Richardson number ($0.1 \le Ri \le 100$), Reynolds number ($10 \le Re \le 200$), Darcy value ($10^{-5} \le Da \le 10^{-1}$), Hartmann number (0 (no field)$\le$ Ha $\le$70), volume fraction (0 (no particle)$\le \phi \le$2%), treating porosity value ε = 0.6 and amplitude (A =1.0) fixed, and frequency magnitude chosen as f = 1 to 7. Results are demonstrated by means of flow path using streamlines, temperature distribution by isotherms, energy flux by visualization of heat lines contour and also heat exchanges in the system by Nusselt values.

A. *Impact of half sinusoidal heating frequency f*

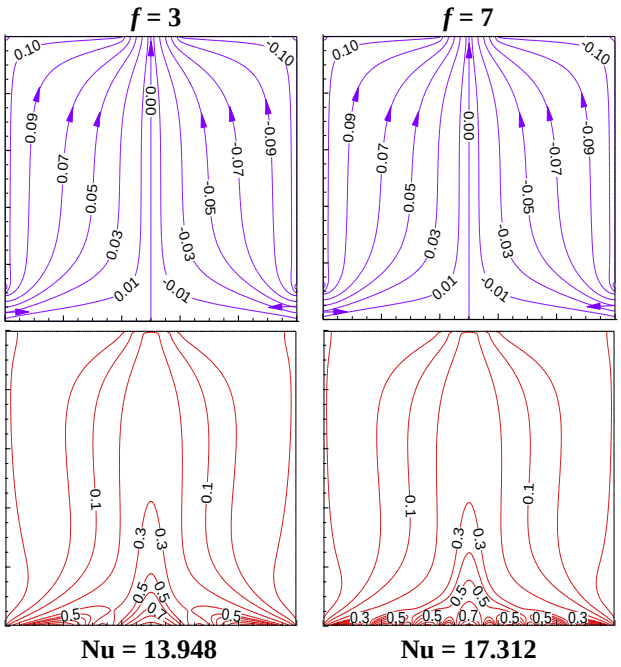

Fig. 2. Impact of *half sinusoidal heating multi frequency on* streamlines (first row), and isotherms (second row) at Re = 100, Ri = 10, Da = 10^{-3}, Ha = 30, ϕ = 0.1%.

Impact of multi frequency of non-uniform half-sinusoidal heating thermal profile on thermos-flow is looked into and exemplified in Fig. 2 for two frequency f = 3, and 7 maintaining other parameters constant as defined. Temperature distribution, demonstrates alike dynamics excepting for bottom section (close to hot wall) of cavity and perseveres for any frequencies as also shown in Fig. 3. Of course, near source wall thermos- flow performance happen to more susceptible and complicated at elevated frequencies. Augment in frequency, flow configurations do not change distinctly, excepting lower section close to source bottom wall. With rise in frequency value, a number of tiny thermal energy recirculation cells appear, and this

number is essentially a function of heating frequency. Temperature allocation (isotherms) closer to source wall specify the existence of unlike peaks numbers as 3 peaks for f = 3, 7 peaks for f = 7 for heating frequency). Obviously, fluid temperature layers, near to hot wall modifies following state of heating. Flow pattern in both frequencies show similar as reflected by streamlines

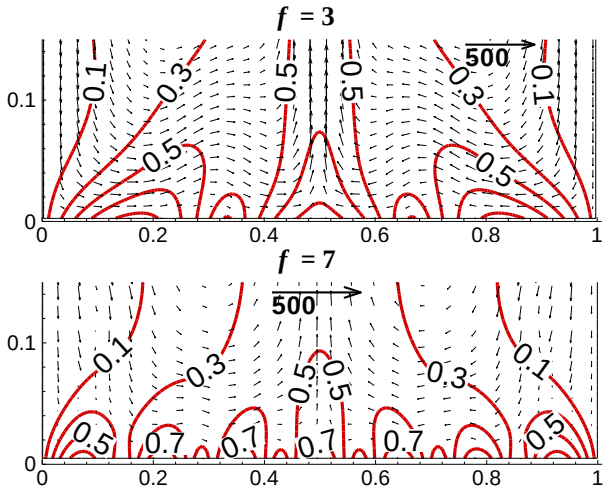

Fig. 3. *Multi frequency impact on* vector and isotherms contour near to hot boundary at Re=100, Ri = 10, Da = 10^{-3}, Ha = 30, ϕ = 0.1%.

B. Impact of flow velocity (Re)

The influence of flow velocity defined by Reynolds number Re on the thermo-hydrodynamics is investigated utilizing different velocities of hybrid nanofluid through active ports of side walls viewed in Fig. 4. Using same fluid and flow domain, unlike velocities are enforced through Re = 10 and 200. Upward velocity of fluid through mid-port of top wall, $v_w = 1$ are considered. Other conditions are taken at Ri = 1, Ha = 30, Da = 10^{-3} and ϕ = 0.1%. At the lower value of Re = 10, the flow structure is dominated by the forced convection. Equivalent heat transfer is governed by thermal conduction. This is obvious from distortion-free isotherms which are disseminated in straightway following profile of active parts of heat source. Energy transportation through heat lines takes place straight forward inflow to outflow allied to hot bottom wall to cold side walls.

However, with augmented Re = 200, the buoyancy dominated flow turn into stronger. The existence of traditional flow-scenarios appears in the enclosure. While Re rises, Gr raises by square of Re. With constant Ri, as Re have an effect on both fluid motion and Gr, elevated Re value severely impacts on flow structures of contour. Energy recirculation in heat lines contours is distributed symmetrically about upright mid-plane which covers entire cavity. Thus, heat flows (from heater to cooler) during long fluid flow paths. Heat lines structure for both low and high Re seems nicely flower vase pattern. The magnitudes of Nu specify heat transmit is radically augmented at higher Re.

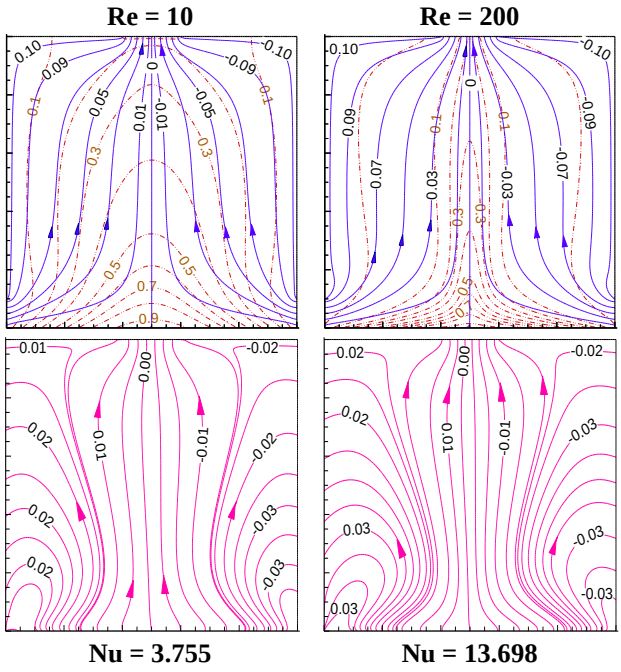

Fig. 4. Reynolds number (Re) impact on streamlines-isotherms coupling (first row), and heat lines (second row) at Ri = 1, Da = 10^{-3}, Ha = 30, ϕ = 0.1%, f = 1.

C. Outcome of Darcy number (Da) *on porous media*

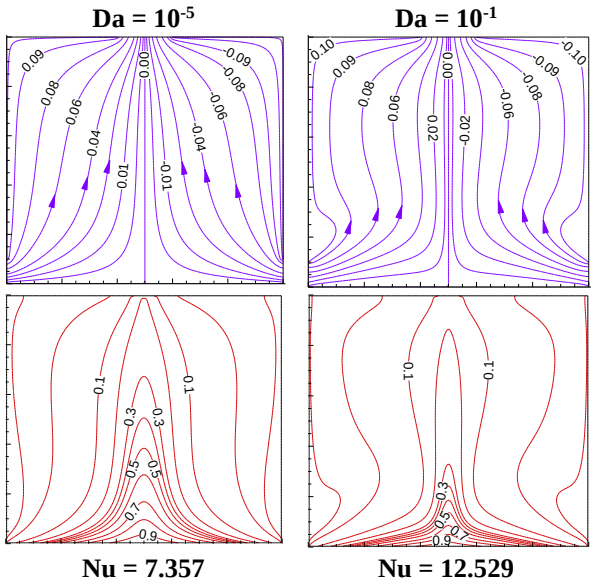

Fig. 5. Porous matrix permeability impact by Darcy number (Da) on streamlines and isotherms at Re=100, Ri = 10, Ha = 30, ϕ = 0.1%, f = 1.

Outcome of Darcy number, Da with unchanging Re = 100, Ri = 10, ϕ = 0.1%, Ha = 30, and f = 1 are represented in Fig. 5 for low to high Da (10^{-5} to 10^{-1}). Normally, less Da is correlated to high resistive porous matrix. Both fluid flows and energy flux progress with high resistance accordingly lessen Nu average value. In augmented Da = 10^{-1}, as knowable with better permeability lesser might be flow resistance. Symmetrical flows come out in plots of streamlines contour and also some distorted contour near inflow path of flow. Subsequent isotherms are symmetrical but curvilinearly disseminated from source to sinks.

Therefore, fluid-based Da indicates a high thermal convection at Da = 10^{-1} comparison to Da = 10^{-5}. Accordingly, overall transmission of heat enhances substantially as reproduced by Nu average values. In addition, choice of Da value manages the thermos-flow heat and cool system along with pathway of nanofluid flow.

D. Intensity of uniform magnetic field (Ha)

MHD impact attributable to horizontal magnetizing field (relating to Ha number) on contours pattern of streamlines and isotherms are visualized in Fig. 6 for varying of Ha = 0(no field), 70 maintain supplementary parameters invariable at Re=100, Ri = 1, Da = 10^{-3}, ϕ = 0.1%, f = 1.

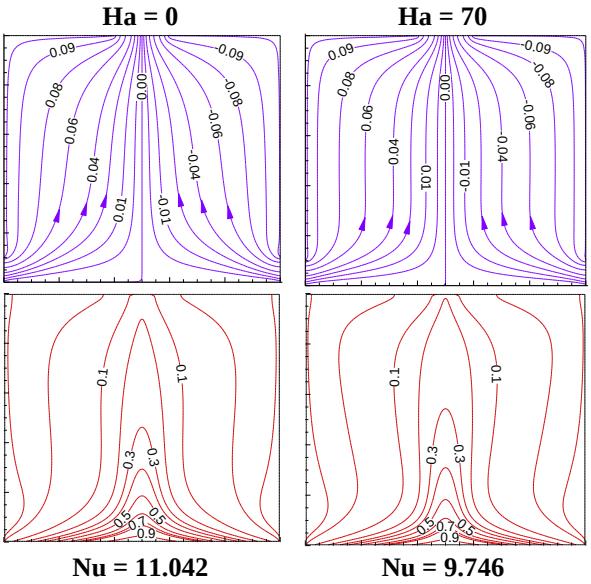

Fig. 6. Magnetic field potency based on Hartmann number (Ha) on contour of streamlines (first row), and isotherms (second row) at Re=100, Ri = 1, Da = 10^{-3}, ϕ = 0.1%, f = 1.

For better investigation, case of absent of magnetic field, Ha = 0 is examined first as epitomized in Fig. 6 followed by high Ha = 70. The flow pattern reflects a symmetric distribution comparative to upright mid-plane. With escalation imposed magnetizing field by increasing Ha value = 70, pattern wise in general flow arrangement are similar with pattern at no field. However, buoyancy-domination becomes weaker which leads to smaller heat transportation and reduction is extreme at elevated Ha = 70.

From the momentum equations as in Eqn. (3), it is perceptible that existence of negative terms with Ha reduces in vertical velocity part as Ha increases. Consequently, magnetizing force counters the positive value of buoyancy force. It governs in further diminution in flow velocity, impacting energy Eq. (4); resulting reduction in energy exchange with rising Ha values. Allied heat transmit rate also reduces as replicated by Nu values.

E. Hybrid Nanoparticles volume fraction (ϕ) influence

The raise in volumetric concentration ϕ = 0.33% and 2% of blended Cu-Al_2O_3 nano-powders and pure water as working fluid on streamlines, isotherms contour and Nu average value are confirmed in Fig. 7 for same values of Re=100, Ri = 100, Da = 10^{-3}, Ha = 30, f = 1.

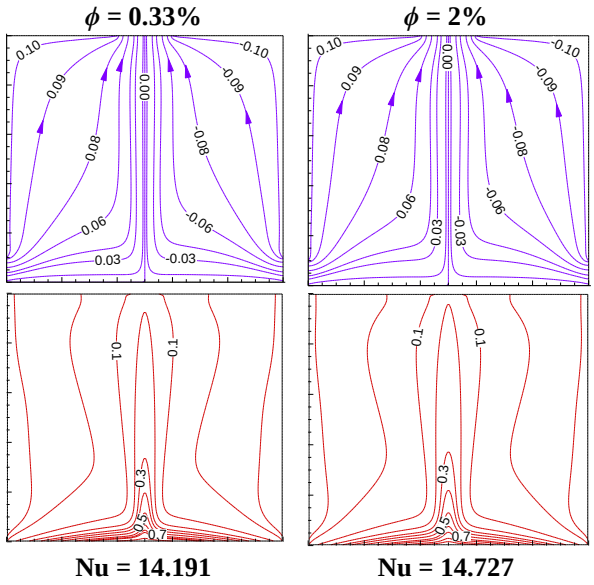

Fig. 7. Inclusion of hybrid nanoparticle volume fraction (ϕ) on streamlines (top panel), and isotherms (bottom panel) at Re=100, Ri = 100, Da = 10^{-3}, Ha = 30, f = 1.

This is reasonably obvious that, inclusion of nanoscale blended hybrid powder in host liquid water owing to augment in flow circulation potency, thereby slight enhancement in heat transport rate. The prime reason behind this augmentation is owing to raise in ϕ governs to increase in effective thermal conductivity of working media as hybrid nanofluid in such mixed convective system.

F. Heat transfer characteristics

Heat transport features shown by Nu curve of the half sinusoidal heated with external flow in and out cavity are plotted in special parametric deviations of Ha, Da, Re, and ϕ for varying Ri within 0.1 to 100 with flow velocity in Fig. 8(a – d). The preset parameters are fixed as f = 1, A = 1, and ε = 0.6. Heat transfer curves are appraised based average Nusselt Nu as formulated in Eq. (13).

Figure 8a reflects Reynolds number variation for an assortment of Re = 10 to 200. With Ri ≤ 1, there is almost analogous consequence of Nu on Re. Though, with Ri = 10 and above, Nu significantly enhances with Re. At elevated Re > 50, heat transmission rate is more. The basis of such augmentation is owing to the truth that as Re raise (with other parameters constant), subsequent Grash of number raises, resulting considerable enhance in buoyancy impact.

Figure 8b reflects Nu curves a continually enhancing trend amid other parameter fixed with increasing of Da value. Rising trend is about analogous for each Ri values. The justification of this verity may be obscured by visualizing the flow configuration at higher Da (as viewed in Fig. 5). As Da increases, resistance to flow through porous media lessens, owing to increase heat transmission.

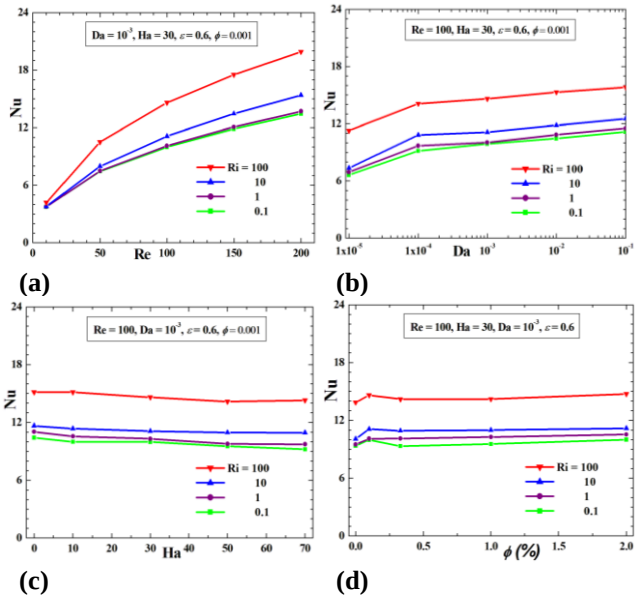

Fig. 8. Heat transport features with altering (a) Reynolds number, (b) Darcy number, (c) Hartmann number and (d) nanoparticle volume fraction

Figure 8c shows consistent declining Nu values with intensifying the magnetizing field, as Ha. This come about buoyancy impact resists the existence of imposed field. Declining trend of Nu plots is almost identical for all 'Ri' value. Buoyant force is counteracted by Magnetizing force that may be actually recognized by observing fluid stream and heat flux flow configuration at higher Ha (as reflected in Fig. 6). Therefore heat transportation progression is affected scrupulously.

Effect of volume fraction alteration of Cu-Al_2O_3 blended nanosize particles for changeable 'Ri' values is shown in Fig. 8d with unvarying parameters. Figure clearly replicates that, with increase in ϕ average Nu increases for 'Ri' values as Nu values for ϕ = 0.33% – 2% shows increasing trend relative to ϕ = 0. This is obvious that at ϕ = 0.1% Nu value is peak which maximizes the option of volume concentration for entire investigation.

V. CONCLUSIONS

A novel investigation leading to active bottom wall with half sinusoidally heating and side walls cooling isothermally along with flow in and out, resulting on transport of heat energy and working fluid medium uniqueness throughout porous area filled with hybrid-nano scale particles blended in base fluid water amid imposed uniform horizontal magnetizing field is analyzed by mathematical simulation adopting FVM. The magneto-thermos-flow phenomena are scrutinized based on exclusive parametric variations like Re, Da, Ha and ϕ. The notable abridgments are accomplished as:

- In MHD based convective system, heat transport characteristic is enhanced significantly for elevated Re and Ri which replicated by the selection of Re, Ri value.
- Intensity of buoyancy supremacy and porous media permeability counteract resistance to flow with intensification in Darcy magnitude within cavity. This outcome for augmentation in heat transfer rate. Such enhancement rate is more prominent at advanced Da.
- Rise in magnetic field strength value, consequence of buoyancy power be in opposition to magnetizing strength following in diminution of heat transmission rate.
- Added blending of hybrid nano-sized particles with base fluid in range of ϕ = 0.33% – 2%, the heat transfer rate increases in respect of host fluid (ϕ = 0) whereas that is maximum at 0.1%.

In finale, this investigation probably will be constructive for designing the exclusive mechanisms where the modest alteration in managing of transport event is a key apprehension. This comprehensive instruction on the present study in view of a blending of solid-fluids flow medium and multi-magneto-thermos-physical circumstances might be the potential opportunity extent of R & D work.

ACKNOWLEDGEMENT

Authors gratefully acknowledge the members of NEPTUNE lab, Mechanical Engineering Department of Jadavpur University, for developing CODE, suggestions and assistance extended by all Professors during this work.

REFERENCES

[1] A. Bejan, I. Dincer, S. Lorente, A. F. Miguel, and A. H. Reis, Porous and Complex Flow Structures in Modern Technologies, Springer, New York, 2004.

[2] Shu-Rong Yan, A. H. Pordanjani, S. Aghakhani, A. S. Goldanlou, and M. Afrand, Effect of nano powder shapes on natural convection of nanofluids inside a square enclosure in presence of fins with different shapes and magnetic field effect, Advanced Powder Technology, 2020, doi.org/10.1016/j.apt.2020.05.009.

[3] N. Biswas, N. K. Manna, and A. J. Chamkha, Effects of half-sinusoidal nonuniform heating during MHD thermal convection in Cu–Al2O3/water hybrid nanofluid saturated with porous media, Journal of Thermal Analysis and Calorimetry, 143: 2021, 1665–1688.

[4] N. Biswas, P. S. Mahapatra, and N. K. Manna, Merit of non-uniform over uniform heating in a porous cavity, International Journal of Heat and Mass Transfer, 78: 2016, 135–144.

[5] N. K. Manna, N. Biswas, and P. S Mahapatra, Convective heat transfer enhancement: effect of multi-frequency heating, International Journal of Numerical Methods for Heat and Fluid Flow, 29(10): 2019, 3822–3856.

[6] N. Biswas, U. K. Sarkar, A. J Chamkha,. and N. K. Manna, Magneto-hydrodynamic thermal convection of Cu– Al2O3/water hybrid nanofluid saturated with porous media subjected to half-sinusoidal nonuniform heating, Journal of Thermal Analysis and Calorimetry, 143: 2021, 1727–1753.

[7] D. Ramakrishna, T. Basak, S. Roy, and I. Pop, Analysis of heatlines during natural convection within porous square enclosures: Effects of amplitudeand thermal boundary conditions, International Journal of Heat and Mass Transfer 59: 2013, 206–218.

[8] T. Tayebi, and A. J. Chamkha, Buoyancy-driven heat transfer enhancement in a sinusoidally heated enclosure utilizing hybrid nanofluid, Computers and Thermal Science 9(5): 2017, 405–421.

[9] N. K Manna, and N. Biswas, Magnetic force vectors as a new visualization tool for MHD convection, International Journal of Thermal Science, 2021.

[10] N. K. Manna, C. Mondal, N. Biswas, U. K. Sarkar, H. F. Öztop, and N. H. Abu-Hamdeh, Effect of spatially intermittently active partial magnetic fields on thermal convection in a half sinusoidally heated porous cavity filled with hybrid nanofluid, Physics of Fluids 33, 2021, doi: 10.1063/5.0043461.

[11] M. K. Mondal, N. Biswas, and N. K. Manna, MHD convection in a partially driven cavity with corner heating, SN Applied Science, 2019, 1–1689.

[12] M. K. Mondal, N. Biswas, N. K. Manna, and Ali J. Chamkha, Enhanced magnetohydrodynamic thermal convection in a partially driven cavity packed with a nanofluid-saturated porous medium, Math Meth Appl Sci. 2021; 1–28, doi: 10.1002/mma.7280.

[13] N. K. Manna, M. K. Mondal, and N. Biswas, A novel multi-banding application of magnetic field to convective transport system filled with porous medium and hybrid nanofluid, Phys. Scr. 96 (2021) 065001, doi.org/10.1088/1402-4896/abecbf.

[14] M. K. Mondal, N. Biswas, A. Datta, and N. K. Manna, Effects of Amplitude on MHD Thermal Convection of Cu-Water Nanofluid Saturated Porous Cavity, ICRAME 2021; NIT Silchar, India.

A narrative loom of multi-banded vertical magnetic field to thermofludic convective porous cavity filled with hybrid nanofluid

Trisha Bhowmik
Mechanical Engineering Department,
Medinipur Sadar Government Polytechnic,
Paschim Medinipur 721102, India
Email: principal.msgp@gmail.com

Joydeep De
Mechanical Engineering Department,
Medinipur Sadar Government Polytechnic,
Paschim Medinipur 721102, India
Email: joy.bibhu@gmail.com

Pratik Roy
Electrical Engineering Department,
Medinipur Sadar Government Polytechnic,
Paschim Medinipur 721102, India
Email: mail2pratik.07@gmail.com

Shovan Dogra
Mathematics Department,
Medinipur Sadar Government Polytechnic,
Paschim Medinipur 721102, India
Email: shovansd39@gmail.com

Ramen Kanti De
Mechanical Engineering Department,
Medinipur Sadar Government Polytechnic,
Paschim Medinipur 721102, India
Email: ramenkantide@gmail.com

Milan K Mondal*
Mechanical Engineering Department,
Medinipur Sadar Government Polytechnic,
Paschim Medinipur 721102, India
*Email: milanmondal@gmail.com

***Abstract* - A CFD based narrative approach of concerning multi-banded vertical magnetizing fields through natural convective system in a linearly heated porous enclosed space is addressed in present study. Transportation occurrence is dealt with heatlines, isotherms, streamlines, and Nusselt values. These results are represented communally for variation of Darcy-Raleigh number, Darcy number, intensity of externally imposed magnetizing field, keeping the fixed value of porosity, and percentage of nanoparticles volume concentration. The special possessions of bandwidths and band numbers of vertical induced magnetizing field are reflective on enduring transport process. The convective strength of flow regime, permeability of the porous medium, strengths of buoyancy and magnetizing fields appreciably control heat and fluid flow. This narrative multi-banding method could be a potential tool to control transportation phenomena involving multi-physics, successfully.**

Keywords* - *Banded vertical magnetic fields; Hybrid nanoscale fluid; Porous enclosure; Natural convection; Magneto-hydro-dynamic.

I. INTRODUCTION

The existence of magnetizing fields in some thermos fluid system develops thermo-magnetic convection, which is recognizable as magneto-hydro-dynamic (MHD) convection. Numerous contemporary devices concerning thermo-magneto structures control underneath assorted multi-physical provisions in existence of porous features, nanofluids or hybrid nanofluids, etc. Appropriate control of transport procedure of such systems is one of the key challenges for researchers. Several modern appliances in bio-engineering (Barnothy1964), such as therapeutic treatment, cancer and tumor treatment with magnetic hyperthermia, control of blood flow through medical surgery, gastro-intestinal treatment, endoscopy, etc. significantly exercise MHD convection. Additional detailed relevance on above subject matter addressed in Refs. (Biswas and Manna, 2018).

The claim for accurate control and sophistication of systems entailing thermos magnetic convection is developing gradually, which demanding novel research in this field. Apart from entire domain magnetizing fields, function of partially discrete fields is an innovative scheme in contemporary period. Such a method of partial magnetic fields could be an effectual means of organizing heat transport process. In common, whenever any system undergoes magnetic field, its hydrodynamic features is affected rigorously resulting localized transport occurrence are changed. The magnetizing force dampens flow velocities, which in sequence lessens convection event (Biswas and Manna, 2018). Subsequently, numerous researchers studied MHD convection in special flow geometry underneath an assortment of multi - physical circumstances like concern of differential heating cavity concerning uniform magnetic fields over entire field, non-uniform fields with line dipoles (Ganguly *et al.*, 2004), and partially applied magnetic fields (Mondal *et al.*, 2019). As of these reports, it is studied that thermos-flow occurrence in a confined area involving to some thermal apparatus can efficiently be managed by concerning magnetizing fields with appropriate modification. The investigation discloses that by regulating the useful magnetizing fields thermos-flow dampened and performance transforms from disordered oscillation to steady position. Very recently, Geridonmez and Oztop explored the thermos-magneto convection with air in differentially heated enclosure filled with (Geridonmez *et al.*, 2019) and without porous media (Geridonmez *et al.*, 2020) amid the impact of partial horizontal and diagonal magnetizing fields. It is observed that transport process in domain is changed depending on position, location, and strength of magnetic fields.

The magneto-hydrodynamic convection arrangement in presence of porous structure turns into more complex (owing to dampening consequence) which leads to decrease in heat transport feature. Such diminution in heat transmit may be recompensed by dissolving one or more dissimilar kinds of nano powders

or their blend into usual fluids that are specified as hybrid nanofluid/ only nanofluid. A detailed review on cited subject topic can be found in Refs. (Manna *et al.*, 2020, Mondal *et al.*, 2019). Very recent, MHD amid convection in blended nanofluid has been reported in a clear domain, porous field (Izadi *et al.*, 2019) incorporating a non-uniform magnetic field. Applying changeable magnetizing fields, they also analyze thermo-magneto convection of hybrid nanoparticles blended fluid-packed porous cavity under the effect of uneven magnetizing fields (Mondal *et al.*, 2021).

With these literature reviews in static temperature magnetic free convection mode, it is found that magnetic field is induced either entire domain or as line dipole. Only few investigations are highlighted on employment of partial active magnetic fields. Moreover, in thermos-magneto convective mode through vertical multi-banded state with active magnetizing fields is absent. In this study, consequence of spatial and partial active vertical magnetic fields on the thermos-magneto convection is scrutinized by numerical simulation. To envisage heat transportation systems and consequently to organize this process, heatlines (Kimura and Bejan, 1983) based study are admitted. Consequently, the investigation is carried out for multi-banding in deviation of band widths (L_b), band numbers along with their positions in vertical direction.

II. PROBLEM DESCRIPTION AND MATHEMATICAL FORMULATION

A diagram of physical domain with the boundary setting is portrayed in Fig. 1. Geometry is of a two-dimensional (in *x*-*y* plane) square enclosure with height, H and length, L composed of superposed hybrid nanofluid-porous substance. The enclosure is heated isothermally at temperature T_h in left wall and right side wall is permitted to remove heat with ambient (at T_c, so that $T_h > T_c$). Both horizontal walls are adiabatic condition. The enclosed space is entirely packed by Cu−Al_2O_3-water based hybrid nanofluid, saturated porous substances. Outwardly imposed magnetic field of strength B can be induced (vertically from bottom to top) either over the entire length of the enclosure (categorized as Case 1: full band) or partially in four equal bands (categorized as Case 2: 4-bands) over equal length of each L_B (= 0.1L) at equal spacing (= 0.1L) at a distance 0.15L from both ends of the left wall, in two equal bands (categorized as Case 3: 2-bands) over equal length of each L_B (= 0.2L) at equal spacing (= 0.2L) and in one bands (categorized as Case 4: 1-band) over equal length of L_B (= 0.4L) at mid-section of bottom wall and also no band is treated as Case 5.

The thermos substantial properties of host liquid with blended nanoparticles of Cu and Al_2O_3 are chosen as constant as given in Manna *et al.*, 2020. Thus the mass, momentum, and energy equations in non-dimensional form are written as:

$$\frac{\partial U}{\partial X}+\frac{\partial V}{\partial Y}=0 \tag{1}$$

$$\frac{1}{\varepsilon^2}\left(U\frac{\partial U}{\partial X}+V\frac{\partial U}{\partial Y}\right)=-\frac{\rho_f}{\rho_{hnf}}\frac{\partial P}{\partial X}+\frac{\nu_{hnf}}{\nu_f}\frac{\mathrm{Pr}}{\varepsilon}\left(\frac{\partial^2 U}{\partial X^2}+\frac{\partial^2 U}{\partial Y^2}\right) -\left(\frac{\nu_{hnf}}{\nu_f}\frac{\mathrm{Pr}}{\mathrm{Da}}+\frac{F_c\sqrt{U^2+V^2}}{\sqrt{\mathrm{Da}}\,\varepsilon^{3/2}}\right)U \tag{2}$$

$$\frac{1}{\varepsilon^2}\left(U\frac{\partial V}{\partial X}+V\frac{\partial V}{\partial Y}\right)=-\frac{\rho_f}{\rho_{hnf}}\frac{\partial P}{\partial Y}+\frac{\nu_{hnf}}{\nu_f}\frac{\mathrm{Pr}}{\varepsilon}\left(\frac{\partial^2 V}{\partial X^2}+\frac{\partial^2 V}{\partial Y^2}\right) -\left(\frac{\nu_{hnf}}{\nu_f}\frac{\mathrm{Pr}}{\mathrm{Da}}+\frac{F_c\sqrt{U^2+V^2}}{\sqrt{\mathrm{Da}}\,\varepsilon^{3/2}}\right)V-\frac{\rho_f}{\rho_{hnf}}\frac{\sigma_{hnf}}{\sigma_f}\mathrm{Ha}^2V+\frac{(\rho\beta)_{hnf}}{\rho_{hnf}\beta_f}\mathrm{RaPr}\theta \tag{3}$$

$$\left(U\frac{\partial \theta}{\partial X}+V\frac{\partial \theta}{\partial Y}\right)=\frac{\alpha_{hnf}}{\alpha_f}\left(\frac{\partial^2 \theta}{\partial X^2}+\frac{\partial^2 \theta}{\partial Y^2}\right) \tag{4}$$

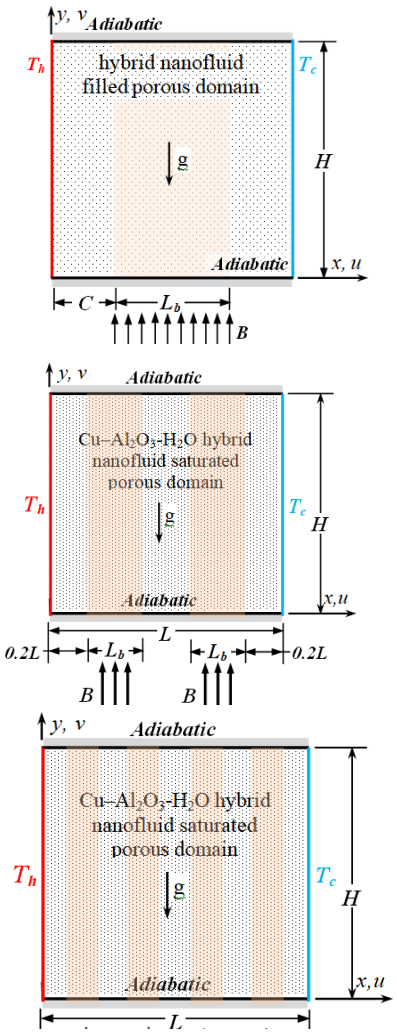

(a) 1-band, 2-bands, 4-bands vertical magnetic field

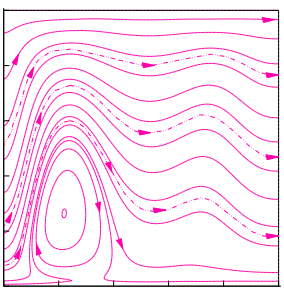

(b) Heatlines

Fig. 1. Problem description involving (a) physical domain with multi-banding (b) heat flow visualization

Above-mentioned all the governing equations (1) – (4) are solved using numerical method and derived by setting up dimensionless variables as written by

$$(X,Y)=(x,y)/L;(U,V)=(u,v)L/\alpha_f; \quad \theta=(T-T_c)/(T_h-T_c);P=(p-p_a)L^2/\rho_f\alpha_f^2 \tag{5}$$

$$\mathrm{Pr}=\frac{\nu_f}{\alpha_f};\ \mathrm{Da}=\frac{K}{L^2};\ F_c=\frac{1.75}{\sqrt{150}}; \tag{5a}$$

$$\mathrm{Ra}=\frac{g\beta_f(T_h-T_c)L^3}{\nu_f\alpha_f};\ \mathrm{Ra_m}=\mathrm{RaDa};\ \mathrm{Ha}=BL\sqrt{\sigma_f/\mu_f}$$

in above equations, dimensionless parameter are Pr, Da, F_c, Ra, $\mathrm{Ra_m}$, Ha, are Prandtl, Darcy, Forchheimer coefficient, Rayleigh, modified Rayleigh and Hartmann number. Pr value is taken as 5.83 for entire simulation.

The subscript '*f*' and '*hnf*' are utilized to indicate thermo-physical properties for host fluid and hybrid nanofluid respectively. Likewise, '*s*' are utilized to indicate solid nano blended particles respectively. The symbol 'ϕ' is utilized to designate the combination of hybrid-nanoparticles volumetric fraction.

The effective density ρ_{hnf}, sp. heat capacity $(c_p)_{hnf}$, coefficient of thermal expansion β_{hnf} of hybrid nanofluid is given by

$$\rho_{hnf}=(1-\phi_{hns})\rho_f+\phi_{\mathrm{Al_2O_3}}\rho_{\mathrm{Al_2O_3}}+\phi_{\mathrm{Cu}}\rho_{\mathrm{Cu}} \tag{6}$$

$$(\rho c_p)_{hnf}=(1-\phi_{hnf})(\rho c_p)_f+\phi_{\mathrm{Al_2O_3}}(\rho c_p)_{\mathrm{Al_2O_3}}+\phi_{\mathrm{Cu}}(\rho c_p)_{\mathrm{Cu}} \tag{7}$$

$$(\rho\beta)_{hnf}=(1-\phi_{hnf})(\rho\beta)_f+\phi_{\mathrm{Al_2O_3}}(\rho\beta)_{\mathrm{Al_2O_3}}+\phi_{\mathrm{Cu}}(\rho\beta)_{\mathrm{Cu}} \tag{8}$$

so that, $\phi_{hnf}=\phi_{\mathrm{Al_2O_3}}+\phi_{\mathrm{Cu}}+H_2O$

The thermal diffusivity α_{hnf} is given as

$$\alpha_{hnf}=\frac{k_{hnf}}{(\rho c_p)_{hnf}} \tag{9}$$

Effectual absolute viscosity of hybrid nanofluid is calculated utilizing classical Brinkman model

$$\mu_{hnf}=\frac{\mu_f}{(1-\phi_{hns})^{2.5}};\ \text{where}\ \phi_{hns}=\phi_{\mathrm{Al_2O_3}}+\phi_{\mathrm{Cu}} \tag{10}$$

Generally, effectual thermal conductivity of hybrid nanofluid k_{hnf} is calculated utilizing classical Maxwell model[43]

$$k_{hnf}=k_f\left[\frac{(k_s+2k_f)-2\phi(k_f-k_s)}{(k_s+2k_f)+\phi(k_f-k_s)}\right] \tag{11}$$

where, k_s, and k_f are the thermal conductivity of nanoparticles and base fluid respectively.

The applied boundary conditions for the present simulation are as follows:

$$U=V=\partial\theta/\partial Y=0 \text{ - top and bottom walls } (Y=0,1),$$
$$U=V=0,\ \theta=1 \text{ - left wall } (X=0), \tag{12}$$
$$U=V=0,\ \theta=0 \text{ - right wall } (X=1),$$

The average allocation of energy transfer rate over the active walls of cavity are formulated by average Nusselt number (Nu) as given by

$$\mathrm{Nu}=\frac{k_{hnf}}{k_f}\int_0^1\left(-\frac{\partial\theta}{\partial X}\bigg|_{X=0,1}\right)dY \tag{13}$$

The local contour profiles of fluid-flow within the simulation domain envisaged employing streamlines, which is computed from velocity fields by producing streamfunction ψ and is stated by

$$-\frac{\partial\psi}{\partial X}=V \text{ and } \frac{\partial\psi}{\partial Y}=U \tag{14}$$

In addition to above, transportation of heat flux flow dynamics is envisaged by using heatlines from elementary viewpoint. As isotherms alone are not sufficient to demonstrate the mechanism of heat energy flow, the concept of heatlines is utilized here to represent the path of heat energy flow. The heatlines are principally generated as of energy equilibrium at steady-state provision and calculated from the heatfunction (Π), which can be expressed as

$$-\frac{\partial\Pi}{\partial X}=V\theta-\frac{\partial\theta}{\partial Y} \text{ and } \frac{\partial\Pi}{\partial Y}=U\theta-\frac{\partial\theta}{\partial X} \tag{15}$$

III. NUMERICAL METHODOLOGY

The equations (1) – (4) in conjunction with suitable boundary setting state a set of nonlinear partial differential governing equations which are solved in sequence using embryonic lab based CFD code implementing FVM loom. The hyperbolic differential equations are initially converted into algebraic forms, which are then solved through iteration using TDMA solver and ADI sweep, by employing the SIMPLE algorithm. Non-uniform staggered grid distributions (200×200) are used for the discretization. The converged solutions are acquired throughout iterative procedure; in anticipation of normalized maximum values of residuals and mass defect go with less than 10^{-8} and 10^{-10}, respectively.

IV. RESULTS AND DISCUSSION

The effects of banded magnetizing fields on the thermal management of blended Cu–Al_2O_3-water nanofluid filled porous cavity heated differentially are evaluated numerically. Results are represented collectively for variant of Darcy-Raleigh number ($\mathrm{Ra_m}$ = 10 - 10^4), Darcy number (Da = 10^{-5} - 10^{-1}), strength of outwardly imposed magnetizing field (Ha = 0, 10 - 70), keeping the fixed value of porosity ε = 0.8, and percentage of nanoparticles volume concentration (ϕ = 0.1%). 1, 2, 4-bands of field and special two extreme cases of no field and whole domain magnetic fields are chosen for study. On the whole results underneath the effects of setting parameters on the thermos-flow and global heat transport presentation are obtainable and discussed elaborately in sub-sections.

A. Effect of multi-banded vertical magnetic fields

Figures 2–4 explain impact of $\mathrm{Ra_m}$, with some common aspects of transportation observable fact. Separately every figure deals with multi-banded impact for Cases 1–4 by contour maps of heatlines, coupled streamlines-isotherms showing Nusselt values. Differentially heated enclosure is inspected from basic view point under control of vertical

magnetic field introduction. As a general aspect, it is observed that only the single CW recirculation (specified by streamlines) produced and isotherms contour possess inclined (ended at adiabatic bottom and top walls). It occurs by reason of static temperature heating of left side wall and cooling of right wall. Heat energy flow portrayed by heatlines is distinctly persuaded by convective flow stream. For the problem domain buoyancy domination is the principal flow dynamic potential. With ascertaining fluid flow, vertical magnetizing fields transform and organize thermos-flow uniqueness by dampening convection system flow. Porous structure proffers resistance to flow. Moreover, hybrid nano scale fluid increases the useful thermal conductivity of fluid. Consequently, here is a key challenge of enhancing heat transport with nanofluid saturated by porous media.

Basis on the above cited common facts and interpretation; key outcome are presented in Figs. 2 - 5 with explanations.

In present computational domain, effects of lowest and highest Ra_m =10 and 10^4 are scrutinized in figs. 2 to 5 keeping supplementary parameters constant. Under the restriction of identical effective width and length of banded fields, transportation processes are examined by contour of heatlines, streamlines- isotherms couple reflecting Nusselt average. All flow configurations are found to endure intensely caused by alteration of vertical banded-outline (Full band, 4-banded, 2-banded, 1-banded) of MHD fields. Figure 2, taking same parameters and band width (0.4 L) of fields for 1- band, the profile of streamlines denoting in enclosure is significantly dissimilar for low to higher Ra_m with enhancing values of Nu. The central part of weak stream of flow has an unlike form and region—say ellipse to distorted parallelogram (1-band) for low to higher Ra_m. As fluid velocity plays key function in transportation, single-banding effect is likewise pronounced through transport of heat flow specified by heatlines contour. The pattern of energy cells markedly suffer by low to higher Ra_m. From source wall to sink wall, the heat flow captures energy cell with non-uniform concentration of flux passed throughout the heatlines passageway.

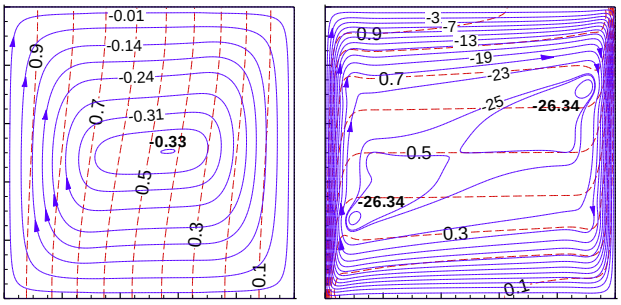

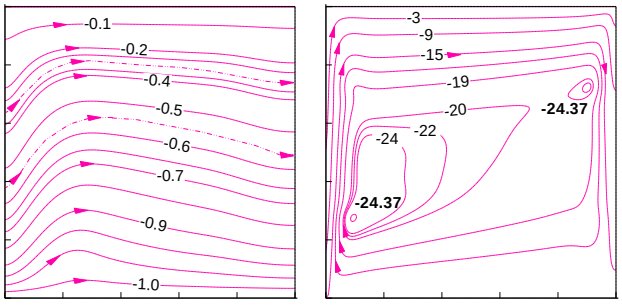

Fig. 2. Convective strength by Darcy-Rayleigh number (Ra_m) on contour couple of streamlines-isotherms (first row), and heatlines (second row), at Da = 10^{-3}, 1-band, Ha = 50, ϕ = 0.1%.

Using combined effect of velocity, temperature, and flow dampening magnetic force, the allocation of static temperature fields revealed by isotherms inclined lines with overall pattern almost same. Almost same observation have been reflected in Fig. 3,4 and 5 for 2-bands, 4-bands and full bands respectively in all contour maps with other parameters fixed as defined. Here it is to be noted that streamlines changes the shape as circular to stretched ellipse with increase in stream function values and same for heatlines also.

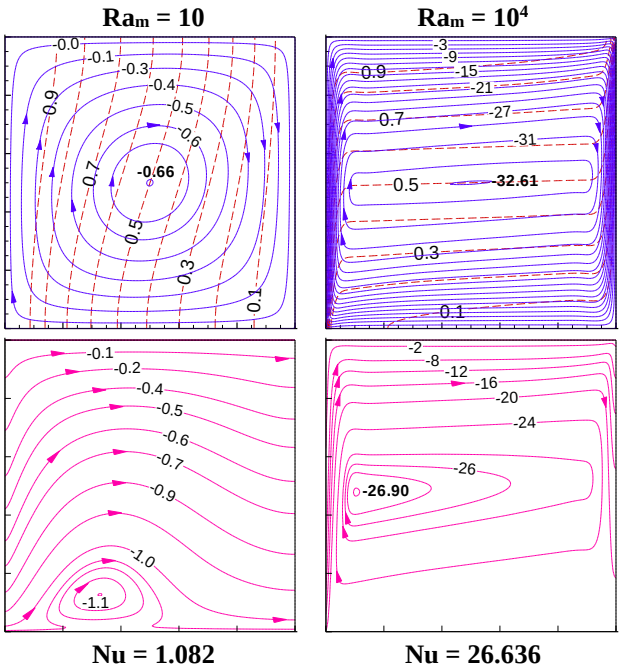

Fig. 3. Convective strength by Ra_m on coupling of streamlines-isotherms (first row), and heatlines (second row) at Da = 10^{-3}, 2-bands, Ha = 50, ϕ = 0.1%.

There is a distinctive alteration in location of streamlines and heatlines in different cases. Compactly allocated contour maps over active walls specify pattern of velocity and boundary layers together with stronger energy-flux. Along with shape and strength centers of cells of flow and heat recirculation are markedly influenced by changing band width and number of imposed magnetic field. The magnitudes of maximum stream function, $|\psi|_{max}$, heat function Π_{max} and Nu are established higher with augmented Ra_m.

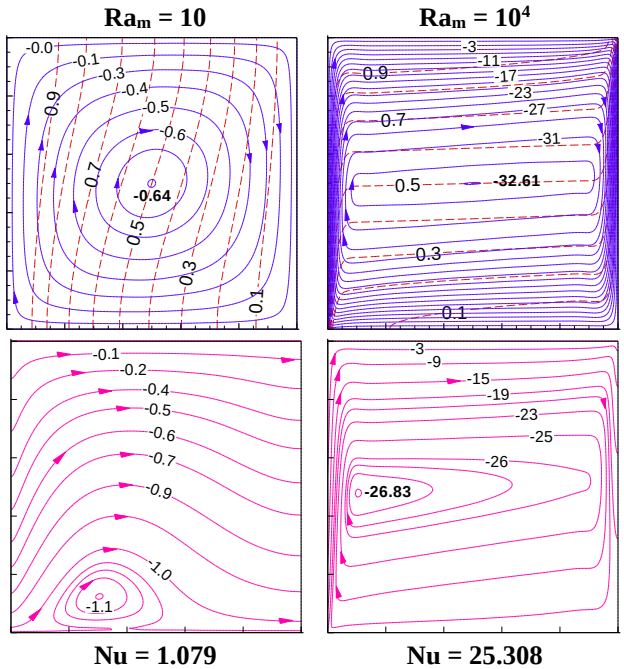

Fig. 4. Convective strength by Ra_m on couple streamlines-isotherms (first row), and heatlines (second row) at Da = 10^{-3}, 4-bands, Ha = 50, ϕ = 0.1%.

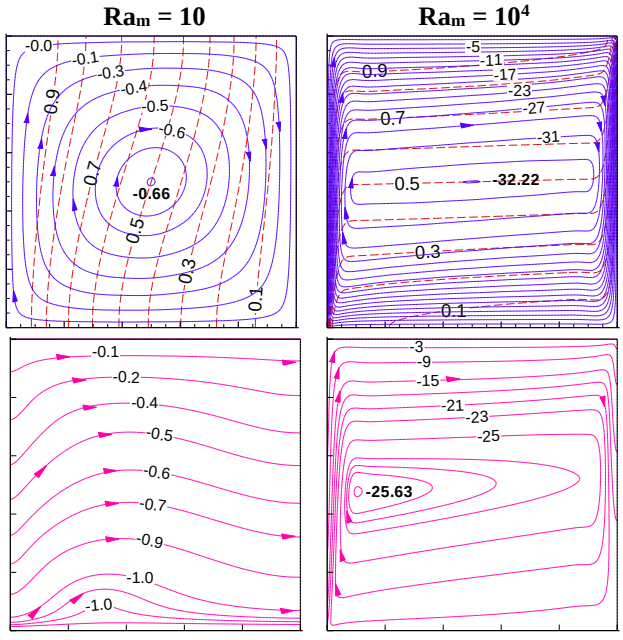

Fig. 5. Convective strength by Ra_m on coupling of streamlines-isotherms (first row), and heatlines (second row) at Da = 10^{-3}, full-band, Ha = 50, ϕ = 0.1%.

B. Outcome of Magnetic field strength (Ha)

Influence of intensity of magnetizing fields underneath multi-vertical banded fields are portrayed in figure 6 for absent of field in domain Ha = 0 to elevated Ha = 50 with at Da =10^{-4}, Ra_m =10^3, ϕ =0.1%. As predictable with no field, Ha=0, figure 6 illustrates 2-bands fields where a minor changes on contour-structures and average values of Nu. Caused by similar effectual width of 2-bands fields, both cases represent nearly alike flow outlines. Every contour of streamlines in respect to mid-section takes a shape of stretched inclined ellipse for intermittent active stronger 2-bands fields. Recirculation of heat fluxes are more pronounced near active wall of source and sink. The magnitudes of maximum stream function, $|\psi|_{max}$, heat function Π_{max} and Nu are established lower with augmented magnetic field.

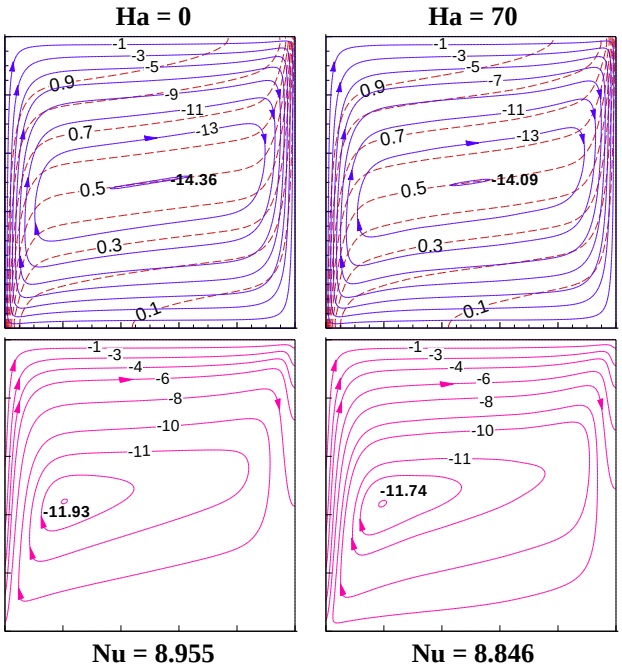

Fig. 6. Vertical magnetizing field potency signified Hartmann number (Ha) on contour couple of streamlines-isotherms (first row), and heatlines (second row) at Ra_m= 10^3, Da = 10^{-4}, 2-bands, ϕ = 0.1%.

C. Consequence of Darcy number (Da) *of porous matrix*

Impact of Darcy number amid multi-banded vertical fields constant at Ha = 50 and ϕ = 0.1% are described in figure 7 for low to high Da (10^{-5}, 10^{-1}) choosing Ra_m =10^3.

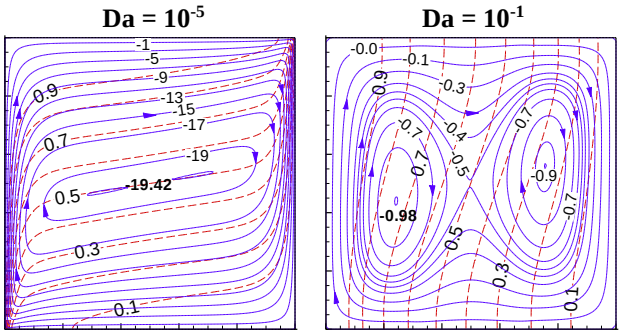

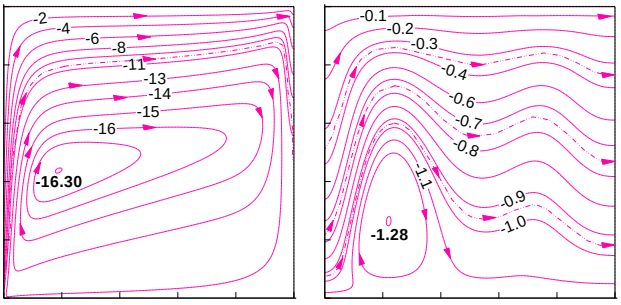

Fig. 7. Porous matrix influence by Darcy number (Da) on contour couple of streamlines-isotherms (first row), and heatlines (second row) at Ra_m= 10^3, 1-band, Ha = 50, ϕ = 1%.

Figure 7 illustrates a elliptically stretched large cells covering entire enclosed space in both stream and heatlines. It ensues as convective strength stronger throughout high resistive porous matrix of Da = 10^{-5}. Usually, low Da is connection to added resistive porous medium. Both energy flux and fluid flows obtain subsequent to enclosed space in elliptic paths. With increased Da = 10^{-1}, as anticipated with improved permeability less flow-resistance, flow can simply go round in the cavity. Distorted multi-vortices come out in the contours of streamlines and nice wavy heatlines. Fascinatingly, two clockwise cells at left and right parts of cavity show because of imposed single-band vertical field.Flow field and related supplementary global parameters turn into appreciably weaker as specified by values of $|\psi|_{\max}$, $\Pi_{\max}$, and Nu. Comparatively lower transportation velocity and heat rate denoted by Nu value as in fig. 7.

D. Heat transfer characteristics

The heat transfer features beneath the multi-banding use of vertical magnetic fields are abridged in Fig. 8 including two results of absence of magnetic field and full domain magnetic field. In Figure 8(a), it is scrutinized that at low Ra_m = 10, 100 Nu values for all 5-cases almost overlap into a single point. This occurs mainly due to domination of heat conduction mode.

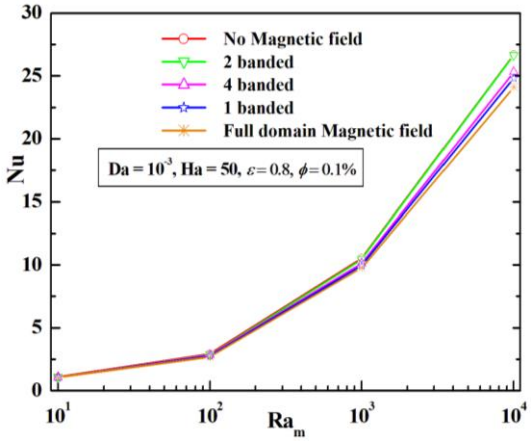

(a)

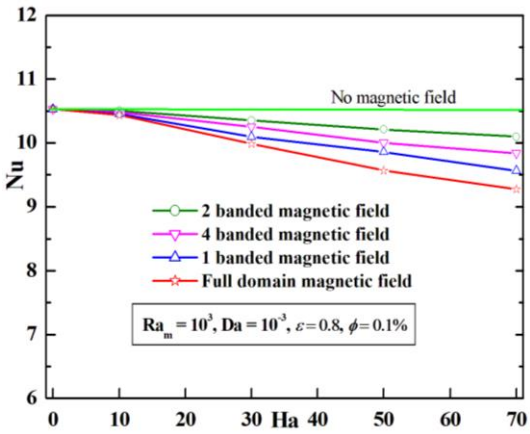

(b)

Fig. 8. Heat transfer by Nu curve with varying (a) Darcy-Rayleigh number (Ra_m), and (b) Hartmann number (Ha)

At $Ra_m \geq 10^2$, convection mode begins to dominate leading to augmented thermos-convection resulting increase in Nu for all five cases. Nu curvature with absent of field denotes a higher level due to lack of flow-dampen force. Consequently, all Nu-curves stretch out in between two special cases of no- field and full domain magnetizing field. The effects of Ha number (replicate magnetizing-field intensity) for the different cases are depicted in figure 8(b). The distinction of average Nu vs. Ha explains a declining fashion for all cases. Moreover, diminution in Nu is important in special case of full domain magnetizing field. Usually, imposed multi-vertical banding fields, lessening in flow velocity are a smaller amount comparison to full domain active field. The case of no-field is represented by a horizontal line as reference to presume fall in Nu with varying Ha. This investigation evidently reveals useful features of multi-banding magnetizing fields with reduction heat transport comparison to absence of magnetic field.

V. CONCLUSIONS

An attempt of present model provides a novel thought of multi-banding function of magnetizing fields to exhibit an enhanced management of convective transports. A considerable alteration in transfer methods is projected to turn out due to intermittent induction in magnetic fields that dampen and un-dampen fields interchangeably in the domain. The novel systems with 4-bands, 2-bands, and 1-band issued to identical width and induction of fields are judged with multi physics. The salient conclusions of study are abridged below:

- Multi-banded role exhibits special flow picture in schemes as band number differ. The variations in the flow outlines with Ra_m, Ha, Da are considerable. Therefore, this method could be a potential tool to manage thermal convection successfully.
- Here heat transport by multi-banded procedure allied with two special cases - no band and full band magnetizing field. So, thermal energy transport can be enhanced (comparison to full band) by implementing multi banded method.

- With 2-bands field, heat transportation is found more for present investigation.

This novel method featuring modifiable conveniences like band number, width, position, and effectual length claims more focus; and thus, it might be opened prospective researches in R & D area.

ACKNOWLEDGEMENT

Authors gratefully acknowledge the members of NEPTUNE lab, Mechanical Engineering Department of Jadavpur University, for developing CODE, suggestions and assistance extended by all Professors during this work.

REFERENCES

[1] M.F. Barnothy, *Biological Effects of Magnetic Fields*, Springer Science +Business Media, LLC, 1964.

[2] N. Biswas, N.K. Manna, "Magneto-hydrodynamic Marangoni flow in bottom-heated lid-driven cavity," J. Mol. Liq. **251**, 249–266 (2018).

[3] R. Ganguly, S. Sen and I.K. Puri, "Thermomagnetic convection in a square enclosure using a line dipole," Phys. Fluids **16**(7), 2228–2236 (2004).

[4] B.P. Geridonmez and H.F. Oztop, "Natural convection in a cavity under partial magnetic field applied from different corners," Int. Commun. Heat Mass Transfer **114**, 104575 (2020).

[5] D.A. Nield, A. Bejan Convection in Porous Media, third ed., Springer, Berlin, 2006.

[6] M.K. Mondal, N. Biswas and N.K. Manna, "MHD convection in a partially driven cavity with corner heating," SN Appl. Sci. 1-1689 (2019).

[7] B.P. Geridonmez and H.F. Oztop, "Natural convection in a cavity filled with porous medium under the effect of a partial magnetic field," Int. J. Mech. Sci. 161–162, 105077 (2019).

[8] M. Izadi, R. Mohebbi, H. Sajjadi, A.A. Delouei, "LTNE modeling of magneto-Ferro natural convection inside a porous enclosure exposed to nonuniform magnetic field," Physica A **535**, 122394 (2019).

[9] M. Izadi, R. Mohebbi, A.A. Delouei and H. Sajjadi, "Natural convection of a magnetizable hybrid nanofluid inside a porous enclosure subjected to two variable magnetic fields," Int. J. Mech. Sci. **151**, 154–169 (2019).

[10] N. Biswas, N.K. Manna, P. Datta and P.S. Mahapatram "Analysis of heat transfer and pumping power for bottom-heated porous cavity saturated with Cu-water nanofluid," Powd Technol. **326**, 356–369 (2018).

[11] M. K. Mondal, N. Biswas, N. K. Manna, and Ali J. Chamkha, Enhanced magnetohydrodynamic thermal convection in a partially driven cavity packed with a nanofluid-saturated porous medium, Math Meth Appl Sci. 2021; 1–28, doi: 10.1002/mma.7280.

[12] N. K. Manna, M. K. Mondal, and N. Biswas, A novel multi-banding application of magnetic field to convective transport system filled with porous medium and hybrid nanofluid, Phys. Scr. 96 (2021) 065001, doi.org/10.1088/1402-4896/abecbf.

[13] M. K. Mondal, N. Biswas, A. Datta, and N. K. Manna, Effects of Amplitude on MHD Thermal Convection of Cu-Water Nanofluid Saturated Porous Cavity, ICRAME 2021; NIT Silchar, India.

[14] S.V. Patankar, *Numerical Heat Transfer and Fluid Flow*, New York NY He

Impact of DG Integration on Protection Coordination & Possible Solutions

Arpan Banerji, Member IEEE
School of Electrical Engineering
IIT Bhubaneswar
Bhubaneswar,India
arpan.sprite@gmail.com

Pratyusha Biswas Deb
Dept. of Electrical Engineering
Narula Institute of Technology,
KOLKATA, INDIA
pratyusha.biswasdeb@nit.ac.in

Ambarnath Banerji, Sr. member IEEE,
Dept. of Electrical Engineering
Narula Institute of Technology,
KOLKATA, INDIA
ambarnath.banerji@nit.ac.in

Sohini Pal
Dept. of Electrical Engineering
Narula Institute of Technology,
KOLKATA, INDIA
sohinip815@gmail.com

Suvargha Ghosh Dastidar
Dept. of Electrical Engineering
Narula Institute of Technology,
KOLKATA, INDIA
suvargha2000@gmail.com

Hiravra Koley
Dept. of Electrical Engineering
Narula Institute of Technology,
KOLKATA, INDIA
koleyhiravra2@gmail.com

***Abstract*—Every power system is armed with its own protection system to protect it from most types of faults. Coordination is maintained between the various protective gears to avoid failure of the protection system. This coordination gets disturbed when a Renewable energy based Distributed Generation is integrated into the distribution system. A number of issues come up, which does not allow the normal protection system to function properly. Many researchers have been presented solutions to overcome these issues. The present work attempts to bring out the impact of these issues on the protection coordination and the possible solutions proposed by various researchers to overcome these problems. The present work will help the potential researchers with a list of protection issues due to impact of DG / microgrid integration & their possible solutions and help them to further their research for more efficient and better protection system.**

Keywords—Microgrid, Protection Coordination, Overcurrent Protection, Distance protection, Adaptive Protection.

I. Introduction

Fast depleting fossil fuel, global warming and environmental sustainability are causing a paradigm shift in the way electricity is generated. Further generation capabilities are being created using renewable energy resources. Most of these generations are small in size and are generated near the loads. These generations are called Distributed Generations (DG). Hence for grid connection these generations are connected to the distribution side of the grid [1]-[3].

Furthermore, most of these DGs are not interconnected. There is a trend to have flexible connection strategies of these DGs and have the benefit similar to that of the grid. The MicroGrid (MG) concept is built out of this desire for a system with flexible interconnection [4]-[5]. Thus a MG is a low voltage (LV) distribution which provides for:

(1) Quality power to the customer with mission critical loads.
(2) Relief to the Distribution Network Operators (DNOs) as their distribution system is already overloaded.
(3) Where the load centre is remote from the utility grid.

II. Protection Issues

A. Basic Issues

A desired power system is one which is free from all types of faults and supplies loads without interruption. Such a system is either not feasible or is beyond reasonable cost. So, protection systems are designed to protect the power systems against most possibly occurring faults.

Sometimes the DGs are connected to directly feed into the distribution network. DGs that operate through synchronous or induction generator units and directly feed into the distribution network cause a change in the fault current level as both kinds of generators can add to fault currents [1].

When Inverter interfaced distributed generation (DGs) units are directly connected to distribution network, fault current is restricted to a smaller number. Inverter interfaced DG supplies limit fault level to about twice its rated value.

Therefore, the contribution of the DGs to fault level is dependent on the capacity of DG, the placement location of DG and finally on the technology used for the DG.

DGs may be interconnected to form a Microgrid. These Microgrids can run in both grid-connected and islanded modes of operation. As required for all types of power systems, it is important to protect the microgrid, in both modes of operation against all types of faults [5]-[6].

B. Effect of DG Integration

1) Over-reach of relay or Loss of relay sensitivity:-

During a grid connected mode of operation of the distribution system a fault downstream of the DG location causes the short circuit current to increase. This is due to the DG adding its contribution to the short circuit current.

$$I_{f\_total} = I_{f\_grid} + I_{f\_DG} \quad (1)$$

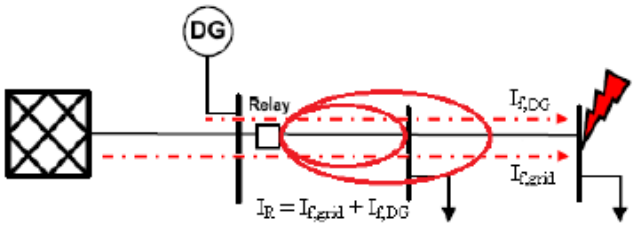

Fig.1 Over-reach of relay due to DG integration

As the fault current increases the relay sees the impedance up to the fault point to be lesser than it actually is. The relay identifies the fault to be much closer (in a different zone) than actual. Thus causing the Over-Reach of the relay [7].

2) Blinding of overcurrent protection or Under-reach

With the grid connected if a fault occurs between the grid and the DG, there is a reduction of current contribution from the grid. This is due to the fact that a part of the fault current is contributed by the DG.

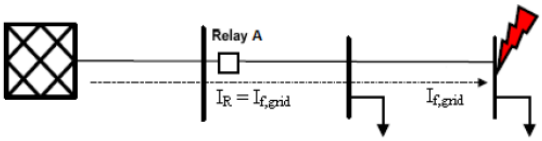

Fig.2 Overcurrent protection without DG

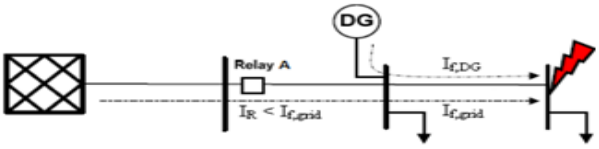

Fig.3 Overcurrent protection with DG integration.

In Fig.2 it is observed that the utility grid is supplying power to the fault that has occurred at the far end of the grid. The whole fault current flows through the relay A. In Fig.3 it is observed that a DG has been connected to the bus in between the relay and the fault point. Therefore, the total fault current supplied by the grid gets decreased. The relay A, due to the reduced current, will see the impedance upto the fault point to be much higher. Therefore, it considers the fault to be much further away. This lead to under-reach of the relay [7].

3) Sympathetic tripping or False tripping of overcurrent protection

With the grid connected to the distribution system and if a fault occurs on a feeder adjacent to that having a DG connected, the DG's current contribution may exceed the pickup setting of the overcurrent relay, if the DG's capacity is sufficiently large as shown in Fig. 4. This leads to a false tripping of the breaker [7].

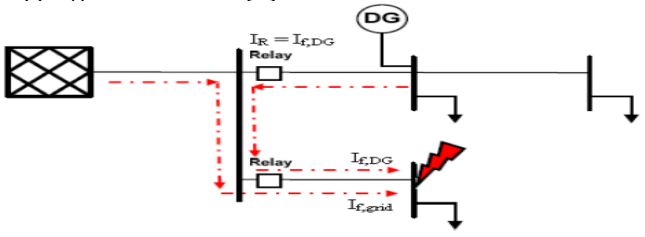

Fig.4 False tripping of overcurrent relay

4) Selectivity problem /protection coordination problem

Presence of DGs within a microgrid causes bidirectional flow of power and fault currents in both modes of operation, grid-connected mode and islanded mode.

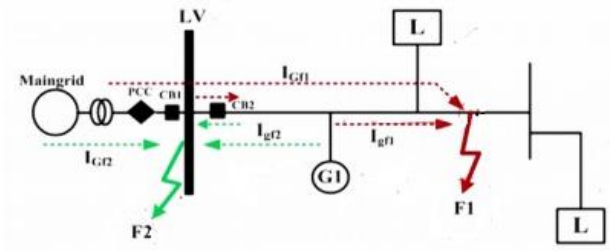

Fig. 5 Selectivity problem in protection coordination

From the Fig. 5 it can be observed that for each fault the direction of fault current changes. Traditional unidirectional overcurrent relays are unable to provide safety protection to microgrid [7].

5) Ineffective use of overcurrent protection

A microgrid in islanded mode and having inverter interfaced DGs has fault current limited to around tywice the rated current of the power electronic devices ued in the inverter.

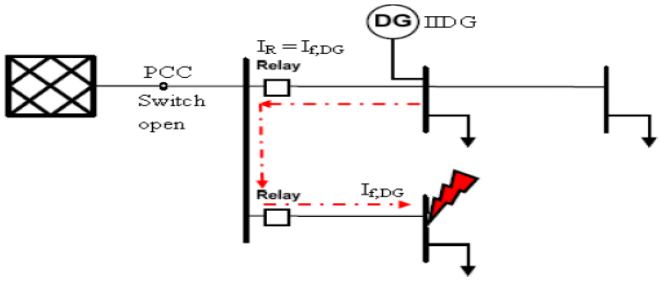

Fig. 6 Ineffective use of overcurrent relays

Insufficient fault current contribution from inverter-interfaced DGs will not exceed the overcurrent setting of the relay causing maloperation of the relay [7].

III. Solutions to Protection Issues

A. Distance Protection

This protection scheme uses either admittance or impedance measurements to detect faults. It has inverse time characteristics according to the different zones of protection. Relays with this scheme can detect faults in all modes of operation whether the microgrid is in islanded mode or in grid connected mode.

They can isolate a fault that happens on either side of the protected circuit. But the important point to be kept in mind is that the reach settings must be different for forward and reverse faults.

The drawbacks being that there might be error in the measured admittance up to fault point. A suitable correction can be applied. Further there might be loss of accuracy which might arise due to problems with fundamental extraction due to harmonics, current transients and decaying DC magnitude [8]-[9].

Distance protection uses measured current and voltage values at the relay location to calculate fault impedance using

$$Z = \frac{U}{I} \quad (2)$$

U and I represent the voltage and current measured at the relay location respectively and Z is the apparent impedance seen by the relay.

If an intermediate infeed in the form of a DG source is present between the relay location and fault point, the DG will feed the fault as well and consequently, the voltage measured at the relay location will be higher. Thus, the relay will see an impedance value higher than the actual. It might infer that the fault is at a higher time-graded zone and introduce unnecessary tripping delay or even not trip at all.

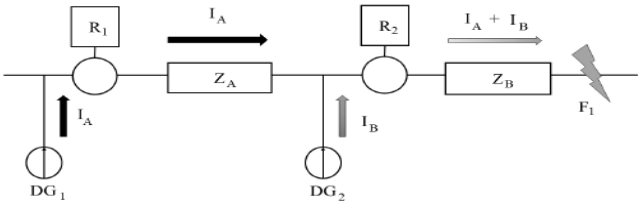

Fig. 7 Distance protection with DGs integrated

In the above situation, for the fault F1, UA and IA are the current and voltage measured by Relay R1 respectively.

$$U_A = I_A Z_A + (I_A + I_B) Z_B \quad (3)$$

$$Z_1 = \frac{U_A}{I_A} = Z_A + \left(1 + \frac{I_B}{I_A}\right) Z_B \quad (4)$$

Therefore there will be difference in the actual and measured Z_1.

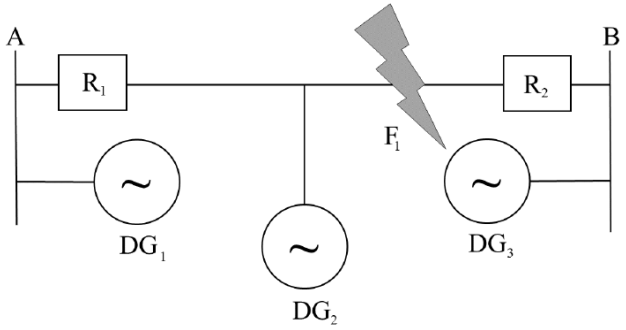

Fig. 8 Distance Protection with communication between relays

In the circuit relay R_2 sends the value of current measured by it to relay R_1. Also, DG_2 communicates its connection status to R_1. Since power can flow in either direction, R_2 also receives the value of current measured by R_1 and the connection status of DG_1. The error in impedance measurement is (IB/IA) times the value of Z_b. If the value of the current measured by R_2 is known, the measurement error can be calculated and subtracted from the impedance measured by R_1.

The expression for corrected impedance value is given by (5)

$$Z_{corrected} = Z_1 - \left(\frac{I_B}{I_A}\right) Z_B \quad (5)$$

B. Current Limiting Protection Schemes

(a) Use of External Devices

Fault Current Limiter (FCL) is used to overcome the impact of fault current feed from DGs. FCL is placed in series with the DGs in the distribution system [7].The DGs' fault current contribution is limited to a magnitude which is less than the trip setting value of the relay by the large impedance of the FCL. This effect is obvious for use with synchronous, induction machine based distribution generation to bring the magnitude of the fault current to the lower level of fault contribution by inverter-interfaced sources of distribution generation

The method has advantage as it retains coordination among original protective devices.

(b) For Inverter based DGs of Islanded Microgrid, protection can be achieved by limiting the current flow through the switches of the inverter [6].

A voltage and current controller of the inverter is used to detect and thereby limit the large current during faults. Voltage/ current signals are transformed from *abc* coordinate to rotating *αβo*-frame, the disturbances are identified, and fault occurrence is detected. Further a signal is sent to a logical controller which causes operation of the circuit breaker/static switch to isolate the faulty section. The healthy phases remain undisturbed. As conventional protection devices like relays are not incorporated, the fault identification to clearance process is very fast.

C. Adaptive Protection Scheme

It is applied to conventional protection system to vary the parameter settings or the relay operating characteristics in response to the changes in the power system [10]. This protection scheme is implemented using extensive communication among the numerical relays. It mainly consists of two stages:

1)Topology Sensing:-

Analyses of actual operating condition of the microgrid are done by continuous measurement of the breaker position, penetration levels of the DGs and other grid parameters. It also detects values to be altered for the adjusted tripping characteristics. During a fault, trip signal to the respective circuit breaker is generated.

2) Calculation of Relay Settings:-

Predicted data of the DG availability is utilized in order to review the range of microprocessor base relays for each new operating condition.

Adaptation takes place if selectivity is not given any longer. If the adaptation is successful and the boundary conditions are not broken, the tripping characteristics of respective relays will be matched. Therefore it makes adjustment to protection function according to the changes in the power system.

The Master Control Protection Unit (MCPU) monitors the Static Switch and C.B status of the microgrid continuously. Whenever there is a change in the monitored breaker position, an interrupt signal is sent to MCPU and the new DGs fault current contribution is calculated and updated in the relay operating data.

But this algorithm may not be appropriate for large microgrid setups because analysis is done offline and requires excessive memory to store all the data.

For any relay, the operating fault current is calculated by,

$$I_{relay}=(I_{fault(grid)} \times OM) + \sum (k_i \times I_{fault(DG)} \times SB) \quad (6)$$

OM = Operating Mode

SB = Status of Breaker

ki= Impact factor of i^{th} distributed generator on the fault current sensed by the relays

D. Genetic Algorithm based Differential zone protection

Differential protection in general uses an ideal number of relays and sensors inside each protection zone. Current sensors is positioned on the secondary side of transformers for every load as well as relays located at the source location of distribution generation [8] [12].

Zone relays detects a fault when the distribution generation source currents go beyond the sum of load currents inside the protection zone.

Then the relays sends a signal to the distribution generation source at the faulty zone and makes it trip.

A genetic algorithm is used to find the best placement for sensors, circuit breakers and relays to decrease total cost to a minimum. The steps involved are:-

1) Short-circuit current (kA) is found by short-circuit analysis.

2) Result of the short-circuit analysis helps to develop the coordination between the protection elements .

3) The complex protection coordination between protection elements is solved and optimized with the help of Genetic Algorithm.

E. Protection Scheme for Loop Based Microgrid

For this protection scheme Illinois Tech microgrid configuration was used as the test bed [12]. The microgrid is operated by the Robert W. Galvin Center in which the power is supplied to various loads by the utility as well as the microgrid sources in normal grid condition.

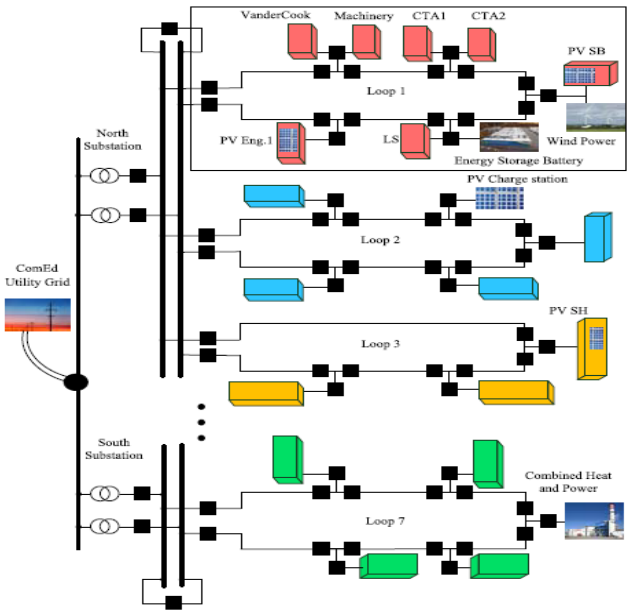

Fig. 9 Layout of Illinois Tech microgrid test bed.

The protection is divided into four levels including

- Microgrid
- feeder
- loop-way
- load-way level

The four levels of protection can be adopted to isolate both internal and external faults in microgrids.

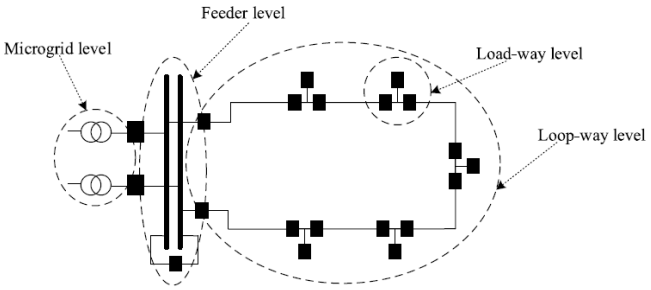

Fig. 10 Different levels of protection for a loop in microgrid

The load-way level is the basic protection element which is integrated with various DGs and loads. The protection zones include Area ‘a’ among breakers and Area ‘b’ of DG/load.

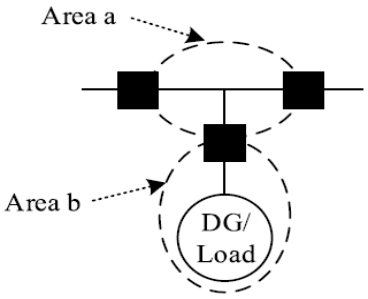

Fig. 11: Protection zones for load –way level.

The short-circuit current in the grid-connected mode is different from that in the island mode because the inverter-based DGs cannot supply sufficient short-circuit currents.

Therefore, a dual-strategy protection is developed for certain parts and a single-strategy protection for others.

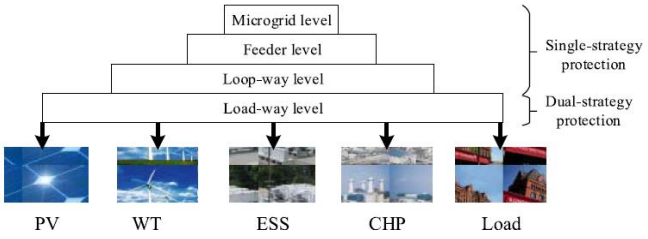

Fig. 12 Strategy allocation for different levels.

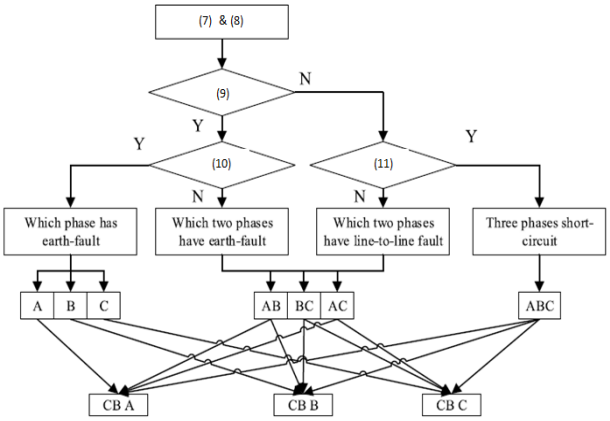

Fig. 13 Flow chart for fault analysis.

(7) and (8) are the initial conditions which are taken at the load loop level.

$$I_{abc}|_{t0+\Delta t} - I_{abc}|_{t0} > I_{se} \quad (7)$$

$$i_a + i_b + i_c > \quad (8)$$

The phase selector criterion is represented by (9)

$$\frac{|I_a + I_b + I_c|}{3} > \varepsilon_1 \quad (9)$$

ε_1 is a small value to check the zero sequence current

The single phase or two phases with an earth fault is identified using (10).

$$\max(\Delta I_{ab}, \Delta I_{bc}, \Delta I_{ca}) >> \min(\Delta I_{ab}, \Delta I_{bc}, \Delta I_{ca}) \quad (10)$$

ΔI_{ab},ΔI_{bc},ΔI_{ca} are differential line currents in Δt time interval.

Identification of the two phases with line-to-line faults or faults that include the three phases is done using (11)

$$\max(\Delta I_a, \Delta I_b, \Delta I_c) >> \min(\Delta I_a, \Delta I_b, \Delta I_c)- \quad (11)$$

ΔI_a,ΔI_b,ΔI_c are differential phase currents in Δt time interval.

IV. Conclusion

This paper presents the various issues that crop up when the DGs are integrated with the distribution. Then when the DGs are pooled together to form a microgrid and which is then integrated with the distribution network more issues crop up due to the fact that the microgrid can operate both in grid connected and islanded mode. The present work summarizes the methods proposed by various authors to overcome the protection issues, when DGs either alone or in the form of a microgrid are integrated with the distribution system. An attempt has been made to collate all the protection issues related to DG integration and various solutions proposed, in this work, so that future investigators can have an insight into the problem in a single paper and can work on more advanced solution to the problem.

References

[1] M. Dahal, A. Kr. Jha and R. M. Ghimire. "Impact of Renewable Distributed Generation on Protection Coordination of Distribution System", International Journal of Engineering and Applied Sciences (IJEAS) ISSN: 2394-3661, Vol-6, Issue-4, April 2019.

[2] Ambarnath Banerji, E. D. Chakrabarty, T. Biswas, D. Bhattacharya, Abhrodip Chaudhury, M. Bhattacharyy, D. Saha, S.K. Biswas, Ayan Banerji and Arpan Banerji, "A Rural Autonomous Grid Delivering Quality Power to its Loads," In Proc. Of IEEE International Conf. on Intelligent Control Power and Instrumentation ICICPI 2016, 21st -23rd October 2016, pp. 204 - 209

[3] P. Chakraborty, S. Duttam, S. Ghosh, S. Chattopadhyay, S. Khan, V. K. Yadav, Ambarnath Banerji, Sujit K. Biswas, "Enhancement of voltage stability of autonomous wind power generation system using DSTATCOM,"In Proc. Of IEEE International Conf. on Power Electronics , Drives and Energy Systems (PEDES) 2014, pp 1-6

[4] Ambarnath Banerji, Sujit K. Biswas and Bhim Singh, "Enhancing Quality of Power to Sensitive Loads with Microgrids," IEEE Trans. Industry Application, Vol. 52, Issue: 1 Pages: 360 - 368, Jan/Feb 2016.

[5] Ambarnath Banerji, Sujit K. Biswas, DebasmitaSen, Ayan K. Bera, Debtanu Ray, Debjyoti Paul, Anurag Bhakat, "MICROGRID : A Review," IEEE Intl. Conf. GHTC-SAS 2013, pp. 27 - 35.

[6] Sindhura Gupta, Susovan Mukhopadhyay, Ambarnath Banerji and Sujit Kumar Biswas, "Fault Management in Isolated Microgrid," 2018 IEEE International Conference on Power Electronics, Drives and Energy Systems (PEDES).

[7] A. R. Haron, A. Mohamed, H. Shareef, H. Zayandehroodi, "Analysis and Solutions of Overcurrent Protection Issues in a Microgrid," 2012 IEEE Intl. Conf. on Power and Energy, (PECon), Malaysia, Dec. 2012.

[8] I. Almutairy, "A Review of Coordination Strategies and Techniques for Overcoming Challenges to Microgrid Protection," IEEE Intl Conf. 2016 Saudi Arabia Smart Grid (SASG), 6-8 Dec. 2016.

[9] Shuchismita Biswas and Virgilio Centeno, "A Communication based Infeed Correction Method for Distance Protection in distribution Systems," IEEE, 2017 North American Power Symposium (NAPS), 17-19 Sept. 2017.

[10] R. Shah, P. Goli and W. Shireen, "Adaptive Protection Scheme for a Microgrid with High Levels of Renewable Energy Generation", 2018 Clemson University Power Systems Conference (PSC), 11 March 2019.

[11] H. Rahbari Magham, M. J. Sanjari, B. Zaker and G.B. Gharehpetian, "Voltage profile improvement in a microgrid including PV units using genetic algorithm," IEEE Iranian Conference on Smart Grids, May 2012.

[12] X. Liu, M. Shahidehpour, Z. Li, X. Liu, Y. Cao and W. Tian, "Protection Scheme for Loop-Based Microgrids," IEEE Trans. on SMART GRID, vol. 8, no. 3, MAY 2017.

Study on mechanical behavior of Concrete Incorporating Alccofine

BLN Sai Srinath
*Research Scholar
Department of Civil engineering,
Gitam University, Andhra Pradesh,
India
srinath296@gmail.com

Chandan Kumar Patnaikuni
Assistant Professor
Department of Civil engineering,
Gitam University, Andhra Pradesh,
India
srinath296@gmail.com

***Abstract*— Making concrete industry sustainable in the present scenario is very important, to reduce its adverse effects on environment. While choosing raw materials for construction it is necessary to go with eco-friendly materials. Alccofine is one such material which is a by-product from steel industry possessing cementitious properties that can be used as replacement of cement in concrete. Concrete mixes of M20 grade with replacement of cement by 0%, 5%, 10%, 15% and 20% of Alccofine were prepared. This concrete's mechanical properties were studied for compressive strength, flexural strength and split tensile strength. It is observed that the strength values are improved by incorporation of alccofine because it accelerates the hydration of cement particles. In the present paper, the results of the study exploring these strength characteristics of Alccofine replacing cement for the curing duration of 28 days. The microstructural analysis was also conducted using a scanning electron microscope (SEM). From the results it was concluded that the addition of Alccofine displays a better strengthening property.**

Keywords*— *Alccofine, SCM, concrete strength

I. INTRODUCTION

Cementitious mediums for concrete that contain aggregates are brittle and allow cementitious materials to adapt. Concrete has been used in the construction industries at an increasing rate, as concrete technology developed. Concrete is primarily composed of cement. Water, cement, coarse and fine aggregates, and admixtures are used in the manufacture of concrete. Concrete is extremely important because cement bonds together with other materials. Alumina, Silica, and Iron Oxide are major raw materials in cement manufacturing. The four major coordinating compounds are formed when these oxides combine at high temperatures in the kiln.

Alccofine is a new generation ultrafine product with low calcium silicate concentration that is readily available in India. It possesses properties that help concrete operate better in both the fresh and hardened states. Alccofine has better qualities than other Indian admixtures. Alccofine is utilized in concrete mixtures with high workability, strength, and modulus of elasticity, as well as high density, dimension stability, low permeability, and chemical resistance. The Alccofine 1203 from Gujarat's Ambuja cement was employed in the experiment.

Researchers Narender and Meena recently concluded that using fly ash and alccofine instead of cement led to concrete that was more eco-friendly than conventional concrete. Compared to the control mix, Saurav and Gupta were able to increase the compressive strength by 46.5% by replacing 10% of cement with alccofine. A mixture of 16% fly ash and 8% alccofine resulted in the greatest compressive strength and flexural strength, according to Deval Soni et al. The addition of alccofine to binder materials resulted in higher particle packing, and high strengths formed early in life, according to Suthar et al. By using fly ash in geopolymer concrete, Jindal et al. developed composite concrete with higher strength than specimens with 0% or 5% fly ash replacement. The compressive strength of pond fly ash based geopolymer mortar in different curing conditions was increased when treated with alccofine, according to Saxena et al. Concrete that contains alccofine showed enhanced microstructural characteristics and improved mechanical properties. As reported by Sagar and Sivakumar, alccofine based HSC behaved under uniaxial stress strains, and a mix with 10% alccofine provided the highest Young's modulus and largest energy absorption capacities than other mixes. To confirm whether it is feasible to develop a more environment-friendly concrete by partially replacing cement with alccofine, this study will conduct an experimental investigation. These results will be applicable for large-scale projects. In this case, alccofine additions will be evaluated on concrete mixes for its effect on mechanical properties. It was found that alccofine was able to significantly influence the studied parameters.

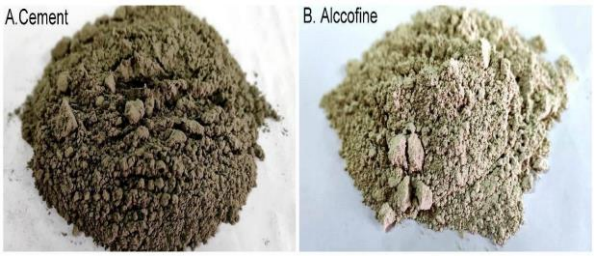

Fig. 1. Cement And Alccofine

II. EXPERIMENTAL WORK

A. Materials

1) Cement

The cement used is standard Portland cement of Grade 53 as shown in figure 1, procured from a single source and meeting IS 12269-2013 standards. As shown in Table 1, cement has the following properties.

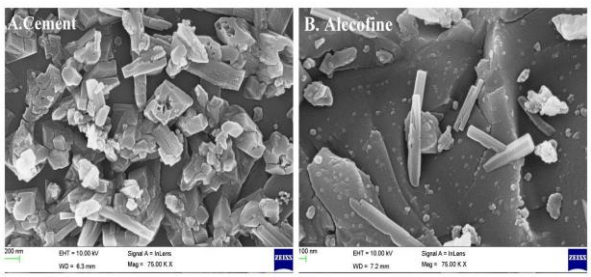

Fig. 2. Sem Images of Cement and Alccofine

2) Alccofine

Alccofine as shown in figure 1, is an ultra-fine slag produced by Ambuja Cement Pvt. Table 1 shows the properties of Alccofine. Figure 2 indicates that the particles are irregularly shaped and have sharp edges. Alccofine was used in this study with a specific gravity of 2.7. The particle sizes ranged from 1 to 75 µm with a major fraction between 20 and 50 µm. In figure 2, you can see images of alccofine scanned using a scanning electron microscope. Table 2 and Figure 3 show the elemental compositions of cement and Alccofine using EDAX.

TABLE I. PROPERTIES OF OPC AND ALCCOFINE

Property	OPC	Alccofine
Bulk density (kg/cum)	1435	660
Surface area (m2/kg)	350	1200
Specific gravity	3.18	2.70
Particle shape	Spherical	Irregular
Color	Grey	Pale white

Based on SEM images of 53 grade OPC cement and Alccofine, it appears that the cement particles are irregular with sharp edges. The figure shows an EDAX image of cement. As a major phase's compound, it has alite, calcite, and larnite.

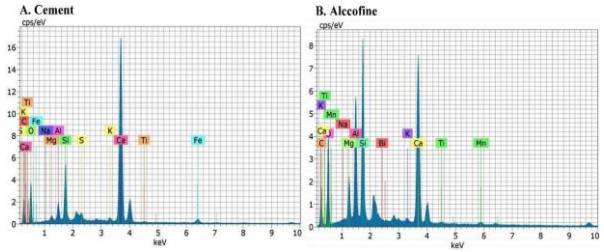

Fig. 3. FIGURE 3 ELEMENTAL COMPOSITION GRAPH OF CEMENT AND ALCCOFINE SAMPLE BY EDAX

TABLE II. ELEMENTAL COMPOSITIONS OF CEMENT AND ALCCOFINE BY EDAX

Elements and compounds	Compound formula	Cement (%)	Alccofine (%)	Composition of cement as per IS 12269-2013 (%)
Calcium	CaO	65.82	39.17	60-67
Silicon	SiO2	14.64	29.22	17-25
Iron	FeO	3.62	-	0.5-6
Aluminium	Al2O3	4.78	20.19	3-8
Sulphur	SO3	2.32	-	1-3
Magnesium	MgO	1.14	6.62	0.1-4
Potassium	K2O	0.4	0.25	0.1-1
Sodium	Na2O	0.22	0.06	0.1-1
Titanium	TiO2	0.07	0.24	-

3) Fine aggregates

In this research, river sand is used, and its physical properties are tested according to IS 383: 2016. Table 3 shows the physical properties of fine aggregates.

4) Coarse aggregate

The gravel of size not larger than 20mm is collected from local supplier which meets the specifications of IS 383: 2016, which describes the physical properties of the material, is used for testing. Given in Table 3, coarse aggregate exhibits the following physical properties.

TABLE III. PROPERTIES OF FINE AGGREGATE AND COARSE AGGREGATE

Property	Fine aggregate	Coarse aggregate
Zone	II	-
Specific gravity	2.65	2.75
Bulk density	1652	Kg/m^3
Fineness modulus	2.77	6.25
Shape	-	Crushed angular
Size	4.75mm	20mm

5) Water

Casting and curing are accomplished with laboratory water from the university, which is added in accordance with the mix design.

6) Superplasticizer

The superplasticizer used in this study is Fosroc Conplast SP430 DIS. Based on the mix, the amount of superplasticizer is adjusted and the final dose is determined by slump testing.

B. CHEMICAL ANALYSIS OF MATERIALS

Using a field emission scanning electron microscope to study material microstructure and surface morphology is very popular in concrete related studies. For examining the chemical composition of concrete and its oxide composition, energy dispersive x-ray analysis (EDAX) is conducted. Using cement and Alccofine as examples, this section discusses the chemical composition of these materials. A FESEM image of cement and alccofine is shown in figure 2.

It can be seen in Figure 2 that the microstructure of the cement sample is spherical. The cement particles also display homogeneous size distributions. The high reactivity of Alccofine is due to its low calcium, silicate content and controlled granulation. Compared to cement, fly ash, and silica, alccofine has a much finer particle size. The amorphous nature of Alccofine is shown in figure 2. Adding Alccofine to concrete increases the cementitious gel, which helps to reduce the permeability of the paste and to improve its durability thanks to its ultra-fineness and calcium oxide content.

III. METHODOLOGY

Figure 4 depicts the overall research methodology used in this study. Concrete mix designs for M20 grade concrete are based on the Indian standard IS: 10262-2019. M20 specimens without Alccofine are used as control mixes1. In this case, water-cement ratio was set at 0.40 and superplasticizer dosage was set at 1% by weight of binding material (Alccofine and cement).

Table 4 outlines the proportions of concrete mix at each level of replacement of 1m3 of concrete. Alccofine is substituted for cement in the following ways (5, 10, 15%, and 20%) in the casting of test specimens. As per Indian standards concrete specimens were prepared in three shapes: cube, cylinder, and beam. Compressive strength is determined by cubes of 100mmx100mmx100 mm size as shown in figure 4.

Fig. 4. COMPRESSION TESTING MACHINE (CTM)

The split tensile strength of cylinder specimens with a diameter of 150mm and a height of 300 mm is also measured as shown in figure 5. For testing the flexural strength of beams, 100mmx100mmx500mm size specimens are used. Lab tests were conducted on all cast specimens after 28 days of curing as shown in figure 6.

Fig. 5. SPLIT TENSILE TESTING

Fig. 6. FLEXURAL STRENGTH TESTING

IV. PARAMETERS STUDIED

Using the Indian standard IS 10262-2019 as a guide, Table 4 under-represents the mix calculations in detail. All the test specimens were evaluated for their flexural, compressive, and split tensile strength after 28 days of curing in this study. In this study, the samples were also analyzed microscopically after they were cured for 28 days.

TABLE 4 MIX PROPORTIONS Kg/m^3 OF ALCCOFINE CONCRETE

Alccofine replacement	**0%**	**5%**	**10%**	**15%**	**20%**
Cement	345	344	326	308	290
Alccofine	0	18	36	54	72
Water	148	152	152	152	152
F.A.	750	652	652	652	652
C.A.	1170	1322	1322	1322	1322
SP	3.45	3.63	3.63	3.63	3.63

V. ANALYSIS AND DISCUSSION

Alccofine was attempted to be used in concrete of grade M20 in this experiment. Concrete was formulated using various proportions of Alccofine (0%, 5%, 10%, 15% and 20%) in order to reduce cement consumption. For experiments to be reported using various tests, it is necessary to detail various properties and visualize them graphically. Therefore, the next section includes details about numerous properties illustrated with graphs of different shades, in order to symbolize comparative standings.

Table 5 represents the results of testing the compressive strength of concrete as per Indian standards IS 516-1959 at 28 days of curing. Concrete specimens were tested for mechanical properties at 28 days after curing, as shown in Table 5. Comparing the specimens with Alccofine up to 15% to the control specimens, the specimens with Alccofine up to 15% achieve the maximum compressive strength. For M20 grade concrete mix 4 with 15% Alccofine replacement exhibited a maximum compressive strength of 30.10mpa 28 days. The compressive strength gain of Mix 4 compared to conventional Mix 1 is 7%.

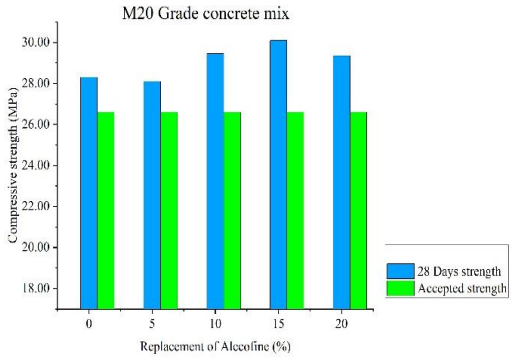

Fig. 7. COMPRESSIVE STRENGTH

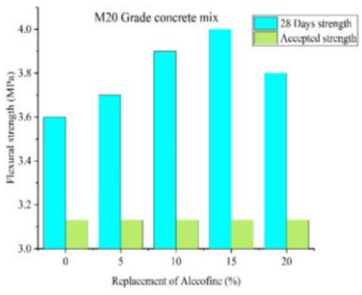

Fig. 8. FLEXURAL TENSILE STRENGTH

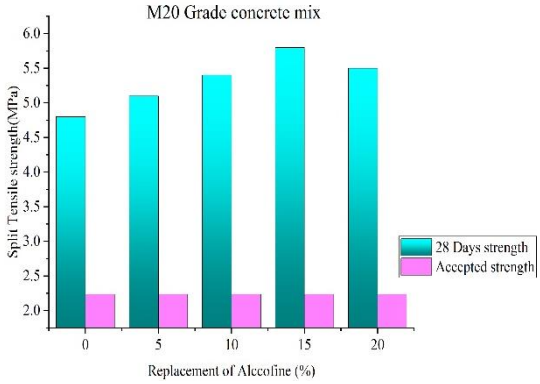

Fig. 9. SPLIT TENSILE STRENGTH

- Increasing split tensile strength occurs at each replacement level. At 28 days after curing, the maximum strength of 15% Alccofine is observed. Alccofine was substituted for up to 15% of the cement in the control mix to achieve the maximum split tensile strength.

- As Alccofine percentage increases, the split tensile strength is shown to decrease suddenly beyond 15 % replacement. Based on this test, a concrete containing 15 % Alccofine showed extremely promising results as compared to concrete with a lower dosage. For 15% replacement of Alccofine in the concrete, the splitting tensile strength of M20 grade concrete is increased from 4.80 N/mm^2 to 5.8 N/mm^2 for 28 days of curing time. Depending on the Alccofine replacement level, the flexural tensile strength of the M20 grade ranged from 3.60 N/mm^2 to 4.0 N/mm^2.

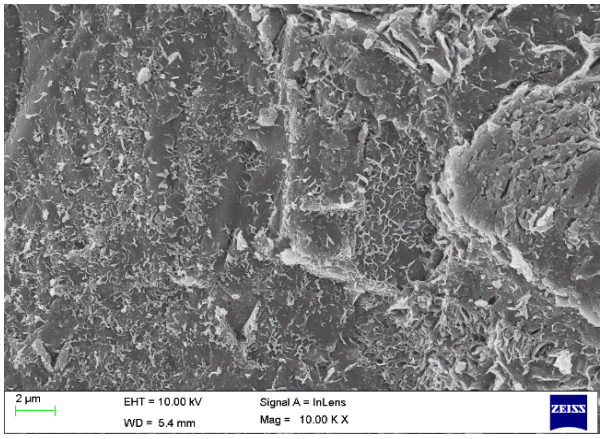

Fig. 10. FIGURE 10 MICROSCOPIC IMAGES OF M20 GRADE CONCRETE AT 15% OPTIMUM DOSAGE OF ALCCOFINE

SCANNING ELECTRON MICROSCOPY

The morphology of M20 grade of concrete shows homogeneous and denser microstructure. As the concrete mix contains ordinary Portland cement (OPC) and Alccofine (ultra-fine slag) as binder which are rich in calcium and silica, there was formation of calcium hydroxide (Ca $(OH)_2$) and calcium silicate hydrate (C-S-H) gels in the microstructure. M20 grade of concrete exhibited slightly denser microstructure which may be due to formation of higher amount of calcium silicate hydrate gels. The calcium hydroxide which represented as hexagonal plate like structure was identified in all concrete mixes, however, it formed in higher amount in the M20 grade of concrete. Further, the formation C-S-H gel was identified as reticular network in the morphology of concrete as shown in the above figure.

VI. CONCLUSIONS

- In terms of hydration process and strength gain, 15% Alccofine Replacement is optimum. Conversely, partial replacements of 10% Alccofine and 20% Alccofine might have behaved as fillers in the concrete's bonding phase.

- With respect to SEM images, it can be understood that in M20 grade concrete, the active reaction of alccofine can be observed. This means that alccofine shows good reaction in concrete when replaced for 15%.

- A marginal improvement can be seen in both flexural and split tensile strength results also, this specifies that there are no negative advantages of using alccofine in concrete.

- Also, from the chemical composition table it is observed that there is silica and alumina difference compared to cement. Silica and alumina are contributing for strength improvement in M20 grade of concrete.

- The formation of CSH gel and CASH gel is improved due to the presence of excessive alumina from alccofine. This means silica and alumina are acting as secondary reactive components which are gaining extra strength to concrete. Also there is a possibility that only alccofine is standing responsible for addition of strength. Calcium has instantaneous reaction for strength, but more calcium is already available in cement, so it only forms a gel, but expecting strength improvement in long term is being possible in the form of secondary reactions.

- Thus, the secondary reaction is not happening just due to cement, but also with the help of a third-party materials that are coming from alccofine i.e., silica and alumina which are excessive in quantity which is deficient in cement. This is the most obvious reason the extra strength gain when alccofine is added to the concrete.

REFERENCES

[1] D. Singhal, B.B. Jindal, S.K. Sharma, Parveen, D.K. Ashish, (2017) Improving compressive strength of low calcium fly ash geopolymer concrete with alccofine, Advances in Concrete Construction: 17-29

[2] Kala TF, Vaidevi C, Kalaiyarrasi (2020) Mechanical and durability properties of self-compacting concrete with marble fine aggregate. Materials Today Proceedings.

[3] Naqash JA, Reddy PN (2019) Properties of concrete modified with ultra-fine slag. Karbala International Journal of Modern Science. Vol 5.

[4] JA Naqash, Reddy N (2019) Effect of alccofine on mechanical and durability index properties of green concrete. IJE Transactions 813–819

[5] PN Reddy, Ahmed JN, (2019) Development of high early strength in concrete incorporating alccofine and non-chloride accelerator. SN Applied Sciences: 755

[6] Naqash JA, Reddy NP (2019) Durability and mechanical properties of concrete modified with ultra-fine slag. International Journal of Innovative Technology and Exploring Engineering: 230–234

[7] Naqash JA, Reddy PN (2019) Strength prediction of high early strength concrete by artificial intelligence. International Journal of Engineering and Advanced Technology: 330–334

[8] Sashidhar C, Jawahar JG, Kavyateja BV (2019) Investigation on ternary blended self-compacting concrete using fly ash and alccofine. International Journal of Recent Technology and Engineering: 447–451

[9] Kaur D, Siddique R (2012) Properties of concrete containing ground granulated blast furnace slag (GGBFS) at elevated temperatures. Journal of Advanced Research: 45–51.

[10] Shah BK, Suthar Sunil B (2013) Study on strength development of high strength concrete containing alccofine and Flyash. Indian Journal of Research: 102–104

[11] Patel PJ, Shah BK, Suthar S (2013) Study on the effect of alccofine and fly ash addition on the mechanical properties of high-performance concrete. International Journal for Scientific Research & Development: 464–467

[12] Ramesh Kumar, R. Venkatasubramani, P. Muthupriya (2013) the experimental investigation on durability characteristics of high-performance concrete, International journal of scientific and technical research. 239-250

[13] Kulkarni S, Soni D, Parekh V (2013) Experimental study on high-performance concrete, with the mixing of alccofine and Flyash. Indian Journal of Research: 84–86

[14] Saurav AK (2014) Experimental study of strength relationship of concrete cube and concrete cylinder using ultrafine slag alccofine. International Journal of Scientific & Engineering Research, 102-107

[15] Patil PN, Patil YO, Dwivedi (2013) GGBS as partial replacement of OPC in cement concrete—an experimental study. International Journal of Scientific Research: 189–191

[16] Saoji AC, Pawar MS (2013) Effect of alccofine on self-compacting concrete. The International Journal of Engineering and Science: 05–09

[17] Venkateswararao K, Swaroop AHL, Kodandaramarao P (2013) Durability studies on concrete with fly ash and Ggbs. Int J Eng Res Appl 3(4):285–289.

[18] K. Gayathri, K. Ravichandran, and J. Saravanan, "Durability and Cementing Efficiency of Alccofine in Concretes", International Journal of Engineering Research & Technology (IJERT), ISSN: 2278-0181, Vol. 5 Issue 05, May-2016, Page 460-467.

[19] LJ Sanjeev Kumar, P Bhuvaneshwari, Moka Eswar and K Aditya Subramanian "Strength Characteristics Of Alccofine Based Light Weight Concrete" International Journal of Advanced Research in Engineering and Technology (IJARET) Volume 10, Issue 1, January-February 2019, pp. 268-275

[20] Author Narender Reddy and T. Meena "An Experimental Study to Find the Optimum Dosage of Admixtures in Blended Concrete" International Journal of Recent Technology and Engineering (IJRTE) ISSN: 2277-3878, Volume-7, Issue-6, March 2019

[21] Keyur S Jasani, S. Manivel, and G. Senthil Kumar "An Experimental Investigation on Strength Properties Of Alccofine 1203 Along With Recycled Aggregate In Concrete" International Journal of Civil Engineering and Technology (IJCIET) Volume 9, Issue 4, April 2018, pp. 138–148

[22] Mohammed Asad Agha, Peta Purnachandra Sai, R Vinay, A Anil Goud "Development Of Early Compressive Strength In High-Performance Concrete Using Perlite And Alccofine" International Journal of Civil Engineering and Technology (IJCIET) Volume 9, Issue 4, April 2018, pp. 382–388.

[23] B.Kaviya, K.Rohith, Soniya Kindo, Manoj Kumar J, Divya P "Experimental Study On Partial Replacement Of Cement Using Alccofine" International Journal of Pure and Applied Mathematics Volume 116 No. 13 2017, 399-405

[24] Nista lama Ghising and Vijay Kumar "Experimental Investigation On Properties Of Concrete With Alccofine1203 As Partial Replacement Of Cement Subjected To Different Curing Regimes" International Journal of Mechanical and Production Engineering Research and Development (IJMPERD) Vol. 10, Issue 3, Jun 2020, 4249–4256.

[25] Rajesh Kumar, AK Samanta and DK Singha Roy, "An experimental study on the mechanical properties of Alccofine based high-grade concrete", International Journal of Multidisciplinary Research and Development, Vol. 2 Issue 10 2015, Page 218-224.

[26] P. Narasimha Reddy and J. Ahmed Naqash "Effect of Alccofine on Mechanical and Durability Index Properties of Green Concrete", IJE TRANSACTIONS C: Aspects Vol. 32, No. 6, (June 2019) 813-819

[27] Mahim Mathur, Ashish Mathur "Performance of Concrete by Partial Replacement of Alccofine -1203" International Journal of Engineering Research & Technology (IJERT) ISSN: 2278-0181 RTCEC - 2018 Conference Proceedings.

[28] Ankit Nainwal, Akshay C, Jaibeer Bhandari, "Comparison between Simple Concrete Cubes and Alccofine Mixed Concrete Cubes (M20 Grade)", IJSRE Volume 05 Issue 2017, Page 6857-6871.

[29] Saurav and Ashok Kumar Gupta. 2014 "Experimental study of strength relationship of concrete cube and concrete cylinder using ultrafine slag Alccofine" Int. J. Sci. Eng. Res. 5(5) 102-7.

[30] R Suganya and Latha Maheshwari, "Experimental Investigation on Alccofine Concrete" Vol. 8 Issue 04, April-2019, International Journal of Engineering Research & Technology (IJERT), 2019.

[31] IS 383. Specification for Coarse and Fine aggregates from Natural Sources of Concrete. Bureau of Indian Standards. New Delhi, India; 1970.

[32] IS 456. Code of practice for Plain and Reinforced Concrete (Fourth Revision). Bureau of Indian Standards. New Delhi, India; 2000. 34. IS 2386. Methods of Tests for Aggregates for concrete. Bureau of Indian Standards. New Delhi, India; 1963.

[33] IS 10262. Concrete Mix Proportioning – Guidelines. Bureau of Indian Standards. New Delhi, India; 2019.

[34] BhanavathSagar, Sivakumar M.V.N 2020 "Mechanical and Microstructure Characterization of Alccofine Based High Strength Concrete", Silicon: springer nature 2021

[35] Bala muralikrishnan R, Saravanan J, "Effect of Alccofine and GGBS Addition on the Durability of Concrete", Civil Engineering Journal Vol. 5, No. 6, 1273-1288.

Job opportunities and challenges to the employability of Fresh Diploma Engineers of West Bengal state in the emerging sector

Suman Sikdar,
Department of Mechanical Engineering,
Technique Polytechnic Institute,
Hooghly, West Bengal, India
sikdar.suman@gmail.com

***Abstract*— Advancement in technology is creating new job opportunities as well as new challenges to the employability of the Fresh Diploma Engineers. Rapid advancement in technology in emerging sectors like solar energy, electric mobility, automation, artificial intelligence, financial technology will affect every occupational group in the future. It has been estimated that 47 % of the current jobs are expected to be taken over by machines and devices during the next two decades. On the other hand, 65,000 (sixty-five thousand) new IT jobs will be created by 2024, mostly in cloud related fields. Changes in consumer behavior generate new opportunity for entrepreneurship in the engineering, technology and management fields. This ever-changing technology creates "skill gap" between the desired skills sets and the available skill sets. This skill gap has to be compensated by learning new skills – both technical skills and professional skills. I have taken into account the following 3 objectives to study the opportunity and challenges in the emerging sector.**

Objective of this research is

- **To estimate the current number of graduating Diploma Engineers from polytechnics in West Bengal and rest of India.**
- **To find out the emerging sectors of Indian economy where job opportunities are created for Diploma Engineers.**
- **To find out the challenges to the employability of Fresher Diploma engineers from West Bengal state in those emerging sectors**

Diploma Engineers, Institute Faculty, Placement agency, Government and Private Skill development agency will be benefited from this study.

Keywords— Employability, Polytechnics of West Bengal , Diploma Engineers, job opportunity, challenges to employability, emerging sectors

I. INTRODUCTION

Employability :

Employability is the quality of being suitable for paid work.

The Confederation of British Industry (CBI) (2009) defines employability as: "A set of attributes, skills and knowledge that all labour market participants should possess to ensure they have the capability of being effective in the workplace – to the benefit of themselves, their employer and the wider economy".

Emerging Sector :

An emerging sector is one that is new or relatively new, is growing fast and is expected to become an important sector in the future. This sector is rising due to the evolving change in the needs, taste and preference of the changing population. This sector is likely to generate higher employment and self-employment for the Engineers and Technocrats. I have identified 10 major emerging sectors of our economy where fresher diploma engineers can secure jobs. These emerging sectors are expected to generate larger employment and better income opportunity . Career growth is faster in these sectors.

Diploma Engineering Programmes :

Diploma Engineers are those who have completed 3 Years Diploma Engineering course from the polytechnics. Major Diploma Engineering courses are Mechanical engineering, Electrical engineering , Civil engineering , Electronics & telecommunication engineering, Computer-Science & Technology, Mining engineering , Architecture engineering, Metallurgical engineering, Footwear Technology, printing technology etc. There are also special Diploma Engineering Courses which can be studied.

Polytechnics in West Bengal :

I have studied about the Polytechnics system education in West Bengal state. All these polytechnics, Government, Sponsored, centrally funded and Self-Financed, are affiliated to West Bengal State Council of Technical and Vocational Education and Skill Development (WBSCT&VE&SD) and approved by All India Council of Technical Education (AICTE). There are currently 183 polytechnics in West Bengal. Every year approximately 25,000 Diploma Engineers complete their courses from polytechnics in West Bengal are ready for jobs or entrepreneurship. This study will guide the budding diploma engineers to acquire jobs in the emerging sectors. They can acquire the skill-sets as per the demand of the job market.

Self-employment / Entrepreneurship :

Entrepreneurship refers to all those activities which are to be carried out by a person to establish and to run the business enterprises in accordance with the changing technological, social, political and economic environments. Entrepreneurs introduce new business ventures to meet the expectations of the changing consumer demands.

Challenges to Employability : The emerging sector comes with new challenges. This ever changing technology creates more Skill Gap. Skill gap is the difference between the desired skill and available skill of an individual / group of individual / employees. This skill gap has to be compensated for through learning new skills – both technical skills and professional skills. Desired skills will not be sufficient to match with the available skills. One has to be a lifelong Learner to remain updated. I have studied those skills to be acquired as well as the challenges faced by the engineering students in the post Covid-19 world.

II. LITERATURE REVIEW

- *PWC Report. Will Robots really steal our Jobs ?*

"any job losses from automation are likely to be broadly offset in the long run by new jobs created as a result of the larger and wealthier economy made possible by these new technologies. We do not believe, contrary to some predictions, that automation will lead to mass technological unemployment by the 2030s any more than it has done in the decades since the digital revolution began"

- *India Skills Report 2021, Powered by Weebox . KEY INSIGHTS INTO THE POST-COVID LANDSCAPE OF TALENT DEMAND AND SUPPLY IN INDIA*

"Forbes states that the online learning market alone is estimated to grow to $350 billion by 2025. With the connectivity of the internet and online learning, a vast Indian talent pool stands to benefit by acquiring skills necessary to the changing employability landscapes."

- *India Skills Report 2022, Powered by Weebox*

"Maharashtra, Karnataka and Tamil Nadu were identified as the top states where maximum hiring activity will occur in the coming year"

III. 1ST OBJECTIVE OF THE RESEARCH

To estimate the current number of graduating Diploma Engineers from polytechnics in West Bengal and rest of India.

THE POLYTECHNIC SYSTEM AND DIPLOMA ENGINEERING EDUCATION OF WEST BENGAL

The 3 Years diploma engineering courses of West Bengal is under the affiliation of West Bengal State Council of Technical and Vocational Education and Skill Development (WBSCT&VE&SD). This can be studied in polytechnic colleges. 40 Diploma Engineering courses are run by the State Council in the Polytechnics under their affiliation. Furthermore, all these polytechnics are approved by All India Council of Technical Education (AICTE). AICTE is the national-level apex body for promotion and development of technical education in the country in a coordinated and integrated manner. AICTE was vested with statutory authority for planning, formulation, and maintenance of norms & standards, quality assurance through accreditation etc.

As on 1st June, 2011, West Bengal had a total number of 65 Polytechnics, 40 being Govt. & Govt. Sponsored and 25 self-financed. Total intake was 17,185 before 1st June, 2011. Substantial growth has been registered and now the total number of Polytechnics across the West Bengal State has reached to 183, out of which 73 are Govt. Polytechnics, 3 are Govt. Sponsored, 2 are Centrally Funded Diploma Institutions and 105 are Self-Financed. The intake capacity in Polytechnics has now gone up to 39,955 in 2020-21.

Major Diploma Engineering course :

Mechanical, Electrical, Civil, Electronics, Computer-Science, Mining, Architecture, Metallurgical, Footwear Technology

Special Diploma Engineering courses :

Automobile, Survey, Instrumentation & Control, Packaging Technology, Geographic Information System and Global Positioning, Chemical, Food Processing Technology, Cyber Forensics and Information Security, Renewable Energy, Printing technology , Photography, Multimedia Technology.

Number of Polytechnics in West Bengal, courses and total intake as on 2020 – 2021

Number of Diploma Engineering courses run by Polytechnics of West Bengal	40
Number of Government Polytechnics (A)	73
Number of Government sponsored Polytechnics (B)	3
Number of centrally funded Diploma Institutions (C)	2
Number of Self-Financed Polytechnics (D)	105
Total Number of Polytechnics In West Bengal (A+B+C+D)	183
Total Intake Capacity of all the polytechnics	39,955

The following chart provides data about the Number of AICTE approved Polytechnic Institutes, approved intake, student passed and the recorded placement of the polytechnics in West Bengal and rest of India.

Year	India / West Bengal / Maharashtra	Number of Institutes	Approved Intake (A)	Student passed (B)	Passed / Intake % (B / A)	Placement (C)	Placement % (= C / B %)
2017 - 2018	All India	3,921	12,11,811	4,58,520	37.8	1,95,379	42.6
2018 – 2019	All India	3,783	11,28,167	4,48,379	39.7	2,04,052	45.5
2019 – 2020	All India	3,711	10,46,335	3,67,279	35.1	2,02,257	55.1
2020 – 2021	All India	3,667	10,11,323	-		1,75,716	
2017 - 2018	West Bengal	150	38,828	26,101	67.2	10,911	41.8
2018 – 2019	West Bengal	149	38,740	27,142	70.1	12,141	44.7
2019 – 2020	West Bengal	159	40,080	21,711	54.2	11,421	52.6
2020 – 2021	West Bengal	183	39,955	-		8,728	
2017 - 2018	Maharashtra	460	1,53,190	60,389	39.4	11,717	19.4
2018 – 2019	Maharashtra	424	1,33,297	61,217	45.9	15,601	25.5
2019 – 2020	Maharashtra	402	1,18,059	44,049	37.3	14,914	33.9
2020 – 2021	Maharashtra	393	1,11,637	43,000	38.5	12,345	

Interpretation of Data

- *West Bengal:* Out of 40 thousand Diploma Engineering seats in West Bengal, 25 thousand are passing-out every and only 11 thousand are getting placement immediately after completion of the course.
- *Maharashtra:* Out of 1.1 Lakh Diploma Engineering seats in Maharashtra, 43 thousand are passing-out every and only 14 thousand are getting placement immediately after completion of the course
- *All India:* Out of 11 Lakh Diploma Engineering seats All India, 4 ½ Lakh are passing-out every and only 2 lakh are getting placement immediately after completion of the course.
- *Placement:* Finding placement immediately after completion of course may be difficult. This placement data is essentially for those who have secured jobs through campus recruitment.

IV. 2ND OBJECTIVE OF THE RESEARCH :

To find out the emerging sectors of Indian economy where job opportunities are being created for Diploma Engineers.

10 EMERGING SECTORS IDENTIFIED AND CLASSIFIED

Emerging Sector: An emerging sector is one that is new or relatively new, is growing fast and is expected to become an important sector in the future. This sector is rising due to the evolving change in the needs, taste and preference of the changing population. This sector is likely to generate higher employment and self-employment for the Engineers and Technocrats. 10 emerging sectors of Indian economy have been identified here. Matching disciplines of the 3 Years Diploma Engineering courses are shown in the chart.

Employment in Emerging Sector : With respect to the job market scenario, it has been observed that courses like Diploma in Mechanical, Electrical and Electronics engineering are a major beneficiary in these emerging sectors. 25,00 Diploma Engineers are passing-out every year from West Bengal currently. These sector, all put together, is able to absorb almost all these Engineers who have the required skill sets and attitude. Example: Mechanical and Electrical students can find jobs in Electric mobility, solar technology, automobile and auto-ancillary, battery technology etc. Computer science / IT / Electronics students can find jobs in Cloud computing, Artificial Intelligence (AI), Machine Learning (ML), Internet of Things (IoT), Blockchain, Data Science etc.

Self – Employment in Emerging sectors: Emerging sector provides new opportunity for self- employment. Innovation is the buzzword now. The talented engineers who are able to develop innovative products and services and are able to form a company, can get self-employed. They can turn out to be good Entrepreneurs. Entrepreneurship refers to all those activities which are to be carried out by a person to establish and to run the business enterprises in accordance with the changing technological, social, cultural, political and economic environments.

Sl. No.	Emerging Sectors	Matching disciplines of 3 Years Diploma Engineering
1	Electric Mobility, Battery operated vehicles, Battery Charging & Infrastructure	Mechanical, Electrical, Automobile, Electronics, Mechatronics, Instrumentation
2	Automotive engineering / Auto-Ancillary	Mechanical, Automobile, Electrical, Electronics
3	Solar Technology, Bio-Fuels	Electrical, Electronics, Instrumentation, Mechanical, Renewable Energy
4	Environmental engineering and sustainability, Survey, GIS / GPS, Mapping, remote sensing, agricultural engineering	Survey, Civil, Geographic Information System and Global Positioning,
5	E-commerce, Supply Chain Management	Any Diploma
6	Telecommunication Infrastructure & Hardware, wired and wireless communication	Electronics, Electrical, Instrumentation,
7	Robotics and Automation, Sensor Networks, Drones technology	Mechanical, Electronics, Instrumentation, Mechatronics
8	Cloud computing, Artificial Intelligence (AI), Machine Learning (ML), Internet of Things (IoT), Blockchain, Data Science, Cyber Security, Educational Technology, Apps Development, Virtual reality, Image and Video Analytics	Computer Science, Electronics, Cyber Forensics and Information Security
9	3D Printing, Modern Manufacturing processes	Mechanical, Electronics, Instrumentation, Mechatronics
10	Financial Technology	Computer Science, Any Diploma

V. 3RD OBJECTIVE OF THE RESEARCH:

To find out the challenges to employability of Fresh Diploma engineers from West Bengal state in those emerging sectors.

THE CHALLENGES TO EMPLOYABILITY FACED BY FRESH DIPLOMA ENGINEERS OF WEST BENGAL

1) *The pandemic effect:* With the coming of the pandemic Covid-19 and lockdowns from March, 2020 till February, 2022, the engineering education has suffered badly. Classes were held online in this period. Engineering streams like mechanical, electrical, electronics, civil, survey, mining where practical classes are much needed, was not held. Consequently, there is a learning gap of 2 years or less for the batches taking admission in the year 2017, 2018, 2019, 2020 and 2021. This has badly affected the skill-sets of the students both in terms of social skills and technical skills. Many of these students are also not willing to relocate to other places due to memory of lockdowns. Also, due to bad health conditions and lethargy some of them are unwilling to take –up field jobs like survey or mapping or machine operator in factory.

2) *The problem of Migration:* Gurgaon, Noida, Delhi-NCR Region, Pune, Chennai, Hyderabad are the geographic locations where majority of the companies are currently located. Also, new factories, service centers, distribution networks are coming up in these geographic locations. Therefore, students of West Bengal will be required to migrate to these places for career opportunities. In most cases the migrating students need to arrange for their own accommodation near the factory; they are required to adapt to the local language, food habits and culture. The starting salary / stipend they get minus the living expenses may not be sufficient for them to save money. Therefore, these students from West Bengal expect a good starting salary. Those who do not get a good starting salary and don't want to migrate may not find suitable and matching job in West Bengal state. This creates unemployable educated youth.

3) *Only One Child of the Parents:* Most students nowadays are from a family where he / she is the only one child of the parents. Some parents, especially from well-to-do families, are reluctant to send their only child to other states for better opportunity. Whatever job they get in the West Bengal state, they adjust to the situation.

4) *Widening Skill Gap:* Skill Gap = Desired Skill Minus the Available skill. The skill gap gets widened with the rapid increase of technology. Engineers unable to upgrade their skills, fall back. New courses will have to be learned, good habits to be cultivated to work in the emerging sectors. This skills gap needs to be reduced as much as possible through continuous skills training programmes.

5) *Need for Skills Training:* It has been estimated that 47% of the current jobs are expected to be taken over by Machines during the next 2 decades. Advancement in technology will affect virtually all occupational group in the future. Skills Training, both soft skills and domain skills, is necessary to work in these emerging sectors. Since the technology used by emerging sectors is new, availability of the good Training institutes and Trainer/Teacher aware of this new technology are very few. These Diploma Engineers will have to self-learn these technologies and make them ready for the industry. Therefore, continuous learning, skilling, re-skilling, upskilling is mandatory for Engineers in the emerging sector.

6) *Newer Professional Skills gaining value:* Professional skills are essentially those related to personality, behaviour and health. These are the professional skills which continue to be in demand both in the current and future job market. Some of the Diploma Engineers lack these skills.

- Teamwork, collaboration, social skills & Emotional balance
- Communication skills & story telling – both written and verbal
- Planning, organizing & problem-solving skills
- Innovation and Creative thinking
- Leadership and Influencing ability
- Good Health and fitness

VI. CONCLUSION

Trust this study gives a clear picture in the minds of the reader about the future job market in the emerging sectors, the current number of graduating Diploma Engineers from polytechnics in West Bengal and the challenges to the employability of Fresher Diploma engineers. This study is expected to benefit fresher Diploma Engineers and those agencies and institutions engaged in technical education and skill development.

REFERENCES

[1] PWC, Impact of Automation on Jobs. Will Robots really steal our Jobs ?

[2] India Skills Report Weebox – 2020, 2021, 2022

[3] A Study On Employability Of Engineering Students In Mumbai And Pune Region, KEERTHI MENON

[4] Role Of Employability Skills In Management Education: A Review Dr M Nishad Nawaz, Dr.B.Krishna Reddy

[5] CURRENT SITUATION OF SKILLS AND EMPLOYABILITY IN INDIA: ENGINEERING EDUCATION PERSPECTIVE. Jagdeep Singh and Mamta Kumari

[6] https://www.mckinsey.com/ Demand for technological, social and emotional, and higher cognitive skills will rise by 2030. How will workers and organizations adapt?

[7] EY , Future of Jobs in India – A 2022 Perspective

[8] Entrepreneurship Management, MBA study material , Pondicherry University

[9] Economic Times

[10] Business Standard

[11] https://webscte.co.in

[12] http://www.wbtetsd.gov.in/

[13] https://www.aicte-india.org/

STUDY OF PERFORMANCE EFFICACY OF SERAMPORE WATER TREATMENT PLANT,WEST BENGAL

Sayantika Saha
Lecturer, Department of Civil Engineering
Technique Polytechnic Institute
Hooghly, West Bengal, India
sayantikasaha92@gmail.com

***Abstract*—The performance efficacy study was undertaken at individual unit of 20 MGD Serampore Water Treatment Plant, West Bengal. Water samples were collected at different stages of treatment units once in a week during study period and analyzed for the major water quality parameters such as pH, turbidity, total dissolved solid, residual chlorine, total hardness, carbonate hardness, magnesium hardness, iron, nitrate, sulphate, total coliform, fecal coliform. Samples from selective points of distribution mains and consumer's end were also collected to assess the quality of supply water. Based on the analysis for physico-chemical parameters, the finished water was conforming to Indian standard for drinking water (IS: 10500,2012) prescribed by APHA guideline in the study period. Result revealed that turbidity removal of clarified water ranging between 81% and 90% have been found. Similarly total coliform and fecal coliform were determined by membrane filter technique. Residual chlorine having 0.2 mg/l was found at the end stage so no bacteria was observed considering post disinfection has been made properly in the treatment system. This research work concludes turbidity values were found satisfactory at different stages except residual chlorine at few points in the distribution system were found less than 0.2 mg/l. Thus, it is concluded that proper disinfection needs to be done including backwashing of rapid sand filter at regular interval.**

Keywords— water treatment, TDS, rapid sand filter, pH, turbidity, total dissolved solid, residual chlorine, total hardness, carbonate hardness, magnesium hardness

I. INTRODUCTION

River is the main inland water resources for all civilizations on earth. They are used by the people for domestic, industrial and irrigation purpose. It must not be polluted. Coming to India ,Ganga is the longest river basin . The water quality of the river has deteriorated due to discharge of pollution load from different sources. The major sources of pollution of the river Ganga are generally the discharge of untreated and partially treated waste water from cities or towns, discharge of untreated and partially treated wastewater from industries, mixing of surface runoff carrying pesticides, agricultural wastes etc. discharge of cattle-shed liquid waste and bathing of cattle in the river and mainly direct disposal of solid waste in the river or mixing of leachate from solid waste dumps. In order to protect the river from contaminations activities relating to abatement of Ganga pollution was taken up by the National River Conservation Directorate under the programme GAP Phase-I and Phase-II.

Kolkata Metropolitan Area (KMA) has got its twofold water source viz: (a) Surface water from the only source of river Hooghly and (b) Ground water source. Out of these two sources, the water from river Hooghly is being treated and supplied to a very limited areas of KMA through the treatment plants and infrastructures that has so far been constructed leaving the vast majority of remaining KMA to depend on the source (b) i.e. Ground water

The Hydraulics of the treatment plant is designed in such a way that water flows by gravity from the collecting well to the clear water reservoir and the sludge generated from the inclined plate settler flows by gravity to sludge sump and ultimately in to the nearest drainage canal.

The overall objective of the proposed research work is to assess the performance of individual unit of Serampore Water Treatment Plant through qualitative analysis.

II. STUDY AREA

Plant Location

The Serampore Water Treatment Plant is located at Chowdhuri Para Lane under Serampore Municipality. The Plant is located at 2-2.5 km East of Serampore Railway station while its intake point islocated about 0.5 Km North of the plant. Both the plant and the intake point are located by the side of river Hooghly.

Figure 1 Clarifloculator

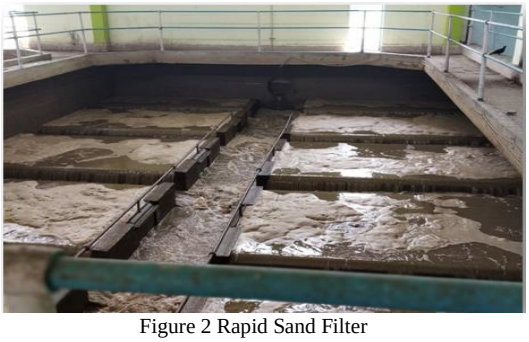

Figure 2 Rapid Sand Filter

The 20MGD Serampore Water Treatment Plant (SWTP) consists of the units which are presented in layout of the plant

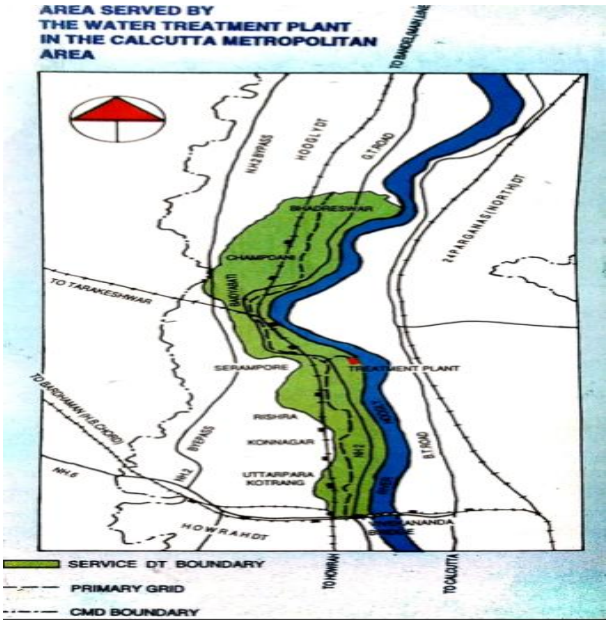

Figure 3 Area served by the Water treatment plant

III. Methodology

Sample collections for Raw and Finished water from the plant were carried out once in a month for a period of 5 months (November,2018 to March ,2019). Samples from clarifier and filter were also collected for the selective physic –chemical parameters during study period. Samples for metals were collected from sludge pocket in month of March, 2019. The samples so collected were preserved properly and brought back to laboratory for further analysis. Samples from selective points of distribution mains were collected for physico-chemical parameters in the month of March, 2019. Samples from selective points of consumer's end were collected for physico-chemical parameters in the month of March 2019.

Samples for Bacteriological parameters such as Total Coliform, Fecal Coliform were collected from Raw water (after pre –chlorination), Clarified water, filtered water and Finished water (after post chlorination) during monthly sampling.

Samples from the selective points of Distribution mains (take off points) were collected for the determination of Total Coliform and Fecal Coliform during supply hours for the month of March,2019.

Samples from the selective points of consumers' end were collected for the month of March, 2019.

Samples so collected were properly preserved and were brought back to School of Water Resources Laboratory for analysis.

Serampore water Treatment plant has two clariflocculators and the clarified water is distributed to ten numbers of filter beds for filtration.

IV. Result and Discussion

- Raw water , clarified water, filter water before chlorination and filter water after chlorination were collected from Serampore Water Treatment Plant for each month and also twice in every month during the study period (from November,2018 to April,2019) for estimation of physic-chemical and bacteriological quality. These results reflect the overall performance of the plant and assure the drinking water quality.
- Water sample from distribution mains and consumer point were also collected to assure the drinking water quality. Avoid combining SI and CGS units, such as current in amperes and magnetic field in oersteds. This often leads to confusion because equations do not balance dimensionally. If you must use mixed units, clearly state the units for each quantity that you use in an equation.
- Physico –chemical and Bacteriological quality of Raw Water (RW), Clarified Water (CW), Filter water Before Chlorination (FWBCL) and Filter water after Chlorination (FW) are summarized in Table I.. to Table V.

TABLE I.

Date of Collection: 16.11.2019		**Month: November, 2019**	
PARAMETERS	***RW***	***CW***	***FWBCL***
Turbidity, NTU	46	8.1	0.8
pH	8.2	7.6	7.5
Conductivity, µmhos/s	338	357	354
Temp., °C	22	21.9	21.8
Residual chlorine, mg/l	-	<0.2	<0.1
TDS, mg/l	169	178.5	177

Date of Collection:29 .11.2019		**Month: November, 2018**	
PARAMETERS	***RW***	***CW***	***FWBCL***
Turbidity,NTU	28	4.3	0.3
pH	8.9	7.6	7.5
Conductivity,µmhos/s	226	342	329
Temp,0C	24.8	24.8	24.8
Residual chlorine,mg/l	-	<0.2	<0.1
Total Hardness,mg/l	100	120	120
Calcium Hardness, mg/l	50	60	60
Iron(as Fe), mg/l	0.05	-	0.05
Chloride(as Cl), mg/l	10	10	10
Alkalinity, mg/l	70	80	80
TSS, mg/l	500	400	300
TDS,mg/l	113	171	164.5
Total Coliform	690/100ML	absent	Absent

TABLE II.

TABLE III.

Date of collection: 07.01.2019		**Month: January, 2019**		
PARAMETERS	***RW***	***CW***	***FWBCL***	***FWR***

Turbidity, NTU	24	7	0.5	0.5
pH	7.9	7.8	7.5	7.5
Conductivity, µmhos/s	460	477	456	450
Temp.°C	21	22	20	20
Residual chlorine, mg/l	-	<0.2	<0.1	0.8
Nitrate, mg/l	-	Nil	Nil	Nil
Sulphate, mg/l	-	Nil	Nil	Nil
Hardness, mg/l	380	374	378	378
TDS, mg/l	89	87	88	85
TC, MPN/100mL	16 x10^4	5 x10^4	absent	absent
FC, MPN/100mL	11 x10^4	4 x10^4	absent	absent

TABLE-IV.

Date of collection: 26.02.2019	***Month: February,2019***			
PARAMETERS	***RW***	***CW***	***FWBCL***	***FWR***
Turbidity(NTU)	46.1	8	0.8	0.7
pH	8	7.8	7.2	7.2
Conductivity, µmhos/s	355	346	323	321
Temp.°C	23.1	23	22	22
Residual chlorine,mg/l	-	<0.2	<0.2	0.7
Nitrate mg/l	-	NIl	NIl	Nil
Sulphate, mg/l	-	NIl	NIl	Nil
Hardness,mg/l	178	162	154	152
TDS,mg/l	150	150	150	150
TC, MPN/100mL	8 x10^4	4 x10^4	absent	absent
FC, MPN/100mL	2 x10^4	1 x10^4	absent	absent

TABLE V

Date of collection: 23 .03.2019	**Month: March,2019**		
PARAMETERS	***RW***	***CW***	***FWBCL***
Turbidity,NTU	82	8	0.7
pH	8.15	8.36	8.31
Conductivity,µmhos/s	357	353	356
Temp.°C	25	25	25
Calcium(as $CaCO_3$), mg/l	74.5	70.6	78.4
Chliride(as Cl),mg/l	19.2	21.2	23.1
Magnesium(as $CaCO_3$),mg/l	51	51	47
Nitrate, mg/l	2.21	1.17	1.6
Sulphate, mg/l	17	20.3	18.5
Iron(as Fe),mg/l	7.71	0.18	0.1
Hardness, mg/l	125.4	121.5	129.4
TDS, mg/l	198	194	196
TC, MPN/100mL	4900	absent	absent

.Discussion

On the basis of secondary data which are collected from the plant laboratory (Jan,2018 to Oct,2018) and some primary data which is collected throughout the study period (from Nov,2018 to March,2019), Turbidity values of Raw water were observed in the range of 35 - 380 NTU Throughout the study period it was observed that during monsoon turbidity value is increases as well as coagulant dosing also increased and during dry season Turbidity level is decreased as well as dosing also decreased. Jar test is conducted to know the dosing value once in a month for dry season and weekly for rainy season.

pH values for Raw Water were observed to be in the range of 8.2 to 7.8 and filter water were 6.5 to 8.31 throughout the study period. It is observed that pH level is increased after coagulant dosing but pH values are under acceptable limit as per IS:10500:2012 specified limit.

Conductivity values for Raw water were observed to be in the range of 465 to 226 µmhos/s and filter water were 456-301 µmhos/s throughout the study period. Conductivity indicates the concentration of ions present in water. These conductive ions come from dissolved salts and inorganic materials present in the water. It is observed that when turbidity value is increased, dosing of chemical is also increased, simultaneously conductivity is also increased

TDS values for Raw Water were observed to be in the range of 198-89 mg/l and filter water were 196-85 mg/l throughout the study period. TDS is a measure of the dissolved combined content of all organic and inorganic substances present in the water. All values were well below the IS :10500:2012 specified limit.

Chloride values for Raw Water of Serampore Water Treatment Plant were in the range of 19.2 to 10 mg/L throughout the study period. Chloride values for filter water were 23.1 to 30 mg/L. Chloride increases the electrical conductivity of water. Chloride concentrations in excess of about 250 mg/litre can give rise to detectable taste in water. All values were well within IS:10500 2012 specified limit

Total Hardness values of Raw water were observed to be in the range of 100-133 mg/L throughout the study period and for finished water were in the range of 120-129 mg/L. These range of values are well below the ISI prescribed limit of 200mg/L

Nitrate and sulphate values for Raw Water were observed to be very low for Serampore Water Treatment Plant.

Total coliform and faecal coliform were determined by membrane filter technique. Residual chlorine having 0.2 mg/l was found at the end stage so no bacteria was observed.

TABLE-VI.

PARAMETERS	***CONSUMER POINTS***	
	CS-1 (near TS-3)	***CS-2(near TN-10)***
TC, MPN/100mL	9	9
FC, MPN/100mL	absent	absent

V. CONCLUSION

Based on the analysis for Physico-chemical parameters, the finished water was conforming to Indian standard for drinking water (IS: 10500,2012) in the entire study period.

Bacteria was present in Raw water above permissible limit which is prescribed in IS: 10500, 2012, though it can be used safely with adequate treatment followed by disinfection in appropriate dose. Total coliform and fecal coliform were determined by membrane filter technique. Residual chlorine having 0.2 mg/l was found at the end stage so no bacteria was observed. Pre-chlorination @ 2.5 mg/l is usually applied in the plant.

These studies were carried out to evaluate the performance of different units of water Treatment Plant and these are summarized hereunder

Though Pre-chlorination is being done at a rate of 2.5 mg/l to the raw water, residual chlorine was observed 0.2 mg /l. No coliform was found at clarifier water.

All rate of Flow water measuring devices in a plant should be checked periodically.

Turbidity removal ranging of clarified water is 81 % to 90 % and coliform reduction ranging for clarified water is 99% to 100 %. Hence it was confirmed that clari-flocculators in the Serampore Water Treatment Plant are working properly

Serampore Water Treatment Plant is supplying potable water to Serampore and adjoining six Municipalities through distribution mains. Data reveal that residual chlorine is below 0.1 mg/l in distribution mains far away from the plant and Total Coliform was found in 2 nos distribution mains out of 4 nos selected distribution mains. Total coliform was also found in two selected consumer end. It indicates post chlorination dosing should be revised.

ACKNOWLEDGMENT

I express my sincere gratitude to my Thesis Advisor Prof. (Dr.) Pankaj Kumar Roy under whose valuable guidance this wholehearted involvement, advice, support and constant encouragement throughout. He has not only helped me to complete my thesis work but also have given valuable advice to proceed further in my life.

REFERENCES

[1] ParagArunKashyupnt ,Mohammad Jawed, Performance Assessment of Clariflocculator of A Water Tieatment Plant-A Case Study, Conference Paper • November 2018

[2] M. A. ElDib , Mahmoud A. AzeemElbayoumy, Evaluation of a Water Treatment Plant Performance – Case Study, Seventh International Water Technology Conference IWTC7 Egypt 1-3 April 2003

[3] Pankaj Kumar Roy , ArunabhaMajumder , Gourab Banerjee , MalabikaBiswas Roy , Somnath Pal , AsisMazumdar, Removal of arsenic from drinking water using dual treatment process, Springer-Verlag Berlin Heidelberg 2014

[4] Wu-yuanJia, Chuan-rong Li, Kun Qin & Lin Liu, Testing and Analysis of Drinking Water Quality in the Rural Areas of High-tech District in Tai'an City, Journal of Agricultural Scienc, Vol. 2, No. 3; September 2010.

[5] N. Rahmanian, SitiHajarBt Ali, M. Homayoonfard, N. J. Ali, M. Rehan,3Y. Sadef, A. S. Nizami, Analysis of Physiochemical Parameters to Evaluate the Drinking Water Quality in the State of Perak, Malaysia, Hindawi Publishing Corporation Journal of Chemistry Volume 2015

[6] AF Shahaby, AA Alharthi , AE El Tarras, Bacteriological Evaluation of Tap Water and Bottled Mineral Water in Taif, Western Saudi Arabia, nternational Journal of Current Microbiology and Applied Sciences ISSN: 2319-7706 Volume 4 Number 12 (2015)

[7] Rakesh Kumar Mahajan , T. P. S. Walia , B. S. Lark &Sumanjit, Analysis of physical and chemical parameters of bottled drinking water, International Journal of Environmental Health Research, 16:2, 89-98, DOI: 10.1080/09603120500538184

[8] Syed Muhammad SqibNadeemRehanaSaeed, Determination of Water Quality Parameters of Water Supply in Different Areas of Karachi City, European Academic Rresearch vol. i, issue 12/ March 2014

[9] Sana Akram , Fazal-ur-Rehman, Hardness in Drinking-Water, its Sources, its Effects on Humans and its Household Treatment, Avens Publishing Group, J Chem Applications June 2018 Volume 4 Issue

[10] Mihir Pal, Nihar R. Samal, Malabika B. Roy , Pankaj k. Roy, Fresh Water Lake Model Application For Seasonal Variation Of Latent And Sensible Heat Fluxes From The Water Surface Of RudrasagarLake,Tripura , Imperial Journal of Interdisciplinary Research (IJIR) Vol-2, Issue-5, 2016

[11] Naeem Khan, Syed TasleemHussain, JavidHussain, NargisJamila, Shabir Ahmed, RiazUllah, ZainUllah, Samina Ali, AbdusSaboor, Chemical and microbial investigation of drinking water sources from Kohat, Pakistan, International Journal of Physical Sciences Vol. 7(26), pp. 4093-5002, 5 July, 2012

[12] Susanta Ray, Pankaj Kumar Roy, ArunabhaMajumder(2016) , Quality of packaged drinking water in Kolkata City,India and risk to public health, 57:59, 28734-28742, DOI: 10.1080/19443994.2016.1196390

[13] Indian Standard (IS) 10500: 2012, Indian Standard,Drinking Water-Specification, Second Rev, 2012.

[14] World Health Organization, Guidelines for Drinking water Quality, fourth ed., Geneva, 2011.

[15] Manual on water supply and treatment ; third edition, Central Public Health and Environmental Engineering Organization, Ministry of Urban Development, New Delhi, May, 1999

[16] Peavy, Howard S. and Rowe, Donald R. , edition 2013, Environmental Engineering

[17] Hussein Janna, Adnan A. Al-Samawi (2014); Performance Evaluation of Al- Karkh Water Treatment Plant in the City of Baghdad *Int. J. of Adv. Res.* **2** (10). 0] (ISSN 2320-5407).

Development of Smart Medicine Box using IoT

Abhishek Dey
Electronics & tele-communication Engineering, TPI
Technique Polytechnic Institute
Hooghly, India
abhishek.dey.ece@gmail.com

Sibasis Bandyopadhyay
Electronics & tele-communication Engineering, TPI
Technique Polytechnic Institute
Hooghly, India
sibasis2012@gmail.com

Suphal Das
Electronics & tele-communication Engineering, TPI
Technique Polytechnic Institute
Hooghly, India
suphaldas406@gmail.com

***Abstract*— In this project our medicine box is targeted on users who regularly take medicine or vitamin supplements or nurses who take care of the older patients. Our medicine box is programmable that allows nurses or users to specify the pill quantity and day to take pills and the save times for each day. Our smart medicine box contains six separate sub-boxes. [7] Therefore, doctors/nurses or users can set information for six different pills. When the pill quantity and time have been set, the medicine box will remind users or patients to take pills using sound and light. A LCD, placed in controller unit will provide the information about the pills. Compared with the traditional pill box it requires users or nurses to load the box every day or every week. Smart medicine box would significantly release nurses or users' burden on frequently preloading pills for patients or users. [2] To make it a grand success, internet of things is one of the latest internet technology developed. Various designs have already been proposed and have advantages as well as disadvantages. The project is a review of smart medicine box based on IOT. [5] Doctors/Nurses can send the entire prescription to the smart medicine box using a mobile application. [2] Our system will store data in its local serve to user in more efficient manner.**

Keywords*— *Smart Medicine Box, IOT, Node MCU, Smart Pill Box

I. INTRODUCTION

Capturing and sharing of vital data of the network connected devices through a secure service layer is what defines IOT. Collection of real-time data and recording database of patients has become easy due to the use of Internet of Things.

One of the most common reasons for the failure of a method to cure a patient is because of not taking the medicine at the prescribed time. People aged 50 or above are prone to diseases such as high blood pressure, diabetes, Alzheimer's and Parkinson's to name a few. Missing a dose for such a patient can prove to be very harmful. Hence it is vital for the patients to take the medicines on time. It has been observed that people in general neglect their health and give preference to other things than taking their medicines.

This project will be helpful for people who forget to take their medicines or even to those who have to take a lot of medicines and get confused about which medicine to take at what time. So this project will help people provide information about the patient's status whether he has taken the medicine or not. In this era, it is difficult for the family members to be present all the time for the aged. Today, most of the families in our society are a nuclear family. [1] Elderly prefer staying independent, but it is a worry for their children. Sometimes despite their best efforts, the aged fail to take the medicine on time. This device is one approach to help them take the medicines effectively.

The Smart Medicine Box is successfully designed in helping the introvert patients taking their medicine without help of others. [7] Our medicine box is targeted on users who regularly take medicine or vitamin supplements or nurses who take care of the older or patients. [4] Our smart medicine box contains six separate sub-boxes. Therefore, doctors/nurses or users can set information for six different pills. When the pill quantity and time have been set, the medicine box will remind users or patients to take pills using sound and light. A LCD, placed in the controller unit will provide the information about the pills. Compared with the traditional pill box it requires users or nurses to load the box every day or every week. Our smart medicine box would significantly release nurses or users' burden on frequently preloading pills for patients or users. To make it a grand success, internet of things is one of the latest internet technology developed.

II. PRODUCT SPECIFICATION

A. *NODE MCU (ESP8266 Wi-fi Module)*

It will give your project access to wi-fi or internet. It is a very cheap device but it will make are your projects very powerful. It can communicate with any microcontroller and make the projects wireless. It is in the list of most leading devices in the IOT platform. It runs on 3.3v and if you will give it 5v then it will get damage.

B. *LCD (16*2)*

LCD (Liquid Crystal Display) screen is an electronic display module and find a wide range of applications. A 16x2 LCD display is very basic module and is very commonly used in various devices and circuits. These modules are preferred over seven segments and other multi segment LEDs. The reasons being: LCDs are economical; easily programmable; have no limitation of displaying special & even custom characters (unlike in seven segments), animations and so on. A 16x2 LCD means it can display 16 characters per line and there are 2 such lines. In this LCD each character is displayed in 5x7 pixel matrix. This LCD has two registers, namely, Command and Data. The command register stores the command instructions given to the LCD. A command is an instruction given to LCD to do a predefined task like initializing it, clearing its screen, setting the cursor position, controlling display etc. The data register stores

the data to be displayed on the LCD. The data is the ASCII value of the character to be displayed on the LCD.

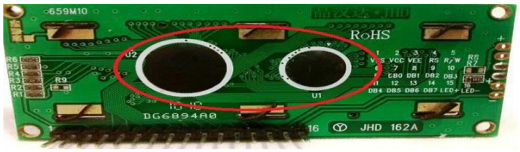

These black circles consist of an interface IC and its associated components to help us use this LCD with the MCU. Because our LCD is a 16*2 Dot matrix LCD and so it will have (16*2=32) 32 characters in total and each character will be made of 5*8 Pixel Dots. So Now, we know that each character has (5*8=40) 40 Pixels and for 32 Characters we will have (32*40) 1280 Pixels.

C. *I2C Buss*

Inter-integrated Circuit (in short I2C) is a two-wire short distance communication protocol. In I2C the external devices have an I2C address for different external devices like LCD Backpack, OLED Display, etc. By using the address the data is sent to the specific device connected on the same I2C Bus.

The message is broken into two frames and sent serially via the I2C Bus. The first frame contains the address, once the address matches with any device on I2C bus, that device will send an acknowledge signal to the master. After receiving the acknowledgment from the slave the data bits are sent. By this method an I2C bus works.

D. *SPDT switch*

A Single Pole Double Throw (SPDT) switch is a switch that only has a single input and can connect to and switch between the 2 outputs. This means it has one input terminal and two output terminals.

A Single Pole Double Throw switch can serve a variety of functions in a circuit. It can serve as an on-off switch, depending on how the circuit is wired. Or it can serve to connect circuits to any 2 various paths that a circuit may need to function in. For example, a SPDT switch can connect to create a Ready Mode and a Standby Mode in a printer.

E. *Female bug strip*

These header pin blocks use the industry standard spacing and are designed for soldering directly into printed circuit boards (PCB's). They are supplied best for extension of pins of Microcontrollers and ICs.

F. *Smartphone*

An android phone is a powerful, high-tech smart-phone that runs on the android operating system developed by Google and is used by a variety of mobile phone manufactures. Pick any one android mobile phone with android version 2.0 or above and have to use applications as per requirement. [3]

III. Working Principle

In this project, the system is going to intimate the patients to take proper dosage according to the prescription at right time. This portable and economical system would help aged patients, especially to the illiterate patients. Our smart pill box can reduce elderly family member's responsibility towards by reminding them to take the medicine on time. [4]

In this pill box, there are six sub boxes. [5] There are six LEDs corresponding to six sub boxes indicates the sub box from which medicine is to be taken. All these LEDs are connected to the pins D3 to D8 of Node MCU through resistor. To make this connection we need to know the functionalities of those pin. VCC and GND have general uses. As prescribed by the Doctor, by using the App developed in the smart phone, first we schedule the time slot when the medicines to be taken. Then as per the time given by the user, Node MCU sends the signal to the corresponding sub box. Pin number D0 in Node MCU is connected to the Buzzer for alarming. A LCD display has been connected to the system using a two wire interface (TWI) for showing the timing of the medicines. TWI uses SCK & SDA pins of the node MCU for enabling serial communication between these two devices as well as for saving GPIO (General Purpose Input/output) pins of the node MCU for other uses.

Now inside a Node MCU a Wi-Fi shield called ESP8266 is used to make the connection to server. The ESP8266 Arduino compatible module is a low-cost Wi-Fi chip with full TCP/IP capability and the amazing thing is that this little board has a MCU (Micro Controller Unit) integrated which gives the possibility to control I/O digital pins via simple and almost pseudo-code like programming language.

The internal connection of ESP8266 to the micro controller is somewhat like this –

UNO	ESP-01
RX	TX
TX	RX
3.3v	VCC
GND	GND

3.3v RST
3.3v CH_PD

So, after making all the connection now our aim is to connect the node MCU to the server. A 'wifi.begin (ssid, password)' command is used to connect node MCU with any wifi network. After making a successful connection we need to create a new Wificlient object. 'Wificlient.connect (server, port)' is used to make connection to the destination server. After connection we need to create a string data in the following format: "<apiKey>&<fieldName><dataToSend>\n\n\n" then using the 'Wificlient.print (data)' command we can upload the data to our desired destination.

It is a combination of physical and digital reminder for a patient that will be helpful for people of any age, but especially helpful for geriatrics who forgets taking their medicines. The main aim is to keep the system easy to handle and make it cost-efficient. We have used MIT app inventor tool for making this android application. IP address of the Node MCU plays an important role to create the connection. By inserting valid IP address displayed in the LCD the user needs to create the connection.

IV. Circuit Diagram

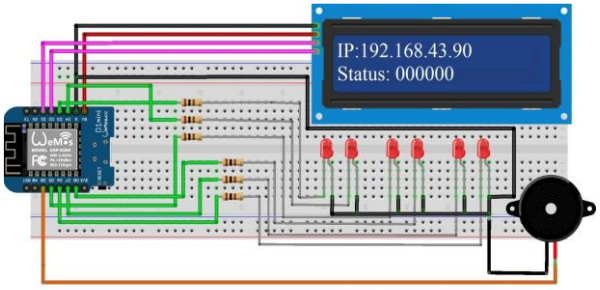

V. Block Diagram

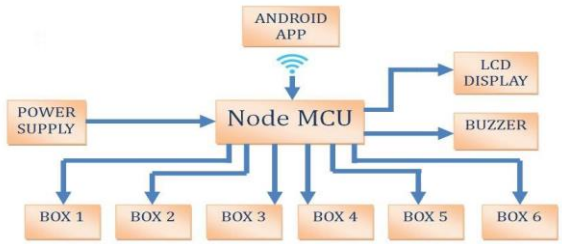

VI. Application

- In this IOT project, users can set a notification time according to a message from the mobile application
- This system is a very good to apply in the hospital because it can make the nurse job easier besides making the patients more comfortable to stay at the hospital. [6]
- The goal of our project is to provide healthy and tension free life to those users who are taking regularly pills and to provide this product at affordable cost also.
- Generates a notification sound and displays a bright light in certain pill boxes, so that the patient will know the specific number of boxes from which they should take out medicine

VII. Scope for Future Development

Although this system was well operating, several adjustments can be made in order to increase its use and ameliorate its behavior. In future we will modify this project using Servo motors for each sub box. [7] By modified in such a way each sub box will automatically open as per the schedule when any patient will take the medicine and after few seconds it will automatically close. In near future we can use this device commercially. Also, the system can be designed using a smaller surface which may lead to a reduced box size.

Acknowledgment

The success and final outcome of this project required a lot of guidance and assistance from many people and we are extremely fortunate to have got this all along the completion of our project work. Whatever we have done is only due to such guidance and assistance and we would not forget to thank them.

On the very outset we would like to extend our sincere & heart full obligation towards all the persons who gave us the golden opportunity to do this wonderful project on the topic "Development of Smart Medicine Box using IoT". [7]

Without their active guidance, help, co-operation & encouragement, we would not have made headway in this project.

We are thankful to and fortunate enough to get constant encouragement, support and guidance from all the teaching staff of Department of Electronics And Telecommunication which helped us in successfully completing our project work.

References

[1] S. Majumder, E. Aghayi, M. Noferesti, H. Memarzadeh-Tehran, T. Mondal, P. Zhibo and M. Deen, "Smart Homes for Elderly Healthcare--Recent Advances and Research Challenges," Sensors, vol. 17, no. 11, pp. 1-32, 2017.

[2] Y. Cha, K. Nam and D. Kim, "Patient Posture Monitoring System Based on Flexible Sensors," Sensors, vol. 17, no. 3, pp. 1-9, 2017.

[3] B.-G. Lee, B.-L. Lee and C. Wan-Young, "Mobile Healthcare for Automatic Driving Sleep-Onset Detection Using Wavelet-Based EEG and Respiration Signals," Sensors, vol. 14, no. 10, pp. 17915-17936, 2014.

[4] S. Sohn, M. Bae, D.-K. Lee and H. Kim, "Alarm system for elder patients medication with IoT-enabled pill bottle," in International Conference on Information and Communication Technology Convergence (ICTC), Jeju, South Korea, 2015.

[5] P. Raga Lavima1, Mr. G. Subhramanya Sarma2, "AN IOT BASED INTELLIGENT MEDICINE BOX", IJCSMC, Vol. 4, Issue. 10, October 2015, pg.186 – 191.

[6] Suneetha Uppala1, B. Rama Murthy2, Smart Medicine Time Indication Box, International Journal of Science and Research (IJSR), Volume 6 Issue 1, January 2017.

[7] Viral Shah, Jigar Shah, Nilesh Singhal, Harsh Shah & Prof. Prashant Uapdhyay, "Smart Medicine Box", Imperial Journal of Interdisciplinary Research (IJIR), Vol-2, Issue-5, 2016.

Groundwater Potential Zone Mapping using AHP technique: A case study of Bankura district, West Bengal

Pinaki Mukherjee
Department of Civil Engineering,
Technique Polytechnic Institute,
Hooghly, India
Email: pinaki.civil.iiests@gmail.com

***Abstract*— Over-exploitation of groundwater and abrupt changes in climate over the years have imposed immense pressure on the global groundwater resources. In the recent years, the studies related to prospects of groundwater and its replenishment have gained much prominence and Geographic Information System (GIS) has been found to be an essential tool in this context. The present study has been undertaken with an objective to delineate the groundwater potential zone of a drought-prone district Bankura located in the state of West Bengal in India using a combination of GIS and Analytic Hierarchy Process (AHP) technique. Four thematic layers such as Geology, Soil, Rainfall and Slope have been utilised for groundwater potential zone demarcation. Weights assigned to each class in all the thematic maps are based on their characteristics and water potential capacity through AHP technique. The groundwater potential zone map thus obtained was categorized into four classes-very poor, poor, moderate and good. The study reveals that about 75.94% of the study area is covered under moderate groundwater potential zone. The poor groundwater potential zones are observed in 22.79% of area.**

Keywords*— *ground water potential zone, AHP, GIS

I. INTRODUCTION

Groundwater is one of the most important and vital natural resource which is stored in the subsurface geological formations in the critical zone of the earth's crust. It serves as a source of water for domestic, industrial and agricultural uses and other developmental initiatives. The ever-increasing demand of water for meeting human requirements and developments has imposed immense pressure on this limited freshwater resource. The occurrence and distribution of groundwater depends on the various natural and anthropogenic factors. The groundwater related problems are severe in most parts of the tropical and subtropical regions that have high population density and economic developments. In a semi-arid country like India, surface water is not available round the year for meeting different purposes and hence people in such areas have to depend more on groundwater resources for their survival. Millions of people in India are facing high to extremely high water stress due to inadequate availability of fresh water. Further, about three-fourth of the households in the country do not have access to portable water at their premises. According to a World

Bank report, if adequate measures are not taken, India will become a water stress zone by the year 2025 and a water scarce zone by the year 2050. All these reiterate the need for better understanding of all the available freshwater resources of the country with special reference to groundwater resource, as it constitutes a major share of India's freshwater resources.

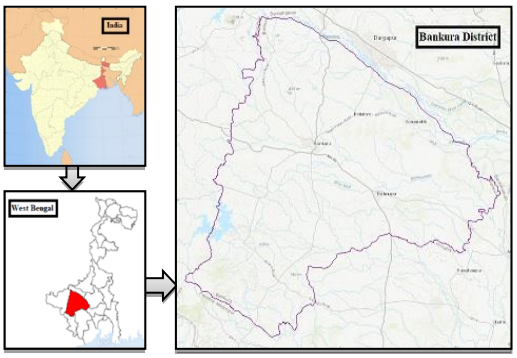

Fig. 1. Study Area

The traditional approaches used to identify, delineate and map the groundwater potential zones are mainly based on ground surveys using geophysical, geological and hydrogeological tools which are generally expensive and time consuming. Geospatial tools, on the other hand, are rapid and cost-effective in producing and modelling valuable data in various geoscience fields. Remote sensing and GIS study with its advantages of spatial, spectral and temporal availability of data converging large and inaccessible areas within a short span of time has become a powerful tool in assessing, monitoring and conserving groundwater resources.

II. STUDY AREA

The entire Bankura district of West Bengal is taken as the study area of the present research work. The entire study area lies between 22038' and 23038' north latitude and 86036' and 87047' east longitude. Water scarcity is a regular threat for the people of Bankura district which has a great negative impact on the socio-economic development of Bankura. Surface water bodies dries up in most of the year during the summer season, people depend on groundwater for domestic, irrigation and other various purposes during this time, but excessive use of groundwater has worsened the situation. Therefore, proper evaluation, planning, and management of groundwater are essential for this region.

III. METHODOLOGY

In the present work slope, rainfall, geology and soil have been considered as major parameters that influence the availability of groundwater at different locations. After the generation of all the thematic maps, the AHP technique was applied to assign the weight of each themes and normalized weight of each layer was obtained. Then a weighted overlay analysis has been performed in a GIS platform to integrate the effects of all the parameters which were considered here. As a resulted overlay map groundwater prospects of different

sites has been identified and the model was validated using groundwater prospects map.

IV. RESULT AND DISCUSSION

GIS model has been used to demarcate the groundwater potential zones in different geographical areas using few thematic layers and validate the result with real data. However, the entire analysis and its accuracy depend on the assigned weights to different factors. In the present study four parameters (Geology, Soil, Slope, Rainfall) were considered as more important for occurrence of groundwater. These layers had been integrated in a GIS environment and different weights had been assigned using AHP (Analytic Hierarchy Process).

A. Slope

Slope is an important parameter of groundwater potential at a location. The amount of groundwater recharge is inversely proportional to the degree of slope. If the slope is high, the rate of drainage is also high and simultaneously the chance of percolation of groundwater through surface gets reduced, so the availability of groundwater at that places also less.

B. Rainfall

The groundwater recharge is directly proportional to the rate of rainfall at a particular location. The rainfall distribution map was prepared by Inverse Distance Weighted (IDW) method by giving the gridded rainfall shape file as an input.

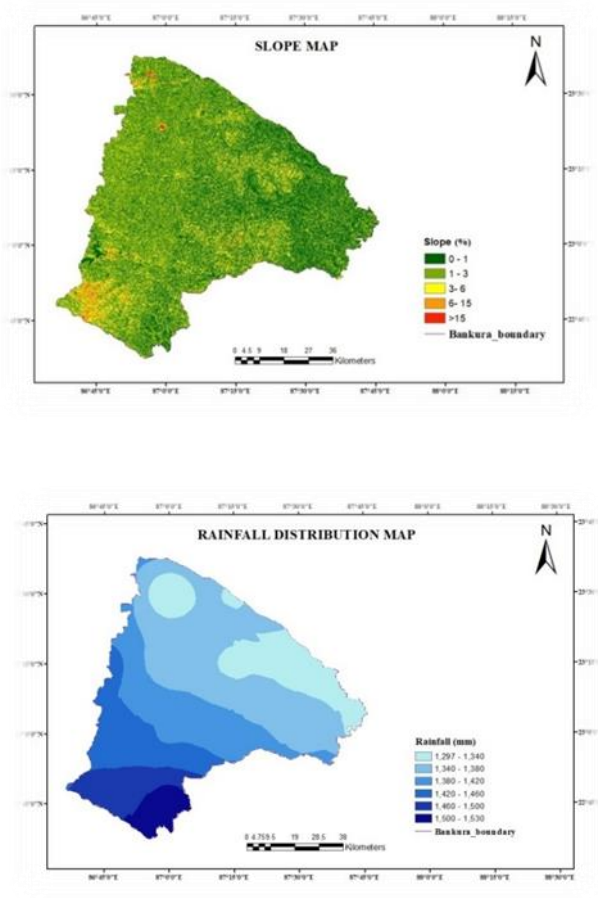

Fig. 2. Slope Map

Fig. 3. Rainfall Map

C. Geology

The word 'Geology' is directly related to the rock formation of the Earth-strata. There are different types of rock structure and each structure has different storage capacity depending on their porosity. So, it can be easily said that geology plays a vital role on the presence of groundwater at each and every location depending on the storage capacity and rate of transmission.

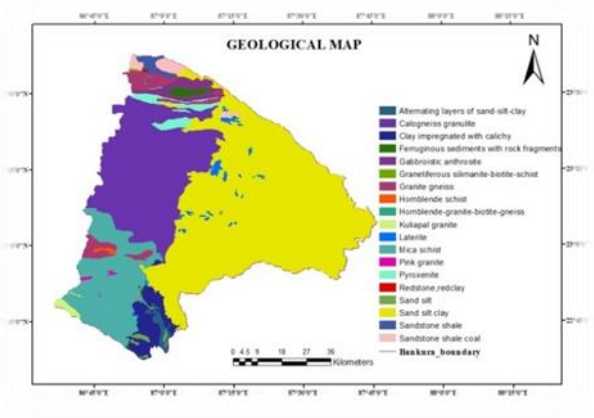

Fig. 4. Geological Map

Deep water, shallow water and water bodies are the excellent sites for groundwater prospect and higher weightage will be given to them. The vegetation areas are considered to have good groundwater potential where settlement areas have least probability of groundwater occurrence.

D. Soil

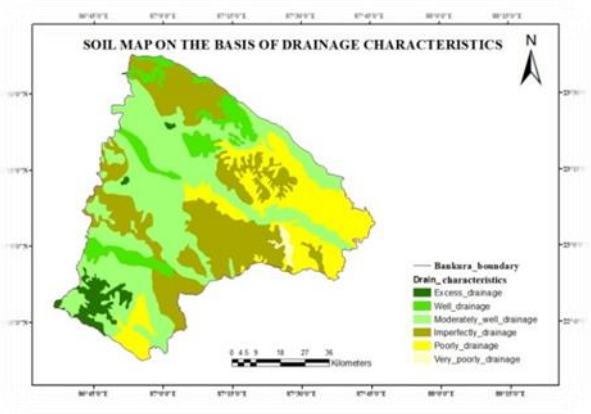

Fig. 5. ` Soil Map

The type of soil is an important factor for the availability of groundwater at a location depending on the porosity, permeability and soil-structure. If the interconnectivity of soil-pores is high, the chance of occurrence of groundwater is high at that place. Drainage characteristics of soil are the major parameter for the occurrence of groundwater in a particular site. The rate of drainage of surface water through the soil pores is considered as the main driving factor for the presence of groundwater on a place and on the basis of

drainage characteristics Soil of the entire study area was classified in six zones.

E. Weighted Overlay Analysis

The weighted overlay analysis is built into ArcTool in the ArcMap 10.4.1 for the integration of different thematic layers. The accuracy of the method lies into the perfection of the weightage analysis of the different themes. Here the concept of normalized weights and rating was applied. Normalized weights represents the relative importance of the different data layers and rating represents the relative weightage of different categories considered in each and every layers.

In the present study, AHP (Analytic Hierarchy Process) proposed by Saaty, 1990 had been used to obtain the normalized weights of the different parameters which has been considered in mapping of groundwater potential zones. The following steps are followed to apply AHP in this study:

- Creating Pairwise Comparison Matrix;
- Calculating normalized weights of different themes
- Checking the consistency

The relative importance values are determined with Saaty's 1-9 scale, where a score of 1 represents equal importance between the two themes, and a score of 9 indicates the extreme importance of one layer compared to another layer. The pairwise comparison matrix which has been prepared on the basis of Saaty'snine point important scale between the various thematic layers, is shown below (Table I).

All the eigen values for the pairwise comparison matrix (Table I) were obtained. Maximum eigen value is 4.07 and corresponding to this value the eigen vector was generated. The normalized weights were calculated of each thematic layer (Table II).

The term '**consistency ratio (C.R)**' was introduced by Saaty to check the errors in judgment of parameter weights.

$$C.R = \frac{C.I}{R.I}$$

TABLE I. PAIRWISE COMPARISON MATRIX

Thematic Layers	Slope	Rainfall	Geology	Soil
Slope	1.00	0.50	0.25	0.33
Rainfall	2.00	1.00	0.20	0.50
Geology	4.00	5.00	1.00	2.00
Soil	3.00	2.00	0.50	1.00

TABLE II. NORMALIZED WEIGHTS OF DIFFERENT THEMATIC LAYERS

Thematic Layer	Eigen Vector Value	Normalized Weights
Slope	0.3513	0.0918
Rainfall	0.5191	0.1357
Geology	1.9549	0.5111
Soil	1	0.2614

C.I represents for Consistency Index, calculated by the following formula

$$C.I = \frac{\lambda max - n}{n - 1}$$

Where, '**λmax**' is the maximum eigen value and 'n' is the number of parameters used.

According to this research work, the value of **λmax** was 4.07 and 'n' was 4.

R.I stands for Ratio Index, the value of which is specified by Saaty using a composite of two different experiments performed by him at the University of Pennsylvania.

If the C.R value is less than or equal to 0.1, then it is accepted. If the value of C.R is greater than 10%, it requires reconsideration of judgment of pairwise comparison matrix.

The value of consistency index and consistency ratio obtained as per my study was 0.023 and 0.026 respectively. Hence the pairwise comparison matrix did not violate the rule of Saaty's AHP technique as the consistency ratio was less than 10%.

The individual rating of each categories of each thematic layers had been given on the basis of their influences on the chance of occurrence of groundwater in a place. The groundwater potential zone map was developed by reclassifying each and every thematic layers and overlaying them by putting their AHP weightage with category rating of each layer in ArcMap. The individual weight of each layer and the category rating were blended and overlay analysis was carried out based on the following equation given below.

$$GWPI = \sum_{i=1}^{n}\sum_{j=1}^{m}[\alpha_i\beta_{ij}]$$

'GWPI' is Groundwater potential index, β_{ij} is rating of the j^{th} class of the i^{th} theme, $\alpha_i$is the weight of the i^{th} theme.

The output overlay map has been reclassified into four categories ('Very Poor', 'Poor', 'Moderate' and 'Good') to classify the study area in different zones in terms of suitability of groundwater prospect. The major parts i.e. about 75.94% of the study area is falling under moderate potential zone. About 22.79% areas have poor groundwater potential. There are very few sites in where the groundwater prospects are good (1.08%) and very poor (0.19%).

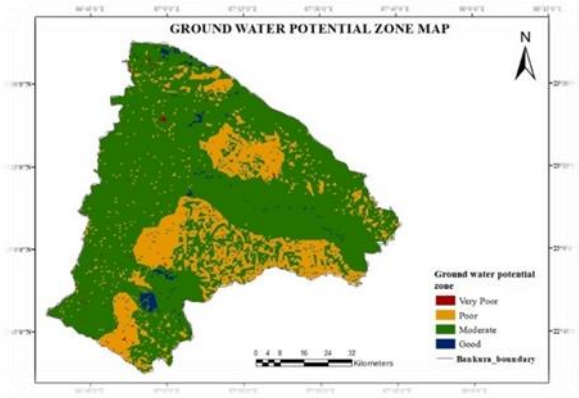

Fig. 6. Ground Water Potential Map

V. CONCLUSION

In this research work, different parameters have been considered as the major driving factors in occurrence of

groundwater in a location. An AHP model was developed successfully to assign the weightage of each thematic layer based on these parameters and a weighted overlay analysis has been performed in a GIS environment to get groundwater potential map of the desired study area. It can be easily illustrated from the resulted potential map that most of the sites i.e. 75.94% of area of Bankura district have moderate groundwater prospect. 22.79% zone of study area is of poor potential of groundwater. There are very few locations in where occurrence of groundwater is high. Finally, it is concluded that the groundwater potential in Bankura district is moderate to poor.

REFERENCES

[1] Agarwal, E., Agarwal, R., Garg, R.D. and Garg, P. K.,"Delineation of groundwater potential zone:An AHP/ANP approach", *Journal of Earth System Science*,122, pp. 887-898, 2013.

[2] Bathis, K.I., and Ahmed, S.A., "Geospatial technology for delineating groundwater potential zones in Doddahalla watershed of Chitradurga district, India",*The Egyptian Journal of Remote Sensing and Space Sciences*, 19, pp. 223-234, 2016.

[3] Chenini, I. and Mammou, A.B., "Groundwater recharge study in arid region; an approach using GIS techniques and numerical modeling",*Computer and Geosciences*, 36, pp. 801-817, June 2010.

[4] Chenini, I. and Mammou, A.B., and May, M.E., "Groundwater recharge zone mapping using GIS based multi criteria analysis;a case study in Central Tunisia (Maknassy basin)",*Water Resources Management*, 24, pp. 921-939,2010.

[5] Chowdhury, A., Jha, M.K. and Chowdary, V.M., "Delineation of groundwater recharge zones and identification of artificial recharge sites in West Medinipur district, West Bengal, using RS and GIS and MCDM techniques",*Environmental Earth Sciences*, 59(6), 1209-1222, 2010.

[6] Dyer, J., Mercer, A., Rigby, J.R. and Grimes, A., "Identification of recharge zones in the Lower Mississippi River alluvial aquifer using high-resolution precipitation estimates", *Journal of Hydrology*, 531, pp. 360-369, 2015.

[7] Ghayoumian, J., Ghermezcheshme, B., Feiznia, S. and Noroozi, A.A., "Integrating Gis and DSS for identification of suitable areas for artificial recharge; case study of Meimeh basin, Isfahan, Iran",*Environmental Geology*, 47, 493-500, 2005.

[8] Jasrotia, A.S., Kumar, R. and Saraf, A.K.,"Delineation of groundwater recharge sites using integrated remote sensing and GIS in Jammu district, India",*International Journal of Remote Sensing*, 28, pp. 5019-5036, 2007.

[9] Kaliraj, S., Chandrasekhar, N. and Magesh, N.S., "Identification of potential groundwater recharge zones in Vaigai upper basin, Tamil Nadu, using GIS based analytical hierarchical process (AHP) technique",*Arabian Journal of Geosciences*, 7, pp. 1385-1401, 2014.

[10] Malekmohammadi, B., Mehrian, M.R. and Jafari, H.R., "Sites selection for managed aquifer recharge using fuzzy rules: integrating GIS tools and multi criteria decision making (MCDM)", *Hydrogeology Journal*, 20, 1393-1405, 2012.

[11] Nampak, H., Pradhan, B. and Manap, M.A., "Application of GIS based data driven evidential belief function model to predict groundwater potential zonation", *Journal of Hydrology*, 513, pp. 283-300, 2014.

[12] Sargaonkar, A.P., Rathi, B. and Baile, A., "Identifying potential sites for artificial groundwater recharge in sub-watershed of river Kanhan, India",*Environmental Earth Sciences*, 62, pp. 1099-1108, 2011.

[13] Senanayake, I.P., Dissanayake, D.M.D.O.K., Mayadunna, B.B. and Weerasekera, W.L., "An approach to delineate groundwater recharge potential sites in Ambalantota, Sri Lanka using GIS techniques",*Geoscience Frontiers*, 7, pp. 115-124, 2016.

[14] Shaban, A., Khawile, M. and Abdallah, C., "Use of Remote Sensing and GIS to determine recharge potential zones: the case of Occidental Lebanon",*Hydrogeology Journal*, 14, 433-443, 2006.

[15] Shereif, H., Mahmoud and Alazba, A.A., "Identification of potential sites for groundwater recharge using a GIS based decision support system (DSS) in Jazan region, Saudi Arabia",*Water Resources Management*, 28, pp. 3319-3340, 2007.

[16] Siva, G., Nasir, N. and Selvakumar, R., "Delineation of Groundwater Potential Zone in Sengipatti for Thanjavur District using Analytic Hierarchy Process", *Earth and Environmental Science*, 80, pp. 12-63, 2017.

[17] Yeh, H.F., Cheng, Y.S., Lin, H.I. and Lee, C.H., "Mapping groundwater recharge potential zone using a GIS approach in Hualian River, Taiwan", *Sustainable Environment Research*, 26, pp. 33-43, 2016.

Mathematical modelling and analysis of HVAC system of modern Buildings using renewables for optimization of Energy consumptions in Indian Scenario

Sushovan Roy
Electrical Engineering Department
Dream Institute of Technology
Kolkata, India
sushovanroy123@gmail.com

Dr. Sandip Chanda
Electrical Engineering Department
Gani khan choudhury Institute of Engineering and Technology
Malda, India
sandipee1978@gmail.com

Dr. Papun Biswas
Electrical Engineering Department
JIS College of Engineeing
Kalyani, india
head_ee.jisce@jisgroup.org

Dr. Abhinandan De
Electrical Engineering Department
Indian Institute of Engineering Science and Technology, Shibpur (Formerly BESU)
Howrah, India
abhinandan.de@gmail.com

***Abstract*— The advancement of technology in domestic comfort specially indoor circulation of conditioned air has resulted in an escalation of household energy consumptions in India specially in summer and due to extensive use of cooling load. Due to high demand for cooling, a country wide energy crisis is witnessed during this time. In this research, a solar water heating of a residential house using the abundant and universal sources is proposed for a residentials house in India for mitigating this energy shortage and for offering a sustainable solution to the problem. The paper presents a mathematical model of the house on TRNSYS simulation software along with the simulation results of coupling of the several components operating in parallel with the cooling systems. The results demonstrated that, the proposed model of household solar cooling system may be satisfactory used for a residential house or HVAC systems in Indian scenario. The system was modeled using TRNSYS software and its components to represent the various parts of the solar heating system. Assumptions, modelling of different components and their limitations of simulations have been depicted as per the requirement of the proposed research work.**

Keywords— Mathematical Modelling, energy efficiency, Solar water heater, TRNSYS software, TRNBuild, HVAC & optimization.

I. INTRODUCTION

There are different literature are available for the Building energy management system at which describes the usefulness of energy efficiency in building sector & how to optimize the efficiency to get the optimum values. Nowadays, energy has been known as one of the most important factors for forming and developing industrial societies [1]. For every residential building, it is the most important issue to effectively manage the energy as well as achieve higher occupant's comfort. The reason behind the fact is that the energy consumption increases rapidly with the passage of time and becomes more and more expensive and the user cannot compromise on his/her comfort. Therefore, the energy consumption minimization and user comfort maximization need to be balanced to achieve both goals. There are many proposals in the literature addressing the issue of user's comfort and energy consumption (management) with keeping different parameters in consideration [2,3]. it was found that a lot of scope is still prevalent in the improvement of energy efficiency through intelligent ways of using solar power. In Persaud of exploring the opportunity this paper presents an energy efficient HVAC based domestic solar cooling system in TRNSYS software in Indian scenario. The paper also proposed various methods of reduction of energy consumptions to optimize the energy efficiency of the building using solar water heater.

II. LITERATURE SURVEY

In recent era, the concepts of optimization of Building energy consumptions and user comfort level has plays an important role. There are various algorithm are used for addressing these building energy consumptions but some techniques are more useful to formulate different components and simulate how much energy that the building should consume. In this literature, using a proposed optimization technique addressing the energy consumptions in the building sector. Moreover, Building Energy Efficiency Optimization methos is also applied for evaluate the Effective Thermal Zones Occupancy. This research presents an innovative and low-cost methodology to reduce buildings' energy requirements through post-occupancy assessment and optimization of energy operations using effective users' attitudes and requirements & it is applied to optimized building energy operations which allow a reduction of primary energy requirements for HVAC, lighting, room-electricity and auxiliary supply. In research activities, it is clear that one of the most important challenges in this century in the world is energy crisis. On one hand, shortage of energy resources and its growing consumption and on the other hand, extreme usage of energy by different users has endangered future life of human and polluted the environment. In order to optimize energy consumption, one must, at first determine a set of consumption standards in different sectors based on the latest levels of technology and other factors affecting energy consumption. Energy efficiency in building stock has become a potential approach to accede sustainability in the built environment and a lucrative source for builders and investors that is discussed in

In this article, due to its definitive impact on energy consumption, building envelope plays a crucial role in the investment and the pattern of energy demands will change after the retrofit of the building. In this literature, Energy Plus has been selected as a tool for building information simulation. Particularly, the jEPlus optimization engine has been selected to optimize multi-objective problems using a genetic algorithm and carry out the energy-simulation. Another literature described in this paper energy management in residential buildings according to occupant's requirement and comfort is of vital importance and in this paper, Artificial bee colony (ABC) optimization technique is used here for maximizing the user's comfort and minimizing the energy consumptions simultaneously in the building energy consumptions. it is again mentioned that Optimization of Energy Consumption in the building Under the requirement of energy savings and emission reduction, building energy consumption, which occupies arising proportion of the total energy consumption in society has become the focus of energy conservation research.

From the above literature survey, it was found that a lot of scope is still prevalent in the improvement of energy efficiency through intelligent ways of using solar power. In Persaud of exploring the opportunity this paper presents an energy efficient HVAC based domestic solar cooling system in TRNSYS software in Indian scenario. The paper also proposed various methods of reduction of energy consumptions to optimize the energy efficiency of the building using solar water heater.

III. METHODOLOGIES OF PROPOSED RESEARCH

A. Performance of Energy Efficient Building modeling

Energy efficiency is the ability to reduce the amount of energy required to deliver various goods or services using less energy for heating cooling and lighting [4]. Energy efficient buildings starts from the building envelope, which includes energy efficient windows, insulation, foundation and the roof to appliances, lights and air-conditioning systems applies to space heating and cooling systems which are aided through the use of automated controls, ventilation, improved duct systems and other advanced technologies. Energy efficiency can also apply to water heating (i.e. solar water heater) when combined with water-efficient appliances and fixtures [5]. There are different methods targeting the decrease of energy consumption of buildings. Considering energy consumption in each phase of structuring is achieved with the analysis of building life cycle. In this respect the Building life cycle is divided into three main phases such as the prebuilding phase, building phase, and post building phase[6]

B. Methodologies of existing Building modeling techniques

The word Modelling comes from the latin word modellus. A model is a simplified version of something that is real. The methodologies used to test the whole building energy modelling and its energy management can be analyzed using three different Techniques, they are as follows,

1. White Box Modeling Technique or Open Box Testing Or Clear Box Testing
2. Black Box Modeling Technique or Close Box Testing Or Opaque Testing
3. Gray Box Modeling Technique or Translucent Testing or Gray Box Modeling = Black Box Modeling + White Box Modeling

C. Proposed architecture design work flow methodology

The proposed architecture is based on simulation & standard optimization techniques. The simulation technique used here are TRNSYS software and using the standard optimization technique one can optimize the energy consumptions and increase the comfortable part of user. TRNSYS is a complete and extensible simulation environment for the transient simulation of systems, including multizone buildings [8]. TRNSYS is a Transient Systems Simulation Program & this software is developed in 1974 by the University of Wisconsin Madison, USA and used by many researchers. TRNSYS is a simulation software for the thermal behavior of buildings and associated systems under dynamic condition [9]. In order to properly utilize the TRNSYS program, an ANSI standard FORTRAN 77 compiler is required. Users without a FORTRAN compiler may still run the program, but will not be able to modify existing components or add new components. It includes the Simulation Studio and TRNBUILD Software [7]

D. Development of HVAC based Domestic House on TRNSYS Software

This model type is useful for estimating heating or cooling loads for a residential house. Walls, factories, flat roofs, doors, and floors are included in this component. The building should be designed according to different dimension and their rating [10]. Also for the design concepts, various elements are incorporated into it & working accordingly. For the modelling purpose, some factors are usually used for designing the whole formation of building. The orientation, hemisphere, calculation (whether it is internal and external surface) and used by surface that have used in orientation place.

E. Implementation of the proposed HVAC based Solar water heater model in TRNSYS Simulation

For modelling the House and Its geometrical perceptions modelling is the best alternative for calculating the whole energy and corresponding indoor outdoor temperature, and some ageing factors like humidity thickness and much more are the required details of a residential building. For the overall progress of the building, one can used TRNBuild is the mechanism of TRNSYS where different types of factors are urgently needed for whole modelling purpose of residential house and also used different measurement for daily, weekly, yearly energy consumption. on the other hand, simulation diagram is the diagram where a model may be implanted with unlimited variations. The simulation diagram is

IV. MATHEMATICAL MODELLING OF SOLAR WATER HEATER

The Proposed system governing some mathematical expressions which is used for Daily, weekly, monthly & yearly energy consumptions in modern buildings using the domestic solar water heater. For better performance, the use of solar water heater is considered only to monthly energy consumption. The daily radiation on the collector system is formulated by the following equation,

$$\overline{H_T} = \overline{H}_b\overline{R}_b + \overline{H}_d\left(\frac{1+\cos\beta}{2}\right) + \overline{H}\rho_g\left(\frac{1\cos\beta}{2}\right)$$

Where, $\overline{H}$ is the monthly average daily radiation on a horizontal surface, $\overline{R}$ is the monthly average ratio of the radiation on a tilted plane to that of a horizontal surface, ρ is the reflectance and β is the collector slope. The subscripts b, d & g denotes the beam, diffuse and ground respectively.

The monthly average absorbed solar radiation per unit area of the collector can be written in this way,

$$\overline{S} = \overline{H}_b\overline{R}_b(\overline{\tau\alpha})_b + \overline{H}_d(\overline{\tau\alpha})_d\left(\frac{1+\cos\beta}{2}\right) + \overline{H}\rho_g(\overline{\tau\alpha})_g\left(\frac{1-\cos\beta}{2}\right)$$

where, $(\overline{\tau\alpha})_b$, $(\overline{\tau\alpha})_d(\overline{\tau\alpha})_g$ are beam, diffuse and ground reflected terms of the monthly average transmittance-absorptance product respectively. The other are described as above.

The governing equation of collector will be obtained by [15],

$$(mC)_c\frac{dT_c}{dt} = A_cF_RS - (A_cF_RU_L - \dot{m}C_p)T_{ci} + A_cF_RU_LT_a - \dot{m}C_pT_{co}$$

where T, $\dot{m}$and C_p are the temperature, mass flow rate and specific heat respectively. A, F_R and U_L are the surface area, heat removal factor and overall heat loss coefficient respectively. S is the absorb radiation per unit area of the collector. The subscripts c, I and o refer to collector, inlet and outlet respectively.

The equation governing the storage tank is given by as follows,

$$(mC_p)_s\frac{dT_s}{dt} + \left(\frac{1}{R} + \dot{m}C_p\right)_sT_s = \frac{T_a}{R_s} + (\dot{m}C_p)_sT_f + (\dot{m}C_p)_{HX}(T_{HXo} - T_{HXi})$$

where, R is heat transfer resistance of the storage tank itself. The subscripts S, HX and f refer to storage tank, heat exchanger and feed water, respectively. All other parameters are as previously defined.

The temperature of the heat exchanger outlet and collector inlet (temperature of the working fluid flowing inside the pipe connecting the storage tank to the collector after losing part of its heat to the ambient before entering the collector) are defined respectively by following relations as follows,

$$T_{HXo} = T_p - exp\left[\frac{-PLU}{(\dot{m}C_p)_{HX}}\right](T_p - T_{HXi})$$

$$T_{Ci} = T_p - exp\left[\frac{-PLU}{(\dot{m}C_p)_{HX}}\right](T_p - T_{HXo})$$

where, T_p is heat exchanger pipe wall temperature, P, L and U are wetted perimeter, length and heat transfer coefficient of the heat exchanger pipe, respectively. Other parameters are as described above.

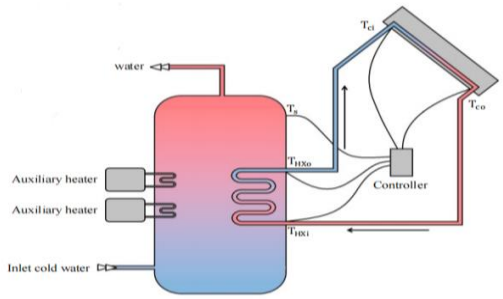

Fig.1: Proposed Solar water heater

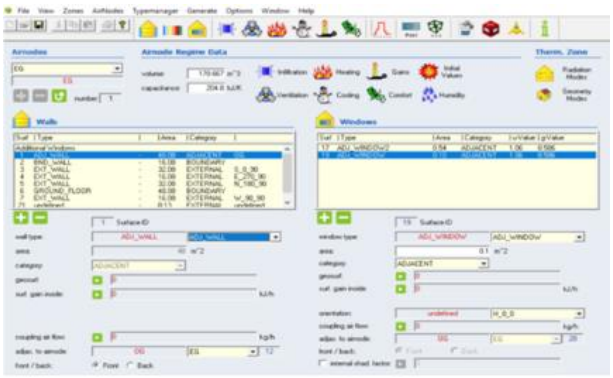

Fig. 2: TRNBUILD mechanism

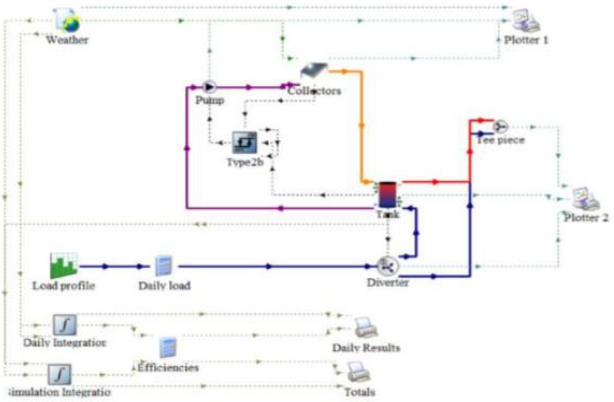

Fig. 3: Proposed model of Solar water Heater in TRNSYS

F. Modelling and Simulation of an Energy efficient building in Western Countries using TRNSYS

The improvement of the building energy efficiency is achieved by reducing the energy consumption and emissions. Since buildings thermal behavior depends on different variables, which complicates the control of predicting energy consumption, the use of buildings thermal simulation models which are based on the building energy balances for each zone is what fits best. To estimate the heating and cooling load and the annual energy consumption, the air temperature is needed. In order to have an overview on the ambient temperature fluctuations, the two followings' graphics

represents respectively the days showing hourly values of the ambient temperature, the daily extreme and the daily mean values of the ambient temperatures [11]. The simulation results also give the status of Energy consumptions are very poor compared to Indian scenario.

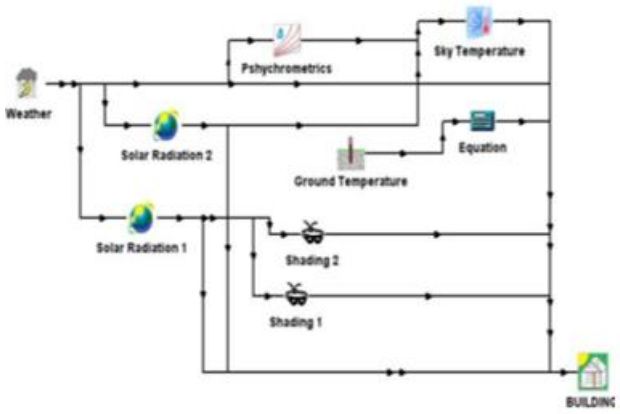

Fig. 4: Simulation Model of Building design in European countries in TRNSYS software

the simulation results are,

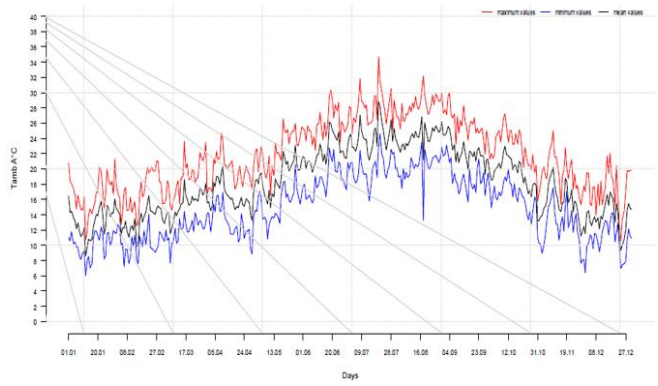

Fig. 5: Simulation results of European countries in TRNSYS software

III. RESULTS & DISCUSSIONS

G. Simulation Results of the Proposed model (Indian Scenario) and discussions

After components are linked properly in simulator, the output results are viewed in terms of simulation output. The figure of output on different parameters are collected together and that's why the discussion are very necessary.

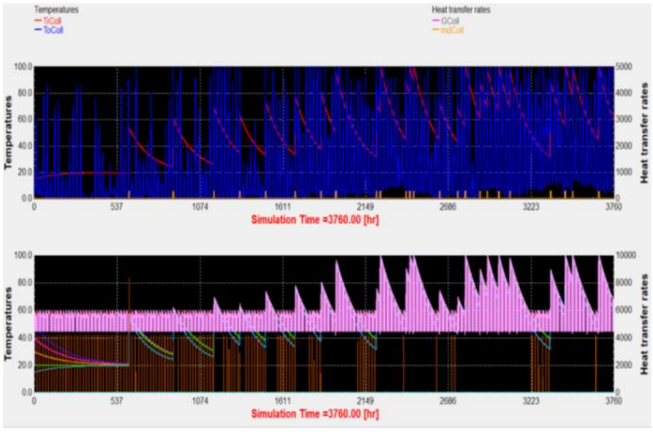

Fig. 6: Output results of simulation in marked as plotter-1

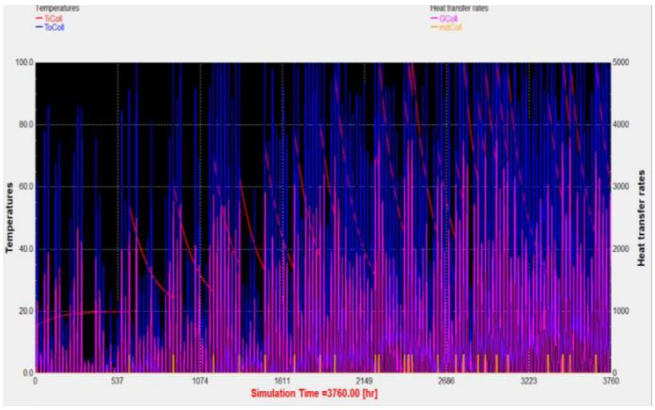

Fig. 7: Output results of simulation in marked as plotter-2

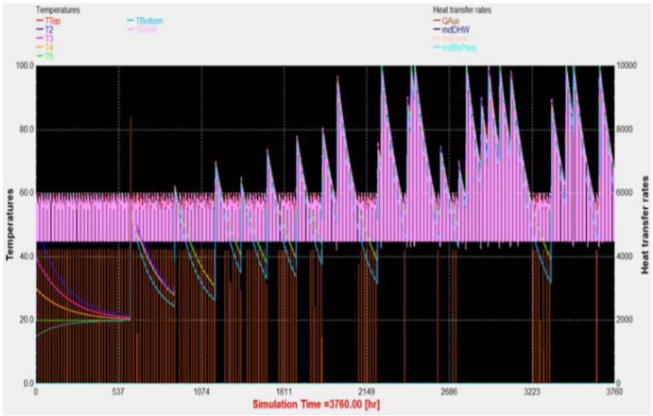

Fig.8: simulation results in plotter-1 in 8760 hours

The solar energy system simulation is transient in nature; therefore the chances of uncertainty and error in simulation are very high. Initially numerical methods were deployed widely in design of solar water heater system but after inception of computer, lengthy and repetitive calculations were obsolete. Numerous simulation tools based on different platform and assumptions have been developed. Extensive research work focused on different components, system configuration and operating conditions are carried out. The

simulation depends upon the programmer; how accurately and precisely the model of consisting components have been designed.

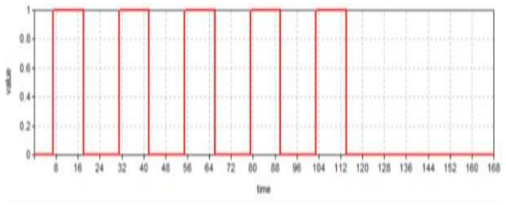

Fig.9: Daily energy consumptions in Building Sector

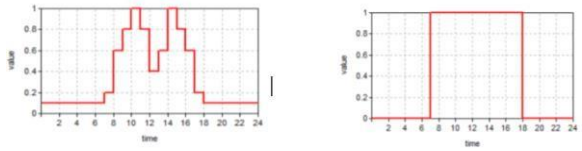

Fig.10: Weekly energy consumptions in Building Sector

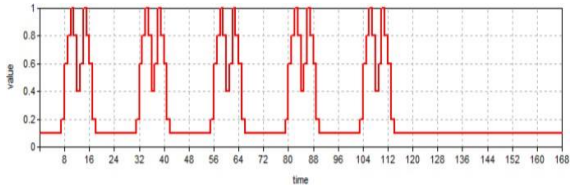

Fig.11: Yearly energy consumptions in Building Sector

Current version of TRNSYS 2017 is a result of constant improvement, regular Updation inclusions of new components and governing parameters. Its modular approach and open-source code facilitate the user to customize and develop the model as per requirement. However, it includes most of the parameters and components are provided to include and modify to suite the requirement [12].

IV. COMPARATIVE STATEMENTS OF PROPOSED LITERATURE

It was found that when we compared the energy consumption between two regions or two scenarios, the energy consumption by daily, weekly monthly and yearly are far better to western regions. Using TRNSYS software we can visualize the different graphs related to this comparative analysis. However, solar energy system simulation is transient in nature; therefore the chances of uncertainty and error in simulation are very high. Current version of TRNSYS 2017 is a results of constant improvement, regular Updation inclusions of new components and governing parameters. Its modular approach and open source code facilitates the user to customize and develop the model as per requirement. However, it includes most of the parameters and components are provided to include and modify to suite the requirement

V. FUTURE SCOPE

Fast growing in solar energy market has been observed worldwide, advance technologies are being introduced in this area. Comprehensive up-gradation of simulation tools to predict more realistic results is need of the day. it is still a thrust area with agenda of accuracy improvement, adding new technologies and report management and cloud application etc. regular updates of simulation are required to account for change in climate, occupants' behavior and technology advancement. Due to dependency on geographical variables, simulation tools developed and validated locally may serve the purpose in better way. instead of going with a single simulation tool, simultaneous analysis of same system on different programs is recommended for future way.

VI. CONCLUSIONS

Simulation of solar water heater includes the transient as well as dynamic parameters. Simulation of SWH depends upon the several factors and many of them are beyond control. current version of TRNSYS 2017 has undergone of constant improvement and development. The quality of results depends upon the degree of accuracy and details considered during modelling. Simulation may be used in best way if acquired through series of experiments is used to train the software accurately [13]. In general, the simulations of solar systems and especially simulations with the TRNSYS program. In the drawbacks of this approach is the effort required to learn and use the program effectively and its cost [14].

VII. REFERENCES

[1] [1] Fazele Azari Sangeli et.al. "Managing and Optimization of Energy Consumption and Offering Strategies to Materialize It" Vol.3, No.3 Special Issue on Environmental, Agricultural, and Energy Science, ISSN 1805-3602

[2] [2] Fazli Wahid and Do Hyeun Kim "An Efficient Approach for Energy Consumption Optimization and Management in Residential Building Using Artificial Bee Colony and Fuzzy Logic" Volume 2016, Article ID 9104735, 13 pages http://dx.doi.org/10.1155/2016/9104735

[3] Fazli Wahid and Do Hyeun Kim "An Efficient Approach for Energy Consumption Optimization and Management in Residential Building Using Artificial Bee Colony and Fuzzy Logic" Volume 2016, Article ID 9104735, 13 pages http://dx.doi.org/10.1155/2016/9104735

[4] Rana Tawfiq Almatarneh "Energy-Efficient Building Design: towards climate-responsive architecture - A case study of As-Salt, Jordan" Advanced Research in Engineering Sciences "ARES" E-ISSN: 2347- 4130; Vol. 1(2) October 2013

[5] Bhagyesh S Pawar and Prof. G.N. Kanade "Energy Optimization of Building Using Design Builder Software " International Journal of New Technology and Research (IJNTR) ISSN: 24544116, Volume-4, Issue-1, January 2018 Pages 6973

[6] Izzet Yu¨ksek and Tu¨lay Tikansak Karadayi "Energy-Efficient Building Design in the Context of Building Life Cycle"

[7] William A. Backam et al. "TRNSYS The most complete solar energy system modeling and simulation software", Renewable Energy, 199

[8] Tiberiu Catelina et al. “Multiple regression model for fast prediction of the heating energy demand” Energy and Buildings 2003

[9] Submitted to Istanbul Aydin University

[10] R. Chargui and Habib Sammouda “Simulation of a Residential House Coupled with a Dual Source Heat Pump System”, International Letters of Chemistry, Physics and Astronomy, 2015

[11] Meriem Labied et al. “Improving the passive building energy efficiency through numerical simulation–A case study for Tetouan climate in northern of Morocco”, Case Studies in Thermal Engineering, 2018

[12] Internet Source

[13] R.L. Shrivastava et al. “Modeling and simulation of solar water heater: A TRNSYS perspective”, Renewable and Sustainable Energy Reviews, 2017

[14] S. Kalogirou et al. “Simple validation method of a TRNSYS model for a thermosyphon solar water heating system”, 2000 10th Mediterranean Electrotechnical Conference. Information Technology and Electrotechnology for the Mediterranean Countries. Proceedings. MeleCon 2000 (Cat. No.00CH37099), 1998

[15] Mohammad Esmaeil Yousef Nezhada and Siamak Hoseinzadehb “Mathematical modelling and simulation of a solar water heater for an aviculture unit using MATLAB/SIMULINK” Article in Journal of Renewable and Sustainable Energy, AIP Publishing, November 2017 DOI: 10.1063/1.5010828

A New Approach to the Construction and Life cycle economic analysis of a Solar Powered Low Voltage Induction Cooking System.

Sujit Dhar
Department of Electrical and Electronics Engineering
Neotia Institute of Technology Management and Science
Kolkata, India
dhar.sujit@gmail.com

Pradip Kumar Sadhu
Department of Electrical Engineering :
Indian Institute of Technology (Indian School of Mines)
\l*Dhanbad, India*
pradip_sadhu@yahoo.co.in

Debabrata Roy
Department of Electrical Engineering
Techno International Batanaga
Kolkata, India
debabrataroy1985@gmail.com

Soumya Das
Department of Electrical Engineering
University Institute of Technology
Burdwan University,
*India*soumya.sd1984@gmail.com

***Abstract*—Induction cooking is considered one of the foremost, efficient and cost-effective technologies involved in cooking. With this technology being properly utilized, 90% of the total energy used up in the process is transferred to the food which when compared to about nearly 40% for gas and 74% for traditional electric systems is comparatively better. This paper deals with the solar energy based induction cooking system where the primary source of power is solar power and also a comprehensive review of economic analysis, lifecycle analysis between normal induction stove and solar powered induction stove. The merits of this research work include designing, life cycle analysis and implementation of a solar power based induction cooking system. Here the full bridge converter is being used by the supply voltage to control the output power by changing the operating frequency.**

Keywords—Induction Cooker, full bridge circuit, battery charging circuit, microcontroller, Life cycle economic analysis.

I. INTRODUCTION

Induction Heating is extensively utilized as of late in domestic appliance due to its cleanness, high effectiveness, assurance, low cost proper quality semiconductors and inordinate by and large execution [1- 2]. The cooker offers power sparing with high speed cooking with numerous temperature levels. This exploration depends on the percept of induction heating and execution of compact acceptance cooker, utilizing inexhaustible supply of intensity as the essential wellspring of supply, enhanced through the network vitality. Acceptance of induction cooking is gotten from the rule of electromagnetic enlistment by prompting swirl flows inside cooking object is made of ferromagnetic material to aid in the process of heating. In this examination the point is to make the cooker an independent, transportable, dazzling and brilliant working gadget through exchanging among sun oriented and mains naturally. This will make the unit a standalone unit whilst at the same time increase the performance of the system [3-5].The excessive frequency harmonics from an instantaneous present-day supply is converted to alternating contemporary the usage of current fed parallel bridge converter. The harmonics delivered by utilizing the bridge circuit is used to create heating inside the induction coil [6-8].The cooker likewise are embedded with batteries which can work for around 4 hours without sun powered and the network being available at the time. The reproduction examine is done at particular frequencies [9-10].

II. PURPOSE OF THE STUDY

The purpose of the study is to present the economic benefits which can be derived from solar powered induction cookers. People prefer food which is cooked fast but with a very low fuel cost. Unlike a normal induction cooker, a solar powered induction cooker does not consume any electrical power from main supply. The initial investment for putting up a solar powered induction cooker maybe high but as solar energy is available in abundance; its fuel cost becomes nil. The solar energy is available in abundance; its generation cost becomes very less. In eastern region (West Bengal) of India, sufficient amount of solar energy is available almost 285 days out of 365 days in a year resulting to which the subject (solar induction cooker) is becoming a field of vast research and development.

III. INDUCTION COOKING SYSTEM

In this type of cooking, a cooking vessel is heated up by electromagnetic induction, instead of by thermal conduction from a flame, or an electrical heating element. The process is rapid through which we can attain high temperature quickly. Three factors governing the operation of an induction stove are skin effect, electromagnetic induction and heat transfer. In this process the input a.c with constant frequency to be converted to d.c first. Then the d.c is fed to the high frequency inverter. The output of the inverter is a high frequency a.c and this high frequency a.c current passes through working coil. Now if any pot is placed on the flat surface of the induction stove the induced voltage will produce an eddy current which will start producing heat on the pot which will increase the temperature of the pot making the pot ready to cook.

A. *Concept behind solar induction cooker*

The simulation model of solar induction cooker is being discussed later. The coil and its working are the two parts where the current version mainly focuses. The distribution of the current is even, which is in turning indicated by the modeled coil. The induction cooker resemblance with the heat generated on the secondary side due to the transformer action because of loading effect of the losses of equivalent resistant is discussed in. Here in the present paper it is discussed in detail about all the coil parameters and how the modern density of the coil is differentiating with respect to the various numbers of turns within the coil. "Hard switching" is the mode of switching in the coil, is studied in the information by showing the electronic power device behaving under worrying switching. Additionally it takes notice on the losses when the transfer is exposed to excessive current and voltage during the same time. During switching, the voltage transients are assisted by the snubber circuits at the transfer. The outcomes correspond with the simulations practically. The solar based induction cooker pinnacle is discussed in. The intention of the paper collectively is to enforce a solar energy based gadget with the high feasibility. Initially the installation cost will be high but subsequently within a span of 5 years; the user can save up to Rs.12000.

IV. BLOCK DIAGRAM AND EXPLAINING OF SOLAR INDUCTION COOKING SYSTEM

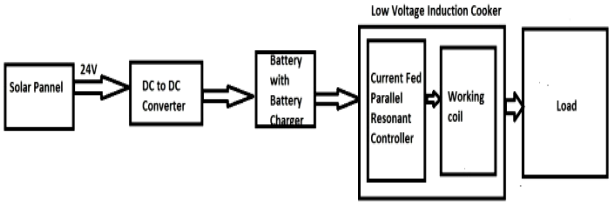

Fig.1. Basic block diagram of low voltage solar power induction cooker

The most important components of a solar power based induction cooking system is as follows: Solar PV array module, Maximum power point tracker (MPPT), Charge controller, Battery bank, Solar powers Induction cooker. In the block diagram (Fig.1) a 24V solar panel is placed on top of the roof with the help of a tracking circuit, which tracks the maximum lighting angle of the day depending on the time and intensity of sunlight throughout the day. This ensures the maximum amount of sunlight falling on the panel in order to get our desired output voltage. Solar panel is used to change the solar energy into electrical energy. The electrical energy available from the photovoltaic cells is converted to direct current. This almost steady d.c voltage is converted to pulsating d.c voltage with high ripple contain and fed into the battery through the battery charger unit. The fully charged battery output is fed to the low voltage side of the solar induction cooker, with the help of the current fed parallel resonant converter circuit and the coil in induction cooker will thus heat up the load. The supply voltage for the induction heater is 24V.Currently no commercial solar induction stoves or any of its literature is somewhat available in research oriented works regarding the induction stoves, which are powered from any d.c power source of such low voltage.

V. DESIGN OF LOW VOLTAGESOLAR POWER BASED INDUCTION COOKING SYSTEM

A. *Solar Pannels*

The solar panel is light weight, frameless and waterproof. These panels consist of solar cells which are much more efficient than the conventional solar panels. They are even effective in low intensity of light. During daytime, PV would be the primary power generator. Each PV module (panel) is rated in accordance with its d.c output power under standard conditions, and typical specification ranges is 300 watts. Fig.2 shows the monthly basis (Jan 2019-Dec 2019) solar radiation chart of the working place (West Bengal, Kolkata, India).

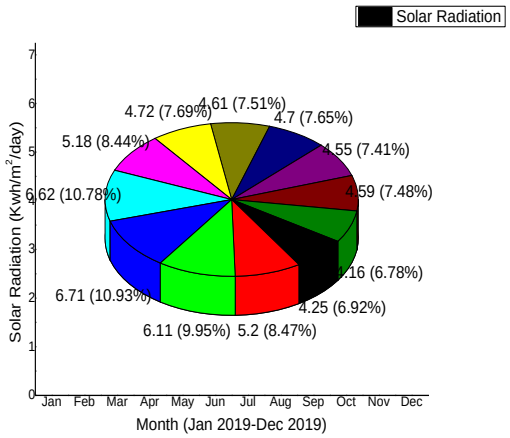

Fig.2. Monthly basis solar Radiation pie chart

B. *Calculation for number of solar panels*

Based on the solar radiation on hourly basis the power generated by the panel can be calculated by the following method: $\boldsymbol{W_{dc} = \eta_{pv} \times I_{irra} \times A}$ …….(1)

where, W_{dc}= power generated by the panels in watt;

A = area of cross section of the panels in m;

I_{irra} = **i**ncident solar radiation falling on the panel;

η_{pv} = **e**fficiency of the solar panels.

Total power rating (N = 1)numbers of solar panel,

$$\boldsymbol{W_{Total} = N \times Wdc} \text{.....(2)}$$

Rating of each solar panel = 300W.

During sunny day, assume sun light available T= 6 hours. Therefore, maximum Energy generated /day,

$$\boldsymbol{E_{max} = T \times W_{Total}} \text{.....(3).}$$

E_{max} = maximum energy generated /day/panel = 1800 wh. Now considering the efficiency of the panel is η = 80%. Therefore, the total energy obtain from panel,

$$\mathbf{E_{total}} = \eta \times \mathbf{T} \times \mathbf{W}_{Total} \quad \text{.....(4)}$$

Therefore, the energy may be collected from the solar panel $\mathbf{E_{total}}$ = 1440 Watts-hours.

Total energy consumed by the proposed solar Induction cooker $\boldsymbol{E}_{Induction}$= 1200 Wh. Number of solar panel required,

$$N = \frac{\mathbf{E_{total}}}{\boldsymbol{E}_{Induction}} = 1.2 \approx 1 \quad \text{……(5)}$$

The array yield is given by,

$$Y_{a\_yield}\,(\%) = \frac{W_{dc}}{W_{PV\ rated}} \quad \text{....(6)}$$

The daily average final yield is $Y_{D_a_f_y(\%)}$the ratio of the generation output to the rated standard test condition (STC).

It is expressed as:

$$Y_{D\_a\_f\_y}(\%) = \frac{g_m}{g_{STC}} \quad \text{.....(7)}$$

Where, g_m = Inclined global radiation in MJ/m2.

The variation of the actual irradiance from the reference is expressed as array capture losses. It can be expressed as:

$$LC = Y_{D\_a\_f\_y} - Y_{a\_yield} \quad \text{.....(8)}$$

TABLE 1 PV MODULE SPECIFICATIONS USED IN INDUCTION COOKER

.Component	Specifications
Solar panel type	Flexible Polycrystalline Silicon.
Dimensions (L×W×D)	1955×982× 36 mm3
Weight	20.5 Kg
Open circuit voltage (V_{oc})	45.58V
STC power Rating	300W
Module peak Efficiency	15.63%
Maximum Power Voltage (V_{mp})	37.05V
Maximum Power Current (I_{mp})	8.1A
Open circuit voltage (V_{oc})	45.58V
Short circuit current(I_{sc})	8.58A
Operating temperature	−20℃ to + 80℃
Normal Operating Cell Temperature (NOCT)	44℃
Temp. Coefficient Power	-0.41%/K
Manufacturer	Vikram Solar Pvt Ltd, India
Indian Market price	Rs 8558 Plus 10% GST

The following panels designed for working in the harshest weather conditions and water-resistant feature for both. The item is easily available in local market because it is an Indian product and the approximate price of solar PV panel is Rs 8558 plus 10% GST. The price of solar module can be varied according to the availability in the Indian market

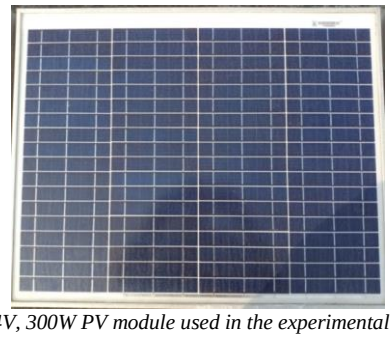

Fig. 3. 24V, 300W PV module used in the experimental set up

C. Battery Charging Power Equations

The maximum power that can be stored in a battery can be calculated as follows:

$$p_{battery_{max}} = \frac{(1 - e^{\theta t})(\theta_{max} - q)}{T} \quad \text{……..(9)}$$

Where, θ = The rate of flow of charge to the battery during peak hours;

Q_{max} = Maximum charge that can be stored by the battery. The calculation of 'Q_{max}' can be obtained as follows:

$$Pmax = \frac{(n \times I \times V)}{1000} \quad \text{. ……. (10)}$$

where, n = The total number of batteries; I = Maximum current; V = Nominal voltage

Equations (9) and (10) are formed on the assumptions of losses of charge:

$$Ploss = \frac{MIN(P_{man-P_{min}})}{N} \quad \text{…..(11)}$$

The function of the battery charger here is to limit the charging current and prevent overcharging of the battery by cutting-off the supply after the set state-of-charge (SOC) threshold is reached.

D. Discharging power Equations of the battery

It's the ability of the battery to discharge the power stored by it to some load. This is calculated as follows:

$$P_{dmax} = nd\left(P_{max}, P_m\right) \quad \text{……(12)}$$

The calculation of the capacity of a lead-acid battery in terms of the rate at which it is discharged can be expressed by Peukert's Law [11].

$$C_{capacity} = T_{discharge}(I_{dischargr})^{K_{con}} \quad \text{……(13)}$$

Where, $C_{capacity}$ is the capacity (one ampere discharge rate) in Ah; $I_{discharge}$ is the discharge current in A; K_{con} is the Peukert's constant; and $T_{discharge}$ is the time of discharge in hours. In this design, two batteries are used, each with the operating voltage of 24V and charges capacity of 150 Ah. When two batteries are combined, they are capable of producing electric power without charging for about four hours.

TABLE 2 Battery Specifications Used in Solar Induction Cooker

Parameters	Specifications
Operating voltage, Stored Energy of a completely charged battery	24 V, 150 Ah, 3.84kWh.
Continuous Disc. Current	12.0 A
Charging Time	8 ~ 10 hour
Weight	28.48kg
Battery Material	Lead acid
Lifetime	6-8 years.
Manufacturer	Exide India Ltd.
Dimension	500×240×220nn3
Indian Market price	Rs 10000 Plus GST Charge.

E. Battery and charging method.

In this design a couple of batteries, each of 24V and 150Ah capacity forming 24V and 300Ah capacity. The battery is partially charged by solar power. During the monsoon season or when charged from the power grid, a separate charger is used for this purpose. The boost converter is used to charge the battery by using the PWM technique. Half bridge series resonant converter is used to convert stored d.c energy to a.c energy of 25 kHz frequency by grid power every day from 6 pm to 2 am (8 hours). This generates 4 hours of battery output (approximately) at night without charging. TABLE 3 gives the technical specification of a battery charger.

TABLE 3 Specifications of a Battery Charger.

Characteristics	Values
Charging Voltage	12/24V, (47-63)Hz
Universal Input	90-260Va.c
Charging Current	5.5-7.5Amps
Weight	2.2 Kg
Charger Dimension	230mm × 160mm ×100mm
Charging Time	8 ~ 10 hour

The battery is charging at home through normal 15/32A three pin plugs, single phase (90-260V, 50Hz) a.c supply with trickle charging facility. The approximate cost of the battery charging unit in Indian market is around Rs 3000/- (excluding 10% GST) and the average lifetime of the charger is around 4-6 years.

F. Flot

The float stage is where the charge voltage is reduced to around 2.25V per cell, which is around (27-29) $V_{d.c}$ and held constant, while the current is reduced to less than 1% of battery capacity. This mode can be used to maintain a fully charged battery pack indefinitely. Some chargers shut off instead of maintaining a float voltage, and monitor the batteries, initiating a charge cycle if necessary. This type of combined chargers is used in charging of the battery system. The utilization of float cum boost charger is as follows: This system is activated when the battery charging is fully charged up at this point it is pointless to charge the battery so in this case the float will bypass the battery charging and will provide direct d.c to the induction coil. In this system, the d.c generated from the solar panel which passes through the d.c to d.c converter then through the charger at this point seeing the battery is fully charged the float will bypass the system resulting of direct supply of d.c from the charger itself.

G. Boost Converter

The use of boost system is to prevent quick discharge of the battery. Boost converter comes in use in such a case if low voltage gets an input to charger the boost converter converts the low input to a desirable high voltage output required by the battery specification. It is in this way boost prevents deep-discharge. So, a combination of this result to float cum boost where one prevents unnecessary charging while other prevents deep discharging of the battery.

H. Solar Induction Cooker

In this approach addresses by the design of a induction stove which is of quite high efficiency (more than87%) powered by a d.c source of 24V. A 24V d.c power supply is one of the most common solar installations output, and mainly only one of few output voltages that are standardized for photovoltaic panels and battery. This in turn makes it perfect for direct integration with a roof top solar-based micro-grid or solar installation.

I. Converter Circuit Topology

In this proposed design, the most suitable converter is current-fed parallel resonant converter [12] used in industrial heating applications, but there is no prior information available about the topologies used in induction cooking. Fig.4 shows the conceptual schematic of a current-fed parallel resonant converter. This type of electrical power converter has within itself a network of capacitors and inductors called resonant tank and also these are resonated and then they are tuned to a specific frequency. Appropriate frequency should be opted depending on the skin-depth requirement and work piece geometry in regard with each application. Among the large number of topologies have been developed in this particular area current-fed and voltage-fed inverters are the most common used [13]. The output power for current source resonant inverter can be controlled only by using phase-controlled rectifier and also by adjusting the d.c- link. A transformer is used for matching load impedance in the conventional current source resonant inverter while high voltage spike and increases on the voltage stress on switches are produced by leakage inductances. And in order for this problem to be solved, the inverter must work with leading power factor load. To decrease the switch's current, more number of legs can be paralleled to the inverter, so that the total efficiency can improved significantly and also the transformer can be removed.

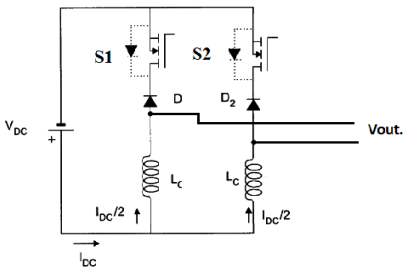

Fig. 4. operating circuit topology for Current-fed parallel resonant converter

J. Induction coil

Fig.5 shows the construction and top view of the induction coil. The metallic strips with huge thickness are used to heat the utensils. With a number of new structures being evolved lately, transverse flux induction heating (TFIH) is doubtlessly very promising and appealing.

Fig. 5. Induction Coil in the proposed design [14].

Journeying wave induction heating (TWIH), as one of the multiphase induction heating systems, has specific features which lead them to appealing for utility to induction cooking system. The main advantages and the precise traits of TFIH and TWIH systems consisting of the effect of slots on prec- ipitated strength distributions has been studied. Throughout the entire cooking process efficiency of the induction heater is almost 83%.

K. Impact of Pan Resistance

The pan resistance (R_{eq}) of the utensils regulates maximum heat generation. To get maximum power, practically pan resistance of utensils needs to be changed. With the change of load power, the heating effect will be maximum. The maximum power is achieved by changing the equivalent resistance (R_{eq}) so as to obtain maximum heating effect. This equivalent resistance is the summation of internal resistance of working coil (R1) and the resistance of cooking pan (R2) which is referred to primary side.

That is: $Req = R1 + R2$ …..…..(14),

Where, R2 is the key regulating parameter of the R_{eq} and which is variable with the change of cooking pan.

L. Operating Frequency

The operating frequency of the design is 45 kHz, which is more or less double the switching frequency of the commercial designs. Also, the presented design has the chances to easily rise up to around 100 kHz and even more. Therefore, the best choice is the IC IRFP4310P of all the 4 switching devices and the specifications are 100V N-channel MOSFETs with 6mOhmRds(on) and 170 nC total gate charge. Lower device stresses due to this low voltage current-fed parallel resonant converter (ZVS) which allows faster device switching than conventional designs. The biggest advantage of the design is that the resonant current energizes entirely the resonant tank. The power electronics device only needs to carry the current actually delivered to the load. 1kW of heating is required for a 24V source for the maximum load current to be 40A.

VI. BLOCK DIAGRAM AND EXPLAINING OF SOLAR INDUCTION COOKING SYSTEM

Fig 6 shows the basic block diagram of the grid charging system. Generally, the battery bank of the solar cooker is partially charged by solar module during sunny day but it is fully charged by normal single phase a.c supply during night/evening time and the approximate time taken for battery charging is (6-8) hours.

A. Supply voltage

The supply main gives a.c during bad weather when there is an inadequate supply of sun light and the rating of supply mains socket is 230V, 65A.

B. A.C to D.C Converter

The output of the converter is fed into d.c to d.c converter through 24V auto selection switch. The firing angle of the converter is controlled by microcontroller. The main function of d.c to d.c converter is to convert the d.c voltage into pulsating and controllable d.c. A booster converter unit is used to boost the charging voltage into nearly 30V of the battery charger.

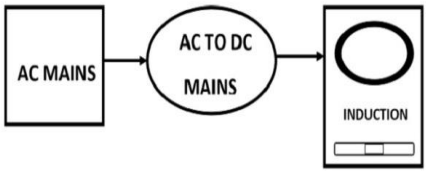

Fig.6: Block-diagram of charging system

VII. BLOCK DIAGRAM OF THE WHOLE SYSTEM

The proposed structure centers additionally around the auto-choice in middle of the two-control sources, to be specific sun based power and mains grid control. The capacity of auto choice is to choose any accessible wellspring of intensity between any of the two. The cooker uses the batteries that will be charged by both solar based and mains yet treating the sun based as a priority so as to advance the utilization of free vitality when it accessible.

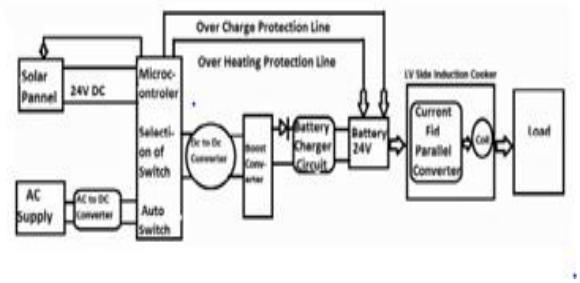

Fig.7: Block diagram of the whole system

Block diagram of the entire solar panel cum main line connection system is to get the d.c voltage to charge the battery and then supply the power to the solar induction cooker subsystem used in this research work is shown in Fig.7.The proposed low voltage d.c induction cooking system consists of several components out of which current-fed parallel resonant converter, Zero crossing detector, and IGBT along with arduino microcontroller (ATmega328) are used to implement the power converter.

A. *Explanation of block diagram*

In this block diagram they are two sections as we see in the diagram first section is for the solar panel part where the d.c current is generated. The other second section has the source from the main supply of 230V which will be on use when there is a lack of d.c supply from the solar panel in case of climatic abnormality. Now let us talk on how different section will function.

First section : in this section solar panel is connected, where a low voltage d.c is generated which is fed to a microcontroller connected with auto switch which can be used to switch over when a microcontroller senses that there is very low d.c generate from the panel (a value is set with a microcontroller for switch over) so the voltage passes to a d.c to d.c converter for improving the voltage of the d.c as required for the battery then it is passed through a boost converter to prevent deep discharge which is feed to the charger which will charge the battery from this source we will connect our induction cooker which hence fourth will heat up the load placed above the cooker. Second section: Mains is considered for the supply. This condition is only used when there is very low voltage generated from the solar panel. Mains current is fed to a.c to d.c converter. The switch over is done with the help of auto switch. Then to d.c to d.c converter and rest of the process will follow as described in first section.

VIII. OPERATION OF THE SOLAR POWER BASED INDUCTION COOKING SYSTEM

A. *Auto Switch Control*

Microcontroller, miscellaneous I/O and signal conditioning components are the main control circuitry of the auto switch control device. The software based auto control broadband is the cause for the digital driving of the switches. Depending on the power demand analysis, availability and the efficiency at that particular moment, the auto select switches helps in the auto selection between solar and the grid. In this analysis, the solar power is the major priority for its economic feasibility, availability and widespread usage. The power levels of the batteries are compared before the switching state selection. In this plan, the auto switching circuits are modified in such a way along these lines that the wellspring of intensity is chosen before each cooking state. On the off chance that the sun based board isn't adequate to supply the required power for the cooking state chosen and for the determined amount of time, the mains power will be chosen and the battery will be charged either from sunlight based or from the mains consequently. Another main function of microcontroller is to provide protection for overheating and overcharging.

B. *Auto Switching*

Based on the power demand analysis, availability and the efficiency at that particular moment, the auto select switches helps in the auto selection between solar and the grid. For economic feasibility, inexpensive usage and widespread usage, the solar power is the major priority of this analysis. The power level of the batteries is compared before the selection of switching state. If the power and voltage level of the battery is sufficient the induction cooker is powered from the battery. In this new design, the software based auto switch is programmed in such a way that before each cooking state the source of power is selected. The mains power will have to be selected and the battery will have to be charged automatically from the solar or from the mains only if the solar panel is not sufficient or in a state to supply the required power for the cooking state selected and also for the duration calculated.

Operation: A negative going ramp but a positive going ramp may also use. The ramp voltage value is continuously compared with the solar charging battery voltage. At the instant the value of is equal to that of battery voltage a coincidence circuit, called input comparator, generates a pulse which opens a gate. Therefore, a logic high input signal will come to auto switch and solar charging circuit is connected to induction cooking equal to that of battery voltage a coincidence circuit, called input comparator, generates a pulse which opens a gate system. Initially the battery of the solar system is fully charged but after some time the battery will discharge to certain value called reference value. The ramp voltage slope is continuing to decrease till it reaches reference level. At this instant another comparator called reference comparator generates a pulse. This pulse comes to auto switch and disconnects the battery of the solar circuit. In this time, the induction cooking system operates through main supply (220 Volt, 50 Hz). Battery is continuously charging through solar panel, again charge is developed and induction cooker is connected to solar circuit automatically through auto switch. This is a continuous process; a huge amount of power will be saved when the cooker is connected to a solar system. FPGA based technology is popular now a days, but in this proposed research, production cost is one of the prime factors, therefore to reduce the production cost, FPGA based circuit are not used.

C. *Sensor, Relay and Flowchart Diagram.*

In the Fig.8 represent a simple logic control operation for controlling of relay with using microcontroller. In this an input line voltage is sent though attenuator and other is sent to the relay.

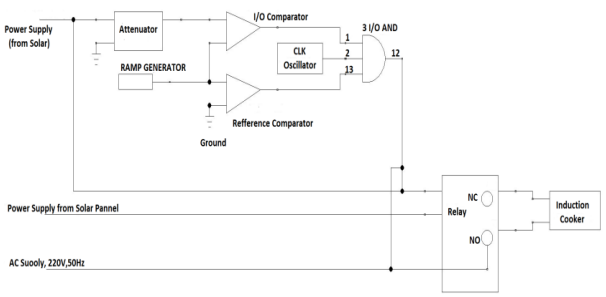

Fig.8: Logical control of relay with the use of microcontroller

The output of attenuator is then sent to a comparator with one is feed with a ramp generator. With the comparator of set voltage logic is generator which will be 1 or 0. This generated output is set as an input for three input AND gate with other input is feed with a clock oscillator and other input is feed from the reference comparator which also has a input from ramp generator. The logic 1 or 0 generated from the 3 input AND gate is set to the relay which will determine

the relay to stay close or open. Fig.9 shows the connection diagram of sensor, relay and microcontroller.

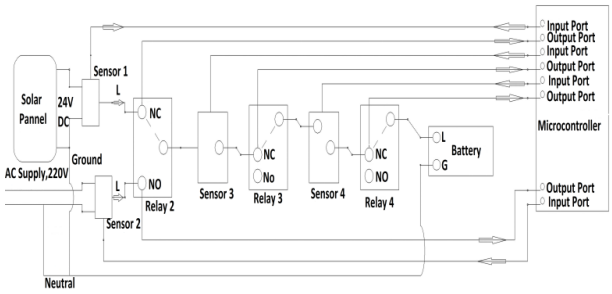

Fig.9: Sensor, Relay, and Microcontroller connection diagram.

D. Flowchart of the System Operation

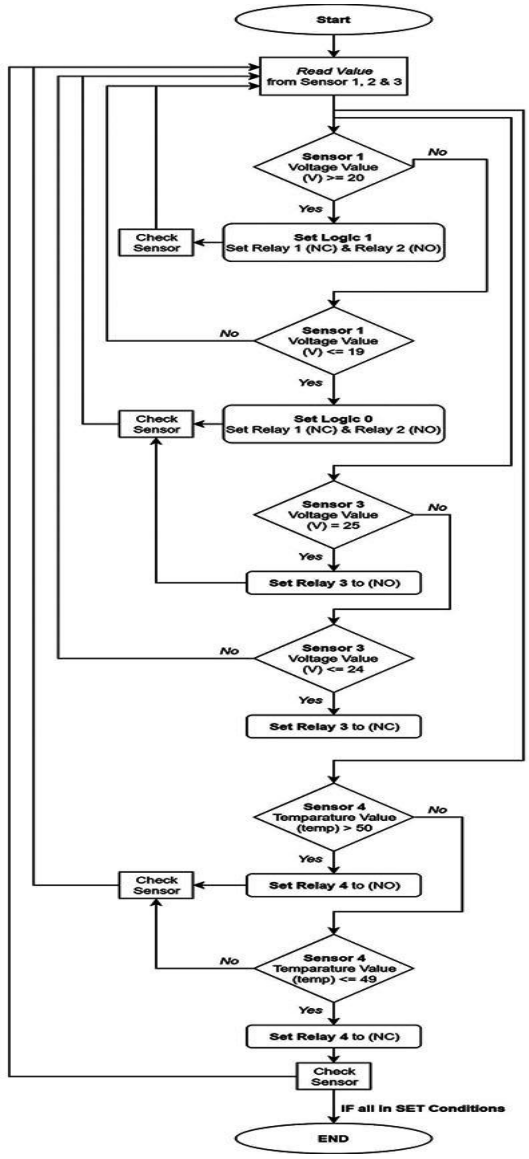

Sensor 1: for observing P.V. generation;
Sensor 2: for observing mains line;
Sensor 3: for observing over load voltage,
Sensor 4: for observing temperature.
Relay 1: NC (Normally closed);
Relay 2: NO (Normally open);
Relay 3: NC (Normally closed);
Relay 4: NC (Normally closed).

Relay 1 connected to solar panel;. Relay 2 connected to main line; Logic 1: Solar panel and relay 1 are connected to auto switch; Logic 0: solar panel is disconnected but connected to main line and relay 2 is connected to auto switch.

Flow chart 1 represents the software program that is uploaded to the microcontroller for controlling the sensors and then relays to operate the function of power system in order to charge the battery.

E. Sensor, Relay and Microcontroller Control circuit

In the fig 7, it is seen that there are 4 types of sensors used as well as 4 relays used. Sensor 1 and 2 are used for checking the voltage change from both the source, whereas relay 1 and 2 are used to change-over supply distribution when solar power production is low.

Sensor 1	Relay 1	Relay 2
0	0 (NO)	1 (NC)

TABLE 4 Logic when Solar Panel has Sufficient Production (V≥ 20)

Sensor 1	Relay 1	Relay 2
1	1 (NC)	0 (NO)

TABLE 5 Logic when Solar Panel Production (V<20)

Sensor 1	Relay 1	Relay 2
0	0 (NO)	1 (NC)

F. Protection against Over load voltage and Temperature change.

Sensor 3 is responsible for checking the over load voltage.

Relay 3 is normally closed but there is an overload which will be set open resulting to the stopping of charging of the battery till the overvoltage decreases.

TABLE 6 Over Load Voltage Logic.

Condition (Over voltage) in V	Sensor 3 logic	Relay 3 Logic condition
V>25	1	NO
V<=24	0	NC

Sensor 4 is responsible for temperature change in the system

Relay 4 will respond to the change in temperature.

TABLE 7 Temperature Change logic

Condition (Temperature Change)	Sensor 4 logic	Relay 4 Logic/ Condition
T >50C	1	NO
T ≤ 49C	0	NC

IX. RESULTS ANDANALYSIS

A. Testing results

Table 8 shows the solar panel voltage(from 24.4V to 10V) that are induced from the different intensities of the sun light. Fig.10 shows the important bar graphs of the battery voltage with respect to time and in Fig.11 the battery voltage, PV module voltage with respect to time for

analysis of the physical conditions and characteristics of PV modules and batteries are being shown. The experimental setup has been developed in a research laboratory; Google map of experimental area has been shown in fig.12.A.c to d.c converter will not operate up to the solar panel voltage of 20V, but it will operate from 19V to 10V. A microprocessor-based auto switch will control that operation. Here, position 1 indicates that selection of the solar power voltage and position 0 indicates the selection of a.c main respectively. Correspondingly, the booster converter voltages, battery voltages and battery temperatures are indicated in TABLE 7. Hence it will conclude that the normal charging voltage of the booster converter lies between 30V to 26.6V. The voltage of the booster converter should not exceed 30V to avoid over-heating, over voltage and over charging problems of the battery and for the life cycle economy analysis it will reduce the life span of the battery.

TABLE 8 Analysis of Solar Charge and Normal Charge System(1: Select Solar power, 0: select A.C Main)
O.V = Over Voltage; N.V = Normal Voltage

SL NO.	Time in hour	Solar Panel Voltage (In Volt)	A.C to D.C Converter Voltage (in Volt)	Position of Microprocessor Control Auto Switch	Booster Converter Voltage in Volt	Battery Voltage in Volt	Selection of Auto Switch	Battery Temperature in C^0	Conclusion
1	09am	23	0	1	29.2	25	solar panel	51	OV
2	10am	23.5	0	1	29.4	25.4	solar panel	52.2	OV
3	11am	24.1	0	1	29.7	25.7	solar panel	53	OV
4	12am	24.4	0	1	30	26	solar panel	53.4	OV
5	01pm	23.6	0	1	29.3	25.2	solar panel	51.5	OV
6	02pm	22	0	1	28	24.3	solar panel	49.9	NV
7	03pm	21.6	0	1	27.5	23.9	solar panel	49	NV
8	04pm	21	0	1	27	23.7	solar panel	48.2	NV
9	05pm	20.1	0	1	26.6	23.4	solar panel	47.3	NV
10	06pm	19	23	0	28.7	23.5	A.C Main	48	NV
11	07pm	16	23.1	0	28.8	24.2	A.C Main	49	NV
12	08pm	13	23.1	0	28.9	24.8	A.C Main	49	NV
13	09pm	10	23.1	0	29	25.3	A.C Main	50	OV
14	10pm	10	23.1	0	29	25.4	A.C Main	50	OV

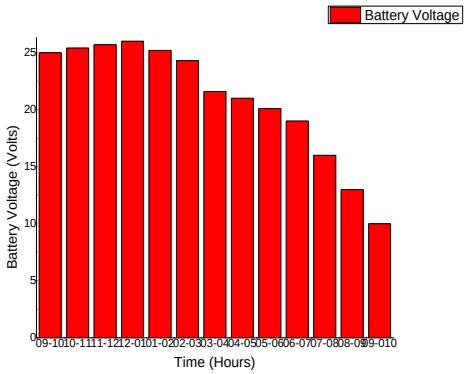

FIG.10: BATTERY VOLTAGE VS TIME

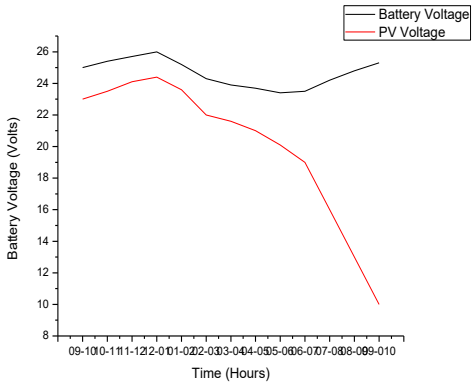

FIG. 11: BATTERY POWER VS SOLAR CHARGING POWER EXPERIMENTAL AREA

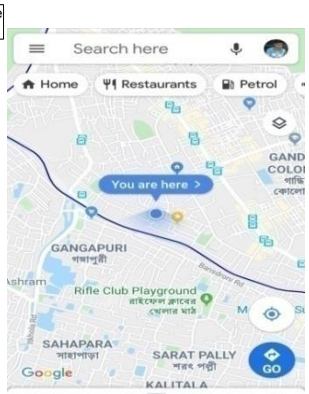

FIG 12: GOOGLE MAP OF THE

B Simulation results

The experimental set up and simulation results are shown in figures 13 to 17 using PSIM software as well as hardware. The switching frequencies are taken from 40 KHz to 100 KHz. Fig.17 shows the experimental set up of the proposed induction cooking system designed in the laboratory.

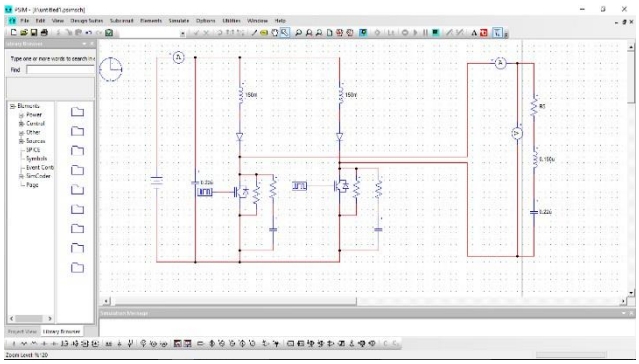

Fig.13: Current-fed parallel resonant converter

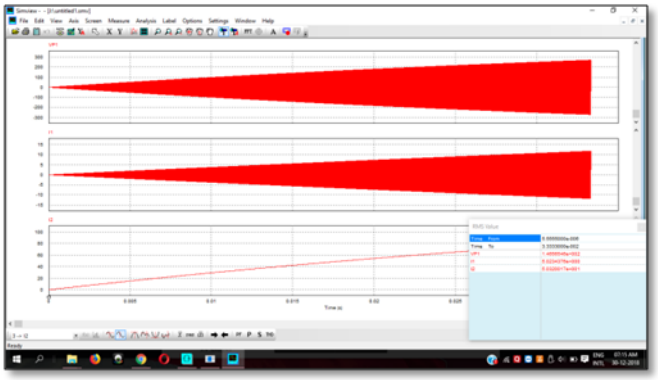

Fig.14: Output current of the proposed induction coking system at 30 KHz.

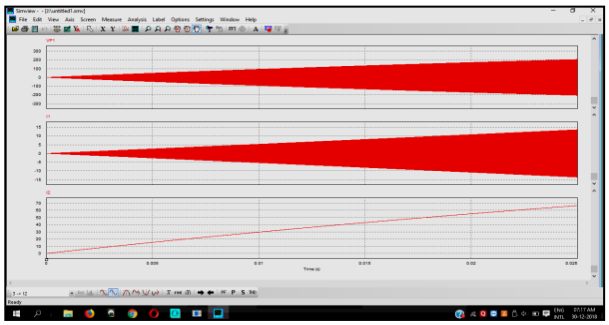

Fig.15: Output current of the proposed induction coking system at 45KHz

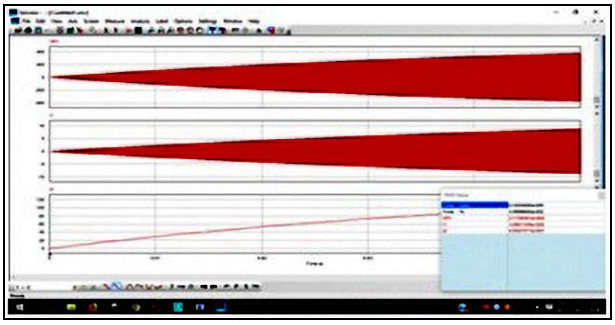

Fig.16: Output current of the proposed induction coking system at 65KHz

Fig 17: Experimental set up of induction coking system.

c. Analysis

TABLE 9 here shows the input the output voltage and the power of the induction heater at three respective frequencies ranges namely 30 KHz, 45 KHz and 65 KHz. The percentages of efficiency achieved are 91.42%, 80.96% and 67.12% respectively. It is observed that there is a sharp drop in the efficiency when it is compared to operation at 30 KHz (91.42%) with the power level two (80.96%). In spite of having this level of efficiency which is somewhat less than the efficiency at 30 KHz, it is still considered one of the best and superior methods to most other cooking methods that are prevalent. The commercial domestic induction cook-top is mostly most used in a domestic setting or at least used for the longest period at the "simmer" power level and the efficiency found at this frequency is 67.12 % (65KHz). TABLE 10 shows the specifications of low voltage solar induction cooker installed in our proposed project.

TABLE 9 Output Voltage and Power at Different Frequency.

Load	V_{rms} in Volts	I_{rms}	Power in Watts	Position of Auto Switch	Types of Supply System
Power Supplied for load 1	24	10.02	240.5	1	Solar Panel
Output power for load 1	23	9.36	215.2	1	Solar Panel
Power Supplied for load 2	23.7	6.34	150.33	1	Solar Panel
Output power for load 2	15.2	8.26	125.7	1	Solar Panel
Power Supplied for load 3	23	3.28	75.4	1	Solar Panel
Output power for load 3	10.3	4.16	43.2	1	Solar Panel
Power Supplied for load 1	24.1	9.97	240.5	0	A.C. mains
Output power for load 1	23	9.43	217	0	A.C. mains

TABLE 10 SPECIFICATION OF SOLAR INDUCTION COOKER

SN	Descriptions	Rating of Low Voltage Induction Tabletop
1.	Construction	Heat resistant ceramic top with SCHOTT glass 600.
2.	Supply system	Single phase, 24V DC supply.
3.	Operating frequency, wattage	45-100 KHz PWM, 1200W
4.	Input current for cook top	9.0 - 10 Amps
5.	Efficiency	>92 %
6.	Temperature Min./Max.	50 /300^{0}C
7.	Working temperature	12-45^{0}C
8.	Noise Level	Less than 45 dB
9.	Temperature control	Thermostat control
10.	Overheating cut-off	Temperature Relay
11.	Cooling System	Axial fan forced air-cooling
12.	Different Protections	Over current / Over voltage
13.	Switching	Zero voltage switching

X. LIFE CYCLE ECONOMIC ANALYSIS (LCEA)

Now with every design of the induction heater, the impact comes directly to the economical cost of the heater. So, with the change in design, economic analysis will also change. The various impacts that affect the economic analysis are discussed in article X.

Life Cycle Economic Analysis (LCEA)is said to be the total calculation of the money that is being spent on a service delivered during the entire life span of a project. Life cycle cost (LCC) analysis is a tool used in statistics which helps assign values to expenses, initial as well as to possible future expenses which provides a cost approximation.

A. Effective present value (EPV)

The life cycle analysis makes us aware of the functionality of the instrument. It helps us to estimate the additional price needed for the instrument in the long run.

B. Net system cost

The total cost of the system of an induction stove incorporates three components related to three different phases considered in analysis of life cycle economic such as Initial capital cost, recurring or regular costs, and replacement or non-recurring costs.

C. Economic criteria

It mainly depends on the life cycle of induction stove under consideration. The economic criteria depend on the availability of raw material in the local market as it reduces the over-all cost of the induction stove.

XI. COMPARATIVE STUDY BETWEEN SOLAR INDUCTION STOVE AND NORMAL INDUCTION STOVE, BOTH OF CAPACITY 1200W.

In this comparative study we are studying the amount of wattage consumption done by 1200W in the duration of 2 hours or 120 min. In the analysis below, we see how much wattage and time is used up when cooking a particular item.

A. Mathematical Analysis.

Normal Induction Stove (with respect to time and wattage).

It is known that an induction stove has the function of changing the wattage requirement according to the type of food which is being cooked. So, let us take a case study for cooking various types of food items for 2-hour (120 min). TABLE 11 shows the normal ac powered induction cooker with different wattage for various type of cooking food.

TABLE 11 Normal Induction Cooker with different Wattage for different Food.

Food being cooked	Wattage required for different types of food (approx)	Time required for cooking in minutes (approx)	Electrical Energy (E) In Wh
Rice	500	30	$E_1 = 250$
Meat	750	40	$E_2 = 500$
Tea	300	10	$E_3 = 50$
Other Item	600	40	$E_4 = 400$

Case Study I.

Total electrical energy required per day, = $(E_1 + E_2 + E_3 + E_4)$ = 1200Wh =1.2KWh ……..(15)

Per Unit cost of electricity = Rs 6.55/-(approximately).

Per day electricity cost of induction stove = Rs7.86/-

Per year electricity cost of induction stove = Rs 2829.60/-Total Electricity cost for 5 years, C_1 = Rs14,184/-.

Replacement or non-recurring costs in 5 years, C_2 = Rs 1000/-(approximately). Initial capital cost for induction stove in Indian market, C_3= Rs 2500/-(approximately).

Total expanses after 5 years,$C_4 = (C_1 + C_2 + C_3)$ ….....(16)

= Rs 17,648 ≈Rs 17,700/-(approximately).

B. Solar Induction Stove (with respect to time and wattage).

So, let us take a case study for cooking various type of food items for two hours (120 min) = 2 hours. TABLE 12 gives the results of a low voltage solar powered induction cooker for the same types of cooking food.

Case Study II.

TABLE 12 A Solar Induction Cooker with Different Wattage for Different Food.

Food being cooked	Wattage required for different types of food (approx.)	Time required for cooking in minutes(approx)
Rice	550	35
Meat	800	40
Tea	350	10
Other item	600	35

Total electrical energy required per day = (320.83 + 533.33 + 58.33 + 350) Wh = 1262.49Wh ≈ 1.26KWh.

Per Unit cost of electricity = Rs 0 (as we are generating our own energy we are not buying from a 3rd party). Per day cost of electricity for induction stove = Rs 0.Per month cost of electricity for induction stove =Rs 0. Per year cost of electricity for induction stove = Rs0.Total electricity cost for 5 years, C_5 = Rs 0

Replacement or non-recurring costs in 5 years, C_6 = Rs 5000/-(Approximately).Initial capital cost for induction stove in Indian market, C_7 = Rs 2500/-.

Therefore, total expanses after 5 years,

C_8 = Rs (C_5+ C_6+ C_7 + C_{11}) = Rs 84,400/- ……(17)

Government giving subsidy 30%, C_9 = C_8×0.3…….(18)

=Rs 25,320/-.

Total investment cost, C_{10}= (C_8 – C_9) = Rs 59,080/- ..(19)

C. Considering Without Government subsidy.

Breakeven point, B_2 = B_1 = C8/C4 ≈ 4.8 years…..(21)

The total installation cost of the proposed project is shown in TABLE 13.

TABLE 13 Installation item cost of the proposed project

Item Used	Makers Name	Quantity	Price Range (Rs)
Solar Panel 300W, 24V D.C	Kenbrook Solar	1	13,500
Float Cum Boost Battery Charger.	Sai-Tech. Engineers	1	10,000
A.C To D.C Converter	Powertek Energy System	1	10,000
D.C To D.C Converter	LM259C D.C To D.C Boost Converter	1	200
Exide Battery 150AH	Exide Insta Brite Battery	4	10,800 × 4 = 43,200

Therefore, the total cost = C_{11} =Rs 76900/-

D. Net Present Value (NPV)

NPV determinate the current rates of investment taking into account the changes in the value of capital over time. Universally recognized principles of assessing the profitability of investment projects determine that the investment is profitable when NPV is higher or equal to zero. TABLE 14 shows the year Vs cash flow study.

$$NPV = \sum_{i}^{n} \frac{\text{nCFt}}{(1+\text{r})^{\text{t}}} \quad \ldots\ldots\ldots\ldots(22)$$

Where, CFt= balance of cash flow in period t; n = duration of project; r = discount rate; t = time unit.

TABLE 14 Year Vs Cash Flow study

Years No.	Cash Flow in Rs	Years No	Cash Flow in Rs
0	59,080	3	17,700
1	17,700	4	20,000
2	17,700	5	20,000

NPV =1,04,200.656 – 59,080 = Rs 45,120.656/-.

E. Internal Rate of Return (IRR)

It is the discount rate which makes the net present value(NPV) equal to zero the discount rate will equate the present value of future cash flowing with initial investment.

$$Here\ , Invesment = \sum_{i}^{n} \frac{\text{nCFt}}{(1+\text{r})^{\text{t}}} \quad \ldots\ldots\ldots\ldots..(23)$$

Let us assume r = 20% = 1.20

Investment= Rs 60,320.327/-.

In 20%, IRR is higher than the investment with a difference of 60,320.327 - 59,080 = Rs 1240.33/-.

Let assume r = 19% = 1.19, Investment = 58,904.67/-

In 19%, IRR is lower than the investment with a difference of (59,080 – 58,904.877) = Rs175.123/-.

To find the value follow the steps.

Step 1: find the closest value of

20% = Rs 1240.327/-; 19% = Rs 175.123/-

Step 2: find the sum of both the closest value:

1240.327 + 175.123 = Rs 1415.45/-

Step 3: calculate the ratio of smallest discount rate:

$$\frac{175.123}{1415.45} = 0.123$$

Step 4: add the value obtained in step 3 to the smallest discount rate: 19 + 0.123 = 19.123%

So IRR is 19.123%

F. Advantage of the proposed design.

- It also uses less energy and cooking is faster than normal stovetop cooking.
- Reduction of manufacturing cost due to elimination of various element.
- Induction heater can also be used when there is an unavailability of a.c. source.
- This design is environment friendly.
- Design has been simplified.
- Design has been done for d.c supply.
- The battery is partially charged by solar power and rest of the charge is done by grid power.
- No electromagnetic wave radiation, suitable for pregnant women, old people and children to use etc

TABLE 15 shows the comparison of dc supply induction cooker Vs a.c supplied induction heater.

TABLE 15 Comparison of D.C supplied induction heater vs A.C. Supplied induction heater

D.C supplied induction heater	A.C supplied induction heater
Manufacturing cost is relatively less as compared to a.c fed induction heater.	Manufacturing cost is more as compared to d.c supplied induction heater.
Environment friendly	Comparatively less environment friendly.
Battery is used for the supply of induction stove.	To use battery as supply d.c. has to be converted to a.c. for the supply
It can work even when there is power surge.	It cannot work when there is a power surge.

XII. BENEFIT OF SOCIAL LIFE WITH THE USE OF SOLAR INDUCTION COOKER

One of the direct benefits towards the social life when using the solar induction stove is that it helps to reduce the pollution which is being caused by the generation of energy. It is well known that the primary sources of energy are generated from non-renewable sources, which are the major contributors of pollution towards our environment. In order to counter the pollution caused by non-renewable resources it is proposed that we start the use of solar powered induction stove, because solar is a renewable source of energy it has no pollution effect towards the environment. With the use of renewable resources, we will not have to fear the depletion of such resources. With the use of solar powered stoves, we are one step closer to make our environment a better place to live in.

CONCLUSION

With the increase in demand for cooking gas day by day and the increase in fuel price, people are looking forward for alternatives. Fire wood/coal is no more an acceptable solution because of the various pollution issues. Induction based cooking system is pollution free and efficient but it consumes too much electrical energy which makes it less economical. People are looking forward to economical, efficient and pollution free options. This is how solar based induction cooking system finds its place. The solar energy is available in abundance for free of cost and over 90% of it has not been utilized. The design provides a standalone product, whereby the solar and the grid power helps in the charging of the battery. When comparing with the conventional heating systems, the solar induction system has various advantages over the former such as in terms of time. In this paper we have made a comparison with the use of solar panel power induction cooker with respect to induction cooker feed from main line.

REFERENCES

[1] Acero, J., Burdio, J. M., Barragán, L. A., Navarro, D., Alonso, R., Ramon, J.,Monterde, F., Hernandez, P., Llorente, S., Garde, I., 2010, Domestic Induction Appliances, IEEE Industry Applications Magazine, 16(2), pp.39–47.

[2] Acero, J., Carretero, C., Millan, I., Lucia,O., Alonso, R., Burdio, J. M., 2011, Analysis and Modeling of Planar Concentric Windings Forming Adaptable-Diameter Burners for Induction Heating Appliances, IEEE Transactions on Power Electronics, 26(5), pp. 1546–1558.

[3] [3] Ahmed, N.A., 2011, High-Frequency Soft- Switching A.C Conversion Circuit With DualMode PWM/PDM Control Strategy forHigh-Power IH Applications, IEEE Transactions on Industrial Electronics, 58(4), pp. 1440–1448.

[4] [4] Aiello, G., Alfonzetti, S., 2002, Finite element computation of axisymmetric eddy currents in an infinite domain, Compel: International journal for computation and mathematics in electrical and electronic engineering, 19(2),pp.167–172.

[5] Aiello, G., Alfonzetti, S., Borzi, G., Dilettoso, E., Salerno, N., 2007, Comparing FEM-BEM and FEM-DBCI for open-boundary electrostatic field problems, The European Physical Journal Applied Physics, 39(2), pp.143–148.

[6] Aiello, G., Alfonzetti, S., Dilettoso, E., 2003, Finite-element solution of eddy current problems in unbounded domains by means of the hybrid FEM-DBCI method, IEEE Transactions on Magnetics, 39(3), pp.1409–1412.

[7] Andree, W., Schulze, D., Wang, Z., 1994, 3D eddy current computation in the transverse flux induction heating equipment, IEEE Transactions on Magnetics,30(5), pp. 3072 –3075.

[8] Andreu, J., De Diego, J. M., de Alegria, I. M., Kortabarria, I., Martin, J. L., Ceballos, S., 2008, New Protection Circuit for High-Speed Switching and Start-Up of a Practical Matrix Converter, IEEE Transactions on Industrial Electronics, 55(8), pp.3100–3114.

[9] Armor, A. F., 1981, 1981 Power Engineering Society Prize Paper Transient, Three- Dimensional, Finite-Element Analysis of Heat Flow in Turbine- Generator Rotors, IEEE Power Engineering Review, PER-1(9), pp. 11 –23.

[10] Aroudi, A. El., Rodriguez, E., Leyva, R., Alarcón, E., 2010, A Design-Oriented Combined Approach for Bifurcation Prediction in Switched-Mode Power Converters, IEEE Transactions on Circuits and Systems II: Express Briefs, 57 (3), pp. 218–22.

[11] M. Barak, “Electrochemical Power Sources–Primary & Secondary Batteries Institution of Electrical Engineers, London, 1980.ISBN 0- 906048-26-5.

[12] Aroudi, A. El., Rodriguez, E., Leyva, R., Alarcón, E., 2010, A Design-Oriented Combined Approach for Bifurcation Prediction in Switched-Mode Power Converters, IEEE Transactions on Circuits and Systems II: Express Briefs, 57 (3), pp. 218–22.

[13] A. Navarro, D. Burdio, J. M., 2009, P Power Measurement by Output-Current Integration in Series Resonant Inverters, IEEE Transactions on6(2), pp.559–567.

[14] S. Dhar, P.K. Sadhu, D. Roy, S. das, 2020, Feasibility Study of the Solar Powered and Induction Cooking Based Mobile Food Court Station in Rural Area of West Bengal, J. Inst. Eng. India Ser. B, DOI 10.1007/s40031-020- 00444-x,Springer.

Failure analysis and cost analysis of C.I. Flange Coupling

Sujit Kumar Garai
Department of Mechanical Engineering
Technique Polytechnic Institute
Chinsurah, India
garaisks@gmail.com

Anupam Barik
Department of Mechanical Engineering
Technique Polytechnic Institute
Chinsurah, India
anupamsantu@gmail.com

Sujay Biswas
Department of Mechanical Engineering
Technique Polytechnic Institute
Chinsurah, India
biswas23.2009@gmail.com

Abhijit Hazra
Department of Mechanical Engineering
Technique Polytechnic Institute
Chinsurah, India
abhijit8944024230@gmail.com

Rohit Jana
Department of Mechanical Engineering
Technique Polytechnic Institute
Chinsurah, India
rohitjana910@gmail.com

***Abstract*— A Coupling is a device which transmits power between two shafts rotating at designed speed. It is the important part of any power transmission system and may continue long time if design and cost analysis is maintained properly and the product can be chosen by the users. The present study of this paper is to reduce the cost of production by selecting proper designing process. The stress analysis that acting on the bolts, keys, hub and flange by making it uniform strengthens. The stress in the threaded part of the bolt will be higher than that in the shank. Hence a greater portion of the bolt will be absorbed at the region of the threaded part which may fracture the threaded portion because of its small length. An axial hole is drilled at the centre of the bolt through the head as far as thread portion such that the stress in the bolt is uniformly distributed along the length of the bolt. This consideration may also be taken in designing hub and flange. A special care should be taken during operation of key way in the hub portion to avoid stress concentration in keys and hub. In this paper there are explanation of detailed designing process for effective cost analysis.**

Keywords*— *Shearing, Crushing, Uniform Strength, Cost analysis.

INTRODUCTION

A coupling is a device that serves to connect the ends of adjacent shafts which are co-axial or non-co-axial. Couplings are basically of two types: 1. Rigid couplings 2. Flexible couplings. Rigid coupling is also classified into - Sleeve or muff coupling, Clamp or split-muff or compression coupling and Flange coupling. Similarly Flexible coupling also classified as - Bushed pin type coupling, Universal coupling and Oldham coupling. The strength of coupling mainly depends on designing process consider, material and workmanship. The cost of coupling is also main considerable factor in the competitive market. In this paper the designing and cost calculations are explained in details.

Objectives of shaft couplings used in machinery are -

- To provide for the connection of shafts of units that are manufactured separately such as a motor and generator and to provide for disconnection for repairs or alternations.
- To provide for misalignment of the shafts or to introduce mechanical flexibility.
- To reduce the transmission of shock loads from one shaft to another.
- To introduce protection against overloads.
- It should have no projecting parts.

Rigid couplings are used when precise shaft alignment is required; any shaft misalignment will affect the coupling's performance as well as its life span, because rigid couplings do not have the ability to compensate for misalignment. Due to this, their application is limited, and they're typically used in applications involving vertical drivers. Requirements of good coupling are - Easy to connect or disconnect the coupling, this does allow some misalignment between the two adjacent shaft rotation axes, no projecting parts, goal should be to minimize the remaining misalignment in running operation so as to maximize power transmission and to maximize machine runtime. It is recommended to use manufacturer's alignment target values to set up the machine train to a defined non-zero alignment, due to the fact that later, when the machine is at operation temperature, the alignment condition is perfect.

DESIGN AND CALCULATIONS

Problem statement:
Design and cost estimation of a C.I. unprotective type flange coupling to transmit 15 kW at 900 r.p.m. from an electric motor to a compressor. The service factor may be assumed as 1.35. The permissible stresses are:
1) Shear stress for shaft, bolt & key = 40 Mpa
2) Crushing stress for bolt & key = 80 Mpa
3) Shear stress for cast iron = 8 Mpa

Input data for CI flange coupling –
1. Power – 15kW
2. RPM - 900
3. Shear stress for shaft, bolt and key =40Mpa
4. Crushing stress for bolt and key =80Mpa
5. Shear stress for cast iron =8Mpa
6. Service factor = 1.35

STEP - 1

Design of Shaft:

$P = \frac{2\pi N T_m x100}{60}$

$T_m = \frac{15x60x1000}{2x\pi x900} = 159.15$ N-m

$T_{max} = 1.35x159.15 = 215$ N-m

$\frac{\pi}{16} * d^3 * \tau = 215 * 10^3 \quad d = \sqrt[3]{\frac{16 \, x \, 215x \, 10^3}{\pi \, x \, 40}}$

=30.13 =35mm (according to market availability)

STEP - 2

Design of Hub:

Outer diameter of hub = D=70mm
Inner diameter of hub = d =35mm

Length of the hub = L =52.5mm

Maximum shear stress developed in the outmost layer of the Hub material = τ_h

Torque (T_{max}) = $\frac{\pi}{16}(\frac{D^4-d^4}{d})*\tau_h$

$\tau_h = \frac{16*215*103*70}{(704-354)*\pi}$

=3.40 Mpa

STEP - 3

Design of Key:

Width of the key = w = $\frac{d}{4} = \frac{35}{4}$ = 10mm

Thickness of key = t = $\frac{d}{6} = \frac{35}{6}$ = 8mm

Length of the key = l_k = 52.5mm

1. Consider shearing failure :

Shearing resisting area = $w*l_k$

$T_{max} = w*l_k*\tau*\frac{d}{2}$

$\tau = \frac{215*103*2}{10*52.5*35}$ = 23.40 Mpa

2. Consider Crushing Failure

Crushing Resisting Area

= t / 2 * l_k

$T_{max} = \frac{t}{2}*l_k*\sigma_c*\frac{d}{2}$

$\sigma_c = \frac{215*1000*4}{52.5*8*5}$ = 58MPa

STEP - 4

Design of Flange:

t_f=17.5mm

Consider shearing failure at the junction of Hub.

Shearing resisting area = $\pi*d*t_f$

$T_{max} = \pi*d*t_f*\tau*\frac{d}{2}$

$\tau_H = \frac{215*1000*2}{\pi*35*17.5*35}$ = 6.38 MPa.

STEP - 5

Design of bolt:

No. of bolt (n) = 4 / 150 * d * 3 4 / 150 * 35 + 3 10^3

= 3.93 ≈ 4

$T_{max} = \frac{\pi}{4}*d_b{}^2*4*\tau*\frac{D1}{2}$

$d_b = \sqrt{\frac{215*8*10^3}{\pi*4*40*105}}$

= 5.70 mm

= 8 mm (according to market availability)

Material Cost of Flange & Hub:

Total volume of flanges and hubs

$= [\frac{\pi}{4}\{(70^2 - 35^2)*52.5 + (140^2 - 70^2)*17.5\}]$

= 3.53x10^5 mm^3

For two flanges and hubs

= 3.53*10^5*2

= 7.06*10^5 mm^3

Density of CI = 7.8gm/cc

Weight of two flanges and hubs

= 7.06*10^5/10^3*7.8/1000

= 5.5 kg

One kg of cast iron price is Rs. 78

Then, 5.5 kg of cast iron price is = 5.5*78

= Rs.430/-

Material Cost of Bolts:

Volume of hexagonal bolt = 2.59*$(8)^2$*8, (where, a = 8)

= 1.32 *10^3 mm^3

Length of the bolt = (17.5+17.5) +8

= 43 ≈ 50mm

Volume of 4 bolts = 4*(1.32*10^3 + 2.51*10^3)

= 15320 mm^3

Total weight of bolts = 15320/1000*7.85/1000

= 0.120kg

Material cost for bolts = 50*0.120

Where, 1kg = Rs.50

= Rs.6/-

Material Cost of Key:

Volume of the key = 10*8*60

= 4800 mm^3

For two keys,

Volume = 4800*2 = 9600 mm^3

Weight of the key = 9600/1000*7.85/1000

= 0.075kg

Cost of the key = 50 * 0.075

= 4/- [Where, 1kg = Rs.50]

So, total material cost for flange coupling = 430+6+4

= Rs.440/-

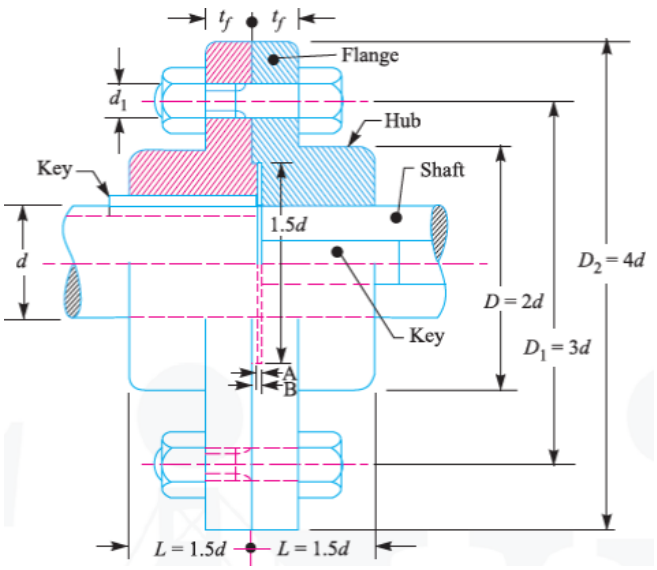

FIGURE I.SECTIONAL VIEW OF FLANGED COUPLING

TABLE I. DETAILS OF STRESS & COST ANALYSIS

Stress and Material cost summary				
Sl. No.	**Component & materials**	**Input stress in MPa**	**Designed stress in MPa**	**Cost per unit (Rs.)**
1	Shaft M.S.	Shear stress 40	Shear stress 25.54	
2	Hub C.I.	Shear stress 8	Shear stress 3.40	430/-
3	Flange C.I.	Shear stress 8	Shear stress 6.38	
4	Bolt M.S.	Shear stress 40	Shear stress 20.37	4 * 1.5/-
5	Key	Shear stress 40	Shear stress 23.40	4/-
	M.S.	Crushing stress 80	Crushing stress 58	
Total Cost				**440/-**

CONCLUSION

From the design calculations of flange coupling it is concluded that all dimensions of different parts of coupling are safe to transmit input power. The cost of the coupling is reasonable in competitive market. For future work, in the analysis process computerized fuzzy logic techniques will be utilized to reduce the error of design calculation and cost calculation.

REFERENCES

[1] Design and stress-Analysis of a Rigid Flange Coupling using FEM by Saurav Rajgadia Vol. 4, Issue 10, October 2015 ISSN(Online) :2319-8753

[2] https://en.wikipedia.org/wiki/Coupling

[3] V.B. Bhandari, Design of Machine Elements, ISBN: 0-07-0681791-1 (978-0-07-068179-8)

[4] Machine design by R.S.Khurmi, ISBN:978-81-219-2537-2

[5] Design and stress-Analysis of a Rigid Flange Coupling using FEM by Saurav Rajgadia Vol. 4, Issue 10, October 2015, ISSN(Online) :2319-8753

[6] Rujuta M. Nakhale and G. K. Gattani "Design and Analysis of Coupling using ANSYS". (IJPRET),2015; Volume 3 (9): 202- 206, ISSN: 2319-507X(IJPRET)

[7] Kondru Nagendra Babu and Dr. D Sunnel"Failure analysis of flange coupling with twodifferent materials". (IJERT), Vol. 4 Issue 04, April-2015, ISSN: 2278-0181

[8] Shivaji G. Chavan "Stress analysis of flangedjoint using finite element method". (IJSR), Volume 3Issue 8, August 2014, ISSN (Online): 2319-7064

[9] Rujuta M. Nakhale and G. K. Gattani "Designand Analysis of Coupling using ANSYS". (IJPRET), 2015; Volume 3 (9): 202- 206, ISSN: 2319-507X (IJPRET)

[10] Chandra Sekhar Katta, Kamana Srinivasa Rao , Design and Analysis of flange coupling , International Journal of Professional Engineering Studies Volume VI /Issue 4 / AUG 2016

[11] Maram Venkata Sunil Reddy, C. Raghunatha Reddy, Design and Analysis of Universal Coupling Joint, International Journal of Engineering Science and Computing, December 2016

[12] Mr. S.B. Jaiswal, Prof. M.D. Pasarkar, Failure Analysis of Flange Coupling in Industry, International Journal of Emerging Technology and Advanced Engineering , Websites- www.ijetae.com (ISSN 2250-2459, Volume 2, Issue 5 May, 2012).

Entropy Generation in Human Respiration System: a Review Paper

Abhijit Hazra
Department of Mechanical Engineering
Technique Polytechnic Institute
Chinsurah, India
abhijit8944024230@gmail.com

Sujay Biswas
Department of Mechanical Engineering
Technique Polytechnic Institute
Chinsurah, India
biswas23.2009@gmail.com

Sujit Kumar Garai
Department of Mechanical Engineering
Technique Polytechnic Institute
Chinsurah, India
garaisks@gmail.com

Anupam Barik
Department of Mechanical Engineering
Technique Polytechnic Institute
Chinsurah, India
anupamsantu@gmail.com

***Abstract*— The irreversible processes involve heat and result in entropy generation, which tends to accumulate within the system. For example, friction heats up and slows down moving parts. The analysis of a number of natural processes can be facilitated by assuming that they are in fact reversible. These processes are called quasi-reversible.**

The respiratory system consists of two lungs, right and left, situated in the thorax and connected via their primary bronchi to the trachea and upper airway of the nose and mouth, The bronchi, or more generally the airways, then form a branching network which, for the most part, is a sequence of bifurcations. Each level of branching is called a generation, starting with the trachea as generation n=0, the primary bronchi, generation n=1, and so on. For a perfectly bifurcating system, there will be 2n airway tubes at generation n. For 0⩽n⩽16, the airways only conduct the gas flow in and out, they do not have any specializes apparatus for exchange of oxygen and carbon dioxide between air and blood. It is the conducting zone. For 17 ⩽n⩽19, there start to appear small air sacs, alveoli, on the airway walls. Alveoli are thin-walled and compliant with a rich capillary blood supply and are designed for gas exchange. These special airways are the respiratory bronchioles.

Keywords*— *quasi-reversible, bifurcations, entropy generation, viscoelasticity.

I. INTRODUCTION

The lungs main function is to help oxygen from the air we breathe that enters the red cells in the blood. Red blood cells then carry oxygen around the body to be used in the cells found in our body. The lungs also help the body to get rid of co2 gas when we breathe out. The lungs are like bellows: as they expand, air is suck in and, as they compress, co2 waste is pushed back out. The energy expand on breathing is used primarily in stretching the lung –chest system and thus causing air flow is normally amounts to one percent of the basal energy requirements of the body but rises substantially during exercise or illness. The respiratory pump is versatile, capable of increasing its output 25 times, from the normal resting level of about 6 litres (366 cubic inches) per minute to 150 litres per minutes in adults. Pressures within the lungs can be raised to 130 cm of water (about 1.8 pound per square inch).

Human breathes to get oxygen to their cells so that they can use oxygen to make cellular energy (ATP). Cells do this by completely breaking down glucose (sugar) into co2 and water. When human breathe in or inhale, their diaphragm contacts (tightens) and moves downward. This increases the space in your chest cavity, into which their lungs explain. The intercostals muscles between their ribs also help enlarge the chest cavity. The contract to pull their rib cage both upward and outward when they inhale.

A reversible process is defined as a process that can be reversed without leaving any trace on its surroundings. That implies that both system and surroundings are returned to their initial states at the end of the process. In some respects, the cardiac cycle might be considered a quasi-reversible process; in fact, myocytes turn chemical energy into mechanical energy, which is subsequently transformed into heat, but at the end of each cardiac cycle the heart tends to return to the initial volume and pressure conditions. However, part of the potential energy that is stored in chemical bonds ends up in less organized forms of energy that contribute to the entropy generation within the system. The possibility of minimizing the entropy production makes the heart move towards a quasi-reversible condition. In some respect, the cycles of the heart may be referred to as the coupled cycles that actually appear in dissipative structures arising in systems maintained far from thermodynamic equilibrium by energy flow.

A thermodynamic quantity representing the unavailability of a system thermal energy for conversion into mechanical work, often interpreted as the degree of disorder or randomness in the system. Entropy the measure of a system's thermal energy per unit temperature that is unavailable for doing useful work. Because work is obtained from ordered molecular motion, the amount of entropy is also a measure of the molecular disorder, or randomness of a system. The concept of entropy provides deep insight into the direction of spontaneous change for many every day phenomena. The static properties of the lungs have been explained by energy change considerations on the elasticity, but this article explains the elasticity if the lungs by entropy-change considerations.

It is the intention of the current work to use Computational Fluid Dynamics (CFD) to demonstrate and quantify the influence of asymmetry and bifurcation geometry on the pressure losses in branching airways, while recognizing that the ultimate flow distribution is largely determined by the particular placement of the bifurcation in the complex network of airways within the lung.

. For example, the flow distribution is often much more influenced by downstream lung volume or heterogeneous lung compliance than the asymmetry of a particular branch. Thus, a parametric analysis is performed where the morphologies and flow conditions are varied independently.

II. LITEARATURE REVIEW

Bejanet. al. [1] developed an analytical and graphical formulation of the constructed law of maximization of flow access in systems with heat and fluid flow irreversibility's and freedom to change configuration. The flow was assumed point to volume and point to area of the system. They have presented the contractual law in the graphical form and generation of new structure.

Dendrites flow structures dominate the design of natural and engineered flow systems, especially in thermal and fluid systems. The starting point is the optimization of the shape of each elemental area or volume, such that the length of the flow path housed by the element is minimized. Proceeding toward larger and more complex structures – from el flow structure developed in the nature Lorentz et al. [2]

David et.al. [3] stated that The effect of lung morphology on the heterogeneity of regional ventilation and particle deposition in the bronchial airways is studied using Herzfeld's regular-asymmetric lung model. Flow distribution among the airways is calculated by solving the whole tree network, assuming laminar flow hydrodynamic resistances without accounting for gravitationally enhanced preferential air flow distribution. It is shown that the fractal dimensions that characterize the morphological properties and the physiological processes are similar, suggesting that all are related and stem from a common underlying attribute—the lung morphology. The variation of particle deposition in the lung, as well as the variation of ventilation and morphological attributes, increases moderately with the lung tree asymmetry.

The contribution introduces an airway scaling procedure, which assumes (a) a fractal anatomy of the human lung and (b) a generation-related variability of bronchial morph metry in a chaotic fashion. Basic scaling of the branching system was conducted by application of an inverse power-law including the fractional dimension of the anatomic object. Simulation of intra subject diversity of the measurements, on the other side, was realized by using a normalized and repeatedly corrected variant of the logistic equation primarily introduced by Verhulst. Two morph metric data sets were theoretically approximated with the help of the scaling procedure, thereby assuming a morph metric diversity covered by a 60%-range – from American association for science & technology Robert et.al.[4]

Liua et.al. [5] developed the inspiratory flow characteristics in a three-generation lung airway have been numerically investigated using a control volume method to solve the fully three-dimensional laminar Navier–Stokes equations. The three-generation airway is extracted from the fifth to seventh branches of the model of Weibel with in-plane and 901 off-plane configurations. Computations are carried out in the Reynolds number range of 200–1600, corresponding to mouth-air breathing rates ranging from 0.27 to 2.16 l/s, or an average height of a man breathing from quiet to vigorous state. Particular attention is paid to establishing relations between the Reynolds number and the overall flow characteristics, including flow patterns and pressure drop. The numerically determined behaviour of $Re^{-0.61}$ assuming the airways to be approximated by two-dimensional channels.

Chang et.al. [6] analysed A thorough analysis of aerosol particle deposition in the human lung requires the knowledge of the distribution of inspired air at respiration. Ventilation distributions were determined under different gravitational force conditions. A larger gravity leads to a greater non uniformity of ventilation between the upper and lower lobes of the lung. When a different gas was inspired instead of air, a preferential distribution of ventilation to the upper lobes was found if the density of the inspired gas was greater than that of the air.

JILL et.al. [7] stated Although the lung is structurally complex, it is suitable for morphometric analysis of the structural determinants of lung function in health and disease. Analysis of the organized branching airways has been problematic because of the need to identify and classify airways before structural characteristics of different- order branches can be determined. Airway casts have been used to identify relationships between branches, measure some structural features, and develop mathematical models that describe simply the relationships between generations. We describe a new approach using tissue sections which combines the classification of airways into Strahler order (SO) with tissue structural analysis. Lung-tissue sections are prepared, and outer (OD) and inner (ID) diameters are determined over a wide range of airways. The line equation relating log OD vs. SO is determined using measured values for SO1 (terminal bronchioles) and SO8 (first branch bronchi). Mean ODs can then be calculated for each of the other SO groups, and measurements can be classified.

DONGYOUB et.al. [8] described a flexible mathematical model of an asymmetric bronchial airway bifurcation is presented. The bifurcation structure is automatically determined after the user specifies geometric parameters: radius of parent air-way, radii of daughter airways, radii of curvature of the daughter branchiopods, bifurcation angles, and radius of curvature of carina ridge. Detailed shape in the region where the three airways merge is defined by several explicit functions and can be changed with ease in accordance with observed lung structure

Alicia et.al. [9] stated Computational Fluid Dynamics simulations of inspiratory airflow in asymmetric bifurcations have been performed in order to determine the influence of the asymmetry and Reynolds number on pressure losses over a physiologically relevant range for pulmonary airways; thus, the results of this work can contribute to the understanding of respiratory ventilation in health and in disease. A key a priori insight to the design of the study is that the flow distribution in respiratory bifurcations can be largely independent of the local losses; and therefore, is predetermined by the boundary conditions in these calculations. The results, presented in the form of pressure loss coefficients, indicate that asymmetry and downstream conditions are significant for severe restrictions and laminar fowl; but are relatively insignificant for turbulent flow conditions and for flow through the healthy branch.

C. G. Caro et.al. [10] developed Swirling flow associated with non-planar arterial geometry encourages interest in

flowing larger human bronchial airways, where bifurcations are planar but consecutive bifurcation planes rotate by an angle (φ)of ca.90°. Steady 'inspiratory' flow has been investigated in a two-generation symmetrically bifurcating human bronchial airway model by studying reddening by acid vapour of a litmus-containing coating as an approximate indicator of relative local wall shear (Sw). The inlet tube Reynolds number (Reit) was 600 or 1800; the branching angle (θ) was 32.5° at first generation and 32.5° or 55° at second generation; φ was 0° or 90° between first and second generations; second-generation daughter tube volume flow rates were the same. Inspiratory flow in larger human bronchial airways is expected to be asymmetric and swirling, with implications for all transport processes including those of particles.

Min-Yeong et.al. [11] stated Characteristics of pressure loss (DP) in human lung airways were numerically investigated using a realistic model bifurcation. Flow equations were numerically solved for the steady inspiratory condition with the tube length, the branching angle and flow velocity being varied over a wide range. In general, the DP co-efficient K showed a power-law dependence on Reynolds number (Re) and length-to-diameter ratio with a different exponent for ReZ100 than for Reo100. The effect of different branching angles on pressure loss was very weak in the smooth- branching airways.

Bahmanet.al. [12] analyzed practical deposition in symmetric bifurcation airways due to inertial impaction was studied numerically for inspiratory flows. Three-dimensional bifurcation models were constructed. The models had different parent and daughter diameters comparable to the airway generation 3-6 of the human lung. Airflow fields in the models were obtained by a finite-element method for different Reynolds number under parabolic and uniform inlet velocity conditions. The calculated flow filed data were used to simulate particle deposition. Based on calculated deposition results, empirical equations were derived for particle deposition efficiency as a function of non-dimensional parameters of stokes number, Reynolds number, and bifurcation angle for a parabolic or a uniform flow.

P. Nithiarasu et.al. [13] states Air flow through a human upper airway has been carried out using a realistic geometry. In addition to explaining the anatomy, problems and importance of patient-specific study of human upper airways, this article also presents some qualitative and quantitative simulation results, As expected, the shear pressure forces are large in or pharynx and laryngopharynx, where the flow passage is narrow. This clearly indicates that these locations should be the focus of any study aimed at understanding the human upper airway collapse in a patient- specific manner.

Srivastava et.al. [14] work on the steady motion of incompressible fluid through a curved tube of circular cross-section is extended. A method using Fourier-series development with respect to the polar angle in the plane of cross-section is formulated and the resulting coupled non-linear equations solved numerically. This theory fill a large part of the gap in existing knowledge of secondary flow patterns, which lies in the upper range of Reynolds number for which flow is laminar. This range is of particular interest in the investigation of the cardiovascular system.

Andrew et.al. [15] states two-phase flow through a rigid curved tube in which a fluid core is surrounded by a film of a second, immiscible fluid, surface tension drives the system towards a configuration in which the film thickness tends to zero on the inner wall of the bend. In the present work he demonstrates that the presence of steady states in which the film thickness remains finite. Analysis of the bifurcation model reveals that the bifurcation structure arises from a perturbation of the translation degeneracy of the interface in a straight tube.

III. EXPERIMENTAL DETAILS

The airflow through the lungs is governed by the Navier- Stokes equation, and the flow in any airway can be characterized by the non-dimensional Reynolds number, (Re)

$$R_e = \frac{\rho V D}{\mu} \qquad \text{..... (1)}$$

Where ρ and μ represent the air's density and viscosity, respectively; V is the mean velocity, and D is the diameter of the airway of interest. The air is assumed to have constant properties: density $\rho=1.225$ kg/m^3 and viscosity $\mu=1.7894\times10^{-5}$ kg/s m. In the current work, the reference Reynolds number is calculated using conditions at the inlet of the parent airway.

$$R_e = \frac{\rho V D}{\mu}$$
$$R_e = \frac{1.225\times7.69\times0.018}{(1.7894\times10^{-5})}$$
$$R_e = 9476.05343$$

Hence the flow is turbulent

Here f is a friction factor whose value depends on the flow regime and Reynolds number Re. For laminar, fully developed flow, f is analytically determined:

$$f = \frac{64}{R_e} \quad \text{when } R_e<2000 \text{----------} \quad (2)$$

For turbulent flow, f is calculated from the Blasiuscorrelation:

$$f = \frac{0.316}{R_e^{0.25}} \qquad When\ R_e \geq 2000 \text{----------} \quad (3)$$

Generation 1-4 Re is turbulent flow because where Re ≥ 2000

$$f = \frac{0.316}{9476.05343^{0.25}}$$
$$f = 0.03202803$$

Generation 5-23 is Laminar flow because where Re < 2000

$$f = \frac{16}{R_e}$$
$$f = \frac{16}{1883.29203} \text{----------} \quad (4)$$

$$f = 0.0084938$$

Values of K were computed for the reference geometry at various flow velocities and daughter lengths, and a best-fit correlation was sought versus Re and geometric parameter L/d_1. All computed K values for $L \leq 10d_1$ fit the following correlations excellently .

$$K \propto R_e^{-\frac{1}{2}} \left(\frac{L}{d_1}\right)^{\frac{1}{2}} \qquad Re \geq 100 \quad (5)$$

$$K \propto R_e^{-1} \left(\frac{L}{d_1}\right)^{3/4} \qquad Re < 100 \text{ ---------- (6)}$$

Our numerical results for the bifurcating tube show very weak dependence of K on branching angle. Also a best-fit correlation for K that considers Re, L/d and θ can be obtained as follows:

$$K \propto R_e^{-\frac{1}{2}} \left(\frac{L}{d_1}\right)^{\frac{1}{2}} \theta^{\frac{1}{20}} \quad \text{..... (7)}$$

This correlation is valid for a short bifurcating tube in laminar flow where Re ≥100, L ≤ 10d1 and d_1/d_0 =0.8.

Generation 1-11 $R_e \geq 100$ When $\theta = 70^0$

For, generation 1,

$$k = (9478.17216)^{-\frac{1}{2}}(6.66667)^{\frac{1}{2}}(70)^{\frac{1}{20}}$$
$$k = 0.03278012$$

Generation 12-23 $R_e < 100$ When $\theta = 70^0$

For generation 12,

$$k = (96.616825)^{-1}(4.58824)^{\frac{3}{4}}(70)^{\frac{1}{20}}$$
$$k = 0.040105134$$

Generation 1-11 $R_e \geq 100$ When $\theta = 90^0$

For generation 1,

$$k = (9478.17216)^{-\frac{1}{2}}(6.66667)^{\frac{1}{2}}(90)^{\frac{1}{20}}$$
$$k = 0.0331503$$

Generation 12-23 $R_e < 100$ When $\theta = 90^0$

For generation 12,

$$k = (96.616825)^{-1}(4.58824)^{\frac{3}{4}}(90)^{\frac{1}{20}}$$
$$k = 0.0406344$$

Generation 1-11 $R_e \geq 100$ When $\theta = 130^0$

For generation 1,

$$k = (9478.17216)^{-\frac{1}{2}}(6.66667)^{\frac{1}{2}}(130)^{\frac{1}{20}}$$
$$k = 0.03382771$$

Generation 12-23 $R_e < 100$ When $\theta = 130^0$

For generation 12,

$$k = (96.616825)^{-1}(4.58824)^{\frac{3}{4}}(130)^{\frac{1}{20}}$$
$$k = 0.0413884$$

Minor Loss Depended on angle

Generation 1-11 $R_e \geq 100$ When $\theta = 70^0$

$$k \times \left(\frac{v^2}{2g}\right) = 0.098801655$$

Generation 12-23 $R_e < 100$ When $\theta = 70^0$

$$k \times \left(\frac{v^2}{2g}\right) = 0.005632707$$

Generation 1-11 $R_e \geq 100$ When $\theta = 90^0$

$$k \times \left(\frac{v^2}{2g}\right) = 0.099917328$$

Generation 12-23 $R_e < 100$ When $\theta = 90^0$

$$k \times \left(\frac{v^2}{2g}\right) = 0.005707038$$

Generation 1-11 $R_e \geq 100$ When $\theta = 130^0$

$$k \times \left(\frac{v^2}{2g}\right) = 0.101959152$$

Generation 12-23 $R_e < 100$ When $\theta = 130^0$

$$k \times \left(\frac{v^2}{2g}\right) = 0.00581294$$

Frictional Loss :-

$\frac{4flv^2}{2gd}$ Where f=friction factor ---------- (8)

l= length in m. v=velocity in m/sec

d=diameter in m.

$$=\frac{4\times0.03202803\times0.12\times7.69^2}{2\times9.81\times0.018}$$

=2.574261345m

Total loss = Frictional loss + Minor loss

= 2.574261345 + 0.98801655

= 2.57117358m

Pressure Loss

From Bernoulli's equation,

$$\left(\frac{p_1}{\rho_g}\right) + \left(\frac{\alpha v_1^2}{2g}\right) - \left(\frac{p_2}{\rho g}\right) - \left(\frac{\alpha v_2^2}{2g}\right) = h_f$$

$$\frac{1}{\rho g}(p_1 - p_2) = h + \alpha\left(\frac{v_2^2 - v_1^2}{2g}\right)$$

$$\Delta p = \left(h_f + \alpha\left(\frac{v_2^2 - v_1^2}{2g}\right)\right)\rho g$$

$$\Delta p = \left(2.013151135 + \left(\frac{13.97^2 - 7.69^2}{9.81}\right)\right)1.225 \times 9.81$$

[α=1 for a blunt velocity profile]

$$\Delta p = 190.8229204\ kg/m^2$$

Entropy Generation We know that,

Entropy , $\Delta s = \frac{\Delta Q}{T}$ ---------(10)

$= \frac{vA\Delta p}{T}$

$= \frac{8.33\times0.0001169\times190.8229205}{309}$

=0.000601349 J/k

IV. RESULTS AND DISCUSSIONS

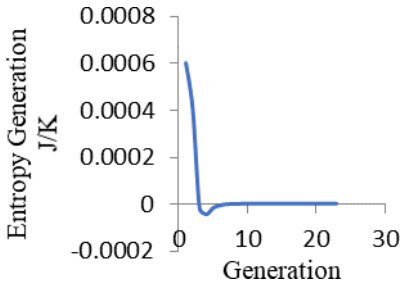

Figure 1 Entropy generation in each generation

The above graph says that the entropy of an isolated system during a process always increases, or in the limiting case of a reversible process remains constant (it never decreases). This is known as the increase of entropy principle. The entropy change of a system or its surroundings can be negative; but entropy generation cannot. But for an adiabatic reversible process the entropy generation is zero. A negative entropy means that "wasted" energy is transformed on work. Entropy remains constant in an adiabatic process which is also reversible. Now, since the process is adiabatic, so the heat transfer is zero and so the entropy change is zero through heat transfer. Here when generation slowly increases, entropy generation gradually decreases. At the stage of this process entropy generation is const. Entropy generation is caused by internal irreversibility thus depends on the nature of path followed during a process.

Total entropy change = Entropy change of reversible process executed in corresponding states + Entropy generation.

V. FUTURE SCOPE

A. Basis on diameters

In this paper we use same diameters of bifurcations. so, we calculate the losses of bifurcation only basis of single bifurcation. But here in future if we work on each & every diameter of bifurcation then we would see some difference in losses which are we actually get. This process will obviously help next generation.

B. Flow ability

A steady flow can be uniform or non-uniform and similarly an unsteady flow can also be uniform or non-uniform. Flow pattern in the airway lumen strongly depends on the geometry of bifurcation, so a realistic geometry model is needed to attain realistic flow fields. Here the flow is uninformed flow. If the flow is uniform then the process would change. In future may be research on this paper.

C. Vascularization

The current literature reveals a surge of interest in bioinspired designs of flow architectures that promise superior properties, for example, distributed and high-density heat and mass transfer. Chief among the new architectures that are being proposed are the tree-shaped (dendritic) designs. A significant stimulus for this new direction is the emergence of constructer theory as a means to explain biological and geophysical design, and as a method for developing new concepts for engineered flow architectures. This growing research activity was reviewed most recently in Refs. [1-3] and is not reviewed again here. Tree-shaped flow structures have multiple scales that are distributed nonuniformly through the flow space.

No equilibrium thermodynamics and maximum entropy production in the Earth system:

The Earth system is maintained in a unique state far from thermodynamic equilibrium, as, for instance, reflected in the high concentration of reactive oxygen in the atmosphere. Entropy production is a general consequence of these processes and measures their degree of irreversibility. The proposed principle of maximum entropy production (MEP) states that systems are driven to steady states in which they produce entropy at the maximum possible rate given the prevailing constraints. Entropy production allow human to quantify an objective direction of Earth system change When a maximum in entropy production is reached, MEP implies that the Earth system reacts to perturbations primarily with negative feedbacks. In conclusion, this no equilibrium thermodynamic view of the Earth system shows great promise to establish a holistic description of the Earth as one system.

Three-dimensional computer modelling of the human upper respiratory tract:

Computer simulations of airflow and particle-transport phenomena within the human respiratory system have

important applications to aerosol therapy and inhalation toxicology. A detailed description of airway morphology is necessary for these simulations to accurately reflect conditions in vivo. Therefore, a three-dimensional (3D) physiologically realistic computer model of the human upper-respiratory tract (URT) has been developed. The final unified 3D computer model may have significant applications to aerosol medicine and inhalation toxicology, and serve as a cornerstone for computer simulations of air flow and particle-transport processes in the human respiratory system.

Lifespan Entropy and Effect of Diet Composition and Caloric Restriction Diets:

The first and second laws of thermodynamic were applied to statistical databases on nutrition and human growth in order to estimate the entropy generation over the human lifespan. The calculations were performed for the cases of variation in the diet composition and calorie restriction diets; and results were compared to a base case in which lifespan entropy generation was found to be 11 404 kJ/K per kg of body mass, predicting a lifespan of 73.78 and 81.61 years for the average male and female individuals respectively. From the analysis of the results, it was found that changes of diet % of fat and carbohydrates do not have a significant impact on predicted lifespan, while the diet % of proteins have an important effect. Reduction of diet protein % to the minimum recommended in nutrition literature yields an average increase of 3.3 years on the predicted lifespan. Changes in the calorie content of the diet also have an important effect, yielding a % increase in lifespan equal or higher than the % reduction in the diet caloric content. This correlates well experimental data on small mammal and insects, in which lifespan has been increased by diet restriction.

Regenerative medicine for the respiratory system: Regenerative medicine (RM) is a new field of biomedical science that focuses on the regeneration of tissues and organs and the restoration of organ function. RM research regarding the respiratory system, including the trachea, the lung proper, and the diaphragm, has lagged behind. In this regard, this article briefly addresses the basics of RM and introduces the keyelements necessary for tissue regeneration, including (stem) cells, biomaterials, and extracellular matrices. In addition, the current status of the (clinical) application of RM to the respiratory system is discussed, and bottlenecks and recent approaches are identified.

Sequencing and Analysis of Globally Obtained Human Respiratory Syncytial Virus A and B Genomes:

Human respiratory syncytial virus (RSV) is the leading cause of respiratory tract infections in children globally, with nearly all children experiencing at least one infection by the age of genotyping, but relatively few whole genome sequences are available for RSV. The goal of our study was to sequence the genomes of RSV strains collected from multiple countries to two. Partial sequencing of the attachment glycoprotein gene is conducted routinely for further understand the global diversity of RSV at a whole-genome level.

VI. CONCLUSION

Pressure loss coefficients have been provided for asymmetric lung bifurcations over a physiological relevant range of incoming Reynolds number, the diameter ratio of parent to daughter, and the flow ratio. The flow ratio was prescribed to account for the fact that individual bifurcations are part of complex lung airway networks.

Pressure loss coefficients have been provided for asymmetric lung bifurcations over a physiological relevant range of incoming Reynolds number, the diameter ratio of parent to daughter, and the flow ratio. The flow ratio was prescribed to account for the fact that individual bifurcations are part of complex lung airway networks.

REFERENCES

[1] Bejan, A. and Lorente, S, "The constructal law and the thermodynamics of flow systems with configuration", Int. J. Heat and Mass Tranf., Vol. 47, pp. 3203-3214,

[2] S. Lorente, W. Wechastol , A. Bejan, "Tree-shaped flow structures designed by minimizing path lengths", Int. J. Heat and Mass Tranf., Vol.45, 2002, pp.3299-3312,

[3] David M. Broday , Yehuda Agnon, "Asymmetric human lung morphology induce particle deposition variation", Aerosol Science, Vol. 38,(2007), pp.701 – 718,

[4] Robert Sturm, " Chaotic Lung Airway Scaling Using Verhulst Dynamics", International Journal of Bioinformatics and Computational Biology , Vol. 2, No. 1, 2017, pp. 1-6,

[5] Y. Liua , R.M.C. Soa, C.H. Zhangb, "Modeling the bifurcating flow in a human lung airway" , Journal of Biomechanics, Vol. 35, 2002, pp. 465–473,

[6] Y. H. Chang, C. P. Yu, "A Model of Ventilation Distribution in the Human Lung" , DEPARTMENT OF MECHANICAL AND AEROSPACE ENGINEERING, STATE UNIVERSITY OF NEW YORK AT BUFFALO,AMHERST, NY 14260, 30 Nov 2010

[7] JILL LIPSETT," Analysis of the Conducting Airway System in the Lung : A New Method Combining Morphometry With Mathematical Modeling for Airway Classification" THE ANATOMICAL RECORD,Vol.266, 2002, pp.51–57,

[8] DONGYOUB LEE, SEONG S. PARK,GEORGE A. BAN-WEISS,MICHELLE V. FANUCCHI,CHARLES G.PLOPPER,AND ANTHONY S. WEXLER," Bifurcation Model for Characterization of Pulmonary Architecture", THE ANATOMICAL RECORD, Vol. 291, 2008, pp.379– 389,

[9] Alicia Clark, Jenn S Rossmann, Ira M Katz, Andrew R Martin and Georges Caillibotte "Pressure Loss Coefficients for Asymmetric Bifurcations of Pulmonary Airways with Predetermined Flow Distributions", J Bioengineer & Biomedical Sci 2015, 5:1

[10] C. G. Caro1, R. C. Schroter, N. Watkins1, S. J. Sherwi,

[11] V. Sauret "Steady inspiratory flow in planar and non-planar models of human bronchial airways", The Royal Society, Vol.458, 2002, pp. 791–809,

[12] Min-Yeong Kang , Jeongeun Hwang , Jin-Won Lee," Effect of geometric variations on pressure loss for a model bifurcation of the human lung airway", Journal of Biomechanics , Vol. 44, 2011, pp.1196-1199,

[13] Lei Zhang, BahmanAsgharian, Satishanjilvel, "Inertial Deposition of Particles in the Human Upper Airway Bifurcations", Aerosol Science and Technology, Vol. 26:2, 2007, pp. 97-110

[14] P. Nithiarsu, O. Hassan, K. Morgan, N. P. Wewatherill,

[15] C. Fielder, H. Whittet, P. Ebden, K. R. Lewis, "Steady flow through a realistic upper airway geometry", int. j. Numer . Meth. Fluids, Vol.57, 2008, pp.631-651,

[16] D. J. Mcconalogue, R. S. Srivastava ," Motion of a fluid in a curved tube", Proc. Roy. A. Vol.307, 1968, pp. 37- 53,

[17] Andrew L. Hazel, MatthaisHeil, Sarah L. Waters, James M. Oliver, " On the liquid lining in fluid-conveying curved tubes", J. Fluid Mech, Vol.705, 2012, pp. 213-323,

Threshold Based Dynamic Approach for the Isolation of the Version Number Attack in IoT

Mr. Debasish Hati
Department of Computer Science and Technology
Technique Polytechnic Institute
Hooghly,India
debasishhati2013@gmail.com

Mr. Sohan Goswami
Department of Computer Science and Technology
Technique Polytechnic Institute
Hooghly,India
sohangoswami@gmail.com

Ms. Soumali Roy
Department of Computer Science and Technology
Technique Polytechnic Institute
Hooghly,India
roysoumali21@gmail.com

***Abstract*— The Internet of Things is the self-configuring type of network in which various nodes can join or leave the network when they want. Due to such nature of the network, various malicious nodes can join or leave the network. The version number attack is the active type of attack which affects network performance. In this research work, technique of threshold is proposed for the detection and isolation of malicious nodes from the network. The proposed technique is implemented in network simulator version 2 and results are analyzed in terms of packet loss, delay and throughput.**

***Keywords*—Version number attack, DODAG, Threshold Technique**

I. Introduction

IoT (internet of things) can be defined as a technology that connects multiple sensors, smart nodes, and objects together for establishing communication among them without any manual intervention. The autonomous functioning of entities or things depends on the connectivity amid them. The nodes in IoT carry out different types of tasks. These tasks include analysis of gathered data for decision making, giving lightweight data and data extraction by getting the excess of the cloud-based resources. The connection between clients, services, sensors and objects is established extremely closely via IoT. There are various application fields that make use of IoTs in extensive manner. These application fields include smart grid healthcare, its (intelligent support system). IoT is highly beneficial from business prospective also as it provides large number of intelligent tools and services [1]. The connectedness of IoT devices on the cloud system is the main reason behind the development of cloud-based iot networks. This makes possible the transmission of data to serve different purposes. In particular, ip based web and iot applications provide transferring using tcp and udp. On the other hand, few commonly used message distribution functions occur amongst the majority of IoT applications. Different applications apply these tasks in interoperable standard manners. The designing of a publish/subscribe protocol framework, extremely analogous to the client/server protocol, is carried out. This is referred as MQTT (Message Queue Telemetry Transport). MQTT protocol becomes highly important because of its uncomplicated structure and capability to prevent the extreme use of CPU and memory. AMQP (Advanced Message Queuing Protocol) is the one more protocol developed for the financial industry. The main motive behind using TLS/SSL protocols is security management. The use of less power and memory embedded devices can be ensured by using CoAP for the communication purpose.

Up to now, several network layer protocols have been designed as well. Among these protocols, IEEE 802.15.4 is the most frequently used IoT standard for MAC protocol [7]. This protocol defines a frame set-up. In this set-up, the address of source and destination is defined in headers along with way through which node can interact with each other. In recent times, the implementation of Low power multi-hop networking is carried out in IoT due to its unsuitability of using frame formats implemented earlier in the conventional networks. They increase the system's overhead. In general, channel hoping and time synchronization are employed to ensure high consistency, inexpensiveness and to satisfy the communication requirements of internet of things. The IPv6 Routing Protocol is a standardized remote vector routing protocol. This protocol is specially designed for RPL network which is lossy and includes low energy. This protocol does not include any cycle, and therefore does not have loop. This occurs due to the way in devices are linked to each other. DODAG with the border routers avoids cycles. These routers are linked to the internet. All devices linked to DODAG are connected online via this border router. The protocol prevents loops when it measures the location of node corresponding to the root node [9]. This position regarding the root node is referred as the rank and the rank increases with the motion away from the border router. Messages from a child node which is going down are ignored to prevent loops. A node contains a parent, which transfers data from the nodes to the border router and may have various children. The node sends the children's packages to the border router.

- *Version Number Attack*

The root node makes use of version number to ensure that the global repair process of rpl is under control and updating of all the nodes existing in dodag is carried out based on their routing location. The occurrence of version number attacks in iot can decrease its service time. The intruder can launch this intrusion with extremely low overhead and the use of global repair scheme included as an immune system of protocol can overload the global repair scheme network. The root starts a global repair in the occurrence of numerous network irregularities. The vn (version number) of dodag is incremented to rebuild the entire dodag. DIO (Dodag Information Object) refers to the control message that carries this version number. Every receiving node compares the earlier version number and the one obtained from its parent. The existing rank information is overlooked, the trickle timers are reset and a novel process to join the DODAG is started in case of higher

received version. This global repair guarantees a loop free topology despite of its too much expensiveness. It is important to notice that the node did not transit to the novel dodag version if dio messages advertize its earlier version. It is essential for the other nodes to not choose such a node as preferred parent. Two versions of dodag may occur simultaneously during global repair. On the other hand, data packets existing in old version can migrate in fresh version to prevent loops. The earlier version is not regarded as dodag. Also, the accessibility of loop free topologies cannot be guaranteed as the network is still away from the convergence state.

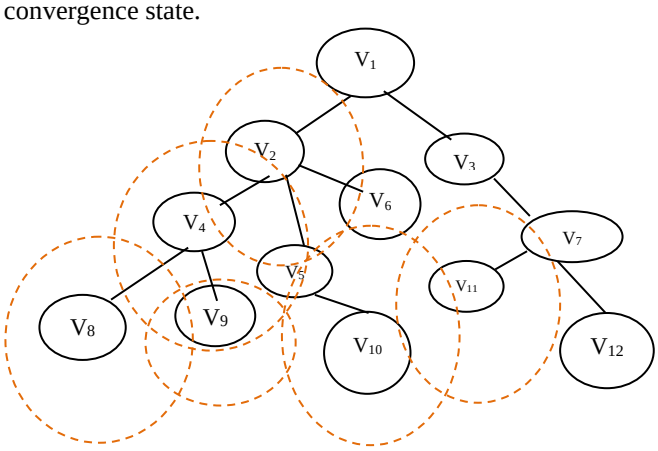

Figure 1: Illustration of a version number attack

In order to prevent any possible irregularities of the network, the version number must be transmitted unaltered across DODAG. RPL does not include ant method to ensure the reliability of version number occurring in the received DIO messages. An attempt made by the malicious node to change this value in its own DIO messages can cause harm to the network. If a malevolent DIO is received with a fresh version number, the trickle timer is reset, the version is updated and the fresh version is promoted to the neighbors by DIO messages. Figure 1 shows the propagation of the illegal version number via the network. In this situation, the genuine network nodes broadcast their increased version number started by malevolent node V_5 in the automatic manner.

II. Literature Review

Ahmet Aris *et al.* [16], presented two new lightweight mitigation schemes for RPL-VNA (Version Number Attacks). These intrusions severely affected the efficiency of IPv6-connected LLNs (Low Power and Lossy Networks). In these intrusions, an intruder cause changes in the version number of the network spitefully. The main aim of the attacker here was to increase the latency and control message overhead. These types of intrusions reduced the service time of network and PDR (Packet Delivery Ratio). This work presented simple at the same time efficient mitigation methods to significantly improve the efficiency of attack affected RPL network. The new schemes reduced the attack caused delay, average power consumption and control message overhead up to 87%, 63%, and 71%. These schemes also showed 86% of increase in the PDR (Packets Delivery Ratio). The new schemes exchanged the mitigation efficiency against the resource outlays while permitting the ordinary RPL function. Hence, these schemes allowed network manager to select the appropriate technique for their RPL network.

Amit Dvir *et al.* [17], presented a novel routing protocol to remove the problems of LLNs (Low power and Lossy networks). This protocol was referred as IPv6 routing protocol. The new protocol made its contribution in the performance of LLNs (Low power and Lossy Networks). RPL provided multiple routes by generating and handling the DAGs (Directed Acyclic Graphs) via single or multiple gateways. Therefore, an adversary deploying a single node close to the gateway could divert a bigger part of the network traffic independently. This work made use of an improve version called DODAG to reconstruct the routing topology. It was also essential to carefully prevent an internal attacker from publishing the reduced rank level that caused a bigger portion of the DODAG for establishing connection to the DODAG root through the intruder and made it enable to listen to a bigger portion of the network traffic forward on its own. Hence, this new security approach was capable enough to prevent the illegal boost in the version number.

Anthea Mayzaud *et al.* [18], proposed a detection technique derived from a distributed monitoring framework with dedicated algorithms. The main aim of this technique was to detect VNAs (version number attacks) in RPL-based networks using a distributed monitoring framework. The new technque successfully identified the malevolent nodes that launched these types of intrusions in RPL networks. A lot of tests were conducted in this work to evaluate the efficiency of the proposed technique. This work considered a monitoring node placement scheme to quantify the scalability of the new technique. The future work would be focused on conducting corresponding tests in real-time architectures with more types of devices applying the RPL protocol. In future, the proposed technique could be evaluated and extended to the case of intruder alliance. It refers to the condition when various adversary nodes occur in the network simultaneously.

Zeeshan Ali Khan *et al.* [19], designed and evaluated some IDS schemes for IoT Networks. These schemes were suitable for the minute devices. These schemes made use of trust management method. This method allowed devices to handle reputation information of their neighbors. This approach efficiently distinguished spitefully behaving elements in a processing and energy-efficient manner. This procedure was carried out in an energy based system. The trust management subjective logic was focused on to recognize the adversary nodes existing in the network. Three variables were presented. These variables were based on negative and positive trust ratings; belief (b), disbelief (d) and uncertainty (u).

$$b = \frac{p}{p+n+k} \quad d = \frac{n}{p+n+k} \quad u = \frac{k}{p+n+k}$$

The adversary node after being detected got immediately eliminated from the network. The new scheme performed better against the three sorts of intrusions launched on RPL protocol. It was possible to use the new scheme against the other sorts of attacks as well. The future work would be

focused on developing a test bed containing Z1 elements to validate the simulation results of MATLAB tool. This work made a discussion on a variety of algorithms to manage the reputation. These algorithms included NBTD (Neighbor Based Trust Dissemination), CNTD (Clustered Neighbor Based Trust Dissemination) and TTD (Tree Based Trust Dissemination).

H. Abdo *et al*. [20], presented a new technique based on both safety as well security during for analyzing the risk in industrial applications. This technique combined bowtie analysis with a fresh improved adaptation of attack tree analysis. The use of bowtie analysis was quite popular to analyze the security while the second approach was presented to analyze the safety of ICS (Industrial Control Systems). The bowtie and attack tree when merged together comprehensively represented the risk conditions by considering safety and security. Afterward, this work presented a technique to evaluate the risk level on the basis of two-folded possibility portions. The first portion was used for the safety while the other one was for the security. This work analyzed a real-time risk case in a chemical factory to represent the purpose of this technique.

Ahmet Aris *et al*.[21], deeply studied the RPL version number attacks and presented the analysis of intrusions from different viewpoints. This analysis gave exclusive factors of this work in a real-time network topology. This topology had both stationary and mobile nodes with different multiplicities. This work was inspired from the IETF routing requirement documents. This work also analyzed the way of affecting the energy consumption of the nodes by the VNA (Version Number Attack). This work presented a probabilistic attacking model. In this model, the intruder launched intrusion attacks with a probability of p (e.g., 0, 0.3, 0.5, 0.7, and 1). This work also provided the performance outcomes in terms of different values of probability of p. The simulation results demonstrated that the outcomes of PDR (Packet Delivery Ratio) and the CPO (Control Packet Overhead) were highly related to the intruder's locality.

Hezam Akram Abdul-Ghani *et al.*[22], presented a novel IoT (Internet of Things) suggestion approach based on the construction of blocks strategy. This was mainly a reference model with four layers. This work presented a wide-ranging IT attack model that had four major stages. The first stage presented an IoT asset based attack level made up of four elements. These elements were identified as software, information, protocol wrapping the complete IoT mass and significant things. The next stage provided a description of the IoT security architecture. The third stage classified the IoT attack for all elements. The last stage detected the infringement of security objectives and relation between each intrusion. This stage also presented various strategies to secure every resource. This was the first ever attempt of developing an IoT attack model based on the building block reference model. The achieved outcomes evidently demonstrated the efficiency of the new model.

Anthea Mayzaud *et al.* [23], presented a detection approach to deal with the VNA **(**Version Number Attack) in RPL environment. This work applied a strategy relied on the distributed monitoring architecture to hold a discussion on node resources. The new approach used the relationship amid monitored nodes for the intruder detection. The intruder started the localization process after getting the detection information from all observing nodes. In this work, several tests had been carried out to evaluate the new approach. It was possible to decrease the FPR (False Positive Rate) by placing the monitoring nodes strategically. The future work would be focused on conducting a large number of corresponding tests on the basis of realistic framework with some other types of devices.

III. RESEARCH METHODOLOGY

There are several stages included in the research method. These stages include implementation strategy, projected results and requirements for hardware and software tools.

The flow-chart of the implementation is given below:

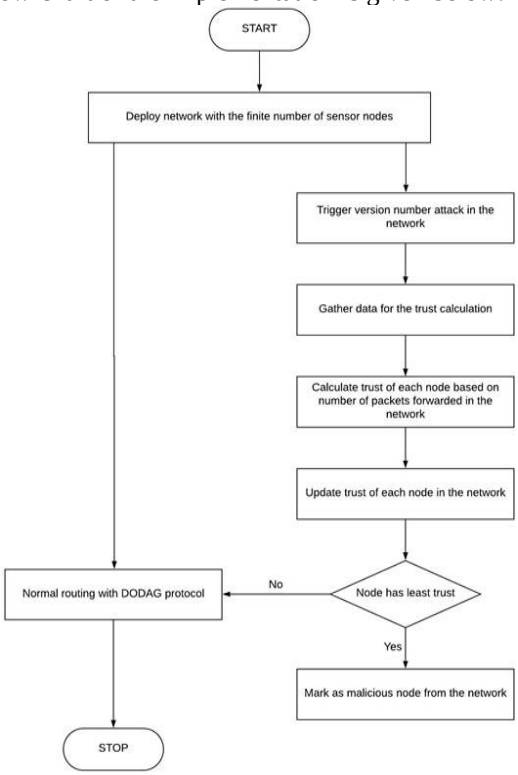

Figure 2: Flow Chart of the algorithm

Here are the different steps of the implementation strategy:-

- **Deployment of the Network: -** The deployment of network will be carried out with the fixed number of sensor nodes and a sink node. The sensor nodes sense different sorts of physical parameters such as temperature, pressure etc. The sensor devices are heterogeneous in nature. This implies that every sensor node possesses different battery and processing energy. The DODAG protocol will sort out the network into a configuration similar to the tree.
- **Trigger of version number attack: -** The malevolent nodes will be formed in the network. These nodes launch version number intrusion. In the DODAG, malicious nodes cause changes in the version number.

The DODAG protocol will choose the route with high version number. This will result in routes based on loop formation in IoT.

- **Trust Calculation:** - This work presents trust based approach to mitigate the version number intrusion. The trust based scheme will perform in the three stages. These stages include pre-processing, trust measurement and trust updating. The sensor nodes with minimum trust will be marked as malevolent nodes.
- **Analyze network performance:** - The final stage will analyze the efficiency of network in terms of some metrics. These metrics include throughput, packet loss and energy consumption. The efficiency of the new method is evaluated using this metrics.

IV. RESULT AND DISCUSSION

This research work is focused on to isolate version number attack in IoT. The version number attack is launched in the DODAG protocol. This chapter compares the three conditions. The first two conditions include DODAG protocol and the effect of version number attack on the efficiency of DODAG protocol with regard to throughput and packet loss. The third case involves the segregation of version number intrusion in DODAG protocol. As per the analysis, the presented case has minimum packet loss and maximal number of throughput in contrast to attack case presented in the base paper.

Table 1: Simulation Parameters

Parameter	Values
Simulator	Ns2-2.35
Number of nodes	32
Area	800 * 800 meter
Antenna type	Omi-directional
Channel	Wireless channel
Propagation Model	Two ray

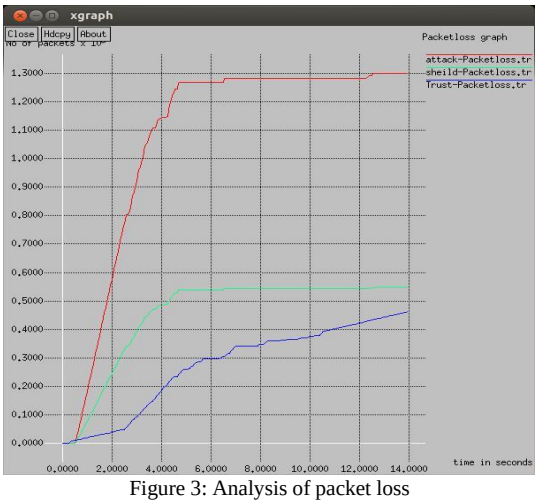

Figure 3: Analysis of packet loss

Figure 3 shows the comparison of attack case, base paper case and proposed case in terms of packet loss. As per the analysis, the presented technique shows minimal number of packet loss in contrast to the other two cases.

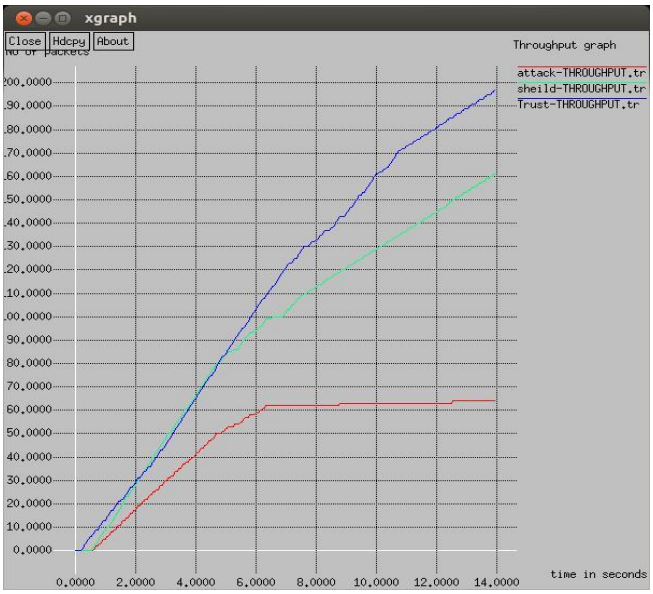

Figure 4: Throughput Comparisons

Figure 4 shows the comparison of attack case, base paper case and proposed case in terms of throughput. As per the analysis, the presented technique shows maximal throughput in contrast to the other two cases.

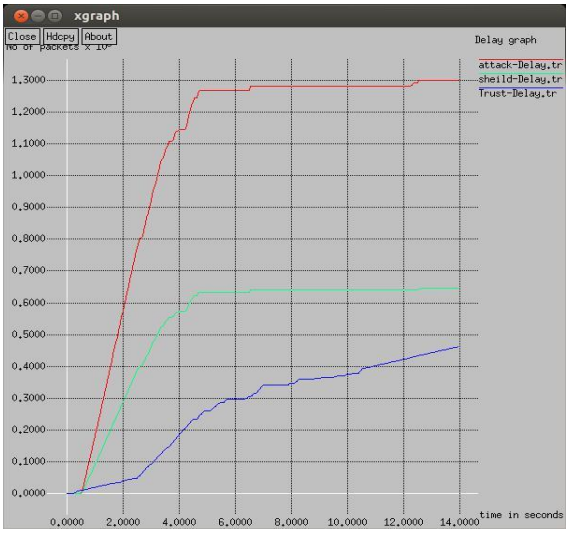

Figure 5: Delay Comparison

Figure 5 shows the comparison of attack case, shield attack and proposed approach in terms of delay. Shield scenario refers to the earlier technique for isolating the version number intrision. As per the analysis, the presented technique shows minimal delay in contrast to the other two cases.

V. CONCLUSION

This work is focused on to mitigate the version number attack in IoT. DODAG is a hierarchical structure. RPL network makes use of this structure for tiny devices where the malevolent nodes increments the version number. In IoT, this results in the formation of path containing loop. This work presents trust based approach to mitigate the version number intrusion from the network, and detecting the malevolent nodes. This approach consumes minimum number of IoT resources. This work makes use of NS2

(network simulator version 2) to implement the presented approach. The analysis of outcomes has been carried out in terms of throughput and packet loss. As per the analysis, the new approach performs better than other two cases in terms of throughput. The packet loss of the presented case is lower than the other two cases.

References

[1] A. Shaddad Abdul-Qawy, P. Pramod, E. Magesh, and T. Srinivasulu, "The Internet of Things (IoT): An Overview", J. Eng. Res. Appl. , vol. 5, no. 12, pp. 71–82, 2015.

[2] D. Bandyopadhyay and J. Sen, "Internet of things: Applications and challenges in technology and standardization," Wirel. Pers. Commun., vol. 58, no. 1, pp. 49–69, 2011.

[3] V. Bhuvaneswari and R. Porkodi, "The internet of things (IoT) applications and communication enabling technology standards: An overview," Proc. - 2014 Int. Conf. Intell. Comput. Appl. ICICA 2014, pp. 324–329, 2014.

[4] S. V. Pote, "Internet of Things Applications , Challenges and New Technologies," vol. 67, no. 978, pp. 45–51, 2018.

[5] E. Hopalı and Ö. Vayvay, "Internet of Things (IoT) and its Challenges for Usability in Developing Countries," vol. 2, no. January, pp. 6–9, 2018.

[6] H. Suo, J. Wan, C. Zou, and J. Liu, "Security in the internet of things: A review," Proc. - 2012 Int. Conf. Comput. Sci. Electron. Eng. ICCSEE 2012, vol. 3, pp. 648–651, 2012.

[7] T. Salman and R. Jain, "Networking protocols and standards for internet of things," Internet Things Data Anal. Handb., vol. 1, no. 1, pp. 215–238, 2017.

[8] Aniruddha Chakrabarti, "Emerging Open and Standard Protocol Stack for IoT | Aniruddha Chakrabarti | Pulse | LinkedIn," vol. 1, no. 1, pp. 2–6, 2015.

[9] Internet Engineering Task Force. RPL: IPv6 Routing Protocol for Low-Power and Lossy

[10] Networks.https://tools.ietf.org/pdf/rfc6550.pdf, 2012. [Online; accessed 02-June 2017].

[11] E. Baccelli, M. Philipp, and M. Goyal, "The P2P-RPL Routing Protocol for Ipv6 Sensor Networks: Testbed Experiments," SoftCOM 2011, 19th Int. Conf. Software, Telecommun. Comput. Networks, Split, vol. 1, pp. 1–6, 2011.

[12] T. Zhang and X. Li, "Evaluating and analyzing the performance of RPL in contiki," Proc. first Int. Work. Mob. sensing, Comput. Commun. - MSCC '14, pp. 19–24, 2014.

[13] J. Posegga, T. Eder, D. Nachtmann, D. Parra, and D. Schreckling, "Conference Seminar SS2013 — Real Life Security (5827HS) Trust and Reputation in the Internet of Things Trust and Reputation in the Internet of Things," pp. 1–19, 2013.

[14] Z. A. Khan, J. Ullrich, A. G. Voyiatzis, and P. Herrmann, "A Trust-based Resilient Routing Mechanism for the Internet of Things," Proc. 12th Int. Conf. Availability, Reliab. Secur. - ARES '17, pp. 1–6, 2017.

[15] L. Gu, J. Wang, and B. Sun, "Trust management mechanism for internet of things", Communi-cations, China, 11:148-156, 02 2014.

[16] J. Guo, I. R. Chen, and J. J. P. Tsai, "A survey of trust computation models for service management in internet of things systems," Comput. Commun., vol. 97, pp. 1–14, 2017.

[17] A. Arış, S. B. Örs Yalçın, and S. F. Oktuğ, "New lightweight mitigation techniques for RPL version number attacks," Ad Hoc Networks, vol. 85, pp. 81–91, 2019.

[18] A. Dvir, T. Holczer, and L. Buttyan, "VeRA - Version number and rank authentication in RPL," Proc. - 8th IEEE Int. Conf. Mob. Ad-hoc Sens. Syst. MASS 2011, pp. 709–714, 2011.

[19] A. Mayzaud, R. Badonnel, and I. Chrisment, "Detecting version number attacks in RPL-based networks using a distributed monitoring architecture," 2016 12th Int. Conf. Netw. Serv. Manag. CNSM 2016 Work. 3rd Int. Work. Manag. SDN NFV, ManSDN/NFV 2016, Int. Work. Green ICT Smart Networking, GISN 2016, pp. 127–135, 2017.

[20] Z. Khan and P. Herrmann, "A trust based distributed intrusion detection mechanism for internet of things", In 2017 IEEE 31st International Conference on Advanced Information Networking and Applications (AINA), pages 1169-1176, Los Alamitos, CA, USA, mar 2017. IEEE Computer Society.

[21] H. Abdo, M. Kaouk, J.-M. Flaus, and F. Masse, "A safety/security risk analysis approach of industrial control systems: A cyber bowtie combining new version of attack tree with bowtie analysis", Computers Security, 72, 09 2017.

[22] A. Aris, S. F. Oktug, and S. B. O. Yalcin, "Rpl version number attacks: In-depth study", NOMS 2016 - 2016 IEEE/IFIP Network Operations and Management Symposium, pages 776-779, 2016.

[23] H. A. Abdul-Ghani, D. Konstantas, and M. Mahyoub, "A comprehensive iot attacks survey based on a building-blocked reference model", International Journal of Advanced Computer Science and Applications, 9(3), 2018.

[24] A. Mayzaud, R. Badonnel, and I. Chrisment, "A distributed monitoring strategy for detecting version number attacks in RPL-based networks," IEEE Trans. Netw. Serv. Manag., vol. 14, no. 2, pp. 472–486, 2017.

Smart Home Automation System with Voice Control

Swapnadip Guha
Department of Computer Science and Engineering
JIS College of Engineering Kalyani, Nadia, West Bengal
swapnadip.guha@gmail.com

Sumanta Chatterjee
Department of Computer Science and Engineering
JIS College of Engineering Kalyani, Nadia, West Bengal
sumanta.chatterjee@jiscollege.ac.in

Anupam Dutta
Department of Computer Science and Engineering
JIS College of Engineering Kalyani, Nadia, West Bengal
anupamdutta27121998.in@gmail.com

Shubhranil Mazumder
Department of Computer Science and Engineering
JIS College of Engineering Kalyani, Nadia, West Bengal
onlysubhranil1998@gmail.com

***Abstract*— Home automation is the new era in the field of technology where we all can control our regular electrical home appliances. It is very useful and it's used in today's tech world. Everything can be controlled from anywhere in the world because the distance is not a boundary anymore. Although now in the current market we all can see that there are some smart devices which are very costly. Nowadays smart led light are dominant over normal lights. So, for that reason, we need a middle system that can convert our regular home to a smart home. By using voice command, you can be able to turn on and off that device easily from anywhere in the world. This research paper presents a very useful low-cost IoT work that is very flexible with our current non-smart electrical devices which has the potential to convert our traditional electric devices to an IoT-enabled devices. It can simply connect to the internet by using home Wi-Fi or any hotspot.**

Keywords*— *Electrical Devices, IoT, Internet, Voice command.

I. INTRODUCTION

Most of the people in our society work in some private company, for their jobs, they have to leave their homes to attend the office early in the morning and they will return back to their houses in late night. In that stated scenario, it is very obvious that time & money is a very important thing for everyone. Let's consider a person who lives alone has no other choice to return home if he/she forgets to turn off any electrical device before leaving the house for office, it is a very bad thing for him because, there is no one in the home to turn off that electric device & this is the big reason for electricity wastage & maybe some kind of electrical hazard.

In today's world the concept of smart appliances which can be connected with the internet and accessed by their users anywhere in the world is becoming a necessity. Suppose in the time of summer you are returning to your home from your office and you have to wait a few minutes after turning on your Air conditioner to cool your room, in this situation if you have the option to turn on your air conditioner five or ten minutes before you reach your home then it will be the more peaceful situation. So, for solving that issue we are introducing a new idea by using the IoT in our homes. The person needs a middle device that can allow him to turn on or off that regular air conditioner or any regular electrical appliances from anywhere through the internet and it is possible when he/she will use our concept.

II. LITERATURE SURVEY

In the Year 2011 R. Piyare and M. Tazil published a paper named "Bluetooth based home automation system using a cell phone" in the "2011 IEEE 15th International Symposium on Consumer Electronics" in Singapore [1], they proposed the method which was very useful although there concept is very useful and secure there is a limitation of distance, as Bluetooth signal is not capable enough to connect a device above 5 - 10 meters, and Bluetooth is not capable enough to communicate or establish a connection with a home Wi-Fi router so the range is becoming a big concern because although their concept is implemented in a particular area globally the connectivity will not be possible this concept is useful in intranet domain but not fully useful in the actual internet domain. Previously In the Year 2015 Sonali Sen, Shamik Chakrabarty, Raghav Toshniwal, Ankita Bhaumik published a paper named "Design of an Intelligent Voice Controlled Home Automation System" [2] in the International Journal of Computer Applications, they proposed the method of voice recognition based home automation concept which was amazing and future-ready but the main problem was that it was using Bluetooth for communicating with the Arduino module. So, in that case, the Arduino module is not accessible via the internet and it limits its usability. Earlier in the year 2017 M. Abivandhana, K.Divya, D. Gayathri, R. Ruhin Kouser published a paper named "Smart Home Automation Based on IoT and Android Technology" in IJESC [3]. In their research paper they explained home automation through Bluetooth and GSM communication technology which is actually used locally by using Bluetooth signals and global by using traditional GSM signal. A paper published by J. Vijaya Kumari & Pavithra Neelam in the year 2021 named "IoT Based Smart Home Automation System" in JETIR [4] also demonstrates the IoT by using NodeMCU, but speech recognition technology was not embedded with that. Previously in the year 2019 K. Lova Raju, V. Chandrani, SK. Shahina Begum, M. Pravallika Devi published a paper named "Home Automation and Security System with Node MCU using Internet of Things" [5] in the International Conference on Vision Towards Emerging Trends in Communication and Networking (ViTECoN), the study on the overall IoT based system using nodemcu and the system security was discussed by them. In the year 2020 a paper on "Wireless Home Automation with Security System" was published in the International Journal of Electrical Engineering and Technology (IJEET) [6] by Jolan

Baccay Sy, Shegaw Melak Akele & Edward B. Panganiban briefly researched an RFID based authentication system with home automation.In the year of 2017 Menal Dahiya was also published a paper named “Bluetooth Remote Home Automation System using Internet of Things” [7] in the International Journal of Innovative Research in Computer and Communication Engineering, discussing about the home automation using Bluetooth technology. A paper was also published in the year of 2019 by A. Senthil Kumar & Easwaran Iyer named “An Industrial IoT in Engineering and Manufacturing Industries – Benefits and Challenges” [8] on International Journal of Mechanical and Production Engineering Research and Development (IJMPERD) discussed about the industrial benefits & challenges & implementation of the IoT & IIoT in industry level.

III. RESEARCH METHODOLOGY

A. Hardware Requirements

- NodeMCU ESP 8266 Board (Fig 1, Fig 2):- A NodeMCU is a 32bit microcontroller used in IoT projects. It is an open-source microcontroller. It has a total of 11 I/O Digital Pins and 1 Analog Input Pin. It has an ESP 8266 Wi-Fi module on-chip for communication and internet connectivity. It has 4MB of flash storage and the clock frequency is 80MHz. The NodeMCU is a very low-cost IoT platform and it has an initial firmware that runs on esp8266 SoC. The firmware of NodeMCU uses Lua-based firmware. It has also a memory of 128Kb. It has a total of 30 pin headers. It can be easily programmed with Arduino

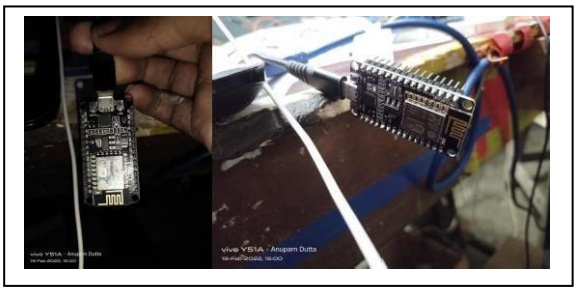

Fig. 1. NodeMCU ESP 8266 Board

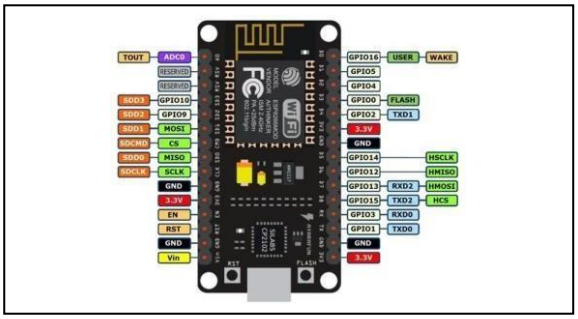

Fig. 2. NodeMCU ESP 8266 Board Pin Diagram

- 4 Channel Relay Module (Fig 3): - The 4-channel relay module is used as an interconnector between the low voltage and high voltage devices. The module contains 4 relays which are used as a switch. The relay module has one +5V Vcc & one Ground Connector pin and four input pins through which the microcontroller sends the needed digital input in terms of HIGH & LOW (0 or 1) for controlling the relays.

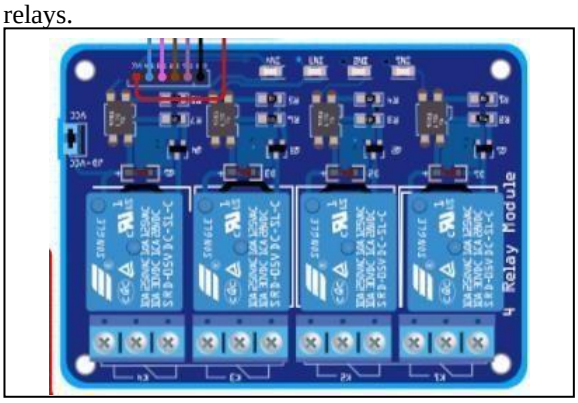

Fig. 3. Channel Relay Module

- LDR Module (Fig 4):- LDR sensor module is an analogue sensor module that can measure and dig out light intensity. This sensor has a Light Dependent Resistor that helps to detect light. This module has 4 terminals. There is a “DO” pin which is a digital output pin. The “AO” pin is an analogue output pin. When light is absent the output of the module is high and when there is a presence of light then the output becomes low. Also, there is a potentiometer knob that is required for the adjustment of the sensitivity of the sensor. This sensor is also known as the Photoresistor sensor. This sensor consists mainly of the LM393, Comparators, Variable Resistor(Trim Pot), Output LED, Power LED. The LDR works on the principle of “Photo Conductivity”. The resistance of the LDR changes according to the light intensity that falls on the LDR. When the intensity is high then the resistance will decrease and vice-versa. When intensity is high on the surface of the LDR then LDR resistance decreases. After that, the maximum voltage will pass across the resistor’s a minimal voltage from the LDR is put to the inverting input of the IC. In this scenario, the voltage taken as input is less than the threshold voltage. Due to this sensor output goes to LOW. And the opposite goes for HIGH”. The microcontroller takes that input value through the analogue input pin.

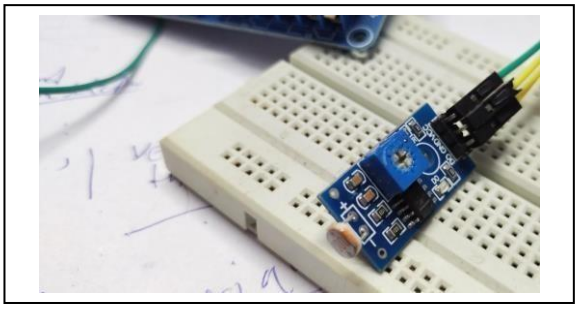

Fig. 4. LDR Module

- PIR Motion Sensor Module (Fig 5):- PIR or passive infrared sensor is a motion sensor that senses the motion by taking and analysing the infrared light

radiating by the moving object. The PIR Motion sensor detects the motion by analysing the infrared radiation or radiant heat reflected from any moving thing. It has 3 pins one is for 3.3V DC Vcc and the Other one is for GND and the middle one is a Data or Digital Pin for the output if motion detects it provides “High” as an output otherwise it gives “LOW” as output in binaries 1’s and 0’s where 1 is for High and 0 is for Low. As the PIR sensor provides the output in digital like 0’s and 1’s its output/data pin is normally connected with the digital pins of the NodeMCU board. The PIR module has 2 types of modes one is the single trigger and the second one is the Repeat trigger. This PIR sensor it has two potentiometers one is for detection range and another one is for delay setting.

Fig. 5. PIR Motion Sensor Module

B. Workflow diagram (Fig 6):-

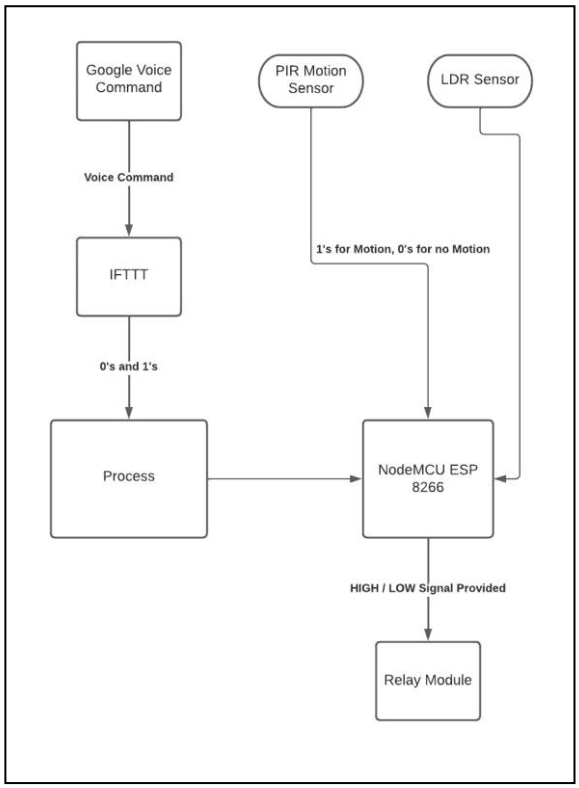

Fig. 6. Workflow Diagram

C. Circuit Diagram (Fig 7):-

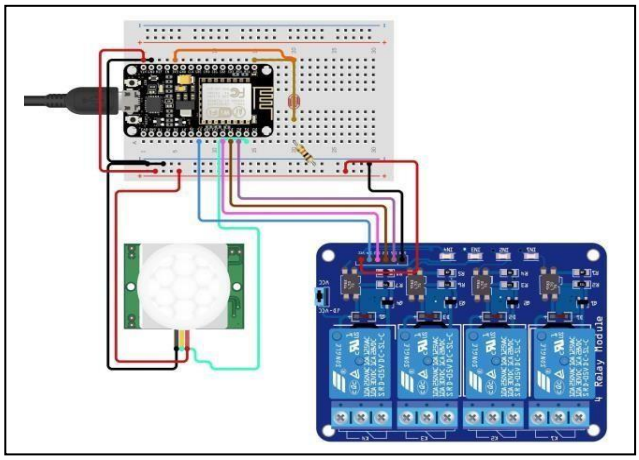

Fig. 7. Circuit Diagram

IV. WORKING PRINCIPLE

Our research paper is based on home automation by using some hardware like NodeMCU which is our main microcontroller and 4 channel relay module which acts as the smart switch which operates on traditional electric appliances. We are also using a PIR motion sensor which will sense the motion and LDR which we use to sense the environment's light intensity. The motion sensor provides the digital input to the microcontroller LDR sensor provides an analogue signal to the microcontroller. The software like Google Assistance, Blynk, and IFTTT are used in our research. At first according to the circuit diagram all the connections will be made electrically then we have to install the Blynk app to our smartphone and configure each relay. Now we have to configure the google assistant with Blynk and IFTTT. Now everything is done, thus the whole system is ready to be used through the Blynk app & Google assistant. The microcontroller sense the data from LDR and PIR motion Sensor, when the environment light and motion are detected, then it selects a specific relay to active state.

Fig. 8. Application Working model

V. RESULT AND DISCUSSION

When any person provides the voice comment to activate or deactivate any electrical appliances the system will do so. Several observations on the research model are done to verify its working in a practical scenario. Total 5 types of observations are taken on the research model, the 1st one is the voice assistance working or functioning in terms of command given as “Turn on & Turn off Light” 2nd observation is based on the voice command given as “Turn on & off Fan”, 3rd observation is based on controlling water Pump by providing command as “Turn On and Turn Off- Pump” and 4th one is the observation on Chimani by proving some voice command to Turning on and off that Chinami by using voice, all though we get total 98% accuracy for above 4 observation, the fifth observation was automated by the system, the system will turn a light on when motion is detected by the sensor and there is no light in the environment, The LDR sensor is responsible to sense the light intensity and the PIR module is responsible to detect motion by using passive infrared the model get 97% accuracy on the 5th observation. By getting all observations the average accuracy of our model is 97.5%. Most of the time our system behaves perfectly which is should be.

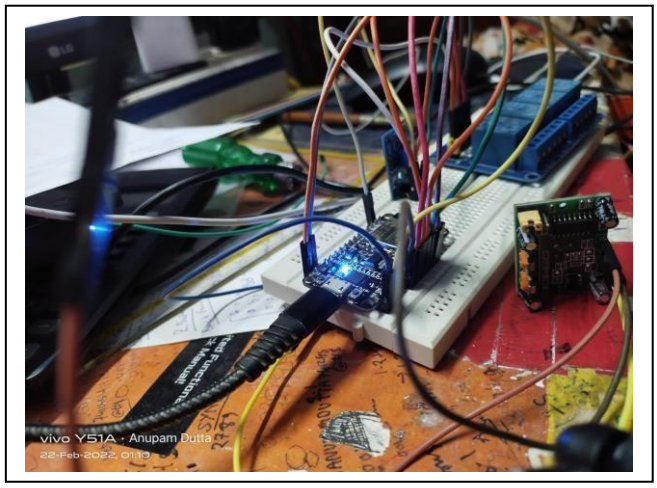

Fig. 9. Hardware Working Model

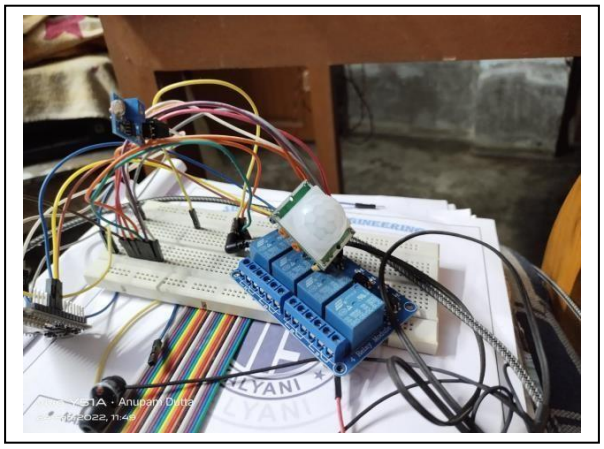

Fig. 10. Hardware Working Model

TABLE I. EXPERIMENTAL DATA ANALYSIS FOR THE VOICE COMMAND TO CONTROL THE LIGHTS.

Sl. No.	Sample	Instruction Given	Result	Performance State (%)
Command Given When Light Current State is Off				
1	1	Turn On Light	Light Turned On	100
2	2	Turn On Light	Light Turned On	100
3	3	Turn On Light	Light Turned On	100
4	4	Turn On Light	Light Turned On	100
5	5	Turn On Light	Light Turned On	100
6	6	Turn On Light	Light Turned On	100
7	7	Turn On Light	Light Turned On	100
8	8	Turn On Light	Light Turned On	100
9	9	Turn On Light	Light Turned On	100
10	10	Turn On Light	Light Turned On	100
Command Given When Light Current State is On				
11	1	Turn Off Light	Light Turned Off	100
12	2	Turn Off Light	Light Turned Off	100
13	3	Turn Off Light	Light Turned Off	100
14	4	Turn Off Light	Light Turned Off	100
15	5	Turn Off Light	Light Turned Off	100
16	6	Turn Off Light	Light Turned Off	100
17	7	Turn Off Light	Light Turned Off	100
18	8	Turn Off Light	Light Turned Off	100
19	9	Turn Off Light	Light Turned Off	100
20	10	Turn Off Light	Light Stays On	0

TABLE II. EXPERIMENTAL DATA ANALYSIS FOR THE VOICE COMMAND TO CONTROL THE FAN

Sl. No.	Sample	Instruction Given	Result	Performance State (%)
Command Given When Fan Current State is Off				
1	1	Turn On Fan	Fan Turned On	100
2	2	Turn On Fan	Fan Turned On	100
3	3	Turn On Fan	Fan Turned On	100
4	4	Turn On Fan	Fan Turned On	100
5	5	Turn On Fan	Fan Turned On	100
6	6	Turn On Fan	Fan Turned On	100
7	7	Turn On Fan	Fan Turned On	100
8	8	Turn On Fan	Fan Turned On	100
9	9	Turn On Fan	Fan Turned On	100
10	10	Turn On Fan	Fan Turned On	100
Command Given When Fan Current State is On				
11	1	Turn Off Fan	Fan Turned On	100
12	2	Turn Off Fan	Fan Turned Off	100
13	3	Turn Off Fan	Fan Turned Off	100
14	4	Turn Off Fan	Fan Turned Off	100
15	5	Turn Off Fan	Fan Turned Off	100
16	6	Turn Off Fan	Fan Stays On	0
17	7	Turn Off Fan	Fan Turned Off	100
18	8	Turn Off Fan	Fan Turned Off	100
19	9	Turn Off Fan	Fan Turned Off	100
20	10	Turn Off Fan	Fan Turned Off	100

TABLE III. EXPERIMENTAL DATA ANALYSIS FOR THE VOICE COMMAND TO CONTROL THE WATER PUMP.

Sl. No.	Sample	Instruction Given	Result	Performance State (%)
Command Given When Pump Current State is Off				
1	1	Turn On Pump	Pump Turned On	100
2	2	Turn On Pump	Pump Turned On	100
3	3	Turn On Pump	Pump Turned On	100
4	4	Turn On Pump	Pump Turned On	100
5	5	Turn On Pump	Pump Turned On	100
6	6	Turn On Pump	Pump Turned On	100
7	7	Turn On Pump	Pump Turned On	100
8	8	Turn On Pump	Pump Turned On	100
9	9	Turn On Pump	Pump Turned On	100
10	10	Turn On Pump	Pump Turned On	100
Command Given When Pump Current State is On				
11	1	Turn Off Pump	Pump Turned Off	100

12	2	Turn Off Pump	Pump Turned Off	100
13	3	Turn Off Pump	Pump Turned Off	100
14	4	Turn Off Pump	Pump Turned Off	100
15	5	Turn Off Pump	Pump Stays On	0
16	6	Turn Off Pump	Pump Turned Off	100
17	7	Turn Off Pump	Pump Turned Off	100
18	8	Turn Off Pump	Pump Turned Off	100
19	9	Turn Off Pump	Pump Turned Off	100
20	10	Turn Off Pump	Pump Turned Off	100

TABLE IV. EXPERIMENTAL DATA ANALYSIS FOR THE VOICE COMMAND TO CONTROL THE CHIMNEY

Sl. No.	Sample	Instruction Given	Result	Performance State (%)
Command Given When Chimney Current State is Off				
1	1	Turn On Chimney	Chimney Turned On	100
2	2	Turn On Chimney	Chimney Turned On	100
3	3	Turn On Chimney	Chimney Turned On	100
4	4	Turn On Chimney	Chimney Turned On	100
5	5	Turn On Chimney	Chimney Turned On	100
6	6	Turn On Chimney	Chimney Turned On	100
7	7	Turn On Chimney	Chimney Turned On	100
8	8	Turn On Chimney	Chimney Turned On	100
9	9	Turn On Chimney	Chimney Turned On	100
10	10	Turn On Chimney	Chimney Turned On	100
Command Given When Chimney Current State is On				
11	1	Turn Off Chimney	Chimney Turned Off	100
12	2	Turn Off Chimney	Chimney Turned Off	100
13	3	Turn Off Chimney	Chimney Turned Off	100
14	4	Turn Off Chimney	Chimney Turned Off	100
15	5	Turn Off Chimney	Chimney Stays On	0
16	6	Turn Off Chimney	Chimney Turned Off	100
17	7	Turn Off Chimney	Chimney Turned Off	100
18	8	Turn Off Chimney	Chimney Turned Off	100

TABLE V. EXPERIMENTAL DATA ANALYSIS FOR THE MOTION AND ENVIRONMENT LIGHT DETECTION.

Sl. No	Sample	Real Condition		System Output		Relay O/P	Performance State (%)
		Motion	Light	Motion	Light		
1	1	YES	YES	YES	NO	HIGH	100
2	2	YES	YES	YES	YES	LOW	100
3	3	YES	YES	NO	YES	LOW	100
4	4	YES	YES	YES	YES	LOW	100
5	5	YES	YES	YES	YES	LOW	100
6	1	NO	YES	NO	NO	LOW	100
7	2	NO	YES	YES	NO	HIGH	0
8	3	NO	YES	YES	YES	LOW	100
9	4	NO	YES	NO	YES	LOW	100
10	5	NO	YES	NO	YES	LOW	100
11	1	YES	NO	YES	NO	HIGH	100
12	2	YES	NO	NO	NO	LOW	100
13	3	YES	NO	YES	NO	HIGH	100
14	4	YES	NO	YES	NO	HIGH	100
15	5	YES	NO	YES	NO	HIGH	100
16	1	NO	NO	NO	NO	LOW	100
17	2	NO	NO	NO	NO	LOW	100
18	3	NO	NO	YES	NO	HIGH	100
19	4	NO	NO	NO	NO	LOW	100
20	5	NO	NO	NO	NO	LOW	100

VI. CONCLUSION & FUTURE SCOPE

In this paper, we have developed and given a concept about how the IoT can change regular home appliances and provide more flexibility to us in our daily life. As the technology is upgrading day by day, we also have to take some measures to modify our regular devices with smart ones, but for reducing the cost we have proposed our concepton those aspects.

As our research paper is based on IoT it has a lot of scope for future expansion and upgradation. Firstly, our research should be incorporated with other sensors like humidity and temperature sensor so that our operations will be more useful and relevant. Secondly, in our research, we didn't use any camera module for video or image processing purposes, but nowadays it is very important to use Machine Learning algorithms for getting more accurate results and data, in future we add a camera and by using a video processing

algorithm the System will accurately take a needed decision. If the System detects that the person at the home is sleeping but forgot to turn off the light then the system will automatically be able to turn them off. Thirdly, our provided concept has a drawback because in case of Wi-Fi router failure the system will not work, so, we are planning to make some changes in the future and add the GSM and Bluetooth module for solving that issue. Otherwise, lots of up-gradation is possible in the future in this IoT domain.

REFERENCES

[1] R. Piyare and M. Tazil, paper on "Bluetooth based home automation system using cell phone," published on *Consumer Electronics (ISCE), 2011 IEEE 15th International Symposium on, Singapore*, 2011, pp.192-195 | Conference Paper | Publisher:IEEE

[2] Sonali Sen, Shamik Chakrabarty, Raghav Toshniwal & Ankita Bhaumik, paper on "Design of an intelligent voice-controlled home automation system", published on *International Journal of Computer Applications*, vol. 121, no.15, pp. 39-42, 2015

[3] M.Abivandhana, K.Divya, D.Gayathri, R.RuhinKouser, paper on "Smart Home Automation Based on IOT and Android Technology", published on *International Journal of Engineering Science and Computing*, March 2017, Volume 7 Issue No.3

[4] J.Vijaya Kumari, Pavithra Neelam paper on "IoT Based Smart Home Automation System", published in *International Research Journal of Engineering and Technology (IRJET)* January 2021, Volume 8, Issue 1.

[5] K. Lova Raju, V. Chandrani, SK. Shahina Begum, M. Pravallika Devi paper on "Home Automation and Security System with Node MCU using Internet of Things", published in 2019 *International Conferenceon Vision Towards Emerging Trends in Communication and Networking (ViTECoN)* | Conference Paper | Publisher: IEEE.

[6] Jolan Baccay Sy, Shegaw Melak Akele & Edward B. Panganiban paper on "Wireless Home Automation With Security System (WHASS)", published in *International Journal of Electrical Engineering and Technology (IJEET), Volume 11, Issue 9*, November 2020, pp. 101- 110, Article ID: IJEETConference Paper | Publisher: IAEME | Scopus Indexed.

[7] Menal Dahiya paper on "Bluetooth Remote Home Automation System using Internet of Things", published in International Journal of Innovative Research in Computer and Communication Engineering, Vol. 5, Issue 5, May 2017, ISSN(Online): 2320-9801, ISSN (Print): 2320-9798

[8] A. Senthil Kumar & Easwaran Iyer paper on "An Industrial IoT in Engineering and Manufacturing Industries – Benefits and Challenges", published in *International Journal of Mechanical and Production Engineering Research and Development* (IJMPERD), ISSN(P): 2249- 6890; ISSN(E): 2249-8001, Vol. 9, Issue 2, Apr 2019, 151-160.

[9] Baotong Chen, Jiafu Wan, Antonio Celesti, Di Li, Haider Abbas; Qin Zhang paper on "Edge Computing in IoT-Based Manufacturing", published by IEEE, published in *"IEEE Communications Magazine"* in 2018.

[10] Swapnili Karmore, Rushikesh Bodhe, Fadi Al-Turjman, R Lakshmana Kumar, Sofia Pillai paper on "IoT Based Humanoid Software for Identification and Diagnosis of Covid-19 Suspects", published by IEEE, in IEEE Sensors Journal, 2020.

Sensor-based secured real-time intelligent health monitoring and alert system using IoT

Pabitra Kumar Bhunia
Department of Computer Science and Engineering
JIS College of Engineering Kalyani, Nadia, West Bengal
pabitrabhunia2056@gmail.com

Sumanta Chatterjee
Department of Computer Science and Engineering
JIS College of Engineering Kalyani, Nadia, West Bengal
sumanta.chatterjee@jiscollege.ac.in

Poulami Mondal
Department of Computer Science and Engineering
JIS College of Engineering Kalyani, Nadia, West Bengal
poulamimondal164@gmail.com

Monalisa De
Department of Computer Science and Engineering
JIS College of Engineering Kalyani, Nadia, West Bengal
monaderima@gmail.com

Amarta Kundu
Department of Information Technology
JIS College of Engineering Kalyani, Nadia, West Bengal
amartakundu247@gmail.com

***Abstract*— From the last ten to fifteen years the lifestyle of the whole human being has become so much concerned that they don't get time even to take food or sit down to relax for some moment and for this reason the well-being of every humankind gets neglected nowadays. But in this increasing era of technology, the more humankind is becoming developed day by day the more the nature around us is changing like pollution, climate change, etc. which are becoming a threat to humankind and also from 2020 a new bad time named COVID added to humans which brought a pause to human daily lifestyle. So, in this environment, humans have to take care of their health in a proper way. Then for our today's technology-based smart lifestyle we need some smarter way to look after our health and for this, we designed this device through which people can take care of their health along with their family members because some time there stays some old or paralyzed person in the home but for them always it is not possible to call or say other home members about their problems or some abnormality happening to their body so this device can help them to inform their family members to say their problems. Also, it can help doctors or nurses to monitor patients all 24 hours. Thus, this device will help the whole of mankind to superintend their and their family members' well-being.**

Keywords*— *Real-time, IoT, Health monitoring

I. INTRODUCTION

In this era of the twenty-first century humans are so fast and so busy from day to night. People get out of their house early in the morning and return home late at night from work. So, people also cannot get time to take care of their health. But every human being has to take proper care of his or herself and also of their family members especially of children and old persons. But maximum time in some cases all of the young family members who have to take care go out for their workplace like school, colleges, offices, etc. for an almost full day and there will no one to take care of children or old persons and also always keeping a nurse or a babysitter in the house is not possible for everyone and also getting busy in work for the whole day people who work outside, they cannot take care of their health and in this way, human healthcare comes neglected day by day. On other hand keeping ourselves healthy is most important and most necessary. Because in this current situation of COVID and also in this modern era where pollution is the most there, keeping ourselves healthy is much more important than any other work. And also, in our busy daily routine most of the time we have to take lunch, breakfast, etc. outside where food is left in the open air. So, in this situation, we have to look after our health more importantly without any fail. So, when our daily lifestyle is becoming busier and smarter day by day with high technology then we have to search for a smarter way of caring for our health. So, when there are smart appliances for every work, different types of mobile applications are there then also there should be a smart way out for health monitoring. This device is a smart health monitoring system where there will be band-like equipment where heart beat sensor, sweat sensor, oxygen level measuring sensor, measuring footstep, and calorie burn sensor will present. Also, if there will be any type of abnormality in anyone's body as soon as possible a message will be served to his or her mobile and also to his or her family members. In this way, people can take care of their own and their family members' health at any time even in between their work. Also, with the help of this device doctors or nurses can all time take care of any patients, especially paralyzed and cardiac patients. Because doctors or nurses can't take care of every patient every minute. So, this will be a smarter way to look after the well-being of every human being.

II. METHODOLOGY

A. STM32F407VGT6 M Cortex-M4 32bit MCU (Fig 1).

STM32 is the micro controller of high frequency which supports rapid data interpretation with the help of advance cortex score and enhanced data binding it contains up to 196 kb of secondary memory. It can provide two timing matric manipulation of data. The incorporated RAM of 1 Mb simulates high TensorFlow processing speed.

B. High Accuracy Temperature Sensor (Fig 2).

12C High Accuracy Temperature Sensor (MCP9808) MCP 9808 is a microchip integrated high accuracy module. It can measure temperature -40°C to 125°C and it is highly accurate. Also, through this sensor temperature can be sensed.

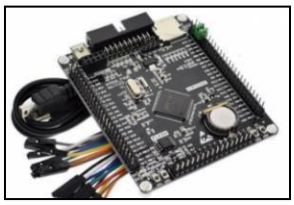

Fig. 1. M Cortex-M4 32bit MCU

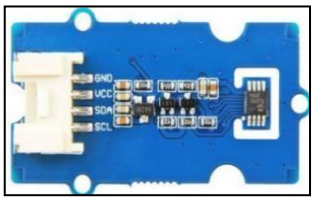

Fig. 2. Temperature sensor

C. MAX30100 Pulse Oximeter Heart Rate Sensor Module (Fig 3).

MAX30100 is an integrated pulse oximeter which can sense heart-beat. It gets its readings from two LEDs which emit two wavelengths- a red and an infrared and then with the help of photodetector measures the pulsing blood absorbance. MAX30100 can be operated in range of 1.8 to 3.3 V.

D. Pedometer Sensor Module (Fig 4).

DSPX01 can be used for 3D pedometer applications and it is made of 3 axes acceleration sensor. This sensor sense data from physical movements. At the time of walking or running it measures the steps and give the output as a high-level pulse. The output pulse is of 50ms width. This pedometer sensor works at 2.5-3.3 V.

Fig. 3. Pulse Oximeter Heart Rate

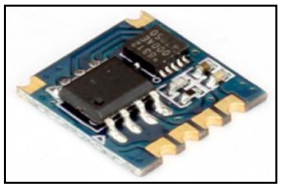

Fig. 4. Pedometer sensor Sensor.

E. Mini cellular GSM module (Fig 5).

Mini cellular GSM GPRS module helps us to access the internet connectivity and as well as the location. GSM module is a cellular based module.

F. 3.7V 5000mAH (Lithium Polymer) Rechargeable Battery Model (Fig 6).

This battery is thin, powerful and light and widely used in Bluetooth speaker, power bank, MP4 player, IoT and other industrial applications.

Fig. 5. Mini cellular GSM module

Fig. 6. 5000 mah battery

G. Sweat sensor (Fig7).

This sensor detects metabolize and biomarkers that is present in human sweat execrated by the skin and it automatically calculates the salt and humidity ratio of our skin. A higher version of this device may determine sweat glucose and blood glucose level of the investigating patient. This integrated circuit performs very efficiently with low voltage microcontrollers.

H. M131Loudspeaker (Fig 8)

It is an Arduino compatible speaker. It requires quite low power but gives high sound. It will be used as an alarm or buzzer here.

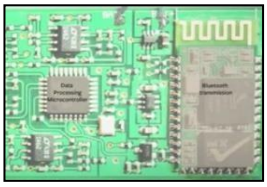

Fig. 7. Sweat sensor

Fig. 8. Loud Speaker

III. WORKFLOW DIAGRAM

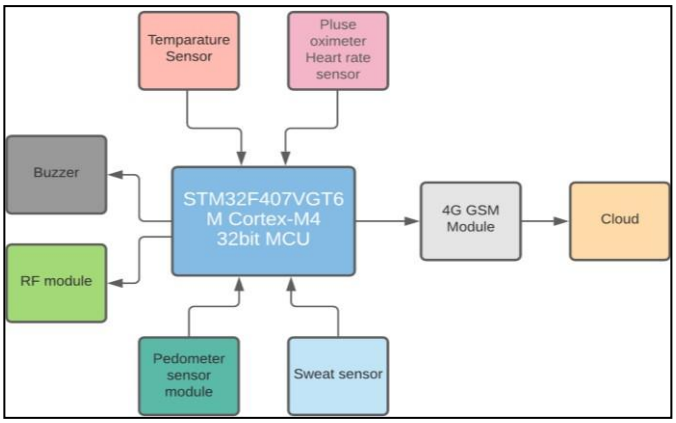

Fig. 9. Work Flow diagram

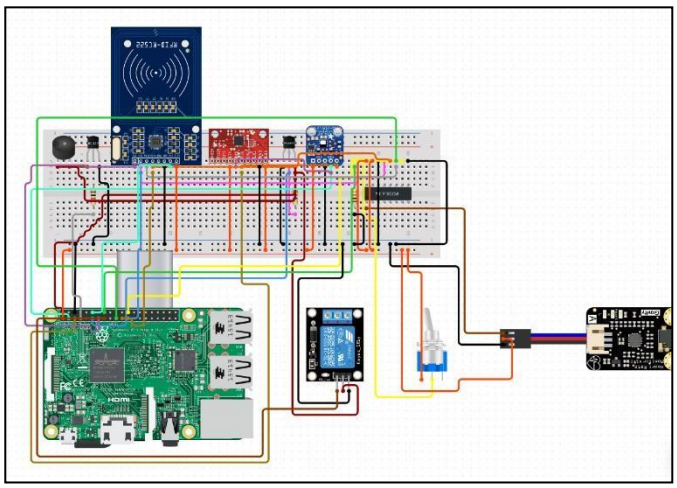

Fig. 10. Circuit diagram

IV. Working Principle

The microcontroller used here is STM32F407VET6 Arm Cortex-M4 which will gather all the information body parameters from the attached sensors. The handy sensors like body temperature sensor, sweat analyzer, and BPM sensor will obtain power from the microcontroller and pass accurate digital values of sensors to the microcontroller and will process all the data with machine learning reinforcement algorithms which can interpret even the lowest suspicious data among large ratio. If the system will compare the incoming data with predefined values. If any abnormality is detected then the buzzer will come to action and thus will predict the upcoming danger. The module is also connected with could along with a 4G GSM that will provide the network. In the end, we can find all the details just by logging in to the cloud with any device authorized by the out network.

V. Result and Discussion

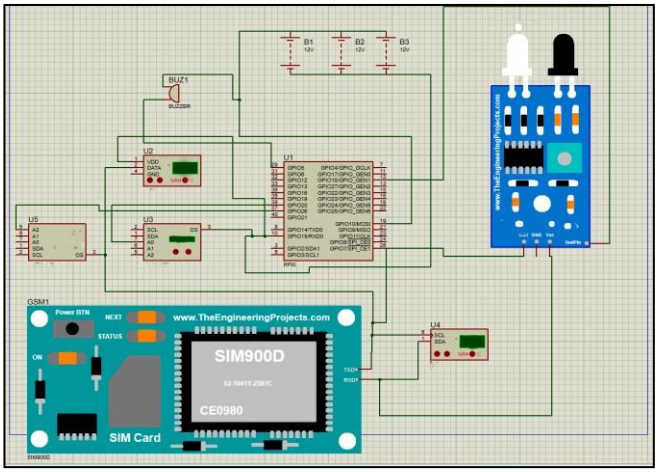

Fig. 11. Simulation process of the device

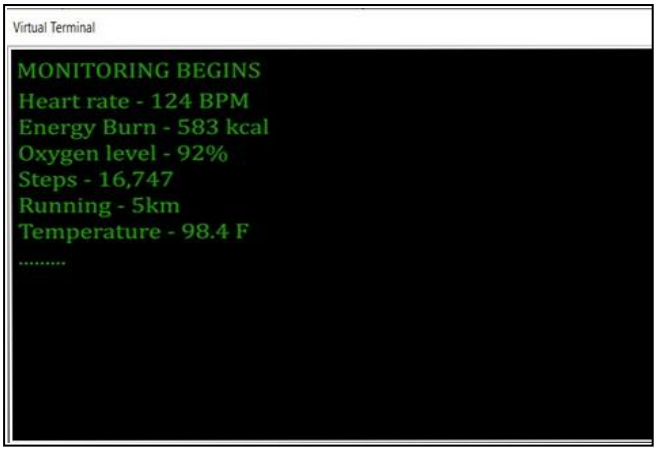

Fig. 12. Output of simulation

Sl. No.	Sub	Sample	Heart Rate	Body temp	Action
1	1	1	<60bpm	<36.1◦C	Message sent
2	1	2	<60bpm	<36.1◦C	Message sent
3	1	3	<60bpm	<36.1◦C	Message sent
4	1	4	<60bpm	<36.1◦C	Message sent
5	1	5	<60bpm	<36.1◦C	Message sent
6	1	6	<60bpm	<36.1◦C	Message sent
7	1	7	<60bpm	<36.1◦C	Message sent
8	1	8	<60bpm	<36.1◦C	Message sent
9	1	9	<60bpm	<36.1◦C	Message sent
10	1	10	<60bpm	<36.1◦C	Message sent
11	2	1	60 bpm	<36.1◦C	Message sent
12	2	2	60 bpm	<36.1◦C	Message sent
13	2	3	60 bpm	<36.1◦C	Message sent
14	2	4	60 bpm	<36.1◦C	Message sent
15	2	5	60 bpm	<36.1◦C	Message sent
16	2	6	60 bpm	<36.1◦C	Message sent
17	2	7	60 bpm	<36.1◦C	Message sent
18	2	8	60 bpm	<36.1◦C	Message sent
10	2	9	60 bpm	<36.1◦C	Message sent
20	2	10	60 bpm	<36.1◦C	Message sent
21	3	1	<60bpm	37◦C	Message sent
22	3	2	<60bpm	37◦C	Message sent
23	3	3	<60bpm	37◦C	Message sent
24	3	4	<60bpm	37◦C	Message sent
25	3	5	<60bpm	37◦C	Message sent
25	3	6	<60bpm	37◦C	Message sent
27	3	7	<60bpm	37◦C	Message not sent
28	3	8	<60bpm	37◦C	Message sent
29	3	9	<60bpm	37◦C	Message sent
30	3	10	<60bpm	37◦C	Message sent
31	4	1	65bpm	>37.2◦C	Message sent
32	4	2	65bpm	>37.2◦C	Message sent
33	4	3	65bpm	>37.2◦C	Message sent
34	4	4	65bpm	>37.2◦C	Message sent
35	4	5	65bpm	>37.2◦C	Message sent
36	4	6	65bpm	>37.2◦C	Message sent
37	4	7	65bpm	>37.2◦C	Message sent
38	4	8	65bpm	>37.2◦C	Message sent
39	4	9	65bpm	>37.2◦C	Message sent
40	4	10	65bpm	>37.2◦C	Message sent
41	5	1	66bpm	37◦C	Message not sent
42	5	2	66bpm	37◦C	Message not sent
43	5	3	66bpm	37◦C	Message not sent
44	5	4	66bpm	37◦C	Message not sent
45	5	5	66bpm	37◦C	Message not sent
46	5	6	66bpm	37◦C	Message not sent
47	5	7	66bpm	37◦C	Message not sent
48	5	8	66bpm	37◦C	Message not sent
49	5	9	66bpm	37◦C	Message not sent
50	5	10	66bpm	37◦C	Message not sent
51	6	1	>100bpm	<36.1◦C	Message not sent
52	6	2	>100bpm	<36.1◦C	Message sent
53	6	3	>100bpm	<36.1◦C	Message sent
54	6	4	>100bpm	<36.1◦C	Message sent
55	6	5	>100bpm	<36.1◦C	Message sent
56	6	6	>100bpm	<36.1◦C	Message sent
57	6	7	>100bpm	<36.1◦C	Message sent
58	6	8	>100bpm	<36.1◦C	Message sent
59	6	9	>100bpm	<36.1◦C	Message sent
60	6	10	>100bpm	<36.1◦C	Message sent
61	7	1	90bpm	<36.1◦C	Message sent
62	7	2	90bpm	<36.1◦C	Message sent
63	7	3	90bpm	<36.1◦C	Message sent
64	7	4	90bpm	<36.1◦C	Message sent
65	7	5	90bpm	<36.1◦C	Message sent
66	7	6	90bpm	<36.1◦C	Message sent
67	7	7	90bpm	<36.1◦C	Message sent
68	7	8	90bpm	<36.1◦C	Message sent
69	7	9	90bpm	<36.1◦C	Message sent
70	7	10	90bpm	<36.1◦C	Message sent
71	8	1	>100bpm	37◦C	Message sent
72	8	2	>100bpm	37◦C	Message sent
73	8	3	>100bpm	37◦C	Message sent
74	8	4	>100bpm	37◦C	Message sent
75	8	5	>100bpm	37◦C	Message sent
76	8	6	>100bpm	37◦C	Message sent
77	8	7	>100bpm	37◦C	Message sent
78	8	8	>100bpm	37◦C	Message not sent
79	8	9	>100bpm	37◦C	Message sent
80	8	10	>100bpm	37◦C	Message sent

81	9	1	90bpm	>37.2◦C	Message sent
82	9	2	90bpm	>37.2◦C	Message sent
83	9	3	90bpm	>37.2◦C	Message sent
84	9	4	90bpm	>37.2◦C	Message sent
85	9	5	90bpm	>37.2◦C	Message sent
86	9	6	90bpm	>37.2◦C	Message sent
87	9	7	90bpm	>37.2◦C	Message sent
88	9	8	90bpm	>37.2◦C	Message sent
89	9	9	90bpm	>37.2◦C	Message sent
90	9	10	90bpm	>37.2◦C	Message sent
91	10	1	90bpm	37◦C	Message sent
92	10	2	90bpm	37◦C	Message not sent
93	10	3	90bpm	37◦C	Message not sent
94	10	4	90bpm	37◦C	Message not sent
95	10	5	90bpm	37◦C	Message not sent
96	10	6	90bpm	37◦C	Message not sent
97	10	7	90bpm	37◦C	Message not sent
98	10	8	90bpm	37◦C	Message not sent
99	10	9	90bpm	37◦C	Message not sent
100	10	10	90bpm	37◦C	Message not sent

Accuracy 98%

VI. Conclusion

Through recent years humankind has changed from normal to technology-based and till now people are developing to spend their lifestyle in smarter than smarter ways and based on mankind's demand different kinds of smart devices and mobile applications are invented almost every day. There are different mobile applications and devices for almost every type of working like grocery, shopping, etc. and so here is also a device to look after people's health like this device will measure people's heartbeat, calorie burn, footsteps, oxygen level, etc. In this way, people who always get busy in work can also take care of his or her and their family members through a band like property where almost all body parameters measuring sensors are present and through this device also doctors and nurses can sense any types of abnormality or problem creating in patients' body.

VII. Future scope

If the more advanced sensor is used the circuit can produce a more accurate result. By applying some modification, the circuit can be made more lite therefore it can be light weight. If this circuit can be implemented in a larger scale it will be lower price. This device can also be implemented in wrist,

References

[1] E. Sutjiredjeki, E.M. Dewi and D. Budiman.: Air constituent Prediction Using Modern algorithm, 2018 International Conference on Applied Science and Technology Year: 2018 | Conference Paper | Publisher: IEEE

[2] Yair Enrique and Rivera Julio.: Development of a Prototype Arduino system for analyzing bacteria, Conference on Computer Aided System Engineering Year: 2015 | Conference Paper | Publisher: IEEE

[3] Vemuri Richard Ranjan Samson, U Bharath Sai, P Malleswara Rao and S Pradeep Kumar.: Simulation Based Design of Deep Ultraviolet LED Array Module, 2017 International Conference on Big Data Analytics and Computational Intelligence Year: 2017 | Conference Paper | Publisher: IEEE

[4] Md.Hasibur Rahman and Mohiuddin Ahmad.: Air filter sterilization using a one atmosphere uniform glow discharge, 2018 4th International Conference on Electrical Engineering and Information & Communication Technology Year: 2018 | Conference Paper | Publisher: IEEE

[5] Lazuardi Umar, Irfan Firmansyah and Rahmondia Nanda Setiadi.: Smart Pulse Oxygen monitoring with heart ventricle Rate Signal, 2018 3rd International Instrument Measurement Year2018 | Conference Paper | Publisher: IEEE

[6] Felix Liang, Iris Preston and Jas doon parkour.: Virus Propagation Model and Node Defense Strategy of Single Operation System Virus, 2016 IEEE International Symposium Conference and Room Year: 2016 | Conference Paper | Publisher: IEEE

[7] Martin Striegel and Amelie Hagelauer.: The ultraviolet offense: Germicidal UV lamps destroy vicious viruses, 2018 IEEE tropical agenda Conference on the topic of Wireless Sensors and Sensor Networks Year: 2018 | Conference Paper | Publisher: IEEE

[8] L. Mattias Andersson, kisimoto, Ryotaro Miura and Koji Yoshioka.: Air-gap data transmission using screen brightness modulation", 2015 IEEE International Conferenece of Remote SENSORS Year: 2015 | Conference Paper | Publisher: IEEE

[9] Z. A. Weinberg and S. A. Cohen.: Advances in air filter sterilization using a one atmosphere uniform, IEEE Transactions Biomedical Engineering International Seminar for Youth Meidcs Year: 1983 Journal Article | Publisher: IEEE

[10] S. Deepthi, Anjaly Krishna Sai and Guttappa.: Sajjan Improved air filtration and filter sterilization using DC electric fields, International International Conference on Electrical and Computer Engineering Year: 2019 | Conference Paper | Publisher: IEEE

Vehicle Accident Alert System

Biswayan Das, Student
Electronics and Telecommunication Engineering
Technique Polytechnic Institute
Hooghly, India
biswayandas10@gmail.com

Antara Banerjee Bhowmick
Electronics and Telecommunication Engineering
Technique Polytechnic Institute
Hooghly, India
bhowmick.antara@gmail.com

Madhurima Santra
Electronics and Telecommunication Engineering
Technique Polytechnic Institute
Hooghly, India
madhurima757.santra@gmail.com

Abstract*—- The advancement of technology has made our lives easier. Any technology has its advantages as well as its disadvantages. The advancement in automobile technology has increases the rate of road accidents which causes huge loss of life. Keeping this in our mind we have prepared a project,' Vehicle Accident Alert System' which may provide a solution of this problem to some extent. Here we have used Arduino, GPS (Global Positing System), GSM (Global System for Mobile Communication) and Accelerometer. Accelerometer detects the sudden change in the axes (X, Y, Z direction) of vehicle and GSM (Global System for Mobile Communication) module send the alert message on specified Mobile Phone with the location of the accident.

Keywords— Arduino, GPS, GSM, Accelerometer

I. INTRODUCTION

Now a days with the increase of population and advancement in automobile industry the number of vehicles in the road increases which leads the traffic jams and road accidents [4]. In the entire world 80% death is caused by vehicle accident. This is because of the lack of best emergency facilities available in our country [3]. Keeping this in our mind we decided to develop a project 'Vehicle accident alert system' which can mitigate the loss of lives. It can detect accidents in significantly less time and sends the basic information about the accident such as geographical coordinates and the time of the vehicle accident to first aid center, nearest police station and relatives. As this alert message will reach to the rescue team in a short time, they will be able to rush to the place quickly which will help in saving the valuable lives.[4][6]

To prepare the prototype of this project we have used Arduino UNO as microcontroller unit which is the brain of this project along with GSM module (Global System for Mobile Communication), GPS module (Global Positioning System) LCD (Liquid Crystal Display) and ADXL335 which is an accelerometer sensor.

II. METHODOLOGY

The Prototype of this Vehicle Accident Alert System uses the following steps:

1. ADXL335 is an accelerometer sensor which is used to detect the vibration in X, Y, Z axis of the vehicle. The vibration limit is pre stored in the EEPROM (Electronically Erasable Programmable Read-Only Memory. If the vibration level increases the pre stored vibration limit then ADXL335 accelerometer will send signal to microcontroller unit. This sensor has 5 pins VCC, GND, X, Y, Z which are connected to Digital Pins of Arduino.
2. GPS module (GLOBAL POSITIONING SYSTEM) is used to detect exact geographical Location
3. (Latitude & Longitude) where the accident happened. It collects coordinates from satellite for each and every second with time and date and sent as message to the rescue team through GSM. It has 4 pins VCC, GND, RX, TX which are connected to Arduino.
4. GSM MODULE (GLOBAL SYSTEM FOR MOBILE COMMUNICATION) is used to send SMS to Victim's family member. It consists of SIM slot in which SIM can be inserted. When accident happened, microcontroller receive data from GPS and transmit to GSM. Then it sends SMS to the mobile numbers which are pre stored in the EEPROM.
5. LCD DISPLAY – Here we have used 16*2 LCD Display. It is used to show different functions, Latitude & Longitude and some other information that helps understand whether the system is working properly or not.
6. POWER SUPPLY – For running all the modules, we need a power supply. Here Arduino, ADXL335, LCD Display works on 5V. GPS, GSM works on 12V. So, we have used 12v Power adapter and rest with good quality power bank which provide output of 5v.
7. Last but not the least the microcontroller which controls the entire circuit module that has been used in this project.

III. PRODUCT SPECIFICATIONS

A. ARDUINO UNO

The Arduino Uno is a microcontroller board based on the ATmega328. It has 20 digital input/output pins (of which 6 can be used as PWM outputs and 6 can be used as analog inputs), a 16 MHz resonator, a USB connection, a power jack, an in-circuit system programming (ICSP) header, and a reset button. It contains everything needed to support the microcontroller; simply connect it to a computer with a USB cable or power it with a AC-to-DC adapter or battery to get started.

1	Operating voltage	5V
2	DC current per I/O Pin	40mA
3	DC current for 3.3 volt Pin	50mA
4	Clock frequency	16 MHz

B. GSM Module

GSM is a mobile communication modem; it is stands for global system for mobile communication (GSM). The idea of GSM was developed at Bell Laboratories in 1970. It is widely used mobile communication system in the world. GSM is an open and digital cellular technology used for transmitting mobile voice and data services operates at the 850MHz, 900MHz, 1800MHz and 1900MHz frequency bands.

GSM system was developed as a digital system using time division multiple access (TDMA) technique for communication purpose. A GSM digitizes and reduces the data, then sends it down through a channel with two different streams of client data, each in its own particular time slot. The digital system has an ability to carry 64 kbps to 120 Mbps of data rates.

C. ADXL335 Accelerometer Module

An accelerometer is an electromechanical device that will measure acceleration force. It shows acceleration, only due to cause of gravity i.e. g force. It measures acceleration in g unit. The ADXL335 gives complete 3-axis acceleration measurement.

- This module measures acceleration within range ±3 g in the x, y and z axis.
- The output signals of this module are analog voltages that are proportional to the acceleration.
- It contains a polysilicon surface-micro machined sensor and signal conditioning circuitry.

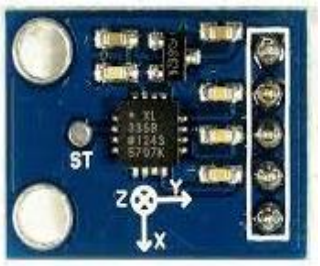

Pin configuration

VCC: Power supply pin i.e. connect 5V here.
X_OUT: X axis analog output.
Y_OUT: Y axis analog output.
Z_OUT: Z axis analog output.
GND: Ground pin i.e. connect ground here.

ADXL335 accelerometer provides analog voltage at the output X, Y, Z pins; which is proportional to the acceleration in respective directions i.e. X, Y, Z.

D. GPS Module

GPS stands for Global Positioning System by which anyone can always obtain the position information anywhere in the world.

NEO-6MV2 GPS Module Pin Configuration

The module has four output pins and we will describe the function each pin of them below. The powering of module and communication interface is done through these four pins.

Pin Name	Description
	
VCC	Positive power pin
RX	UART receive pin
TX	UART transmit pin
GND	Ground

E. LCD display

LCD modules are very commonly used in most embedded projects, the reason being its cheap price, availability and programmer friendly. Most of us would have come across these displays in our day to day life, either at PCO's or calculators. The appearance and the pinouts have already been visualized above now let us get a bit technical.

16×2 LCD is named so because; it has 16 Columns and 2 Rows. There are a lot of combinations available like, 8×1, 8×2, 10×2, 16×1, etc. but the most used one is the 16×2 LCD.

Features

- Operating Voltage is 4.7V to 5.3V

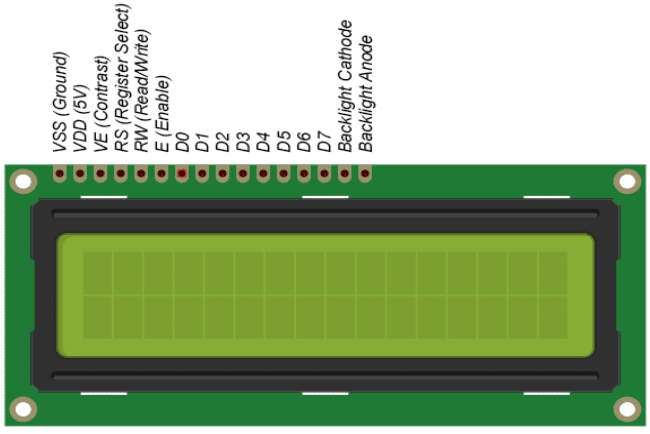

- Current consumption is 1mA without backlight

- Alphanumeric LCD display module, meaning can display alphabets and numbers
- Consists of two rows and each row can print 16 characters.
- Each character is build by a 5×8 pixel box
- Can work on both 8-bit and 4-bit mode
- It can also display any custom generated characters
- Available in Green and Blue Backlight

IV. Flow Chart

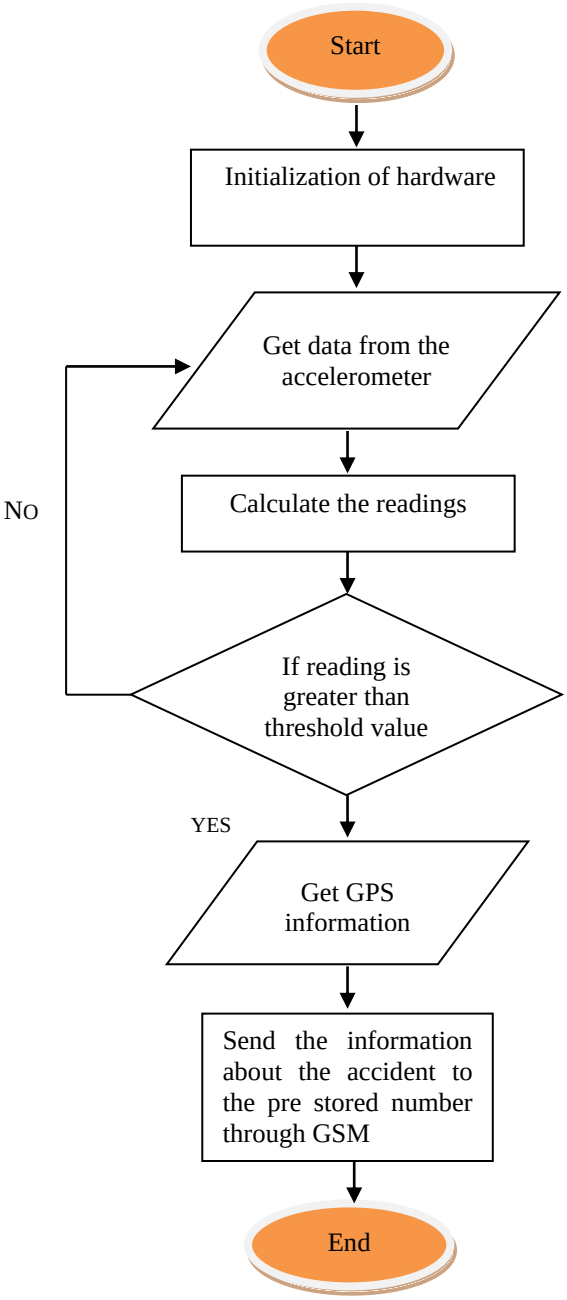

VI. Circuit Diagram

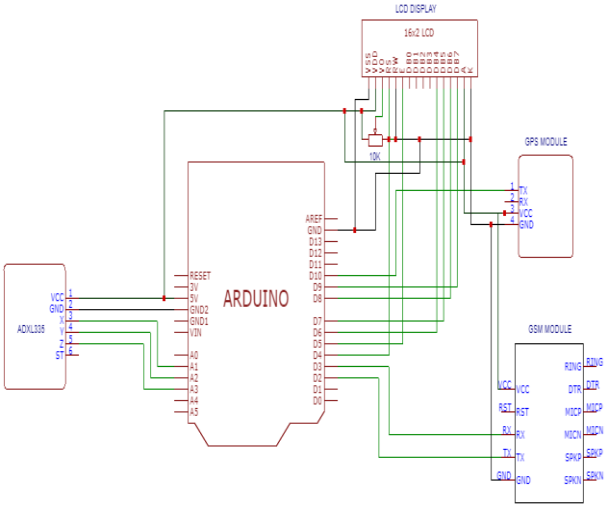

VII. Hardware Structure of the Project

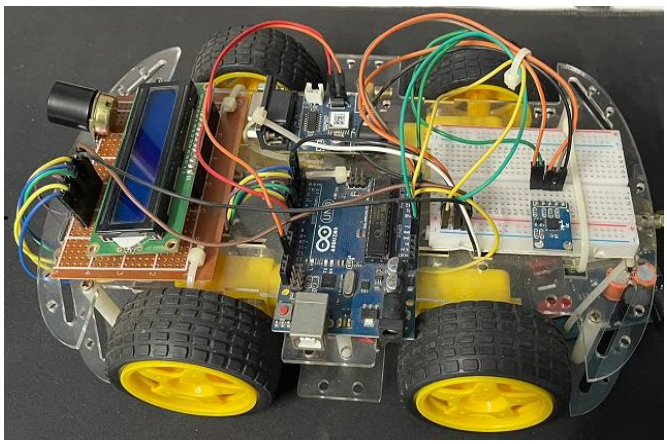

VIII. Advantages

- System is reliable.
- Design is simple and can be interface in any system easily.
- Alerts police and medical units about accidents.
- Easy to operate and maintenance.
- Easy to operate by the user.
- As each module are separated to each other to it is easy to identify the fault.

IX. Disadvantages

- If the phone battery is dead by any means, then it can't able to provide information about the accident to those pre stored number.
- If the vehicle faces an accident in the tunnel or in underground road, the GPS module may not be able to provide exact location.

Though the research work is going on for tracking the position of the vehicle even in dark clumsy areas where there is no network is available.

X. Future Scope

In future few features can be added to improve its functionality:

1. A wireless webcam can be added to capture the images which will help in providing driver`s assistance.
2. We can minimize the impact of the accident by using auto breaking system.
3. Also, we can modify it by using the concept of engine locking system if the pollution level of the vehicle exceeds the desired level.

XI. Conclusion

The aim of his project is to detect accident and provide automatic emergency assistance services. This system will send SMS to the nearest Emergency assistance service provider as well as to the relatives of the victim from accident location with exact latitude and longitude. If this feature can implemented in vehicles the death rate caused by accidents can be reduced.

XII. Acknowledgment

We wish to express our sincere gratitude to Mr. Avijit Karmakar, Principal and Mr. Sibasis Bandhyopadhyay, H.O.D of Electronics and Telecommunication Engineering Department of Technique Polytechnic Institute for providing us an opportunity to do our project work. This project bears on imprint of many people. Finally, we would like to thank our colleagues and students who helped us in different ways to complete this project successfully.

Referances

[1] R. Ganiga, Rohit Maurya, Archana Nanade, “Accident detection system using Piezo Disk Sensor”, International Journel of science, Engineering and Technology Research (IJSETR) volume6, Issue3, March 2017, ISSN 2278-7798.

[2] Khyati Shah, Vile Parle, Swati Bairagi, Vile Parle “Accident Detection and Conveyor System using GSM and GPS Module” International journal of Computer Applications (0975-8887).

[3] Nasr, Elie, Elie Kfoury, and David Khoury. "An IoT approach to vehicle accident detection, reporting, and navigation." 2016 IEEE International Multidisciplinary Conference on Engineering Technology (IMCET). IEEE, 2016.

[4] Gowshika., Madhu Mitha, Jayashree, S. Mutharasu. “Vehicle Accident Detection System By Using Gsm And Gps” International Research Journal of Engineering and Technology (IRJET), Volume: 06 Issue: 01 | Jan 2019, e-ISSN: 2395-0056, p-ISSN: 2395-0072.

[5] Kattukkaran, Nicky, Arun George, and TP Mithun Haridas. "Intelligent accident detection and alert system for emergency medical assistance." 2017 International Conference on Computer Communication and Informatics (ICCCI). IEEE, 2017.

[6] Goud, Varsha. "Vehicle accident automatic detection and remote alarm device." International Journal of Reconfigurable and Embedded Systems 1.2 (2012): 49.

[7] Mr. S. Kailasam, Mr Karthiga, Dr Kartheeban, R.M.Priyadarshani, K.Anithadevi, “Accident Alert System using face Recognition”, IEEE, 2019.

[8] Rajvardhan Rishi, Sofiya Yede, Keshav Kunal, Nutan V. Bansode”, Automatic Messaging System for Vehicle Tracking and Accident Detection, Proceedings of the International Conference on Electronics and Sustainable Communication Systems, ICESC, 2020.

[9] Harit Sharma, Ravi Kanth Reddy, Archana Karthik, “S-CarCrash: Real-time Crash Detection Analysis and Emergency Alert using Smartphone “, ICCVE, 2016.

[10] Pooja Shindalkar, Aasiya Fatema Shaikh, Chaitanya Mate, “Arduino Based Vehicle Accident Detection System”, International journal of Innovative Research in Computer and Communication Engineering (An 3297:2007 certified organization) Vol.5, Issue 4.

A CFD Study of a rectangular fin having different geometry exposed to natural convection

Aditya Kumar
Post-Graduate Student
Birla Institute of Technology
Sindhri

Sudip Chakraborty
Assistant Professor
Department of Mechanical Engineering
Adamas University
Kolkata

***Abstract*— The purpose of the paper is to investigate the heat transfer from a longitudinal fin by varying geometrical configurations. In this problem, heat from the base wall which is made of mild steel, is transferred through conduction and conducted heat is interacting with atmosphere through natural convection by the extended surface to enhance the heat transfer rate. Two different profiles are chosen for the study namely rectangular profile with single step change (RFSSC) and rectangular profile with double step change (RFDSC). Convective heat transfers, End-tip temperatures and Effectiveness are calculated for the chosen profiles and compared with the orthodox CRF profile. The best profile based on the application is identified to increase heat transfer is shown in this paper. ANSYS 19.0 is used to design the different configurations and to carry out the simulation to get the results. The simulated data have been verified analytically using Finite Difference Method and the equations are solved in MATLAB to get the desired data to be compared with fluent data. Few exhortations have been made about the possible application areas of the identified profiles.**

Keywords*— *Fin; CRF; RFSSC; RFDSC; CFD; Finite Difference Method; MATLAB; Convective heat transfer; Effectiveness.

I. INTRODUCTION

Heat transfer domain deals with generation of heat, absorption of heat and transportation of heat. Fin is nothing but the extended surface which helps to enhance the heat transfer by providing extra area. Application of fins are huge in mechanical devices such as IC engines, compressors, heat exchangers etc., even it is being used in space vehicles and in cooling of electronic components. The geometrical configurations are crucial since the volume and weight of the devices increase, consequently manufacturing cost raises when fins are used. For this reason only, fins with different geometry have been used to get the best profile which can save some manufacturing costs. Cuce E. et al.[1] investigated the effect of concavity level on performance parameters of a parabolic fin under the influence of natural convection and radiation. Total heat transfer, effectiveness and fin efficiency were calculated and this has been observed that heat loss due to convection and radiation decreases exponentially with the concavity of the profile. The volume of the profiles decreases with the concaveness of the profile as well. They have concluded that profiles with higher concavity provide the cheap and effective profile in terms of heat loss. Aziz A. [2] et al. applied finite element method to investigate the 2D performance of rectangular, trapezoidal, triangular and concave parabolic profile based fins under the mutual effect of convection and radiation. They have identified few parameters on which the total heat transfer rate is dependent, these parameters are fin size parameters, Biot number, radiation-conduction parameters and environment temperatures. Observations were done for each and every profiles and it was observed that profile with concave parabolic shape provided the best heat transfer rate and lowest was achieved for rectangular profile. Few assumptions were made in this study such as uniform convective heat transfer coefficient, constant base temperature and absence of radiative interaction between the fin profile and base surface. Kraus D. [3] reviewed the literatures of fins in the period of 1922-1987. The review was commenced with the NACA report of Harper & Brown and it was winded up with the work of Marto Wanniarachchi, Rose, Mitrou, and Razelos. The review was done based on non-uniform heat transfer coefficient, heat transfer solely on radiation, combined mode: Convection and Radiation, non-steady state heat transfer, non-homogeneous fin material, heat sources within the fin etc. Ullmann A. [4] et al. studied the efficiency and optimized dimensions of annular fins using different cross section areas. They took a constant mass system for different profiles and heat transfer rate was observed. Fin efficiency was calculated for the optimized profile and practical applications were discussed. Fabbri G. [5] developed a genetic algorithm for fin profile optimization. 2D distribution of temperature on the longitudinal section was observed using finite element method. Heat transfer was compared for generic profile with the rectangular profile with same length and volume. Generic algorithm was applied on polynomial profiles to determine polynomial parameter values which optimize the fin effectiveness. Azarkish H. [6] et al. worked on the geometry optimization of a longitudinal fin with volumetric heat generation under the influence of convection and radiation. The main objective was to investigate the maximum heat loss for a given volume of fins. Maximize object function was achieved corresponding to the optimized profile applying modified generic algorithm. The effect of the base temperature, heat transfer coefficient, temperature distribution along the fin length, fin efficiency etc. were calculated in this study. Finite volume method was applied to solve the 1D heat transfer problem and B-spline curves are used to generate the profile and optimal shape was found by optimizing the locations of a few control points by applying generic algorithm. Malekzadeh P. [7] et al. used differential quadrature element method (DQEM) for shape optimization of fins exposed to radiation and convection. In this study, thermal conductivity is assumed to be varied linearly with temperature and optimization of fins with uniform and stepped cross section was investigated. Accuracy of the work was measured by Adomian's decomposition technique, Taylor transformation technique and finite difference method. It was observed that DQEM happens to be the

propitious technique in practical engineering simulations where complex boundary conditions are imparted.

The objective of the work is to investigate the two novel profiles exposed to natural convection only. The two novel geometrical configurations are shown in figure 1, namely rectangular fin with single step change (RFSSC)and rectangular fin with double step change (RFDSC). Heat loss due to convection, End-tip temperatures and Fin-effectiveness have been investigated and based on the results, the profile has been identified. The results have been compared with common rectangular profile (CRF) and the verification of the computational result has been verified using finite difference method. The obtained equations from FDM have been solved using MATLAB.

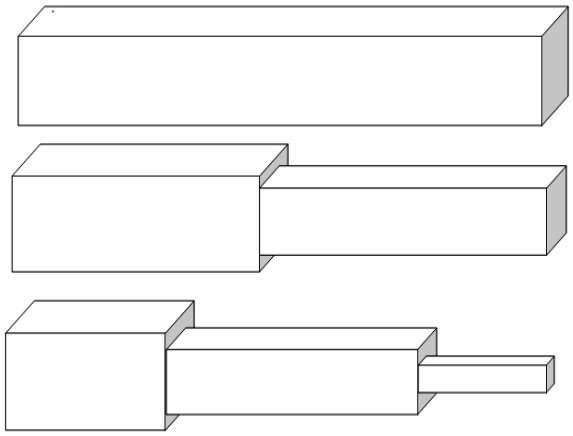

Fig. 1. fin profiles investigated in the study (Upper: CRF, Middle: RFSSC and Lower: RFDSC)

II. Mathematical Analysis

The general energy equation for a fin profile exposed to natural convection, can be written as –

$$\frac{d^2T}{dx^2} + \frac{hp}{kA}(T\text{-}T_s) = 0$$

Boundary condition: $T(0) = T_A$

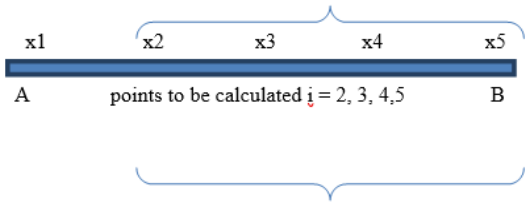

Finite difference form of the energy equation is –

$$\frac{T_{i-1} - 2T_i + T_{i+1}}{h^2} - \beta(T_i - T_s) = 0, \text{ where } \beta = \frac{hp}{kA}$$

$$T_{i-1} - (2 + h^2\beta)\,T_i + T_{i+1} = -h^2\beta T_s$$

When i=2

$$-(2+h^2\beta)\,T_2 + T_3 = -(h^2\beta T_s + T_1)$$

When i=3

$$T_2 - (2+h^2\beta)\,T_3 + T_4 = -h^2\beta T_s$$

When i=4

$$T_3 - (2+h^2\beta)\,T_4 + T_5 = -h^2\beta T_s$$

When i=5

$$T_4 - (2+h^2\beta)\,T_5 + T_6 = -h^2\beta T_s \text{ (T_6 is the atmospheric temperature)}$$

These equations can be presented in matrix form as [a][T] = [c]; the system can be written as –

$$\begin{bmatrix} -(2-h^2\beta) & 1 & 0 & 0 \\ 1 & -(2-h^2\beta) & 0 & 0 \\ 0 & 1 & -(2-h^2\beta) & 1 \\ 0 & 0 & 1 & -(2-h^2\beta) \end{bmatrix} \begin{bmatrix} T_2 \\ T_3 \\ T_4 \\ T_5 \end{bmatrix} = \begin{bmatrix} -(h^2\beta T_s) + T_1 \\ -(h^2\beta T_s) \\ -(h^2\beta T_s) \\ -(h^2\beta T_s) + T_6 \end{bmatrix}$$

III. Problem Statement

Common rectangular fin (CRF) made of aluminium having length (L) = 80 mm and width (w) = 25 mm has been taken for the reference and other profiles namely RFSSC and RFDSC are being used to investigate the change in different parameters compared to CRF. Optimization will be done by taking five different cases for RFSSC and RFDSC which is illustrated in table 1.

Atmospheric temperature has been taken as 293 K.

Three different cases (in mm) for optimization are illustrated as table 1.

Cases	L1	L2	L3	L4	L5	L6	t1	t2	t3	t4	t5	t6
1	80	50	30	30	20	30	3	3	2	3.6	2.4	1.8
2	80	40	40	40	20	20	3	3	2.2	2	3	4
3	80	25	75	20	30	50	3	2.5	4.5	2.3	3.5	4

In this study, the temperature of the base wall has been taken as 373 K and aluminium has been chosen as fin material. Thermal conductivity and heat transfer coefficient have been taken as 240 w/m/K and 40 w/m^2/k. Step length of the FDM analysis has been taken as 0.016.

IV. Verification of Computational Results

The accuracy of the FLUENT results will be verified using finite difference method (FDM) for a specific case (CRF). Finite Difference Method will be used to find out the temperature distribution of the fin. We will find the temperature distribution at i-1, i, i+1, i+2… nodes. These values will be compared with the FLUENT data. The FDM generated equations have been solved using MATLAB after representing those into matrix format and we will generate a graph between temperature and fin length.

Above matrix form is being used to get the different temperatures along the fin length. After putting the values of input parameters, the matrix can be represented as –

$$\begin{bmatrix} -2.052 & 1 & 0 & 0 \\ 1 & -2.052 & 1 & 0 \\ 0 & 1 & -2.052 & 1 \\ 0 & 0 & 1 & -2.052 \end{bmatrix} \begin{bmatrix} T_2 \\ T_3 \\ T_4 \\ T_5 \end{bmatrix} = \begin{bmatrix} -388.23 \\ -15.23 \\ -15.23 \\ -308.23 \end{bmatrix}$$

This system has been solved in MATLAB and the data have been captured for the temperatures where T2 = 352.503 K, T3 = 335.106 K, T4 = 319.604 K and T5 = 306.108 K. These values have been compared with the fluent data for verifying the fluent result.

These graphs show the similarity of trends of the temperature distribution using FLUENT and MATLAB. It indicates that the distribution which we have got using computational technique, has been verified using the analytical method. It can be surmised that computational method can be used for other profiles in order to get different outcomes. This comparison has been done just to check whether the computational method can be used for further analysis or not.

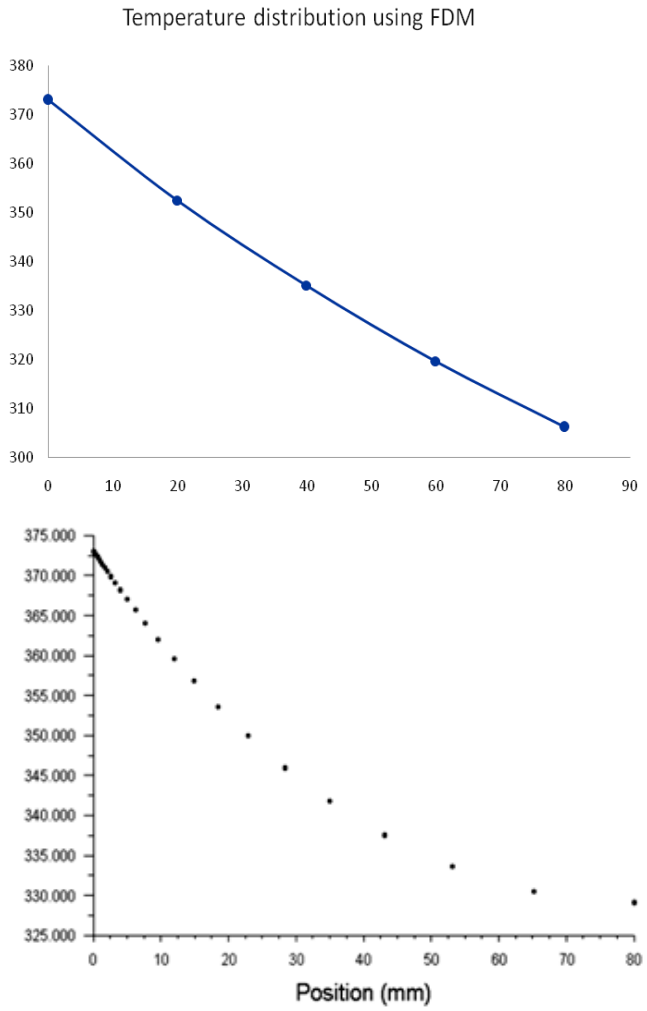

Fig. 2. Comparison of FLUENT and MATLAB results for validation

V. Analysis of Rectangular Fin with Single Step Change (RFSSC)

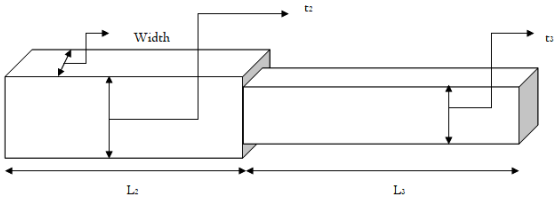

Fig. 3. Schematic diagram of RFSSC

CFD analysis has been performed on RFSSC profile using three different geometrical configurations. Heat loss due to convection, End-tip temperatures and fin effectiveness.

Different Configurations for RFSSC are shown in table 2:

Case	L_2 (mm)	L_3 (mm)	t_2 (mm)	t_3 (mm)
1	50	3	3	2
2	40	40	3	2.2
3	25	55	2.4	1.8

After doing analysis on RFSSC, three output parameters such as total convective heat transfer and end-tip temperature, have been analysed and represented for every case.

VI. Analysis of Rectangular Fin with Double Step Change (RFDSC)

CFD analysis has been performed on RFDSC profile using three different geometrical configurations. Heat loss due to convection, End-tip temperatures and fin effectiveness.

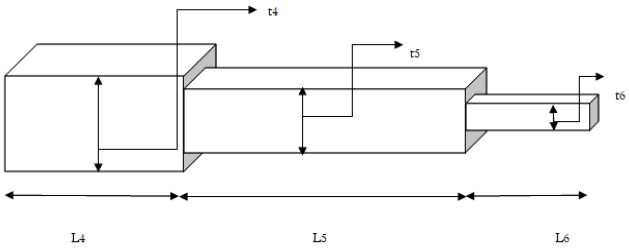

Fig. 4. Schematic diagram of RFDSC

Different Configurations for RFDSC are shown in table 3:

Case	L_4 (mm)	L_5 (mm)	L_6 (mm)	t_4 (mm)	t_5 (mm)	t_6 (mm)
1	30	20	30	3.6	2.4	1.8
2	40	20	20	3.4	2.2	1.6
3	20	30	30	3.2	2.0	1.2

After doing analysis on RFDSC, three output parameters such as total convective heat transfer and end-tip temperature, have been analysed and represented for every case.

VII. Results

After analysing the two novel profiles namely RFSSC and RFDSC, all the data associated to heat loss and end-tip temperature have been tabulated and represented to identify the best profile depending upon the applications.

Table 4 Convective heat transfer through different profiles

Profile	Convective Heat Transfer (10^5 W/m^2)
CRF	1.05
RFSSC1	1.25
RFSSC2	1.48
RFSSC3	1.42
RFDSC1	1.00
RFDSC2	1.04
RFDSC3	1.02

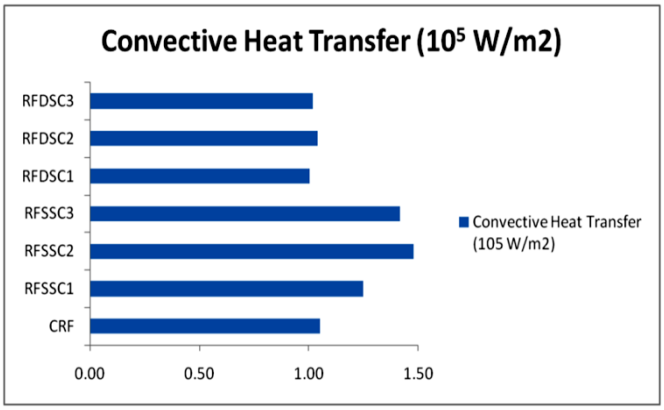

Fig. 5. Convective heat transfer through different profiles

Table 5. End-tip temperatures of different profiles

Profile	End tip temperature (Degree Centigrade)
CRF	67.62
RFSSC1	70.15
RFSSC2	68.28
RFSSC3	66.86
RFDSC1	43.73
RFDSC2	43.59
RFDSC3	38.34

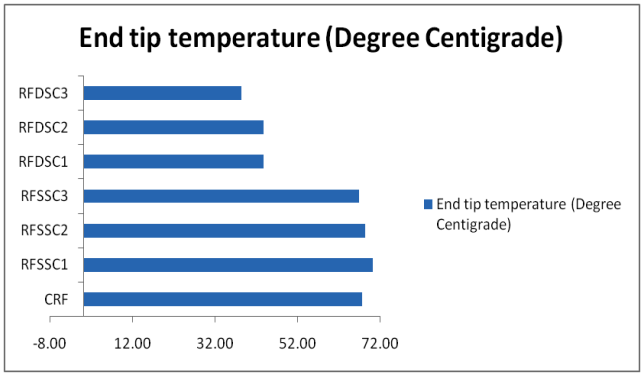

Fig. 6. End-tip temperatures of different profiles

Table 6. Fin effectiveness of different profiles

	Fin effectiveness
CRF	5.44
RFSSC1	6.47
RFSSC2	7.67
RFSSC3	7.34
RFDSC1	5.19
RFDSC2	5.40
RFDSC3	5.28

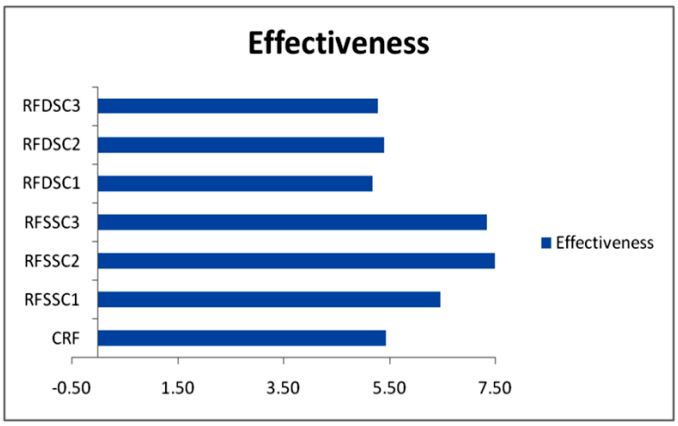

Fig. 7. Fin effectiveness of different profiles

VIII. Comparative Results

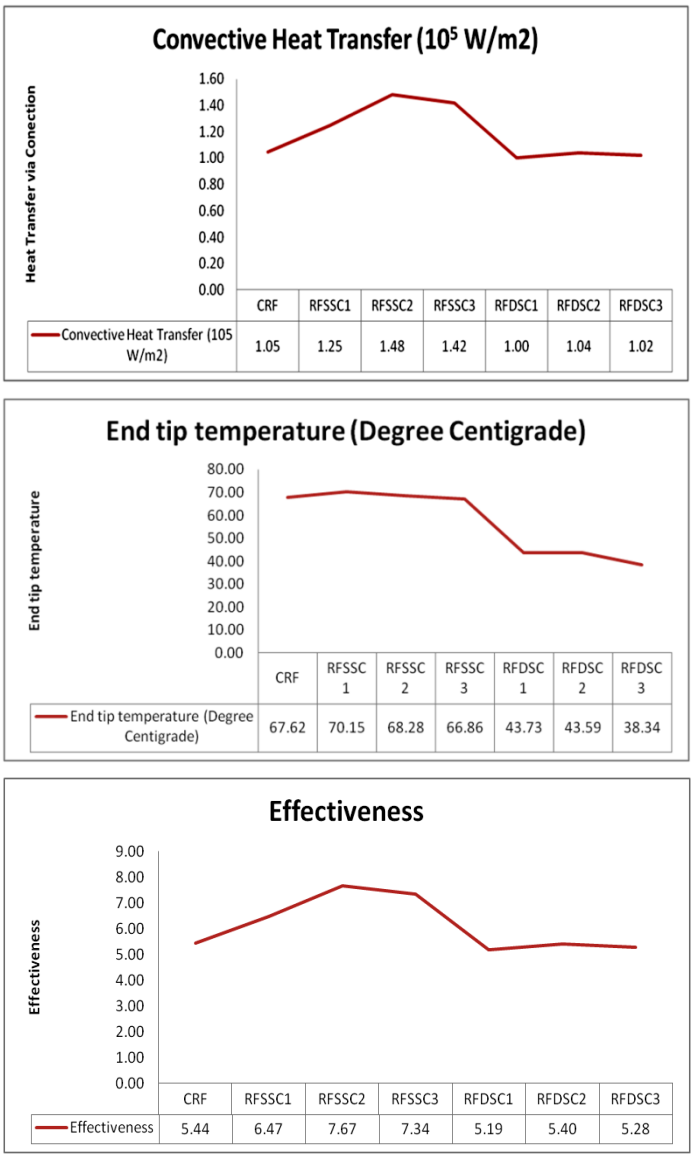

Fig. 8. Comparative results of different output parameters

In this work, CFD study was done on two novel profiles with different geometrical configurations to identify the best profiles based on the application. Here we have observed –

Rectangular fin with single step change (Case2) is showing the best result based on the heat loss due to convection which is 1.48 X 105 W/m^2.

Rectangular fin with double step change (Case3) is showing the best result based on the end-tip temperature which is 38.340 C where the base temperature was 1000 C and ambient temperature was 200 C

Rectangular fin with single step change (Case2) is showing the best result based on the fin effectiveness which is 7.67.

Based on the previous observation, this can be concluded that Rectangular fin with single step change (Case2) (RFSSC2) is to be identified as the best profile with the specific geometrical configurations for overall applications.

REFERENCES

[1] *Aziz A, Nguyen H.* Two-dimensional performance of convecting–radiating fins of different profile shapes. Waerme Stoffuebertrag 1993;28:481–7.

[2] *Kraus AD.* Sixty–five years of extended surface technology. Appl Mech Rev 1988;41:321–64.

[3] *Mikk I.* Convective fin of minimum mass. Int J Heat Mass Transfer 1980;23:707–11.

[4] *Ullmann A, Kalman H.* Efficiency and optimized dimension of annular fins of different cross-section shapes. International Journal of Heat Mass Transfer 1989;32:1105–10.

[5] *Kobus CJ, Cavanaugh RB.* A theoretical investigation into the optimal longitudinal profile of a horizontal pin fin of least material under the influence of pure forced and pure natural convection with a diameter-variable convective heat transfer coefficient. J Heat Transfer 2006;128:843–6.

[6] *Fabbri G.* A genetic algorithm for fin profile optimization. Int J Heat Mass Transfer 1997;40:2165–72.

[7] *Yeh RH, Liaw SP, Chang M.* Optimum spacings of longitudinal convective fin arrays. J Mar Sci Tech 1997;5:47–53.

[8] *Mueller DW, Jr, Abu–Mulaweh HI.* Prediction of the temperature in a fin cooled by natural convection and radiation. Appl Therm Eng 2006;26: 1662–68.

TECHNIQUE POLYTECHNIC INSTITUTE

PANCHROKHI, SUGANDHYA, HOOGHLY, 712102